

1-1-2013

# Removal of Synthetic Organic Compounds and NOM by Single-Walled Carbon Nanotubes-Ultrafiltration and Forward Osmosis Membrane System

JI YONG HEO

*University of South Carolina*

Follow this and additional works at: <http://scholarcommons.sc.edu/etd>

---

## Recommended Citation

HEO, J. (2013). *Removal of Synthetic Organic Compounds and NOM by Single-Walled Carbon Nanotubes-Ultrafiltration and Forward Osmosis Membrane System*. (Doctoral dissertation). Retrieved from <http://scholarcommons.sc.edu/etd/2357>

This Open Access Dissertation is brought to you for free and open access by Scholar Commons. It has been accepted for inclusion in Theses and Dissertations by an authorized administrator of Scholar Commons. For more information, please contact [SCHOLARC@mailbox.sc.edu](mailto:SCHOLARC@mailbox.sc.edu).

REMOVAL OF SYNTHETIC ORGANIC COMPOUNDS AND NOM BY SINGLE-  
WALLED CARBON NANOTUBES-ULTRAFILTRATION AND FORWARD OSMOSIS  
MEMBRANE SYSTEM

by

Jiyong Heo

Bachelor of Engineering  
Korea Army Academy at Yeongcheon, 2002

Master of Science and Engineering  
Seoul National University, 2006

---

Submitted in Partial Fulfillment of the Requirements

For the Degree of Doctor of Philosophy in

Civil and Environmental Engineering

College of Engineering and Computing

University of South Carolina

2013

Accepted by:

Yeomin Yoon, Major Professor

Joseph R.V. Flora, Committee Member

Navid B. Saleh, Committee Member

Namguk Her, Committee Member

Lacy Ford, Vice Provost and Dean of Graduate Studies

© Copyright by Jiyong Heo, 2013  
All Rights Reserved.

## DEDICATION

This dissertation is dedicated to my family who has supported me all the time. Especially, this dissertation is dedicated to my beloved wife, best lifetime companion, Hyeun Park, who has been share joys and sorrows of my work and a great source of motivation and inspiration. She has been always support me and patience with my work since the beginning of my studies.

## ACKNOWLEDGEMENTS

First of all, I would like to acknowledge my sincere gratitude to my advisor, Dr. Yeomin Yoon, for his consistent inspiration and advice. He gave me a great opportunity to learn, prepared me to do great things, and allowed me to perform the research that is presented in this body of work. I would also like to express my appreciation to my committee members, Dr. Joseph R.V. Flora, Navid B. Saleh, and Namguk Her for their invaluable advice and guidance in the preparation of this dissertation. I would also like to thank my colleagues in CEE at the USC. None of this would be possible without their help and support. I would like to thank to Dr. Nicole Berge, who has set up the instruments for analysis and provided critical advisement of it that has thoroughly enhanced the quality of this dissertation. I would also like to give a special appreciation to Dr. Heebum Lee, who has given me endless support and kindness for military overseas education. I greatly acknowledge to the Republic of Korea Army overseas education scholarship that offers me the opportunity to pursue a Ph.D. in Civil and Environmental Engineering at USC under their generous financial support. This research was also conducted using the funding provided by the GS Engineering and Construction Co. and the Korea Ministry of Environment.

Most of all, I greatly thank to my parents, my parents-in-law, my family and friends for their continual support and belief, no matter what it took me. All this would not have been possible without their constant support.

## ABSTRACT

This overall theme of this dissertation is to investigate the potential engineered application of low pressure membranes incorporated with single-walled carbon nanotubes (SWNTs) and forward osmosis (FO) membrane systems for the removal of synthetic organic compounds (SOCs) and natural organic matter (NOM) from drinking water sources. The focus is on the use of SWNTs-ultrafiltration (UF) and FO membrane systems to facilitate the removal of these compounds and potential applications of these membrane system designs for reducing the energy demands and membrane fouling in environmental water filtration process and seawater desalination. The SWNTs-UF results indicate that SOCs transport is influenced by NOM, which fouls the membrane through pore blockage and cake/gel formation. A strong linear correlation between the retention and adsorption of SOCs was observed, indicating that retention by the SWNTs-UF membranes is mainly due to the adsorption of SOCs onto the membrane, the SWNTs, and/or NOM. The performance of SWNTs–UF was also evaluated on the basis of a resistance-in-series model, filtration laws, and NOM transportation mechanisms. The addition of SWNTs to the UF process did not significantly exacerbate the permeate flux decline and total membrane resistances. Further, it appeared that the effect of SWNTs on membrane fouling is a function of hydrodynamic and operational conditions. The results suggest that the NOM transportation in SWNTs–UF systems depends, to a significant extent, on the concentration polarization and cake/gel layer formation at the membrane boundary. In the application for artificial seawater in SWNTs-UF, the presence of

SWNTs shows 20% increase in membrane flux and a strong linear correlation between retention and adsorption of SOCs was obtained. In FO membrane systems, the cellulose triacetate based FO membrane exhibited the better separation properties than that of polyamide based reverse osmosis (RO) membrane. And, in active layer (AL)-facing-feed solution (FS) configuration in FO mode, the RO membrane exhibited higher removal efficiency at the expense of severe internal concentration polarization (ICP) and flux reduction. Under higher cross-flow velocity operations in FO mode, both reduced external concentration polarization and retarded SOC diffusion from the reverse flux of sodium chloride contributed to the improved SOC removal performance. The FO membrane removal behavior was principally related to size exclusion, while the RO membrane removal behavior was related to interactions between hydrophobicity, size, and electrostatic repulsion. The results significantly confirmed the dominant role of ICP, and the trade-off between flux and removal efficiency depends on the porous supporting layer in AL-facing-FS configurations in the FO process.

## TABLE OF CONTENTS

DEDICATION .....	iii
ACKNOWLEDGEMENTS.....	iv
ABSTRACT .....	v
LIST OF TABLES .....	x
LIST OF FIGURES .....	xii
CHAPTER I INTRODUCTION AND MOTIVATION .....	1
CHAPTER II OBJECTIVE AND SCOPE .....	6
CHAPTER III LITERATURE REVIEW AND BACKGROUND.....	11
3.1 MECHANISMS FOR ORGANIC SOLUTES RETENTION OF MEMBRANE TREATMENT	11
3.2 DISSOLVED ORGANIC MATTER (DOM) TRANSPORT MODELS.....	15
3.3 APPLICATION OF SWNTs-UF IN WATER TREATMENT .....	24
3.4 FORWARD OSMOSIS SOLUTION-DIFFUSION MODEL AND CROSS-FLOW TEST UNIT	27
CHAPTER IV REMOVAL OF BPA AND EE2 IN SWNTs-UF MEMBRANE SYSTEMS .....	31
4.1 INTRODUCTION .....	32
4.2 MATERIALS AND METHODS .....	35
4.3 RESULTS AND DISCUSSION .....	45
4.4 CONCLUSIONS.....	69



CHAPTER V NATURAL ORGANIC MATTER REMOVAL IN SINGLE-WALLED CARBON NANOTUBES-ULTRAFILTRATION MEMBRANE SYSTEMS .....	71
5.1 INTRODUCTION .....	72
5.2 MATERIALS AND METHODS .....	75
5.3 RESULTS AND DISCUSSION .....	79
5.4 CONCLUSIONS.....	102
CHAPTER VI REMOVAL OF MICRO-POLLUTANTS AND NOM IN CARBON NANOTUBE-UF MEMBRANE SYSTEM FROM SEAWATER .....	104
6.1 INTRODUCTION .....	105
6.2 MATERIALS AND METHODS .....	109
6.3 RESULTS AND DISCUSSION .....	115
6.4 CONCLUSIONS.....	125
CHAPTER VII REMOVAL OF SYNTHETIC ORGANIC COMPOUNDS BY FORWARD OSMOSIS AND REVERSE OSMOSIS MEMBRANE .....	127
7.1 INTRODUCTION .....	128
7.2 MATERIALS AND METHODS .....	132
7.3 RESULTS AND DISCUSSION .....	139
7.4 CONCLUSIONS.....	165
CHAPTER VIII OVERALL CONCLUSION AND FUTURE RECOMMENDATIONS .....	167
REFERENCES .....	172
APPENDIX A – MD SNAPSHOT OF OPTIMUM SOCs WITH FO AND RO MEMBRANE COMPLEXES IN AQUEOUS SOLUTION.....	195



## LIST OF TABLES

Table 4.1 Ultrafiltration membrane characteristics .....	36
Table 4.2 Characteristics of BPA and E2 .....	37
Table 4.3 Equations and constants description of fitted isotherm models.....	39
Table 4.4 The BPA and EE2 fitted isotherm models constants on membrane in the absence and presence of SWNTs and NOM .....	49
Table 4.5 Ultrafiltration flux declines with the accumulated adsorbed mass of the micropollutants by UF and SWNTs-UF processes in the absence and presence of NOM .....	60
Table 4.6 Equations of different fouling mechanisms for dead-end filtration.....	63
Table 5.1 Ultrafiltration membrane characteristics .....	77
Table 5.2 Characteristics of the fouling layer and resistances as a function of unit retained DOC mass in the absence and presence of SWNTs and various operating conditions according to resistance in series model. ....	86
Table 5.3 Membrane fouling analyses for HA filtration in UF and UF-SWNTs without stirring .....	90
Table 5.4 Empirical dead-end filtration blocking laws in their linearized form with blocking indexes.....	93
Table 5.5 Observed and real rejection results of HA in UF and UF-SWNTs according to concentration polarization model. ....	100

Table 6.1 Characteristics of BPA and EE2.....	110
Table 6.2 Ultrafiltration membrane characteristics .....	111
Table 6.3 Characteristics of standard seawater salt and ionic composition of ASW .....	112
Table 7.1 Properties of the target compounds spiked to the feed solution. ....	133
Table 7.2 Properties of the selected FO and RO membranes .....	139

## LIST OF FIGURES

Figure 3.1 EDC/PPCP percentage removed from spiked DI water (pH 7) in a dead-end membrane filtration system using a separate NF and UF membrane. ....	13
Figure 3.2 Batch adsorption with ESNA membrane in the presence from deionized water and presence ( $4 \text{ mg L}^{-1}$ ) of NOM. ....	14
Figure 3.3 Conceptual schematic of concentration polarization by film theory and cake layer formation; concentration profile under steady-state conditions. ....	17
Figure 3.4 Characterization of single walled carbon nanotubes: (a) HR-TEM images of SWNTs aggregates; (b) zeta potential at pH 4.0, 7.5, and 11.0; (c) Raman spectra; and (d) SWNTs aggregate diameter. ....	26
Figure 3.5 Schematic diagram of bench-scale FO membrane system. ....	29
Figure 3.6 Bench-scale FO membrane system. ....	30
Figure 4.1 Schematic diagram of SWNTs-UF membrane testing unit. ....	41
Figure 4.2 Comparison of adsorption to UF5K membrane: (a) BPA and (b) E2 between the membrane area and the bulk solution in the absence and presence of NOM and SWNTs. ....	46
Figure 4.3 Isotherm model data fitting for BPA and E2 onto UF membrane: (a) Langmuir isotherm fit of data in no NOM/SWNTs; (b) linear form of Langmuir isotherm data in SWNTs only and NOM/SWNTs. ....	48
Figure 4.4 The average adsorption coefficients of BPA and E2 onto UF membrane in the absence and presence of NOM and SWNTs. ....	51

Figure 4.5 Comparison of partition coefficient of (a) BPA and (b) E2 between the membrane and the bulk solution in the absence and presence of NOM and SWNTs.....	53
Figure 4.6 Comparison of (a) delivered and adsorbed mass accumulated and (b) adsorbed mass and retention for BPA and E2 in the UF5K filtration in the absence and presence of NOM and SWNTs. ....	56
Figure 4.7 Comparison of retention and adsorption for BPA and E2 in the UF5K end of filtration (cumulative permeate volume of 500 mL) in the absence and presence of NOM and SWNTs. ....	58
Figure 4.8 The experimental data fitting of the flux decline using different fouling mechanisms: (a) complete blocking; (b) standard blocking; (c) intermediated blocking; and (d) cake filtration.....	64
Figure 4.9 Comparison of (a) retained DOC and adsorption for BPA and E2 and (b) applied pressure, DOC rejection, and retained DOC in the UF5K filtration in the presence of NOM and SWNTs. ....	65
Figure 4.10 Comparison of delivered and adsorbed mass accumulated, and adsorbed mass and retention for BPA and E2 in three UF (UF5K, UF10K, and UF30K) membrane filtration in the presence of NOM and NOM+SWNTs.....	67
Figure 4.11 Three-dimensional AFM image (a) cleaned membrane, (b) fouled in the absence of SWNTs, and (c) fouled membrane in the presence of SWNTs ....	68
Figure 5.1 Influence of SWNTs concentrations on flux decline and HA rejection. Flux decline and HA rejection as a function of SWNTs concentration for the 10 kDa PES membrane: (a) Flux decline at 300 rpm, (b) flux decline without stirring, (c) HA rejection based on UV <sub>254</sub> , and (d) HA rejection based on DOC .....	80
Figure 5.2 Influence of pH on flux decline and HA rejection based on DOC in the absence and presence of SWNTs: (a) Normalized flux decline and (b) HA	

rejection based on DOC at different pH conditions. ....	84
Figure 5.3 Influence of ionic strengths on flux decline and HA rejection based on DOC in the absence and presence of SWNTs: (a) Normalized flux decline and (b) HA rejection based on DOC at different ionic strength conditions. ....	84
Figure 5.4 Comparison of UF fouling resistances as a function of unit retained DOC mass in the absence and presence of SWNTs. ....	88
Figure 5.5 Flux decline analyses for HA filtration in the absence and presence of SWNTs: (a) Flux modeling and (b) membrane fouling analyses ....	91
Figure 5.6 Influence of stirring on filtration law analyses for HA filtration in UF-SWNTs: (a) Cake filtration and complete blocking analysis and (b) standard blocking and intermediate blocking analysis. ....	94
Figure 5.7 Influence of applied pressure on flux decline and HA rejection based on DOC in the absence and presence of SWNTs: (a) Normalized flux decline and (b) HA rejection at different applied pressures. ....	96
Figure 5.8 Comparison of HA rejection trends with respect to both VCF and pressure in the absence and presence of SWNTs: (a) In the absence of SWNTs and (b) in the presence of SWNTs. ....	98
Figure 5.9 Application of transport mechanisms for real rejection trends and transport Parameters of humic acid with UF-SWNTs. ....	99
Figure 6.1 The relationship between dissolved organic carbon (SHA) and UVA absorbance at various pH values in (a) DI water and (b) ASW. ....	116
Figure 6.2 Comparison of (a) delivered and adsorbed mass accumulated, (b) adsorbed mass and retention, (c) adsorption and accumulated retention, and (d) mass of permeate, retentate, membrane adsorption, and CNT adsorption for BPA and EE2 in the CNT-UF system with DI water and ASW. ....	118
Figure 6.3 Comparison of flux-decline, rejection trends based on UVA <sub>254</sub> (a) ASW only	

and (b) ASW+CNTs. ....	123
Figure 6.4 Three-dimensional AFM image (a) cleaned membrane, (b) fouled in the absence of CNTs in ASW, and (c) fouled membrane in the presence of CNTs (ASW). ....	125
Figure 7.1 Pure water flux and NaCl rejection trends with respect to applied hydraulic pressure in the RO-mode: (a) FO membrane and (b) RO membrane .....	140
Figure 7.2 Water flux and specific water flux (flux normalized by osmotic driving force) as a function of time for two FO membrane experiments and one RO experiment: (a) FO membrane (3 and 18 GPH) and (b) RO membrane.....	143
Figure 7.3 SEM image of FO-CTA and RO-BW30 membrane: (a.1) FO membrane cross-section ( $\times 150$ ), (a.2) FO membrane cross-section of supporting layer ( $\times 1K$ ), (a.3) FO membrane back side ( $\times 1K$ ), (b.1) RO membrane cross section ( $\times 150$ ), (b.2) RO membrane cross-section of supporting layer ( $\times 1K$ ), and (b.3) FO membrane back side ( $\times 1K$ ). ....	146
Figure 7.4 Reverse salt flux as a function of time for two FO membrane experiments and one RO experiment: (a) FO membrane (3 and 18 GPH) and (b) RO membrane.....	147
Figure 7.5 Comparison of (a) SOCs concentration in permeate and (b) SOCs retention as a function of time with FO membrane in the FO-mode at the cross-flow velocity of 3 GPH. ....	149
Figure 7.6 Comparison of (a) SOCs concentration in permeate and (b) SOCs retention as a function of time with FO membrane in the FO-mode at the cross-flow velocity of 18 GPH .....	150
Figure 7.7 Comparison of (a) SOCs concentration in permeate and (b) SOCs retention as a function of time with RO membrane in the FO-mode at the cross-flow velocity of 3 GPH. ....	151



Figure 7.8 Comparison of (a) SOC's retention between FO and RO membrane and (b) the normalized SOC's adsorbed mass onto FO and RO membrane .....	153
Figure 7.9 Comparison of SOC's adsorption onto (a) FO membrane and (b) RO membrane as a function of time.....	157
Figure 7.10 Representative MD snapshot of optimum (a) FO membrane with EE2 and (b) RO membrane with EE2 complexes in aqueous solution.....	160
Figure 7.11 Binding energy of SOC's onto FO and RO membrane with respect to log Kow values.....	161
Figure 7.12 Flux decline and SOC's retention as a function of VCF in RO-mode: (a) flux decline between FO and RO membrane, (b) SOC's retention with FO membrane, and (c) SOC's retention with RO membrane .....	163

## CHAPTER 1

### INTRODUCTION AND MOTIVATION

The synthetic organic compounds (SOCs), including endocrine disrupting compounds (EDCs), and pharmaceuticals and personal care products (PPCPs) have been detected in water supplies and wastewater effluents worldwide [1-4]. Some SOC have documented adverse ecological impacts that have raised concern among public and regulatory groups about the fate of such compounds during potable water treatment, as well as human exposure to them in drinking water [5-7]. Some EDC/PPCPs are more polar than the currently regulated polyaromatic contaminants. This, coupled with their occurrence at trace levels (parts per trillion), creates unique challenges to analytical detection and the assessment of removal performance by potable water treatment plant processes [3]. Drinking water treatment relies primarily upon adsorptive and oxidative processes to remove or transform organic materials. Previous studies of selected groups of EDC/PPCPs, pesticides, and herbicides have indicated that coagulation, sedimentation, and filtration achieve minimal levels of removal [8-10].

Natural organic matter (NOM) has been related to the most problematic issue of water treatment. NOM can affect carcinogenic as a precursor to disinfection by-products and making complex it with metals and hydrophobic synthetic compounds, which are more difficult to remove it during water treatment processes. NOM cannot be significantly rejected during ultrafiltration (UF) since UF has relatively larger nominal molecular weight cut-off (MWCO) compared to the molecular size of NOM [11, 12].

Furthermore, NOM has been well known as a major contributor to membrane fouling, which deteriorates the extensive application of UF process in advanced water systems, as it clogging the membrane pores or forming cake layer on the membrane surface [13-16]. But most of all, the humic acid (HA), major hydrophobic fractions of dissolved NOM (DOM), are usually considered to be responsible for severe membrane fouling [17, 18]. HA are anionic macromolecules having a wide range of molecular weights comprise both aromatic and aliphatic components with primarily carboxylic (carboxylic functional groups account for 60–90% of all functional groups) and phenolic functional groups in aquatic environments [19]. HA is found to have the largest impact on membrane fouling as causing great pore adsorption (irreversible fouling) onto membranes compared to other fractions of DOM.

For over the past few decades, membrane filtration process has attracted increasing attention as a promising technology for the elimination of SOCs, including EDC/PPCPs from water and wastewater. The process of membrane filtration has significant advantages, because it is easy and safe to perform and produces a minimal amount of toxic byproducts. In recent years, low pressure membranes (LPMs) including UF and microfiltration (MF) are widely used as a separation technology in the filtration of aqueous mixtures for drinking water and wastewater treatment [20, 21]. LPM treatment has become one of the most important technologies for water treatment due to its outstanding efficacy in producing high quality water, its relatively small footprint, and its relatively low costs [21, 22]. However, membrane fouling associated with reversible and irreversible foulants (i.e., colloids, particles, algae, and bacteria) needs to be overcome for achieving water quality objectives [23].

Seawater desalination is a general term for the process of removing salt from seawater to produce fresh water. For seawater desalination, reverse osmosis (RO) desalination installations have been significantly increasing and have accounted for 75% of new production capacity in 2003 [24]. Furthermore, forward osmosis (FO) using the osmotic pressure driving force has drawn special research attention by providing reasonably low cost and energy under a high recovery rate [25-30]. FO involves spontaneous water movement by means of a natural chemical gradient in which a solution tends to move from a state of lower osmotic pressure to a higher one through a semi permeable membrane, which can remove target solutes from the sample [31]. Also, the FO process depends more on the molar concentrations of the solutions instead of the actual identity of the solutes. This makes the overall process much more versatile in order to filter different kinds of solutions with the same system. Nevertheless, FO is not fully developed; thus, it cannot be used in commercial practice, but the whole process technology is in developing stages [31]. First of all, the specialized membranes (i.e. low internal concentration polarization) must be found in order to create the most efficient FO system along with high osmotic pressures for creating the high gradient for water to move from the feed solution. So far, only a handful studies have focused on FO mode runs for the retention of SOC's for the FO application to the environmental filtrations.

The seawater sources often include particulate and colloidal contaminants, as well as hydrocarbons from oil contamination and biological contaminants (e.g., algal blooms and other microorganisms) [32]. These foulants need to be pretreated to lower the fouling propensity of water in RO and FO membrane system. Conventional pretreatment processes (acid addition, coagulant/flocculant addition, and disinfection) have been

widely used for seawater and RO plants. However, various feed water chemistry conditions can cause variations in conventional pretreatment efficacy, since colloids and suspended particles often pass through conventional pretreatment and contribute to difficult to remove (and possibly irreversible) RO membrane fouling [33]. A new trend in pretreatment has been a movement towards the use of UF and MF membranes to pretreat of FO/RO feed water [32]. Commonly used pretreatments (i.e., coagulation, adsorption, and preoxidation) for LPM filtration can transform the physicochemical and/or biological properties of feed water and improve the performance of LPMs.

The most intensively studied adsorbent for LPM filtration in water treatment is powdered activated carbon (PAC). The efficacy of PAC in removing organic contaminants is strongly dependent on PAC type [34, 35], dose, properties of the organics [10, 36], and the competition of other aquatic constituents [37]. Since their discovery in 1991, carbon nanotubes (CNTs) have demonstrated such extraordinary mechanical, electrical, thermal, and chemical properties that they have become candidates for numerous applications, such as nanocomposites, energy storage, microelectronics, and medical devices [38, 39]. Several studies projected the production of CNTs at millions of tons in 2010, and a \$1 trillion worldwide market for nanoproducts by 2015 [40, 41]. Studies have indicated that CNTs are good adsorbents, due to their high adsorption capacities for heavy metals [42], phenols [43], and other organic chemicals [44]. In addition, CNT technology has the potential to support point of use in water treatment since unlike many microporous adsorbents, CNTs possess fibrous shape with high aspect ratio, large accessible external surface area, and well developed mesopores, all contribute to the superior removal capacities of these macromolecular biomolecules and

microorganisms [45]. Due to these unique characteristics of CNTs, the potential applications of CNT-UF/MF can be enormous in water/wastewater treatment/reclamation and seawater desalination, although they have not been studied.

Regardless of rapid growth in membrane-based water pretreatment capacity, the key disadvantages of each conventional pretreatment for LPMs include that (i) coagulation may exacerbate fouling and be ineffective in mitigating the fouling by hydrophilic neutral organics, (ii) adsorption possibly exacerbate LPM fouling, and (iii) preoxidation forms disinfection by-products and may damage membranes incompatible with oxidants [23]. This research, UF incorporated with SWNTs, can provide solutions to overcome the possible exacerbation of LPM fouling readily shown in conventional hybrid adsorbent-UF/MF processes, also it is include that the potential applications of FO membrane systems for reducing the energy demands and membrane fouling in the environmental filtration by efficiently removing SOCs with optimization of draw solution recovery in near future.

## CHAPTER 2

### OBJECTIVES AND SCOPE

In competing with conventional water treatment processes, the high removal pressure driven membrane technologies have been a long-standing issue for membrane fouling resistance. Thus, the single-walled carbon nanotubes (SWNTs)-UF membrane and FO membrane system have been drawn on the unique characteristics for improved flux, low fouling, and high removal efficiency of SOC<sub>s</sub> and NOM in water treatment and seawater desalination. *The overall objective of this study is to evaluate UF membrane process coupled with the use of SWNTs and FO membrane system in order to understand the fate and transport of a representative selection of SOC<sub>s</sub> and NOM in water treatment and furthermore potentially apply to optimization of various pretreatment system designs for reducing the energy demands and membrane fouling in water treatment and seawater desalination process.* This research entails the study and development of next-generation FO membrane processes to enhance micropollutants removal and membrane fouling reduction, which could have extensive applicability for sustainable water purification, including seawater desalination, as well as the aspects of fouling and energy consumption of drinking water and wastewater treatment. The novelty of using both ultrafiltration and SWNTs adsorption processes is, at one level, a relatively simple approach that involves the combination of two existing technologies (i.e., filtration process and adsorption). However, little work has been performed to specifically assess the influence of membrane fouling and SWNTs on the fate and transport of a broad range

of SOCs of emerging EDC/PPCPs and NOM. Also, it is currently unknown what mechanisms in FO process can affect to the transport of SOCs. The preliminary results about CNTs adsorption with micropollutants suggest that significant enhancement is feasible. In addition, this study provides benefits of FO membrane compared to that of RO membrane and offers SOCs removal behaviors in both FO- and RO-mode experiments under various operating conditions that have not been previously recognized.

This research plan is guided by four hypothesis-driven studies. The hypotheses are drawn from both the preliminary results and relevant sources in the literature.

#### ***Study I: Determination of Adsorption and Retention of EDCs on SWNTs-UF Systems***

***Hypothesis:*** The effect of the SWNTs adsorbent on membrane fouling may be a function of the physicochemical properties of the adsorbent (e.g., size, charge, and hydrophobicity), membrane characteristics (e.g., pore size, charge, and hydrophobicity), and solution water chemistry (e.g., pH and conductivity). SWNTs will be effective at removing the majority of hydrophobic EDCs through adsorption mechanisms. Although hydrogen bonding affinity and  $\pi$ - $\pi$  EDA interactions are the key parameters used to predict the adsorption with SWNTs, this is somewhat difficult to ascertain for the emerging EDCs including BPA and EE2. Acknowledging these limitations, it is hypothesized that EDC removal will be related to the octanol–water partition coefficients ( $\log K_{ow}$ ) of neutral compounds. The retention and adsorption trends of the EDCs in SWNTs-UF were significantly influenced by the interactions between NOM-SWNTs-UF and EDCs. In addition, the adsorption of EDCs onto UF membrane decreased in the



presence of NOM due to competition for adsorption sites and pore blockage by NOM in UF.

***Study II: Evaluation of SWNTs Contributions to Remove NOM in SWNTs-UF Systems***

***Hypothesis:*** The SWNTs-UF will exhibit increased rejection trends as a result of SWNT binding sites adsorbing HA during volume concentration factor (VCF)-dependent fouling runs under various feed water hydrodynamic and solution conditions. Further, the addition of SWNTs to the UF process will not significantly exacerbate the permeate flux decline, which may be due to the stacking of SWNTs on the membrane surface, thereby maintaining a porous layer that permits the passage of water without any additional fouling resistance. In addition, while applying a resistance-in-series model, where HA fouling resistances will be mainly attributed to adsorptive fouling, and it appears likely that SWNTs-UF provides a greatly reduced membrane resistance per unit retained DOC mass, compared to UF alone. In addition, the characteristics of the fouling layer and resistances will be more dependent on HA deposition and/or HA adsorptive fouling rather than a fouling contribution from SWNTs; this is presumably because the SWNTs are too large to block the membrane pores. Overall, SWNTs-UF will be shown to be effective at improving membrane performance through neither attenuate flux nor total membrane resistances.

***Study III: Investigation of Potential Feasibility of SWNTs-UF as Pretreatment to Enhance the Removal of NOM, EDCs and Fouling Control in Seawater Environments***

**Hypothesis:** As ionic strength increases in solution, adsorbent hydrophobicity generally increases, which may contribute to as the more hydrophobic non polar compound adsorption remain. It is hypothesized that adsorption of NOM and EDCs, and exchange of ions can be attributed to the hydrophobic CNTs functionalized and will thus increase as ionic strength increases. For seawater conditions, adsorption capacity of SWNTs will increase as ionic strength increases due to the "screening effect", which reduces electrostatic repulsions of surface charge. In addition, enhancing of hydrophobic-organic adsorption onto SWNTs could be affected by "salting-out effect", which increases adsorption capacity with decreasing solubility of organic compounds in aqueous salt solutions. However, detailed mechanisms associated with NOM, EDC, and ion removal by functionalized CNTs are still unclear with seawater. The information gained during this experiment will be incorporated into a process model that can be used to predict compound transport through SWNTs-seawater environments and UF membranes.

**Study IV: Investigation of the bench-scale FO and RO mode experiments with both FO and RO membranes in order to address the retention and adsorption behaviors of the relative hydrophilicities of several SOCs.**

**Hypothesis:** Previous studies have shown that RO and nanofiltration (NF) membranes are an effective approach to retain SOCs by retention mechanisms, such as size/steric exclusion, electrostatic repulsion, and hydrophobic interactions between solutes and membranes. Until now, very few studies on FO retention mechanisms of micropollutants have been reported in the literature. As a result, the understanding fouling and retention mechanisms of FO processes are basically unsure. Nevertheless, through next-generation

bench scale FO system setting, some of the critical and fundamental questions will be answered based on the assumption of that the FO-mode is not a pressure-driven process, but its retention mechanisms are expected to follow those of conventional RO processes: (1) whether various operating conditions process in FO mechanistically alters the membrane's fouling and SOCs retention behaviors and (2) what mechanism is more dominant to remove those SOCs including solute parameters such as molecular weight (MW), hydrophobicity ( $\log K_{ow}$ ), and solubility. It shall be tested that other aspects of a FO membrane process including the effect of internal concentration polarization (ICP), reverse salt flux, and specific water flux.

## CHAPTER 3

### LITERATURE REVIEW AND BACKGROUND

#### 3.1 Mechanisms for Organic Solutes Retention through Membrane Treatment

##### 3.1.1 Hydrophobic Interaction (Adsorption)

Partitioning will be the main phenomenon in hindered diffusion of organic compounds when partitioning is dominated by the hydrophobic interaction (adsorption) mechanism between the target hydrophobic compounds and hydrophobic membrane. In the previous study [46], model and natural waters were spiked with >30 EDC/PPCP compounds at environmentally relevant concentrations and subjected to membrane treatment using a dead-end stainless steel membrane system both *tight* NF (MWCO = 200 Daltons) and UF (MWCO = 8,000 Daltons) membranes. Contact angle and streaming potential (zeta potential) measurements showed that those membranes were relatively hydrophobic and negatively charged [47]. The molecular weight of the compounds ranged from 150 to 300 Daltons except iopromide (790 Daltons). Therefore, it was expected that the NF membrane could reject greater than 90% of the compounds due to steric/size exclusions (Figure 3.1 – for spiked laboratory DI water). However, the retention was positively correlated with the hydrophobicity based on the octanol- water partition coefficient ( $\log K_{ow}$ ) of the compounds. Furthermore, the negatively charged/hydrophobic UF membrane also removed greater than 70% of the relatively high hydrophobic compounds (e.g., oxybenzone, triclosan, fluoxetine, progesterone, erythromycin, gemfibrozilmore)

due to mainly hydrophobic adsorption and fairly electrostatic exclusion even though the membrane has much larger membrane pore size than the size of the compounds. The less hydrophobic compounds (iopromide, meprobamate, sulfamethoxazole, pentoxifylline, acetaminophen, and trimethoprim) were slightly rejected by the NF membrane. Log Kow values are reported for neutral molecules. Many of the compounds are deprotonated at the ambient pH tested. For example, the pKa values are  $< 8.0$  for diazepam, diclofenac, dilantin, ibuprofen, naproxen, sulfamthoxazole, triclosan, trimethoprim, and TCEP; therefore a fraction of these compounds exist in ionic form susceptible to electrostatic interaction with membrane surfaces. The bench-scale data from similar dead-end membrane tests using a larger number of EDC/PPCP spiked compounds into Passaic Valley water (PVW; DOC = 3.5 mg/L,  $UVA_{254} = 0.09$  1/cm, SUVA = 2.6 L/mg-m, conductivity = 40.7 mS/m, pH = 6.8) [48]. Although certainly, this NF membrane exhibited a greater retention than adsorption, many compounds had high adsorption, indicating that the retention of these compounds was controlled by adsorption. In addition, the effect of DOC in PVW decrease removals of some compounds, presumably as DOC competed with EDC/PPCPs for adsorption sites, and increased removal of other compounds during UF, presumably due to DOC changing the charge of the UF membrane surface. It can be concluded that the hindered diffusion of hydrophobic organic compounds can be significantly influenced by adsorption while the electrostatic repulsion mechanism is dominant for the hindered diffusion of anions through a negatively charged membrane.

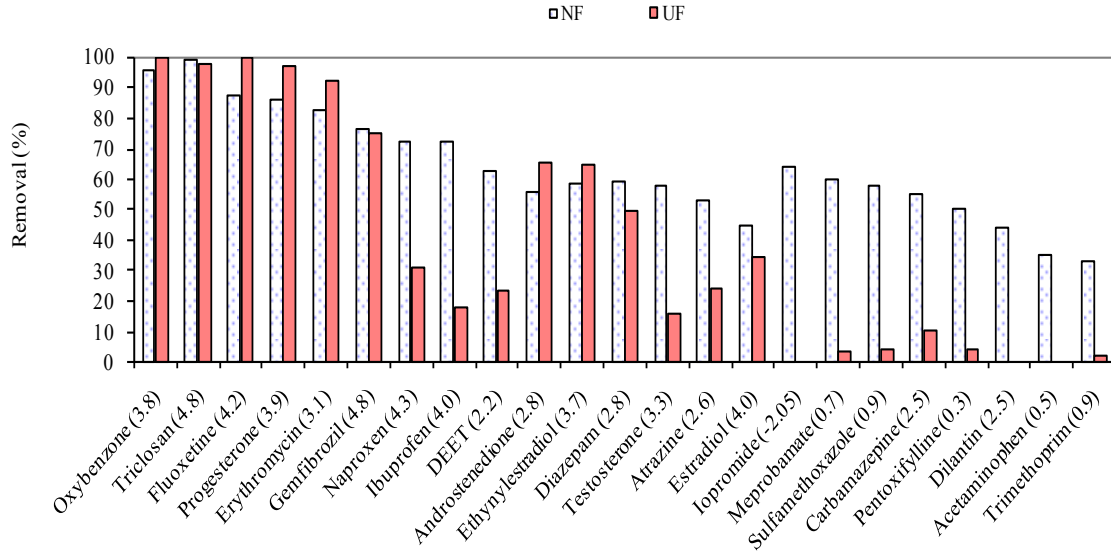


**Figure 3.1** EDC/PPCP percentage removed from spiked DI water (pH 7) in a dead-end membrane filtration system using a separate NF and UF membrane (From American Water Works Association Research Foundation - AwwaRF Project #2758).

### 3.1.2 Membrane Batch Adsorption Tests

The partition coefficient of the compounds between the membrane and the bulk solution was evaluated per unit volume of membrane (membrane area  $\times$  membrane thickness) using the following equation:

$$K = \frac{Q}{C_b} \quad (\text{Eq. 3.1})$$

where  $K$  is the partition coefficient (dimensionless),  $Q$  is the adsorption amount per unit volume of membrane ( $\mu\text{g m}^{-3}$ ), and  $C_b$  is the concentration of the compound in the bulk solution ( $\mu\text{g m}^{-3}$ ). The membrane thickness, including the top layer and microporous support layer, was 200  $\mu\text{m}$  for UF5K, as measured using an electronic digital micrometer

(733xflz-3, Starrett, Athol, MA, U.S.A.), which has a measuring limit of 1.0  $\mu\text{m}$ . A previous study highlighted that the sorption experiments of pesticides, hydrophobic compounds, and humic acid should include not only the adsorption on the membrane surface, but also the adsorption by the membrane skin layer, the membrane support layer, and/or the membrane pore [49-51]. In a previous study by the Investigators the results of bench-scale membrane testing (NF & UF) with three EDCs was presented [52]. Two estrogenic compounds (17 $\beta$ -estradiol and fluoranthene) and a more polar compound (parachlorobenzoic acid (PCBA)) were investigated. 17 $\beta$ -estradiol (E2), fluoranthene (Flu), and PCBA were applied to the membrane in the presence and absence of NOM. Both batch adsorption and dead-end stirred-cell filtration experiments indicated that adsorption is an important mechanism for transport/removal of relatively hydrophobic compounds, and is related to the log Kow values. The three compounds had different extents of adsorption in the batch experiments (Figure 3.2). Partition coefficients (H) of 0.44 to 4.86 measured in this study increased with log Kow and membrane pore size.

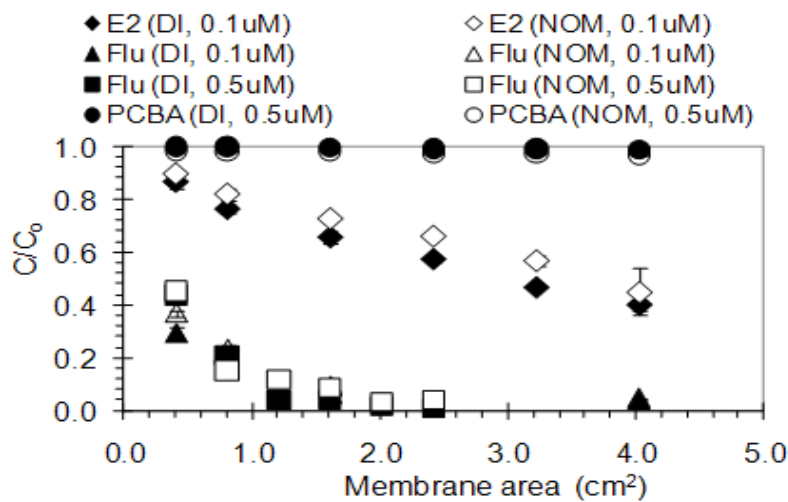


**Figure 3.2** Batch adsorption with ESNA membrane in the presence from deionized water and presence ( $4 \text{ mg L}^{-1}$ ) of NOM (contact time = 72 h) [53].

### 3.2 Dissolved Organic Matter (DOM) Transport Models

The UF membrane process is regarded as the physical barrier that rejects macromolecules larger than the membrane pore size. HA rejections cannot be explained only by size exclusion mechanisms because HAs consist of various ranges of macromolecules with different functional groups influencing NOM charge and hydrophobicity. Thus, macromolecule rejection cannot be explained on the basis of size exclusion alone. In addition, various mechanisms such as electrostatic repulsion, hydrophobic interaction, and adsorption occur simultaneously during membrane filtration. Therefore, prediction of DOM transportation in UF is more complicated. To understand the DOM transportation mechanisms in various hydrodynamic conditions, resistance-in-series model, filtration laws, and DOM mass transfer mechanisms should be considered during membrane filtration.

#### 3.2.1 Resistance in Series Model

Darcy's law can be used to describe the permeate flux ( $J_v$ ) for flow through UF membranes.

$$J_v = \frac{\Delta P}{\eta R_m} \quad (\text{Eq. 3.2})$$

where  $J_v$  is the volumetric water flux through porous membranes ( $\text{L m}^{-2} \text{h}^{-1}$ ),  $\Delta P$  is the pressure drop across the membrane (bar),  $\eta$  is the dynamic viscosity of the fluid ( $\text{kg m}^{-1} \text{s}^{-1}$ ), and  $R_m$  is the hydrodynamic resistance of the membrane. During membrane filtration, various factors contribute with different extent to the total resistance to flow; (i)



resistance as a result of adsorption or pore-blocking ( $R_a$ ), (ii) cake resistance forming a gel and/or a porous cake as the buildup and accumulation of some solute on the membrane surface ( $R_c$ ), and (iii) highly concentrated layer resistance toward mass transfer (i.e. concentration polarization) near the membrane surface ( $R_{cp}$ ). These resistances totally depend on the source water qualities as well as the type of the membrane operating conditions and module. In most encountered UF application of water and wastewater treatment, this appears that the CP is not capable of any further effect to increase resistance, once forming the cake layer near the membrane surface [54]. This implies that  $R_{cp}$  becomes the negligible resistance factor to  $J_v$ . Hence, the typical forms of the resistance-in-series model for the quantification of the filtration characteristics through a UF membrane containing a cake layer can be expressed as shown resistances in Figure 3.3 and Eq. 3.3 [55, 56];

$$J_v = \frac{\Delta P}{\eta (R_m + R_{IR} + R_R)} = \frac{\Delta P}{\eta (R_m + R_c + R_a)} \quad (\text{Eq. 3.3})$$

where  $R_{IR}$  is the irreversible fouling resistance ( $m^{-1}$ ),  $R_R$  is the reversible fouling resistance ( $m^{-1}$ ),  $R_c$  is the cake layer resistance ( $m^{-1}$ ), and  $R_a$  is the adsorptive fouling resistance. Consequently, in this study, Eq. 3.3 was used to evaluate the fractions of these different resistances ( $R_m, R_c, R_a$ ).

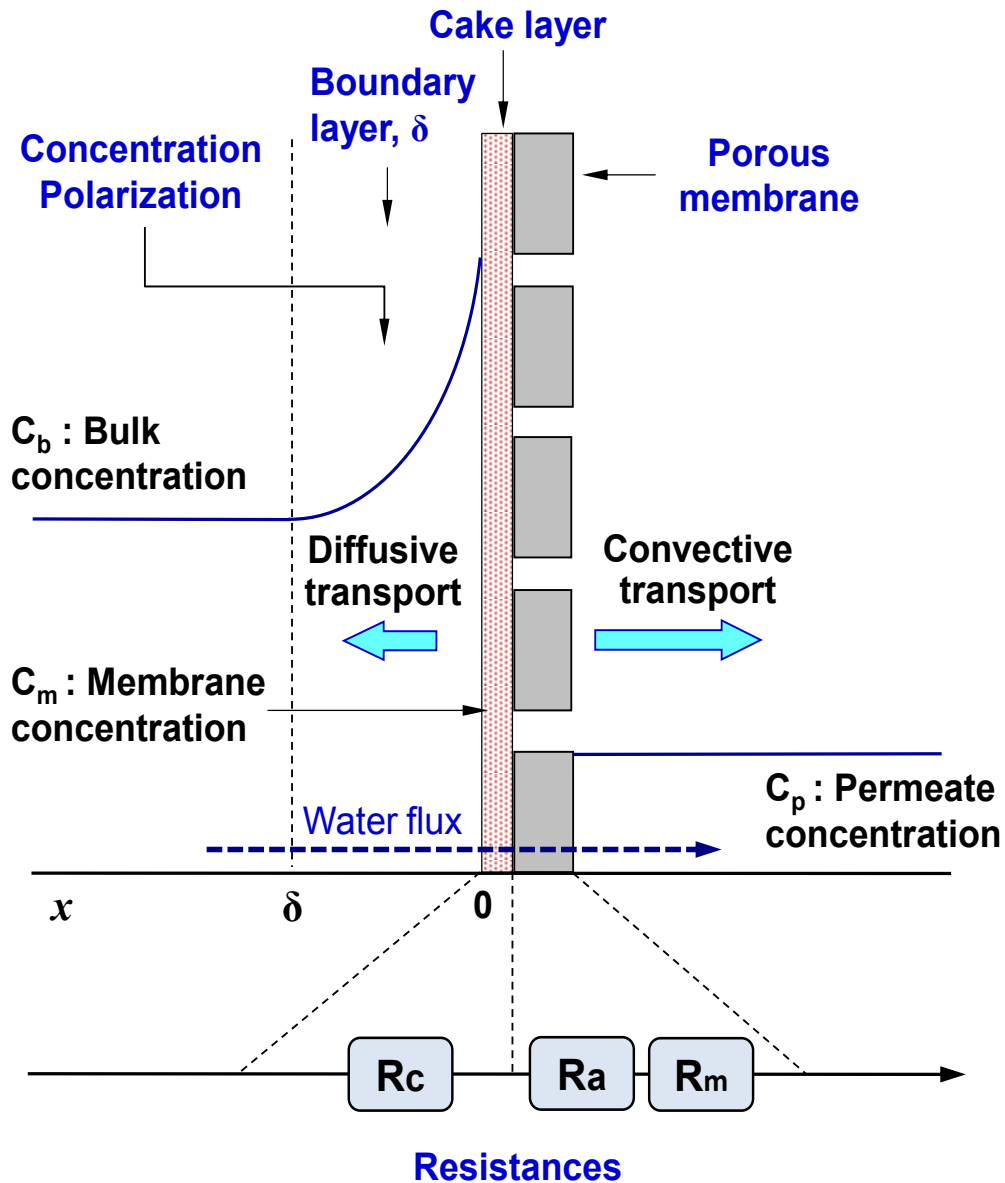


**Figure 3.3** Conceptual schematic of concentration polarization by film theory and cake layer formation; concentration profile under steady-state conditions.

### 3.2.2 Concentration Polarization by Film Theory

One of the critical factors affecting the ratio of solute rejection is the transportation mechanisms of DOM on the membrane surface. In the application of UF, the

concentration polarization (CP) is caused by increasing of the bulk solution concentration through inner membrane cell as the pressure-driven flow convectively transport solute to the upstream boundary layer. By the mass movement to meet the concentration balance between bulk concentration ( $C_b$ ) and membrane concentration ( $C_m$ ), it finally keeps the equilibrium between solvent flux ( $J_v$ ) by applied pressure and back diffusion of the solute from the membrane surface to the bulk solution. The concentration of upstream membrane is reached the steady state conditions when the permeate flux, back diffusion caused by the accumulation of solute, and convective transportation of solute are in equilibrium as shown in Figure 3.3.

This phenomenon can be expressed by the CP model derived from back diffusion of solute on membrane surface [56]. Depending on the mass-balance approach of constituent concentration ( $\partial C/\partial t$ ), convection through membrane pores ( $J_v \cdot \partial C/\partial t$ ) and back diffusion ( $D \cdot \partial^2 C/\partial^2 t$ ), CP model can be written as Eq. 3.4;

$$\frac{\partial C}{\partial t} + J_v \cdot \frac{\partial C}{\partial x} + D \cdot \frac{\partial^2 C}{\partial x^2} = 0 \quad (\text{Eq. 3.4})$$

Eq. 3.4 can be integrated between the boundary conditions  $C = C_b$  at  $x = \delta$ ,  $C = C_m$  at  $x = 0$ , under steady state conditions, yields Eq. 3.5;

$$J_v = k \cdot \ln \left( \frac{C_m - C_p}{C_b - C_p} \right) \quad (\text{Eq. 3.5})$$

where  $k$  is the mass transfer coefficient ( $\text{m s}^{-1}$ );  $k = D \delta^{-1}$  [ $D$  is the diffusion coefficient ( $\text{m}^2 \text{s}^{-1}$ ),  $\delta$  is the boundary layer ( $\text{m}^{-1}$ )].

### 3.2.3 DOM Transport Parameters Estimations

Mass transfer in UF membranes is influenced by the effects of solute CP on membrane surface and hindered partitioning and diffusion. Bulk flow comes in and convection occurred towards membrane and at the same time back diffusion occurred from the membrane surface by solvent flux flowing through membrane. Due to the CP on membrane surface, solute should come back from the area of membrane surface to bulk area. This is referred to the back diffusion phenomenon in the area of CP of membrane surface. What mechanism of mass transfer is more dominant in stirred membrane cells can be explained by the extended Nernst-Planck equation combined with a CP model. Bowen and Mohammad suggested more specifically how much contribution is influence to the mass transfer in membrane cells by the equation on the basis of the Nernst-Planck Equation [57]. And, to know the real rejection of membrane, we have to derive the diffusion coefficient of HA. Common equation about mass transfer coefficient ( $k$ ) derived from the diffusion coefficient in the stirred cell can be expressed as Eq. 3.6 [58];

$$k = 0.104 \left( \frac{D_{eff}}{r} \right) \left( \frac{\omega r^2}{\eta} \right)^{\frac{2}{3}} \left( \frac{\eta}{\rho D_{eff}} \right)^{\frac{1}{3}} \quad (\text{Eq. 3.6})$$

where  $D_{eff}$  is the effective diffusion coefficient,  $r$  the stirring radius,  $\omega$  the stirring velocity, and  $\rho$  the solution density. And applying the CP model, we can find the

concentration of membrane surface and the real rejection ( $R$ ) of membrane. Also, membrane selectivity ( $\sigma$ ) and  $k$  are influenced with interactions between HA and membrane, which merit prediction of the HA transportations with respect to various operating conditions. However, we should not apply Eq. 3.6 for  $k$  (mass transfer coefficient) because the humic substances have the wide range of molecular weight. Thus, by applying similar approach of Tandon [59], it will produce the value of the  $1/k$  and  $\sigma$  (it could be estimated with the regression analysis by plotting the  $\ln(1-R_{obs}/R_{obs})$  against  $J_v$ ). Assuming that the local equilibrium of mass transfer in membrane cells with a thermodynamic point of view, the real rejection can be estimated by Kendem-Katchalsky (K-K) equation is as follows Eq. 3.7 [60];

$$\frac{1}{R} = \frac{1}{\sigma} + \frac{P_m}{\sigma \cdot J_v} \quad (\text{Eq. 3.7})$$

where  $R$  is the real solute rejections,  $P_m$  is the solute diffusive permeability ( $\text{m s}^{-1}$ ). It was resulted in Eq. 3.8 [59, 61] by substituting Eq. 3.7 to Eq. 3.5 with  $R_{obs} = (C_b - C_p)/C_b$  and  $R = (C_m - C_p)/C_m$  for the term of  $R_{obs}$ ;

$$\ln\left(\frac{1 - R_{obs}}{R_{obs}}\right) = \ln\left(\frac{1 - \sigma}{\sigma} + \frac{P_m}{\sigma \cdot J_v}\right) + \frac{J_v}{k} \quad (\text{Eq. 3.8})$$

In this thermodynamic approach (Eq. 3.8), it is very important note that the how much contribution is influence to the mass transfer in membrane cells by defining the  $P_e = J_v \cdot (1 - \sigma) / P_m$  (denoted pore Péclet number,  $P_e$ ). Referring to the  $P_e$ , it is interesting to note

that if the  $P_e$  is much larger than 1, then the solute transport by convection will definitely control the mass transfer process. In the case of the  $P_e$  is much smaller than 1, then the diffusion mechanism is dominant to mass transfer in membrane process. Thus, the K-K equation simply expressed by neglecting that  $1/(\sigma \cdot Pe) \approx 0$  or  $J_v/k \approx 0$  and yields Eq. 3.9 and 3.10 [59, 61];

$$\ln\left(\frac{1 - R_{obs}}{R_{obs}}\right) = \ln\left(\frac{1 - \sigma}{\sigma}\right) + \frac{J_v}{k} \quad (\text{if } P_e \gg 1) \quad (\text{Eq. 3.9})$$

$$\frac{1 - R_{obs}}{R_{obs}} = \frac{1 - \sigma}{\sigma} + \frac{P_m}{\sigma \cdot J_v} \quad (\text{if } P_e \ll 1) \quad (\text{Eq. 3.10})$$

### 3.2.4 Membrane Fouling Blocking

It was developed the four conceptual filtration, known as the blocking laws under specific laboratory operating conditions, such as constant pressure and straight identically cylindrical pore diameter and length with non-Newtonian fluids [62]. Also, that was applied the successive steps of blocking mechanisms during dead-end microfiltration (MF) mode with unstirred and constant TMP [63]. These blocking laws have been used for studying fouling mechanisms involving porous membrane filtration with NOM and microorganisms. The four different blocking models are; complete blocking, standard blocking, intermediate blocking and cake filtration, which can be expressed in a mathematical form given as Eq. 3.11 [62].

$$\frac{d^2t}{dV^2} = \beta \left( \frac{dt}{dV} \right)^\varphi \quad (\text{Eq. 3.11})$$

where  $V$  in the total permeate volume (L),  $t$  is time (s), and the exponent  $\varphi$  (blocking index, unit-less) describes the filtration model;  $\varphi = 0$  for cake filtration,  $\varphi = 1$  for intermediate blocking,  $\varphi = 1.5$  for standard blocking, and  $\varphi = 2$  for complete blocking, respectively. The units of the constant  $\beta$  vary depending on  $\varphi$  of the model, which influenced by the initial flow rate and solute characteristics. Taking the logarithm of term in Eq. 3.11 can be expressed in linear form as Eq. 3.12.

$$\ln\left(\frac{d^2t}{dV^2}\right) = \varphi \ln\left(\frac{dt}{dV}\right) + \ln(\beta) \quad (\text{Eq. 3.12})$$

By plotting  $\ln(d^2t/dV^2)$  against  $\ln(dt/dV)$ , the blocking index  $\varphi$  can be determined in the filtration process. For complete blocking, it is thought that certain pore is blocked from each fouling particle, so no fluid can pass through this pore. Complete pore blocking leads to the presumption that particles are not superimposed upon one another, so the deposit is single layer. In case of standard blocking, it is assumed that the each particle arriving to the membrane, pore volume is decreased by proportional to particle depositing on the inner pore walls. Intermediate blocking is formed by the complete blocking, and increased with the single layer deposition by accumulating each other particles on membrane surface. For cake filtration, it is relevant to cake/gel layer on the membrane surface, and each particle was accumulated on the membrane surface in order to form a cake layer/gel due to the no rooms for direct accumulation on the membrane surface.

These blocking laws can be expressed with linearized form of empirical dead-end filtration [64].

### 3.2.5. Cake Filtration and Membrane Filtration Index (MFI)

An alternative way to identifying the fouling mechanism is the application of the cake-filtration model. Also, this cake filtration model widely used to assess the membrane filtration index (MFI) in UF, which originally obtained to perform fouling tests in reverse osmosis (RO) though. The MFI is defined as the slope of the straight line after an initial linear section by plotting between  $t/V$  versus  $V$  ( $t$ : filtration time,  $V$ : permeate volume). In this cake-filtration model, the solute is considered to be exerts the cake layer as retaining it on the membrane surface. The flux decline can be fully determined by a resistances-in-series model, in which the growing cake layer buildup leads to a continuous flux decline. The flux across the membrane can be defined as the flux across two resistances in series, which is comprised of the cake resistance ( $R_c$ ) and the membrane resistance ( $R_m$ ). The cake-filtration model equation including MFI in constant pressure can be given as Eq. 3.13 in the form of  $t/V$  against  $V$  [56];

$$\frac{t}{V} = \frac{\eta R_m}{A \Delta P} t + \frac{\eta \alpha C_f}{2 \Delta P} V = \frac{\eta R_m}{A \Delta P} t + \text{MFI} \cdot V \quad (\text{Eq. 3.13})$$

where  $C_f$  is the AHA concentration in the feed ( $\text{mg L}^{-1}$ ), and  $\alpha$  is defined as the specific cake resistance per unit thickness of cake layer, which is often expressed as Kozeny-Carmen relationship ( $\text{m g}^{-1}$ ). In this study, the permeate flux modeling approach, which was used by Danis et al. [35], was applied to calculate MFI as one-fourth of the  $\beta$



constant through Eq. 3.13 and Eq. 3.14 for the whole process, not only for linear slope after an initial section between  $t/V$  versus  $V$  [65].

$$J^2 = \left[ \left( \frac{\eta R_m}{\Delta P} \right)^2 + \left( \frac{2 \eta \alpha C_f}{\Delta P} \right) t \right] \quad (\text{Eq. 3.14})$$

where Eq. 3.14 can simply expressed in the form of  $J^2 = (\alpha + \beta t)$ . Curve fitting determining model constants ( $\alpha$  and  $\beta$ ) are carried out using SigmaPlot<sup>®</sup> 11.2 (Systat Software, Inc.) for non-linear regression analysis [66].

### 3.3 Application of SWNT-UF in Water Treatment

#### 3.3.1 Characterization of SWNTs

The HR-TEM image (Figure 3.4a) shows evidence of the single graphite layer, which consists of the aggregation of SWNTs. The majority of the SWNTs had few impurities; this observation also confirms the manufacturer's claim of greater than 95% SWNT purity. Figure 3.4b displays the ZP as a function of pH for the SWNTs. The values of ZPs were found to range from -21 to -67 mV. The net charge present on the SWNTs is due to the formation of an electrical double layer that was a few angstroms thick. This layer prevents the aggregation of particles, resulting in the stabilization of the suspension. As the pH increases, the negative charge on the SWNTs also increases. Charge density on the SWNTs was determined using the pH of the solution because pH affects the extent of ionization and, therefore, adsorption. The properties of the SWNTs were further studied using the radial breathing mode (RBM) of Raman spectroscopy. Figure 3.4c shows the Raman spectra of the SWNTs. The RBM transition positions for the SWNTs at low

frequencies ( $< 300 \text{ cm}^{-1}$ ) were found at  $211.2 \text{ cm}^{-1}$ . The diameter of the SWNTs calculated using the following equation [67]:

$$d = \frac{223.75}{\omega - 14} \quad (\text{Eq. 3.15})$$

where  $d$  is the estimated diameter of the SWNTs (nm), and  $\omega$  is the respective frequency ( $\text{cm}^{-1}$ ). Using this equation, the diameter of the SWNTs was calculated as 1.13 nm based on the peak observed at  $211.2 \text{ cm}^{-1}$  in the Raman spectrum, which can be justified by the data provided by the manufacturer. Figure 1c also shows a second group of Raman peaks, appearing at  $1257.7 \text{ cm}^{-1}$  and  $1579.6 \text{ cm}^{-1}$ , which correspond to the D and G bands, respectively. Minor amorphous carbon and defective structures of hollow graphite cylinders induce the D band, while the strong intensity of the G band is related to the graphitization of the SWNTs [68, 69]. The hydrodynamic diameters of SWNTs aggregates are presented in Figure 3.4d. It was observed that the SWNTs aggregate size varies to around 1327 of SWNT with an average value of 1500 nm.

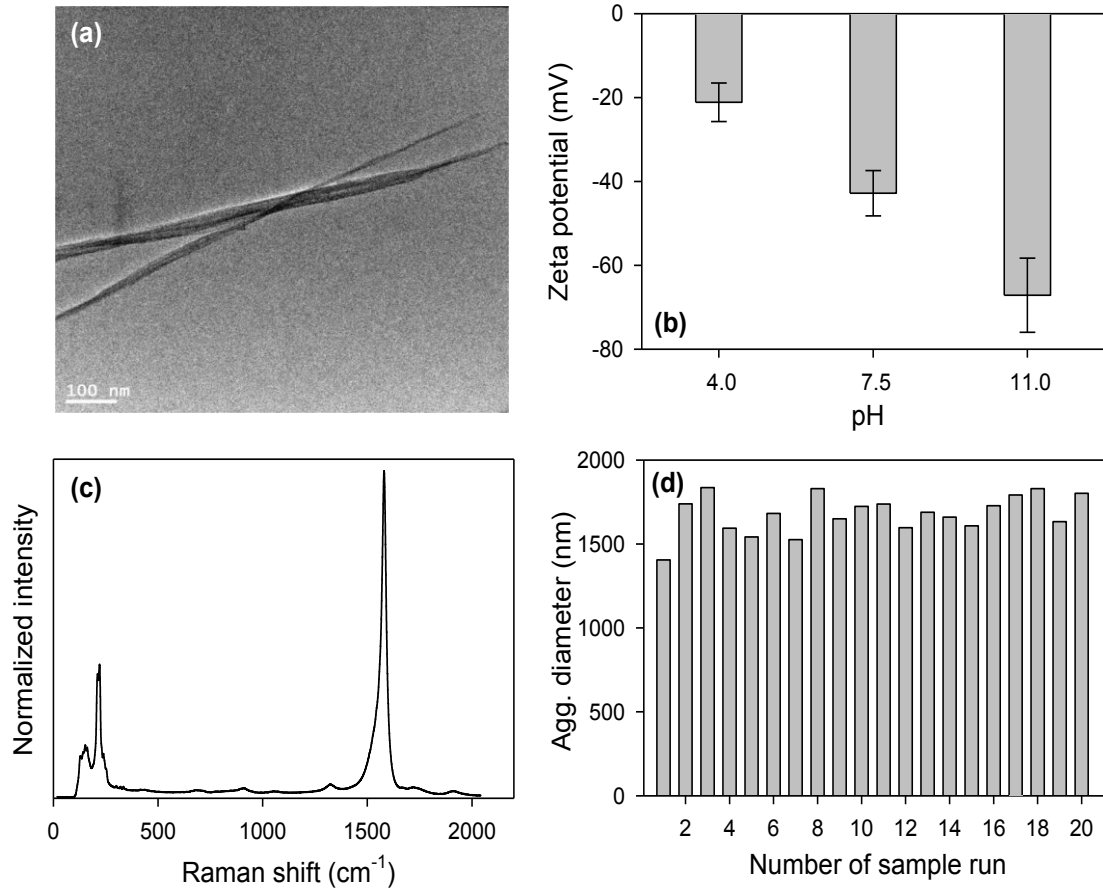


**Figure 3.4** Characterization of single walled carbon nanotubes: (a) HR-TEM images of SWNTs aggregates; (b) zeta potential at pH 4.0, 7.5, and 11.0; (c) Raman spectra; and (d) SWNTs aggregate diameter [70].

### 3.3.2 Implications and Costs

Low pressure membranes (LPMs) coupled with other pretreatment processes including coagulation/flocculation, adsorption, and oxidation have become more popular in drinking water and wastewater treatment to meet more stringent treatment goals. Practically, the results obtained in this SWNTs-UF study demonstrate the feasibility of SWNT applications to enhance membrane flux and removal efficiency in water and wastewater treatment. More specifically, in the case of removal efficiency due to adsorption using CNTs, several studies have reported that the adsorption capacities to

remove BPA, EE2, endrin, microcystins, Zinc and Cd were higher compared to those by activated carbons [71-74]. Therefore, SWNTs-UF systems can be beneficial to overcome the key disadvantages of LPMs coupled with those existing treatment processes: (i) Coagulation may exacerbate membrane fouling and be ineffective in removing the recent emerging micropollutants including EDC/PPCPs, (ii) conventional adsorbents including activated carbons may exacerbate LPM fouling, and (iii) preoxidation forms disinfection by-products and may damage membranes [23, 46]. For SWNTs-UF field systems, it is expected that SWNTs be added to the feed raw water upstream for the removal of EDC/PPCPs, heavy metals, and synthetic organic compounds as well as taste and odors. Since SWNTs are considerably larger than UF membrane pores, the transport of SWNTs through UF membrane pores unlikely occurs. However, it should still be noted that one of the current major challenges of CNTs-UF use in large scale water treatment plants is the high cost of CNTs, since PAC costs approximately \$0.5–1.8/kg while the price for CNTs is still quite high (approximately \$10/kg) [45]. However, continuous mass production of CNTs will possibly provide large quantities of CNTs with economically viable prices for large scale applications in the near future [45].

### **3.4 Forward Osmosis solution-diffusion model and cross-flow test unit**

#### **3.4.1 Solution-diffusion model in Forward Osmosis**

The basic properties of FO and RO membranes (i.e. ICP) can be characterized based upon the solution-diffusion (SD) model. Although, the SD model approach has been applied in detail in some recent FO studies, we briefly summarize some key equations for dilutive ICP. It can be shown that [28, 31]:

$$K = \left(\frac{1}{J_W}\right) \ln \left(\frac{S_P + W_P \pi_{High} - J_W}{S_P + W_P \pi_{Low}}\right) \quad (\text{Eq. 3.16})$$

$$S_P = \frac{(1 - R) W_P (\Delta P - \Delta \pi)}{R} \quad (\text{Eq. 3.17})$$

where K the solute resistance to diffusion within porous support layer,  $W_p$  the pure water permeability coefficient,  $S_p$  the salt permeability coefficient in active layer of membrane, R the salt rejection,  $\Delta P$  the hydraulic pressure difference,  $\Delta \pi$  osmotic pressure difference across the composite membrane and  $\pi_{High}$  and  $\pi_{Low}$  the osmotic pressures on draw and feed solution side, respectively. In these equations, K is related to the ratio of the solute diffusion coefficient over the membrane structural parameters (i.e., porosity, thickness and tortuosity of support layer), can be used to successfully predict to ICP based upon mass transfer of the solute from the concentration of the bulk feed and draw solution interfaces.

### 3.4.2 Forward Osmosis cross-flow test unit

In FO mode experiments, a bench-scale stainless steel plate and frame of FO cell coupled with a feed tank, a draw solution tank, a temperature controller (Fisher Scientific Isotemp Chillers, Pittsburgh, PA), variable gear pumps (Micropump, Vancouver, WA), and pressure transducer (Omega Eng., CT, USA) was employed as shown in Figure 3.5 and 3.6.

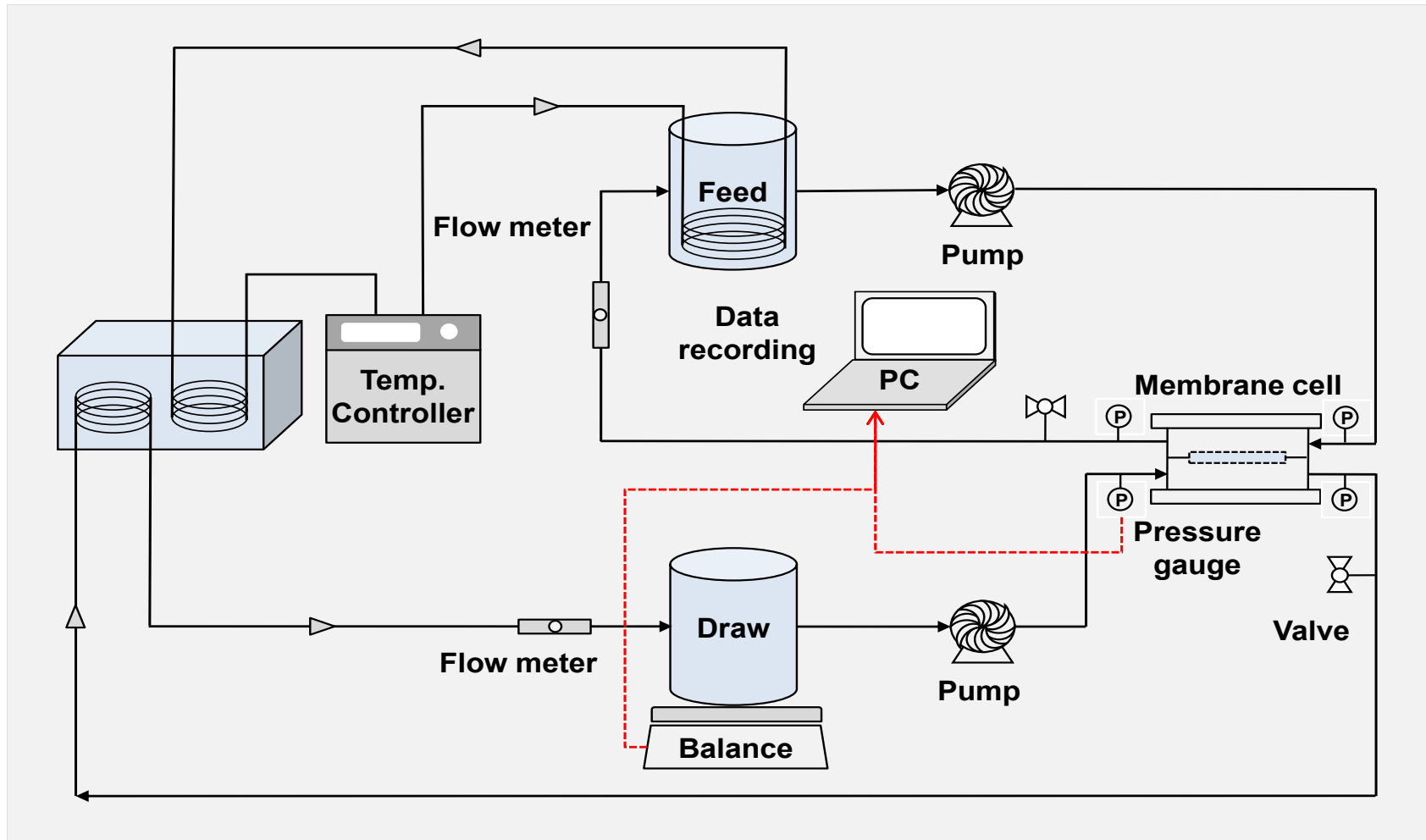
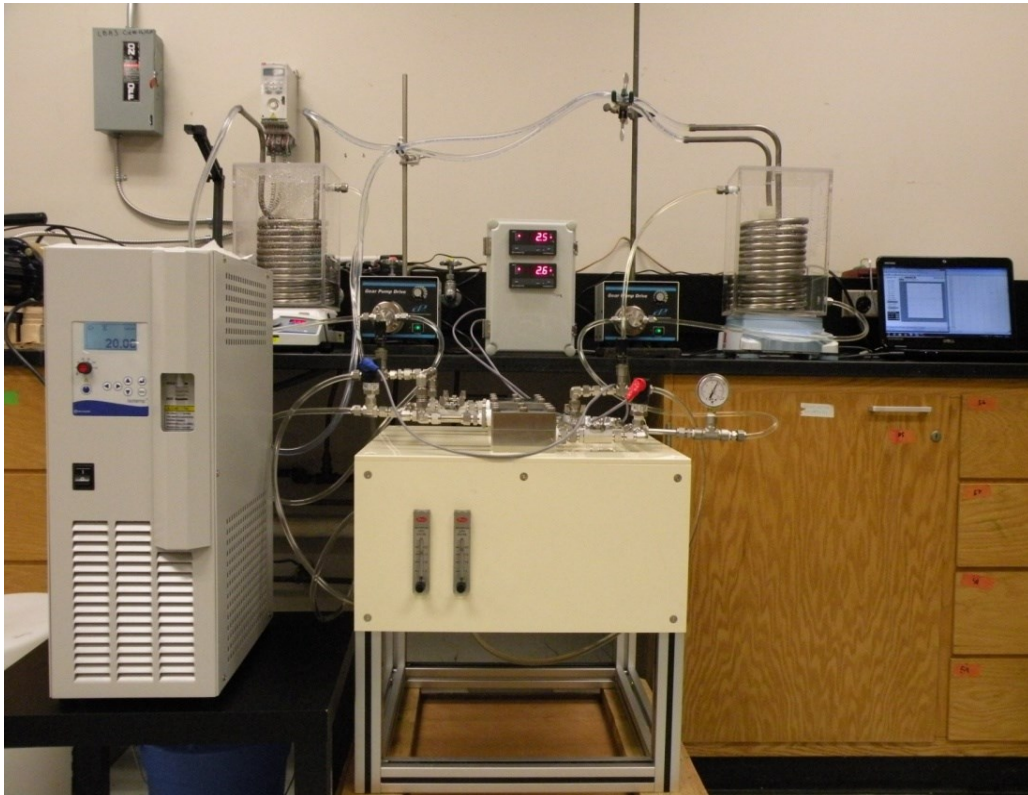


Figure 3.5 Schematic diagram of bench-scale FO membrane system.



**Figure 3.6** Bench-scale FO membrane system.

## CHAPTER 4

### REMOVAL OF BPA AND EE2 IN SWNTs-UF MEMBRANE SYSTEMS\*

\*Reprinted here with permission of publisher: Heo et al., Removal of bisphenol A and 17 $\beta$ -estradiol in single walled carbon nanotubes-ultrafiltration (SWNT-UF) membrane systems, Separation and Purification Technology 90 (2012) 39-52.

#### **Abstract**

The retention and adsorption of bisphenol A (BPA) and 17 $\beta$ -estradiol (E2) were examined using three commercially available ultrafiltration (UF) membranes. A stirred cell operated within a batch dead-end stirred cell was employed to study the solute retention and the membrane flux of solutions both in the absence and presence of natural organic matter (NOM) and single-walled carbon nanotubes (SWNTs). The batch adsorption and stirred-cell filtration experiments indicated that adsorption was an important mechanism for the retention of hydrophobic compounds and was dependent on the octanol–water partition coefficient. The results also suggested that BPA and E2 transport was influenced by NOM, which fouls the membrane through pore blockage and cake/gel formation. The NOM fouling was presumably attributed to the adsorptive hydrophobic interactions, which decreased the membrane pore size and caused the flux decline. A strong linear correlation between the retention and adsorption of BPA and E2 was observed, indicating that retention by the UF membranes was mainly due to the adsorption of BPA and E2 onto the membrane, the SWNTs, and/or the NOM. Size



exclusion is unlikely to be a key factor in the retention of E2, however, BPA retention showed a slight dependence on the membrane pore size.

*Keywords:* Bisphenol A; 17 $\beta$ -estradiol; Ultrafiltration; Single walled carbon nanotubes; Adsorption; Retention

#### **4.1 Introduction**

Endocrine-disrupting compounds (EDCs), pharmaceuticals, and personal care products (PPCPs) are an emerging group of trace contaminants detected in wastewater and water supplies worldwide [75-81]. Bisphenol A (BPA), one of the well-known EDCs, is a manufacturing intermediate in epoxy, polycarbonate, polysulfone, and certain polyester resins [82]. Previous studies have shown that BPA is released from polycarbonate flasks during autoclaving and displays estrogenic activity. Thus, the health effects of BPA are a controversial issue [83, 84]. The sex hormone, 17 $\beta$ -estradiol (E2), is the most active estrogen and also a type of EDC [85].

Numerous EDC/PPCPs including both BPA and E2 are frequently detected in water and wastewater [86-89], suggesting that conventional drinking and wastewater treatment plants cannot completely remove all EDCs and PPCPs [79]. Coagulation alone is generally ineffective for the removal of trace-level organic pollutants, but is effective for the removal of hydrophobic compounds associated with high organic carbon particulate or colloidal materials [10, 90, 91]. Various advanced technologies have been developed for the removal of EDCs and PPCPs from water and/or wastewater, such as biological degradation [92, 93], activated carbon adsorption [10, 37, 94], advanced oxidation processes [10, 95-97], and membrane filtration [48, 98].

Nanofiltration (NF) and ultrafiltration (UF) membranes are used to recover drinking water from wastewater by removing micropollutants and natural organic matter (NOM). Several studies have shown that NF and UF membranes can effectively remove EDCs and PPCPs from drinking water and wastewater [48, 50, 51, 53, 99-104]. In these studies, various removal mechanisms, including hydrophobic adsorption, size/steric exclusion, and electrostatic repulsion were investigated. The NF membrane results suggested that the rejection of uncharged trace organics by the membranes was influenced by hydrophobic adsorption and steric hindrance, whereas the rejection of polar trace organics was due to electrostatic repulsion. For the UF membrane, steric exclusion was an important factor due to NOM adsorption even when the membrane pore size was reduced [53]. The increased retention resulting from the NOM-associated cake formation was attributed partly to micropollutant-NOM partitioning and subsequent NOM retention, and partly to the fouling layer acting as a second membrane [104]. The removal of various EDCs and PPCPs is dominated by hydrophobic adsorption, which correlates with the octanol-water partitioning coefficient ( $K_{OW}$ ), on NF and UF membranes [48].

Carbon nanotubes (CNTs) are hexagonal carbon lattices that are folded to form helical-like tubular structures. These structures have drawn special attention due to their unique physicochemical properties and variety of potential applications [105, 106]. Unlike many microporous adsorbents, CNT technology could potentially support point-of-use water treatment. CNTs have a fibrous shape with a high aspect ratio, a large accessible external surface area, and well-developed mesopores [45, 106], which render CNTs superior in terms of their capacity to remove organic micropollutants and microorganisms. Further, CNTs have also shown high adsorption capacities for heavy

metals [107, 108] and organic chemicals [109-111]. Recently, researchers examined the adsorptive capacities and mechanisms of various EDCs onto single-walled carbon nanotubes (SWNTs) and/or multi-walled carbon nanotubes (MWNTs) [74, 112]. These studies have shown CNTs to be better adsorbents than the powdered activated carbon (PAC) due to higher adsorption capacities and shorter equilibrium times. However, it should be noted that despite the high adsorption capacities of CNTs in water treatment and purification, they still have several challenges including economic feasibility, health risks, and environmental impacts for practical implementations. Several researchers have reported that the release of CNTs into the environment may cause harmful impacts on ecosystem, such as damage of DNA and organs, due to their toxicity [45, 113, 114]. In particular, CNTs' health effects on human life with water are still a controversial issue [45, 115, 116]. Also, for the CNT use in drinking water treatment plants, one of the possible problems is the escape of CNTs during the membrane filtration process. In addition, CNTs are still relatively expensive for large scale applications in water treatment. However, a recent study has reported that the bulk production cost of high quality CNTs becomes quite low (approximately \$ 10/kg) [45].

The use of adsorbents such as PAC, heated aluminum oxide particles, aluminum sulfate, and ferric chloride in combination with UF and microfiltration (MF) membranes is an emerging technology for the removal of colloids, NOM, and/or organic micropollutants from drinking water [12, 117-122]. Nevertheless, these studies have shown somewhat contradictory results concerning the effect of the adsorbent on membrane fouling. Some studies revealed an enhancement of the permeate flux or longer filtration runs without chemical washing, while others showed similar flux behavior or an

exacerbated flux decline. The effect of the adsorbent on membrane fouling may be a function of the physicochemical properties of the adsorbent (e.g., size, charge, and hydrophobicity), membrane characteristics (e.g., pore size, charge, and hydrophobicity), and solution water chemistry (e.g., pH and conductivity).

The purpose of this study is to investigate the role of SWNTs in controlling membrane fouling and to discuss the potential mechanisms for the removal of EDCs using membranes. In this study, two estrogenic compounds, BPA and E2, were added to model water samples. In the presence and absence of SWNTs and NOM, the water samples were filtered using commercially available UF membranes with varied membrane properties (e.g., pore size, charge, and hydrophobicity). In addition, the feasibility of adding SWNTs to conventional water treatment plants (WTPs) for the removal of selected estrogenic compounds was investigated.

## **4.2 Materials and Methods**

### **4.2.1 UF Membranes**

Three commercially available UF membranes were evaluated in order to determine their BPA and E2 retention properties. The flat sheet membranes, made of polyethersulfone (PES), were obtained from Koch Membrane Systems Inc. (Wilmington, MA, USA) and have ionizable functional groups (e.g., carboxylic acids), as specified by the manufacturer (Table 4.1). The pure water permeabilities (PWP) were measured at 827 kPa using a stirred cell, in the range of 0.59 to 2.23 L h<sup>-1</sup> m<sup>-2</sup> kPa<sup>-1</sup>. These relatively hydrophobic UF membranes, featuring different pore sizes based on their nominal molecular weight cut-offs (MWCOs), were selected to allow for a systematic comparison of the hydrophobic

adsorption results and steric exclusion for BPA and E2 retention, but with the same material chemistry. The characteristics of the membranes are shown in Table 4.1. Each new membrane was soaked in ultrapure deionized (DI) water for at least 24 hours prior to use. During this period, the DI water was replaced several times with a new volume of pure DI water. The dissolved organic carbon (DOC) of the final rinse water was checked to ensure that it was at a negligible level.

**Table 4.1** Ultrafiltration membrane characteristics.

Membrane	MWCO (Daltons)	Zeta potential (mV)	Contact angle (°)	Applied pressure (kPa)	PWP <sup>a</sup> (L h <sup>-1</sup> m <sup>-2</sup> kPa <sup>-1</sup> )		
					Average	(min-max)	c.v. <sup>b</sup> (%)
HFK-328 (UF5K)	5k	-24.9	42	800 - 917	0.59	0.55 - 0.64	5.5
HFK-131 (UF10K)	10k	-25.3	48	565 - 607	0.88	0.85 - 0.91	4.8
HFK-141 (UF30K)	30k	-26.8	51	214 - 248	2.23	2.07 - 2.38	9.9

<sup>a</sup>PWP is pure water permeability.

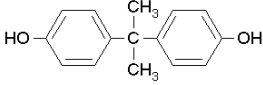
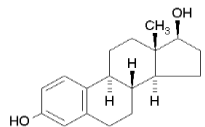
<sup>b</sup>c.v. is coefficient variance

#### 4.2.2 Solutions

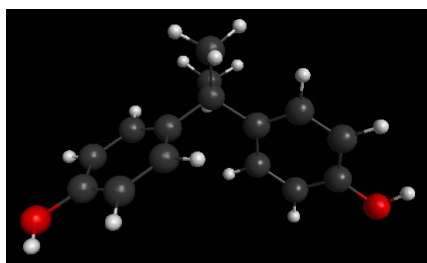
BPA, E2, and humic acid were purchased from Sigma-Aldrich (Sigma, St. Louis, MO, USA). 1 mM stock solutions of BPA and E2 in methanol were initially prepared. The stock solutions of BPA and E2 were then diluted with DI water to five calibration concentrations of 10, 50, 100, 500, and 1,000 nM. Equimolar BPA and E2 solutions of 1 μM concentration were placed in a separate beaker and the methanol was evaporated to minimize the DOC introduced into the experiments by the solvent. Table 4.2 describes the characteristics of the compounds used in this study. For batch adsorption experiments and membrane filtration measurements, BPA, which is a plasticizer, and E2, which is a natural estrogen, were introduced to the membranes in a model water sample with 1 mM

Na<sub>2</sub>HPO<sub>4</sub>. Experiments were conducted in a mixed compound solution. NOM, in the form of humic acid (8 mg L<sup>-1</sup>), was added in some experiments to represent the DOC. Stock solutions of the NOM isolate were filtered using a 0.7 μm pore size Whatman GF/F glass fiber filters prior to use. The pH was adjusted to the desired values (4, 7.5, and 11) with NaOH or HCl and the conductivity of the solutions was adjusted to 500 μS cm<sup>-1</sup> using NaCl.

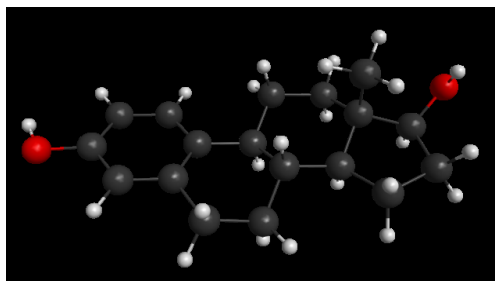
**Table 4.2** Characteristics of BPA and E2.

Common name (Abbreviation)	Use	Molecular weight (g mol <sup>-1</sup> )	LogK <sub>ow</sub>	pK <sub>a</sub>	Structure
Bisphenol A (BPA)	Plasticizer	228.1	3.3	9.6 to 10.2	
17β-estradiol (E2)	Reproductive hormone	272.3	3.9	~10.5	

3D structure model <sup>c</sup>



Bisphenol A (BPA)



17β-estradiol (E2)

<sup>c</sup> The geometry of 3D structure model is optimized at the level of Hartree-Fock (HF) using the STO-3G basis set in GAMESS (US).

### 4.2.3 Analyses

BPA ( $228 \text{ g mol}^{-1}$ ) and E2 ( $272 \text{ g mol}^{-1}$ ) concentrations were determined using high-performance liquid chromatography (HPLC). The HPLC method employed in this study was described previously [52]. In brief, the detection of BPA and E2 was accomplished using an Agilent 1200 Series (Santa Clara, CA, USA) fluorescence detector at an excitation wavelength of 280 nm and an emission wavelength of 310 nm. A Waters 5- $\mu\text{m}$  LiChrosorb® RP18 analytical column ( $4.6 \text{ mm} \times 100 \text{ mm}$ ) with a 100- $\mu\text{L}$  sample loop was used for the reverse-phase separation. The mobile-phase solvent profile was 45% DI water, acidified with 10 mM  $\text{H}_3\text{PO}_4$ , and 55% MeOH at a constant flow rate of  $1 \text{ mL min}^{-1}$  for 30 min. The elution times of BPA and E2 were 9.4 and 20.3 minutes, respectively. The detection limits were 0.88 nM ( $201 \text{ ng L}^{-1}$ ) for BPA and 0.96 nM ( $283 \text{ ng L}^{-1}$ ) for E2. While these detection limits are higher than most occurrence levels, previous work from this group has demonstrated that the patterns observed at these concentrations are representative of the mechanisms occurring at lower concentrations [53].

#### **4.2.4 Membrane Batch Adsorption Experiments and Partition Coefficient Determinations**

BPA and E2 were placed in contact with the membrane (UF5K, nominal MWCO = Daltons) in the presence and absence of NOM ( $8 \text{ mg L}^{-1}$ ) and SWNTs ( $10 \text{ mg L}^{-1}$ ) at room temperature ( $22 \pm 1 \text{ }^\circ\text{C}$ ). The SWNTs (purity > 90%) were purchased from Cheap Tubes, Inc. (Brattleboro, VT, USA) and used without further purification. The SWNTs range in length from 5 to 30  $\mu\text{m}$  and have an outer diameter of 1–2 nm, as stated by the manufacturer. The areas of the applied membranes ranged from no membrane to  $15 \text{ cm}^2$  with two different contact times (3 and 72 h). For some experiments, duplicates were

conducted to account for experimental errors and to ensure the reproducibility of the measurements. Error bars were based on the standard deviation calculated from duplicate measurements. Amber vials (40 mL) served as the reactors, and were agitated on a shaker at 13.9 rpm. Control reactors contained the solutes but no membrane or SWNTs.

**Table 4.3** Equations and constants description of fitted isotherm models.

Fitted Isotherm model	Equation	Constants description
Langmuir	$q_e = \frac{Q_0 K_L C_e}{1 + K_L C_e}$	$q_e$ is the adsorbed amount per unit membrane area ( $\mu\text{g cm}^{-2}$ ), $Q_0$ is the maximum adsorption capacity ( $\mu\text{g cm}^{-2}$ ), $K_L$ is the Langmuir adsorption constant ( $\text{L } \mu\text{g}^{-1}$ ) and $C_e$ is the equilibrium liquid-phase concentration ( $\mu\text{g L}^{-1}$ ).
	$S_L = \frac{1}{1 + K_L C_0}$	$S_L$ is the shape of the isotherms (unitless), $K_L$ is the Langmuir constant related to the energy of adsorption ( $\text{L } \mu\text{g}^{-1}$ ) and $C_0$ is the initial concentration ( $\mu\text{g L}^{-1}$ ).
Freundlich	$q_e = K_F C_e^{1/n}$	$K_F$ is the Freundlich adsorption capacity parameter ( $\mu\text{g cm}^{-2}$ ) ( $\text{L } \mu\text{g}^{-1}$ ) <sup>1/n</sup> and $1/n$ is the Freundlich adsorption intensity parameter (unitless).

The membrane and SWNTs were removed from the samples for the HPLC-fluorescence analyses. The membrane adsorption isotherm of BPA and E2 in the presence and absence of NOM and SWNTs was obtained using batch adsorption experiments in pseudo-equilibrium. The adsorbed amounts per unit membrane area were calculated through the difference between the initial and pseudo-equilibrium concentrations at 3 and 72 h. A



pseudo-equilibrium time period of 3 h was selected to determine the influence of BPA and E2 adsorption onto the membrane. Both Langmuir and Freundlich models were employed for data fitting of the membrane adsorption isotherms of BPA and E2. Table 4.3 describes the equations and constants of the fitted isotherm models used in this study.

The adsorption constant was calculated as follows:

$$K_d = \frac{q_e}{C_e} \quad (\text{Eq. 4.1})$$

where  $K_d$  is the adsorption constant ( $\text{L cm}^{-2}$ ),  $q_e$  is the adsorbed amount per unit membrane area ( $\mu\text{g cm}^{-2}$ ),  $C_e$  is the equilibrium liquid-phase concentration ( $\mu\text{g L}^{-1}$ ).

#### 4.2.5 SWNTs-UF Membrane Testing Unit

In order to study the SWNTs-UF membrane, a commercial bench-scale stainless steel dead-end stirred-cell membrane unit (HP4750, SterliTech Corp., Kent WA, USA), coupled to a SWNT reactor, was used to evaluate the flat-sheet membrane specimens for retention and flux-decline. Figure 4.1 shows the schematic diagram of the dead-end bench-scale membrane system used in the SWNTs-UF experiments.

This dead-end batch membrane system was used in previous studies to assess the removal of inorganic and organic compounds, and membrane fouling by NOM [14, 58, 123]. BPA and E2, at an initial concentration of 1  $\mu\text{M}$  each, were mixed in the pre-reactor with NOM and/or SWNTs for 2 h before the membrane experiments. Many full-scale WTPs that use PAC employ contact times of 1–5 h and apply PAC dosages of 5–50  $\text{mg L}^{-1}$  [52].

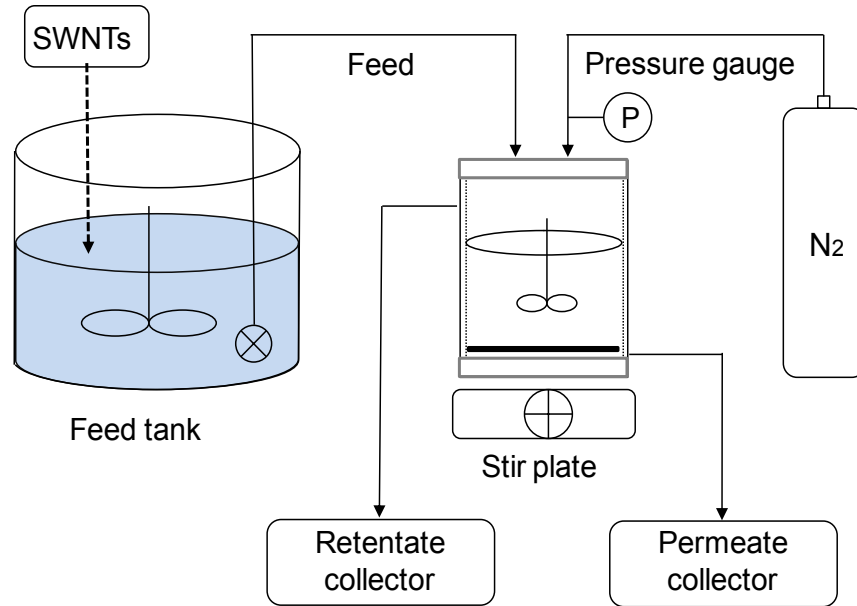


**Figure 4.1** Schematic diagram of SWNTs-UF membrane testing unit.

The cell accommodates  $14.6 \text{ cm}^2$  flat sheet specimens. A stirring speed of 300 rpm, various pH conditions, a constant initial pure water flux ( $12.3 \text{ m d}^{-1}$ ), and pressures of 800–917 kPa, 565–607 kPa, and 214–248 kPa for the UF5K, UF10K and UF30K membranes, respectively were used for the experimental conditions. A fresh membrane was used for each experiment. The membrane was pre-compacted with DI water at a pressure of 827 kPa for further stabilization prior to use. The pure water flux was then measured at a pressure of 800–917 kPa until a constant flux was obtained. At this time, the water in the stirred cell was replaced by the test solution. The stability of the membrane permeability during the experiment was checked by comparing the pure water flux before and after each experiment. Only membranes, with permeability changes less than 5% were included in the data presented here. An initial volume of 100 mL of a specific sample was passed through the membrane until 50 mL of permeate was obtained,

and the corresponding retentate was also obtained. This was repeated 10 times until a total of 500 mL of permeate was collected. The amount of the compound adsorbed onto the membrane was estimated by determining the concentration of compound in the permeate and retentate and subtracting the overall amount from the initial mass of compound in the solution.

The amount of each compound that was removed was calculated and the flux-decline monitored as a function of volume, time, and cumulative delivered or adsorbed mass [53]. Delivered mass is defined as the amount of solute delivered per unit area to the membrane, while adsorbed mass is defined as the amount of solute adsorbed per unit area onto/into the membrane within the stirred-cell, as defined by the following equations:

$$M_{del} = (C_f \times V_f) / A \quad (\text{Eq. 4.2})$$

$$M_{ads} = [(C_f \times V_f) - \{(C_p \times V_p) + (C_r \times V_r)\}] / A \quad (\text{Eq. 4.3})$$

where  $M_{del}$  is the delivered mass ( $\mu\text{g m}^{-2}$ ),  $C_f$  is the feed concentration ( $\mu\text{g m}^{-3}$ ),  $V_f$  is the feed volume ( $\text{m}^3$ ),  $A$  is the effective membrane area ( $\text{m}^2$ ),  $M_{ads}$  is the adsorbed mass ( $\mu\text{g m}^{-2}$ ),  $C_p$  is the permeate concentration ( $\mu\text{g m}^{-3}$ ),  $V_p$  is the permeate volume ( $\text{m}^3$ ),  $C_r$  is the retentate concentration ( $\mu\text{g m}^{-3}$ ), and  $V_r$  is the retentate volume ( $\text{m}^3$ ). The observed percentage of BPA and E2 retentions that were collected  $i$  times,  $R_i$  (%), was calculated using Eq. 4.4:

$$R_i(\text{feed}), \% = \frac{C_f - C_p}{C_f} \times 100 \% \quad (\text{Eq. 4.4})$$

#### 4.2.6. Characterization of Membrane and SWNTs

The membrane streaming and associated zeta potentials were determined using an established procedure [124] at pH 7.5 and a conductivity of  $500 \mu\text{S cm}^{-1}$  using an electrokinetic analyzer (ELS8000, Otsuka Electronics, Osaka, Japan). For the streaming potential measurements, membrane samples were cut to fit the measurement cell and then wetted in a NaCl solution under the same pH and conductivity conditions. The samples were stored in a refrigerator for the specified soaking time in the experimental design. Contact angles were measured using a type of sessile drop method called the water droplet method, which is based on measuring the contact angles between the water droplet and the membrane surface [124]. A goniometer (Rame-Hart Inc., Model 100, Netcong, NJ, USA) was used to measure the contact angle of the membrane. The rinsed membranes were dried in a desiccator prior to measurement. Membrane samples were cut into small pieces and mounted on a support. An approximately  $20 \mu\text{L}$  droplet of pure water was placed on the membrane specimen and the contact angle image was captured by a computer-connected camera and the angle was measured using appropriate software.

A ZetaPALS analyzer (Brookhaven Instruments Corp., Holtsville, USA) was used to measure the zeta potential (ZP) of the SWNTs. The pH values of the SWNTs solutions were adjusted from 4.0 to 11.0 by adding either 1 M NaOH or 1 M HCl solution. The ZP was calculated from the electrophoretic mobilities using the following *Smoluchowski* equation:

$$ZP = \frac{4\pi\mu\nu}{E\epsilon_o} \quad (\text{Eq. 4.5})$$

where  $\mu$  is the dynamic viscosity of water,  $v$  is the electrophoretic mobility of the migrating particle,  $E$  is the electric field at the particle, and  $\varepsilon$  and  $\varepsilon_0$  are the permittivities for water and in vacuum, respectively. The Raman spectra of powdered SWNT samples were collected using a LabRam JY Horiba Raman spectrometer fitted with a confocal microscope, a thermoelectrically cooled charge-coupled device, and a 632.82 nm He-Ne laser for excitation (New Jersey, USA). The integration time was 15 s for each scan with each spectrum representing an average of five scans. High-resolution transmission electron microscopy (HR-TEM) was performed using dry SWNT samples. The SWNT samples were dispersed in ethyl alcohol (JT Baker, ACS Grade) and sonicated for 10 min using a sonic dismembrator (S-4000, Misonix). Suspensions were placed in a bath sonicator (Bransonic-12) for 5 min before the imaging was performed. A drop of the suspension was placed on a 200-mesh copper HR-TEM grid coated with an amorphous carbon holey film (SPI Supplies) and allowed to dry for 2 min. Any excess solvent was removed using filter paper. Images were collected using a JEOL JEM-2100F 200 kV Schottky field emission gun HR-TEM (JEOL Ltd., Tokyo, Japan) with a point resolution of 0.19 nm. The aggregation diameter of the SWNTs was obtained using a dynamic light scattering (DLS) instrument (AVL/CGS-3 system, Langen, Germany) with an optimized laser power of 10 mW. Samples were prepared by dispersing SWNTs in deionized water by mild ultrasonication and depositing them on a 200 mesh nickel grid coated with formvar. Atomic force microscopy (AFM, XE-100, PSIA, Seoul, South Korea) was used to analyze the surface morphology and roughness of the membrane. Small squares of the prepared membranes were cut and glued on a glass substrate. The membrane surfaces were imaged in a scan size of  $10 \mu\text{m} \times 10 \mu\text{m}$ .

### 4.3. Results and Discussion

#### 4.3.1. Membrane Properties

The ZP and contact angle values obtained from our experiments are presented in Table 4.1. The ZPs of the UF membranes do not differ significantly, because as specified by the manufacturer each sample was made of the same material. The standard deviations reflect the relative uncertainty of the measurements. The MWCO data shows that the membranes have various pore sizes. The pure water permeabilities (PWPs) of the UF membranes follow the order of their nominal MWCOs, UF30K > UF10K > UF5K (see Table 4.1), as expected. Pure sulfonated PESs were typically considered hydrophobic materials based on previous contact angle measurements [14, 125]; these UF membranes exhibited similar contact angle values.

#### 4.3.2. Adsorption and Partition of BPA and E2 on the UF Membrane

In the retention of hydrophobic compounds on the SWNTs-UF membrane, the adsorption of the compound on the UF membrane was used to evaluate the membrane performance. Therefore, the batch membrane adsorption experiments were conducted on the UF5K membrane (0–15 cm<sup>2</sup>) both in the absence and the presence of NOM (8 mg L<sup>-1</sup>) and SWNTs (10 mg L<sup>-1</sup>) with a contact time of 3 h (equivalent to the time of the SWNTs-UF membrane experiments) for all samples. For the sample of DI water with only the membrane, a contact time of 72 h was employed to determine the adsorption capacity of UF membranes under equilibrium conditions. Generally, the degree of adsorption of both compounds increased with increasing membrane area, however BPA and E2 exhibited different adsorption trends. The adsorption of BPA was fairly constant in the presence of

NOM, with or without SWNTs, yet increased by approximately 10 to 40% in the presence of SWNTs only, depending on the membrane area, with a contact time of 3 h (Figure 4.2).

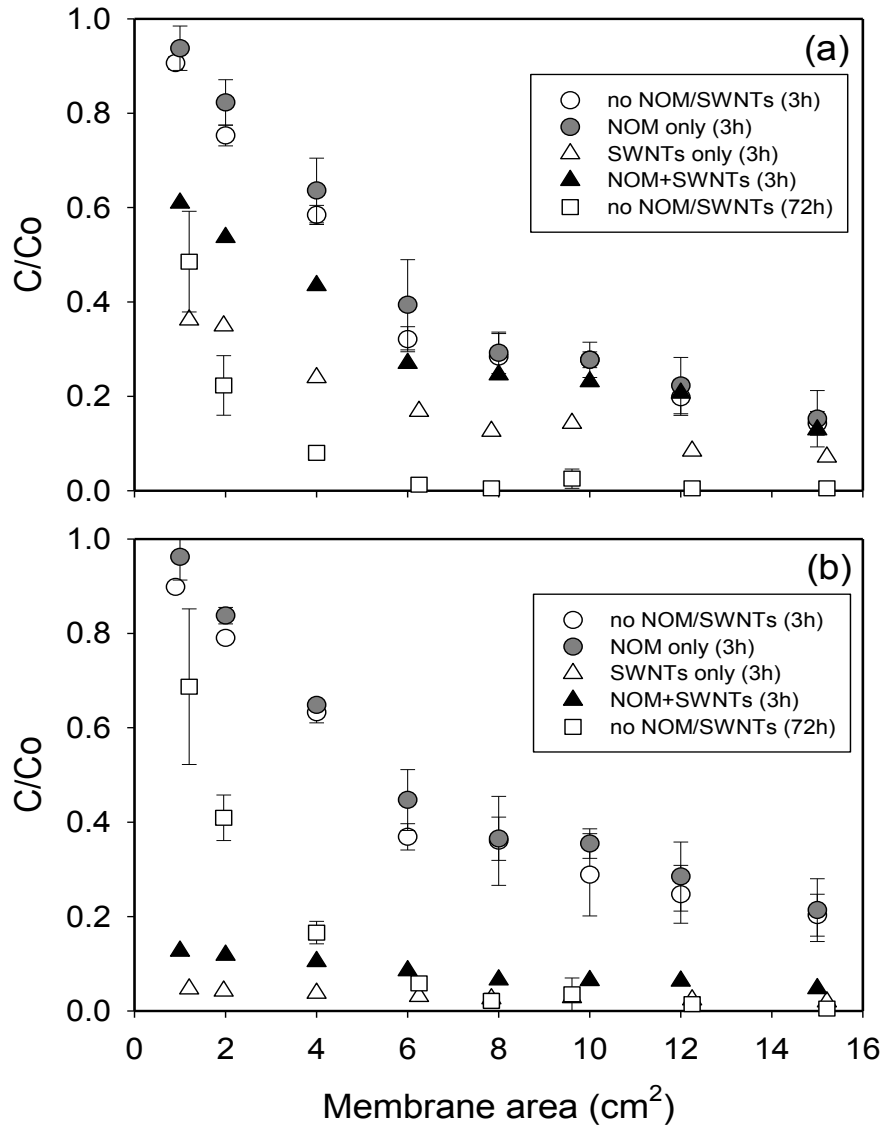


**Figure 4.2** Comparison of adsorption to UF5K membrane: (a) BPA and (b) E2 between the membrane area and the bulk solution in the absence and presence of NOM and SWNTs. Experimental conditions: DOC =  $8 \text{ mg L}^{-1}$ ; SWNTs =  $10 \text{ mg L}^{-1}$ ; conductivity =  $500 \mu\text{S cm}^{-1}$ ; contact time = 3 and 72 h; pH = 7.5.

The conditions that resulted in the highest adsorption of BPA were a contact time of 72 h in the absence of both NOM and SWNTs. However, while the presence of NOM alone did not significantly impact E2 adsorption, the addition of SWNTs resulted in a significant increase in E2 adsorption. The highest E2 adsorption was obtained in the presence of SWNTs only, achieving over 99% adsorption with a membrane area greater than 6 cm<sup>2</sup>. It was reported that the adsorption of BPA and E2 by the UF membrane decreases in the presence of NOM, presumably due to competition of the adsorption sites and pore blockage by NOM. The trend in the percentage of the compound adsorbed in the presence of SWNTs alone and in the presence of NOM and SWNTs positively correlates with the hydrophobicity (log K<sub>OW</sub>) of each compound; E2 (3.9) > BPA (3.3).

To further predict the trends and analyze the membrane adsorption systems in the presence of NOMs and SWNTs, it is essential to establish the most appropriate correlations between the batch pseudo-equilibrium data (3 h and 72 h) and adsorption isotherms. It is noted that contact times of up to 3 h and 72 h are inadequate for representing complete equilibrium. The isotherm of membrane adsorption was obtained by normalizing the adsorbed BPA and E2 capacity as a function of membrane area. This method was used because adsorption on the membrane is dominated by the surface area of membrane. The adsorbed capacity values normalized with membrane area results were well fitted to the Langmuir model and are shown in Figure 4.3 for the samples of BPA and E2 in the absence and presence of NOM and SWNTs. In addition, the fitting parameters of both the Langmuir and Freundlich model are listed in Table 4.4. In all cases, the Langmuir model yields a better linear correlation coefficient ( $R^2 > 0.93$ ) than the Freundlich model. The adsorption data was also analyzed using a partition-adsorption



model (data available on request), but fitting results were comparable to the Freundlich model.

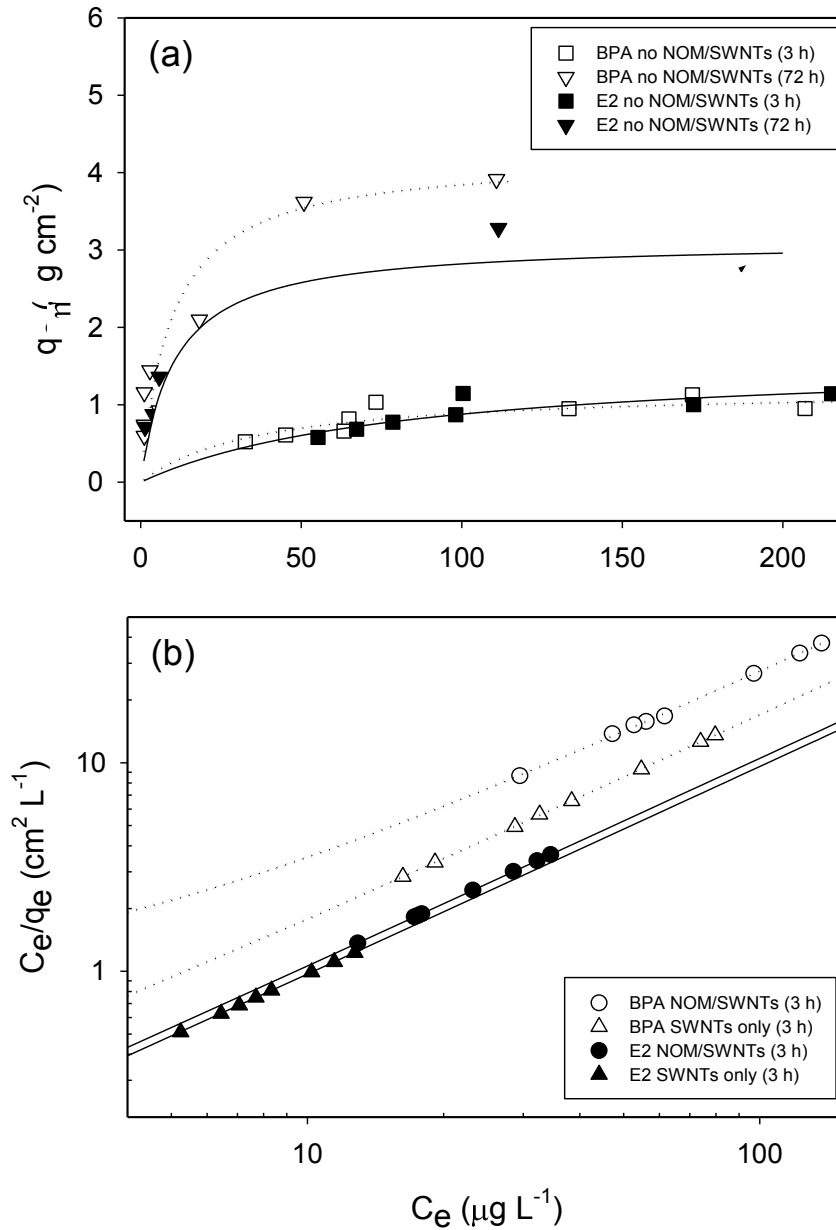


**Figure 4.3** Isotherm model data fitting for BPA and E2 onto UF membrane: (a) Langmuir isotherm fit of data in no NOM/SWNTs; (b) linear form of Langmuir isotherm data in SWNTs only and NOM/SWNTs. Experimental conditions: DOC = 8 mg L<sup>-1</sup>; SWNTs = 10 mg L<sup>-1</sup>; conductivity = 500  $\mu\text{S cm}^{-1}$ ; contact time = 3 and 72 h; pH = 7.5. The data were obtained from Figure 4.2.

The data confirms that only a monolayer accumulation of BPA and E2 occurs on the UF membrane and there is a homogeneous distribution of available sites on the membrane surface. This is based on the Langmuir equation, which assumes that the adsorbate-adsorbent interaction has a constant free-energy ( $\Delta G_{ads} = -RT \ln K_L$ ,  $R$  is the universal gas constant,  $T$  is the absolute temperature in Kelvin, and  $K_L$  is the Langmuir adsorption constant) for all sites.

**Table 4.4.** The BPA and EE2 fitted isotherm models constants on membrane in the absence and presence of SWNTs and NOM.

Fitted isotherm model	Parameters	no NOM/SWNTs (3h)		no NOM/SWNTs (72h)	
		BPA	E2	BPA	E2
Langmuir	$Q_o$ ( $\mu\text{g cm}^{-2}$ )	1.22	1.62	4.21	3.11
	$K_L$ ( $\text{L } \mu\text{g}^{-1}$ )	0.027	0.012	0.105	0.097
	$S_L$	0.141	0.235	0.040	0.037
	$R^2$	0.94	0.93	0.97	0.99
Freundlich	$K_F$ ( $\mu\text{g cm}^{-2}$ ) ( $\text{L } \mu\text{g}^{-1}$ ) <sup>1/n</sup>	0.166	0.115	0.755	0.644
	$1/n$	0.359	0.436	0.357	0.315
	$R^2$	0.72	0.78	0.85	0.93
Fitted isotherm model	Parameters	NOM/SWNTs (3h)		SWNTs only (3h)	
		BPA	E2	BPA	E2
Langmuir	$Q_o$ ( $\mu\text{g cm}^{-2}$ )	3.75	9.53	5.91	10.43
	$K_L$ ( $\text{L } \mu\text{g}^{-1}$ )	0.311	8.966	1.953	9.887
	$S_L$	0.014	0.0004	0.002	0.0004
	$R^2$	0.99	1.00	0.99	1.00
Freundlich	$K_F$ ( $\mu\text{g cm}^{-2}$ ) ( $\text{L } \mu\text{g}^{-1}$ ) <sup>1/n</sup>	2.886	9.343	5.490	10.074
	$1/n$	0.050	0.005	0.016	0.010
	$R^2$	0.69	0.73	0.75	0.83

$R^2$  is the square of the correlation coefficient between the experimental and modeled data.

The separation factor in the Langmuir model also results in a range of  $0 < S_L < 1$  (Table 4.4), indicating favorable adsorption of BPA and E2 is occurring at the membrane

surface. As listed in Table 4.4, the Langmuir model fitted membrane adsorption capacity with no NOM/SWNTs,  $Q_o$ , substantially increased from 1.22  $\mu\text{g cm}^{-2}$  (BPA) and 1.62  $\mu\text{g cm}^{-2}$  (E2) to 4.21  $\mu\text{g cm}^{-2}$  (BPA) and 3.11  $\mu\text{g cm}^{-2}$  (E2) with an increase in the large negative free energy interaction ( $\Delta G_{ads} = -RT \ln K_L$ ). The studies indicate that up to 3 h contact times provides available adsorption sites at the membrane surface, it is inadequate to reach equilibrium from a thermodynamic point of view.

A higher adsorption capacity was obtained in the presence of SWNTs, which indicates that adsorption by the SWNTs is dominant in SWNTs-UF systems (the more specific adsorption mechanisms of SWNTs with BPA and E2 are discussed in the following section). The maximum adsorption capacity values for the Langmuir model and adsorption capacity values for the Freundlich model in the presence of SWNTs and/or NOM with a contact time of 3 h ranked in the following order: E2 (SWNTs only) > E2 (NOM/SWNTs) > BPA (SWNTs only) > BPA (NOM/SWNTs). The adsorption trends are proportional to the average adsorption constant ( $K_d = q_e/C_e$ ) as shown in Figure 4.4. The results indicate that in the presence of SWNTs, the adsorption of E2 onto the SWNTs is more favorable than BPA, while the adsorption of E2 onto UF membrane is less favorable than BPA without NOM/SWNTs. However, the adsorption of BPA and E2 were divergent under membrane only and membrane with NOM conditions, although the adsorption of the more hydrophobic E2 should be greater than BPA based on their log  $K_{ow}$  values.

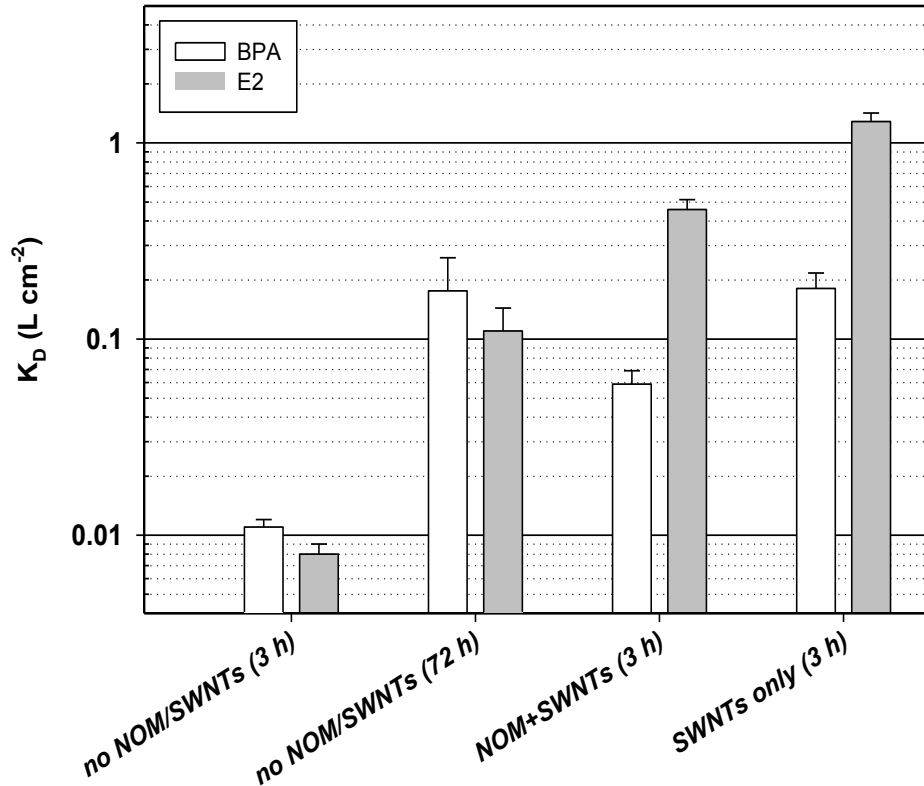


**Figure 4.4** The average adsorption coefficients of BPA and E2 onto UF membrane in the absence and presence of NOM and SWNTs. Experimental conditions: DOC = 8 mg L<sup>-1</sup>; SWNTs = 10 mg L<sup>-1</sup>; conductivity = 500  $\mu$ S cm<sup>-1</sup>; contact time = 3 and 72 h; pH = 7.5.

These results suggest that hydrophobic interactions alone cannot completely explain the interactions among organic chemicals, membranes, NOMs, and SWNTs. The results can, however, be explained by combining the general observations of previous studies and the following phenomena. First, the PES membranes having oxygen in the form of sulphonyl groups (-SO<sub>2</sub>) adsorbed higher BPA than E2, suggesting that multiple mechanisms may occur simultaneously, mainly due to hydrophobic interactions and supramolecular interactions such as hydrogen bonding and  $\pi$ - $\pi$  stacking (e.g., functional groups on the membrane, such as hydroxyl (-OH) and carboxyl (-COOH) groups, induce hydrogen bonding, which may cause the adsorption of EDCs onto the membrane) [126]. Second, in the case of E2 retention increased compared to BPA for the NOM/SWNTs,

indicating that more hydrophobic compounds are preferentially removed using membrane and SWNTs adsorption in the presence of NOM and SWNTs, which positively correlates with  $\log K_{ow}$  [53]. Third, during UF filtration, NOM competes for adsorption sites, resulting in a lower adsorption of EDCs in NOM-containing water, while there is the possibility of micropollutants partitioning onto NOM in solution followed by the retention of NOM [127, 128]. Finally, a high adsorptive capacity of EDCs can be achieved by SWNTs with hydrophobic interactions in evenly distributed hydrophobic sites and  $\pi$ - $\pi$  electron donor-acceptor (EDA) interactions [105].

The partition coefficient ( $\log K$ ) for the compounds is plotted as a function of the membrane area, shown in Figure 4.5. Although some variation was observed in the partition coefficient values due to the relatively small addition of membrane (1–6 cm<sup>2</sup>), the partition coefficient values were consistent for membrane areas in the range of 10–15 cm<sup>2</sup>. Partition coefficient values varied for BPA and E2 depending on the absence or presence of NOM and SWNTs, which was expected. Based on the average  $\log K$  values obtained for 1-15 cm<sup>2</sup> membranes, the partitioning coefficients were lower in the presence of NOM (2.24 for BPA and 2.18 for E2) than without NOM (2.26 for BPA and 2.23 for E2). This observation suggests that E2 and NOM compete for the membrane adsorption sites. A high partition coefficient was calculated with only the membrane and a contact time of 72 h (2.52 for BPA and 2.47 for E2). The partition coefficients increased further in the presence of SWNTs because of the adsorption of BPA and E2 onto the SWNT surface.

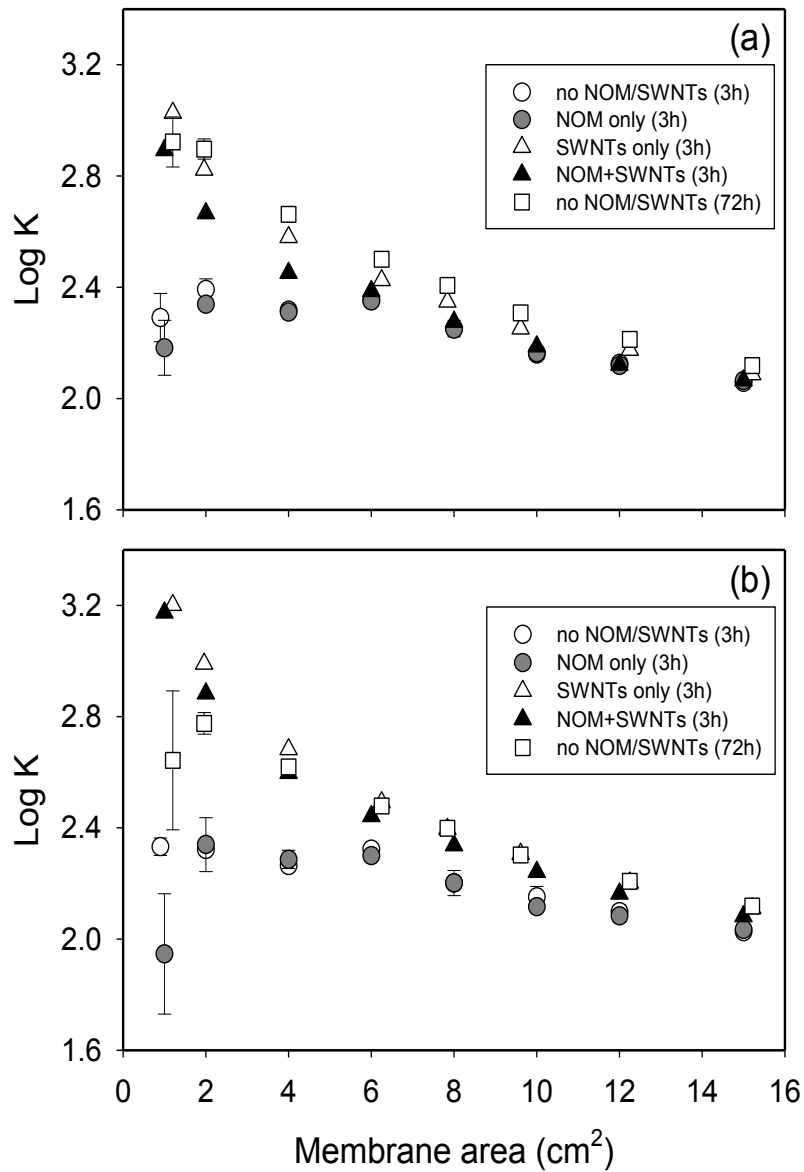


**Figure 4.5** Comparison of partition coefficient of (a) BPA and (b) E2 between the membrane and the bulk solution in the absence and presence of NOM and SWNTs. Operating conditions: DOC = 8 mg L<sup>-1</sup>; SWNTs = 10 mg L<sup>-1</sup>; conductivity = 500  $\mu$ S cm<sup>-1</sup>; contact time = 3 and 72 h; pH = 7.5.

The partition coefficients for the membrane in the presence of SWNTs and/or NOM with a contact time of 3 h ranked in the following order, from highest to lowest: DI and

SWNTs (2.47 (BPA) and 2.56 (E2)) > NOM and SWNTs (2.37 (BPA) and 2.49 (E2)) > DI (membrane only, 2.26 (BPA) and 2.23 (E2)) > NOM (2.24 (BPA) and 2.18 (E2)).

#### **4.3.3 Adsorption and Retention of BPA and E2 by SWNTs-UF**

For the dead-end stirred-cell experiments, simple plots of solute retention and flux-decline versus volume or time have limited scope in the evaluation of organic compound interactions, with NOM and/or SWNTs. This is a result of the variability of retention and flux decline depending on the delivered and adsorbed masses of solute, which are significantly influenced by the physicochemical conditions of the membrane and the solute at the membrane interface. Therefore, the delivered and adsorbed mass of the BPA and E2 per unit membrane area were introduced as more realistic parameters to obtain a reasonable comparison of removal and flux-decline trends. In previous studies, adsorbed mass was used to distinguish between adsorption on the NF and UF membranes and other interaction parameters (e.g., dipole moment, dielectric constant, water flux, molecular weight (MW), and/or octanol-water partition coefficient) [53, 129].

Mass balances of BPA and E2 in the permeate and retentate were conducted over time at various pH levels (4, 7.5 and 11) in experiments with the UF5K membrane. Any significant mass that was unaccounted for was assumed to be adsorbed onto the membrane, SWNTs, and/or NOM, since there was no loss of mass in the control experiments (without SWNTs and NOM). The percentage of BPA and E2 adsorption ranged from 7.3 to 95% depending upon solution pH and the absence or presence of NOM and SWNTs. Generally, while the adsorbed mass increased as the delivered mass of either BPA or E2 was increased, a greater adsorption of E2 than BPA was observed.

This is presumably a result of more hydrophobic interactions due to the larger partitioning coefficient value of E2. The amount of BPA and E2 adsorbed on the membranes, SWNTs, and/or NOM was quantified and plotted as delivered mass versus adsorbed mass, as shown in Figure 4.6a.

The NOM considerably reduced the adsorption of both BPA and E2 when using the UF5K membrane, while their adsorption was significant in the presence of SWNTs only and SWNTs and NOM. The retention and adsorption trends of the EDCs in SWNTs-UF were significantly influenced by the interactions between NOM-SWNTs-UF and EDCs. As previously studied, a decrease in EDC adsorption is expected in the presence of NOM because both direct competition and NOM fractionation occur between the EDCs and the NOM for available interstitial channel sites of the SWNTs for adsorption [111, 130]. In addition, the adsorption of EDCs onto UF membrane decreased in the presence of NOM due to competition for adsorption sites and pore blockage by NOM in UF [53, 104].

The results indicate that in the presence of SWNTs, the adsorption of BPA and E2 onto the SWNTs was dominant, with less adsorption occurring at the membrane surface and pores, as shown in Figure 4.6. The adsorption percentages of BPA and E2 as a result of filtration through the UF5K at pH of 7.5 were 27.8 and 18.4% (DI), 20.2 and 13.4% (NOM), 78.4 and 94.9% (SWNTs), and 60.4 and 79.7% (NOM and SWNTs), respectively. Although the literature suggests that the presence of NOM could enhance the adsorption of BPA and E2 due to NOM-partitioning of the micropollutants [104], our results have shown that competition for adsorption sites and pore blockage by NOM dominate. This results in an overall decrease in BPA and E2 adsorption on the membrane and SWNTs in the presence of NOM.



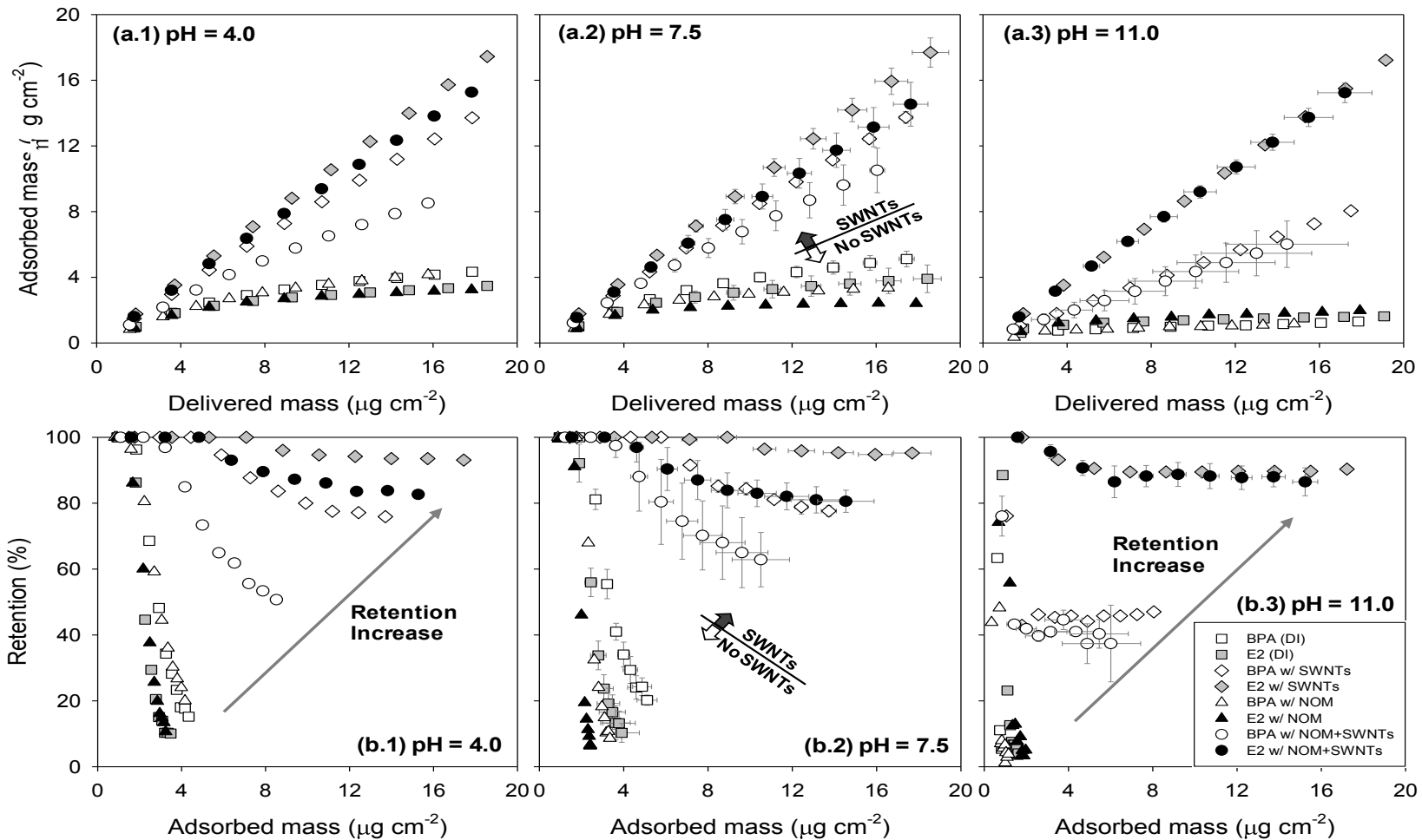


**Figure 4.6** Comparison of (a) delivered and adsorbed mass accumulated and (b) adsorbed mass and retention for BPA and E2 in the UF5K filtration in the absence and presence of NOM and SWNTs. Operating conditions:  $\Delta P = 827$  kPa (120 psi); stirring speed = 300 rpm; recovery = 50%; DOC = 8 mg L<sup>-1</sup>; SWNTs = 10 mg L<sup>-1</sup>; conductivity = 500  $\mu\text{S cm}^{-1}$ ; pre-contact time with SWNTs = 2 h.

Previous studies have reported that the adsorption and retention of hormones (estradiol and estrone) by NF membranes were strongly influenced by pH [103, 131]. The pH dependence of BPA and E2 adsorption and retention by the UF membranes are compared in Figure 4.6. The amounts of retained and adsorbed BPA and E2 showed similar decreasing trends at pH 4 and 7.5. However at pH 11, excluding the results pertaining to E2 with both NOM and SWNTs, both retention and adsorption were observed. Although the results varied significantly depending on the presence of NOM and SWNTs, the effect of varying the pH was attributed to the different log  $K_{OW}$  values of each compound.

The overall decrease in adsorption may be a result of the ionization of BPA and E2 caused by the increase in pH, which reduced hydrophobic interactions with the SWNTs. At pH levels greater than  $\sim 10.5$ , the anionic BPA and E2 species dominates, whereas at pH levels  $< 10.5$ , the neutrally charged BPA and E2 species are the majority. At higher pH, the adsorption was expected to be lower due to charge repulsion between the negatively charged BPA or E2 molecules and the increasingly negatively charged membrane and SWNTs. Another mechanism for BPA and E2 adsorption may be aromatic, specifically  $\pi$ - $\pi$  EDA interactions [105]. If the  $\pi$ - $\pi$  EDA interactions contribute to the adsorption of BPA and E2, decreased adsorption should occur when the pH is greater than the  $pK_a$ , because the chemicals and adsorbent experience increased electrostatic repulsion. In addition, numerous studies have shown that solute retention by the NF and UF membranes is governed by steric exclusion and/or adsorption for associated organic compounds [53, 132, 133] and by electrostatic exclusion for dissociated compounds [103, 131, 134].

The BPA and E2 retention percentage by the UF5K membrane in the absence and presence of NOM and SWNTs at pH 7.5, with a cumulative permeate volume of 500 mL, were 20.2 and 10.3 (DI), 8.6 and 6.3 (NOM), 77.6 and 95.2 (SWNTs), and 62.8 and 80.6 (NOM and SWNTs), respectively (Figure 4.6b). A strong linear correlation between the retention and adsorption of BPA and E2 was obtained, which indicates that retention by the UF membranes is primarily due to adsorption (Figure 4.7).

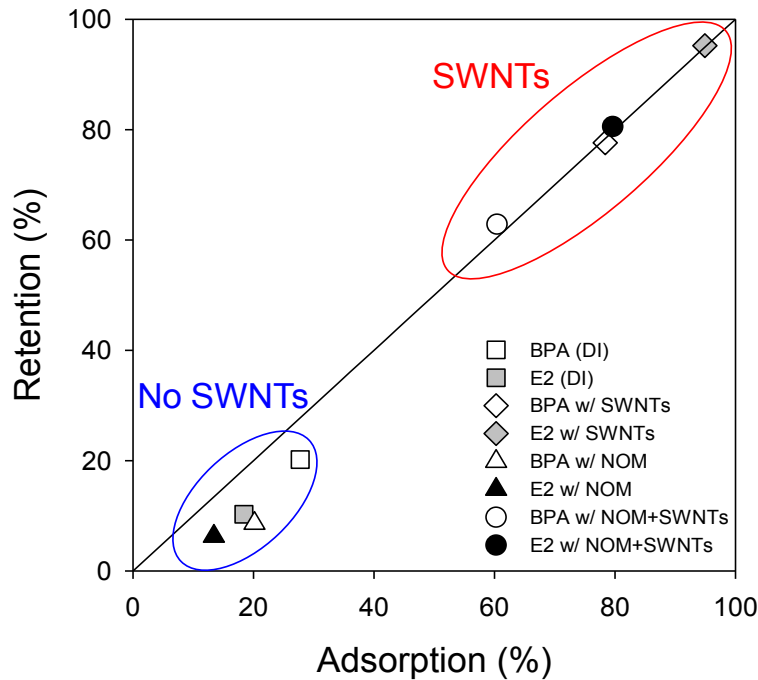


**Figure 4.7** Comparison of retention and adsorption for BPA and E2 in the UF5K end of filtration (cumulative permeate volume of 500 mL) in the absence and presence of NOM and SWNTs. Operating conditions:  $\Delta P = 827$  kPa (120 psi); stirring speed = 300 rpm; recovery = 50%; DOC =  $8 \text{ mg L}^{-1}$ ; SWNTs =  $10 \text{ mg L}^{-1}$ ; conductivity =  $500 \mu\text{S cm}^{-1}$ ; pre-contact time with SWNTs = 2 h.

Other retention mechanisms, such as size-exclusion, are unlikely due to the large pore size of the UF5K membrane ( $\text{MWCO} = 5,000 \text{ g mol}^{-1}$ ) compared to the molecular weights of BPA ( $228 \text{ g mol}^{-1}$ ) and E2 ( $272 \text{ g mol}^{-1}$ ). The larger retention and adsorption of E2 compared to BPA was explained by their relative  $\log K_{\text{OW}}$  values, which suggest a

greater affinity of the membrane for E2, NOM, and SWNTs than for BPA. Despite the fact that similar relationships between retention and adsorption were observed at pH 4 and 7.5, the retention and adsorption decreased significantly at pH 11 for all experiments (with the exception of E2 due to electrostatic repulsion, as described previously). At pH 11, a slight increase (6%) in the retention of E2 was observed in the presence of SWNTs and NOM, while a decrease of 10% occurred without the NOM present, as compared to the results at pH 4 and 7.5. For BPA, the retention was reduced by 30% both in the presence of SWNTs and NOM and with SWNTs alone, upon increasing the pH to 11. These results indicate that the retention of the more hydrophobic E2 was less influenced by pH than that of BPA. A previous study demonstrated that the retention of E2 by the NF membrane increased from 15% in DI water to 70% in the presence of NOM, suggesting that steric exclusion became dominant due to the decreasing membrane pore size caused by the adsorption of the NOM on the membrane surface [53]. However, the results obtained in this study suggest that steric exclusion is minimal with the UF membrane.

#### **4.3.4. Effect of NOM and SWNTs on Fouling**

Flux decline trends for solutions in synthetic water containing BPA and E2 in combination with SWNTs and both SWNTs and NOM were observed with the accumulated adsorbed mass of the micropollutants at the end of membrane filtration (1,000 mL), as summarized in Table 4.5.

**Table 4.5** Ultrafiltration flux declines with the accumulated adsorbed mass of the micropollutants by UF and SWNTs-UF processes in the absence and presence of NOM.

Process	Operating conditions		$J J_o^{-1}$ (%) <sup>d</sup>		Accumulated adsorbed mass (g cm <sup>-2</sup> )			
	pH	Applied pressure (kPa)			BPA		E2	
			NOM free	NOM 8 mg	NOM free	NOM 8 mg	NOM free	NOM 8 mg
<b>UF</b>								
UF5k	4	827	95.7 ± 0.7	20.2 ± 0.4	4.2 ± 0.13	4.1 ± 0.12	3.4 ± 0.10	3.2 ± 0.06
UF5k	7.5	827	96.0 ± 0.4	75.2 ± 0.8	5.0 ± 0.17	3.3 ± 0.05	3.8 ± 0.09	2.4 ± 0.01
UF5k	11	827	92.2 ± 0.7	76.7 ± 0.3	1.3 ± 0.06	1.1 ± 0.05	1.6 ± 0.02	1.9 ± 0.07
UF10k	7.5	586	-	74.0 ± 0.2	-	3.8 ± 0.08	-	2.6 ± 0.01
UF30k	7.5	228	-	67.4 ± 0.1	-	2.3 ± 0.03	-	1.5 ± 0.03
<b>SWNTs-UF</b>								
UF5k	4	827	97.2 ± 0.8	28.2 ± 0.7	13.1 ± 0.91	8.2 ± 0.46	16.6 ± 1.22	14.5 ± 1.03
UF5k	7.5	827	96.7 ± 0.1	78.6 ± 0.3	13.1 ± 0.92	10.1 ± 0.63	16.8 ± 1.24	13.8 ± 0.99
UF5k	7.5	414	-	87.6 ± 0.2	-	7.8 ± 0.43	-	14.6 ± 1.05
UF5k	7.5	137	-	90.1 ± 0.5	-	7.6 ± 0.42	-	14.6 ± 1.07
UF5k	11	827	92.4 ± 0.0	78.6 ± 0.5	7.7 ± 0.56	5.7 ± 0.39	16.4 ± 1.22	14.9 ± 1.10
UF10k	7.5	586	-	79.0 ± 0.7	-	8.4 ± 0.46	-	16.9 ± 1.24
UF30k	7.5	228	-	70.4 ± 0.6	-	6.7 ± 0.38	-	14.0 ± 1.03

<sup>d</sup>  $J J_o^{-1}$  (%) is the normalized flux value of the end of each membrane filtration (1,000 mL).

The numbers in (±) are standard deviation.

As a general observation, the accumulated adsorbed mass of the micropollutants significantly increased in the presence of SWNTs, while it decreased in the presence of NOM over the same period. In addition, neither membrane exhibited significant flux decline in the absence of NOM and in the presence of SWNTs under different pH and applied pressure conditions. This is presumably because at an initial concentration of 1  $\mu\text{M}$ , concentration polarization associated with each compound (in the absence of NOM) does not significantly reduce the membrane flux, but is completely adsorbed onto either membrane surface.

In contrast to the NOM free data, a flux decline of 13 to 80% occurred in the presence of NOM and both NOM and SWNTs because of considerable concentration polarization associated with NOM adsorption at the membrane surface. Conversely, increased flux trends of 2-8% were observed in the presence of SWNTs, indicating that SWNTs are not potential foulants. The effect of SWNTs on fouling at  $10 \text{ mg L}^{-1}$  was insignificant, since the SWNT particles are somewhat too large to block membrane pores. Thus, the SWNTs particles can be stacked on the membrane surface to readily allow the transport of water [135]. Notably, there was an approximately 80% flux decline for the membrane in the presence of NOM alone, and an approximately 72% flux decline in the presence of both SWNTs and NOM for BPA and E2 at pH 4. This is more likely due to an increase in NOM adsorption to the membrane at the low pH. The Aldrich HA NOM filtration was characterized by an initially strong flux decline, followed by a weaker decline in a later filtration stage, indicating that fouling occurs by initial pore blockage and additional cake/gel formation at a later stage [136, 137]. Adsorption of the NOM molecules, which have hydroxyl and carboxyl functional groups, increases at low pH

when the charge on the membrane becomes less negative [14, 138]. Numerous studies have shown that NOM fouling is a major cause of membrane filtration flux decline [19, 125, 139-142]. From the previous reports, it was assumed that the high aromatic content of the feed NOM in the water samples and the hydrophobicity of the UF membrane possibly combined to cause a greater driving force for membrane surface and pore mass adsorption. It was also proposed that humic acid could cause irreversible fouling specifically in the case of interactions between humic acid and hydrophobic membranes.

The complete blocking, standard blocking, intermediate blocking and cake filtration fouling mechanisms (described in Table 4.6) were identified using an approach previously reported by Shen et al. [143], under constant pressure and dead-end filtration. The applied fouling models (Figure 4.8) shows that standard blocking affords an excellent fit ( $R^2=0.999$ ) to the experimental data in SWNTs-UF systems at ambient conditions. The other fittings did not show much variance in  $R^2$  values ranging from 0.777 to 0.798. The data suggests that most of the foulant was associated with inner pore surfaces of the UF membranes. The flux modeling data suggests that HA fouling was associated with inner pore surfaces of the UF membranes (standard blocking), which decreased the membrane pore size related to the inner pore wall particle depositing and caused the flux decline. Specifically, pH=4.0, severe flux decline was strongly related to the adsorptive membrane fouling by standard blocking, allowing for the possibility of complete blocking as listed in Table 4.6 (blocking model results not shown).

**Table 4.6** Equations of different fouling mechanisms for dead-end filtration [77].

Models	Equations	Description
Complete blocking	$J_0 - J = AV$	<p>Particles do not superimposed one upon another and particles arriving at the membranes will block pores : <math>d_{\text{particle}} \cong d_{\text{pore}}</math></p> <p>Particles do superimposed one upon another and particles accumulation increased with the single layer deposition on membrane surface : <math>d_{\text{particle}} \cong d_{\text{pore}}</math></p>
Standard blocking	$1/t + B = J_0/V$	<p>Pore diameter is decreased with proportional to permeate volume on the basis of particle depositing on the internal pore walls : <math>d_{\text{particle}} \ll d_{\text{pore}}</math></p> <p>Particles are retained due to cake layer, and each particle was accumulated on the membrane surface in order to form a bridge like assemblage or a cake layer :</p> <p><math>d_{\text{particle}} &gt; d_{\text{pore}}</math></p>
Intermediate blocking	$\ln J_0 - \ln J = CV$	
Cake filtration	$(1/J) - (1/J_0) = DV$	

Note:  $J$ , flux;  $J_0$ , initial flux;  $V$ , filtrated volume;  $t$ , filtration time;  $A$ ,  $B$ ,  $C$  and  $D$  are constants, respectively.



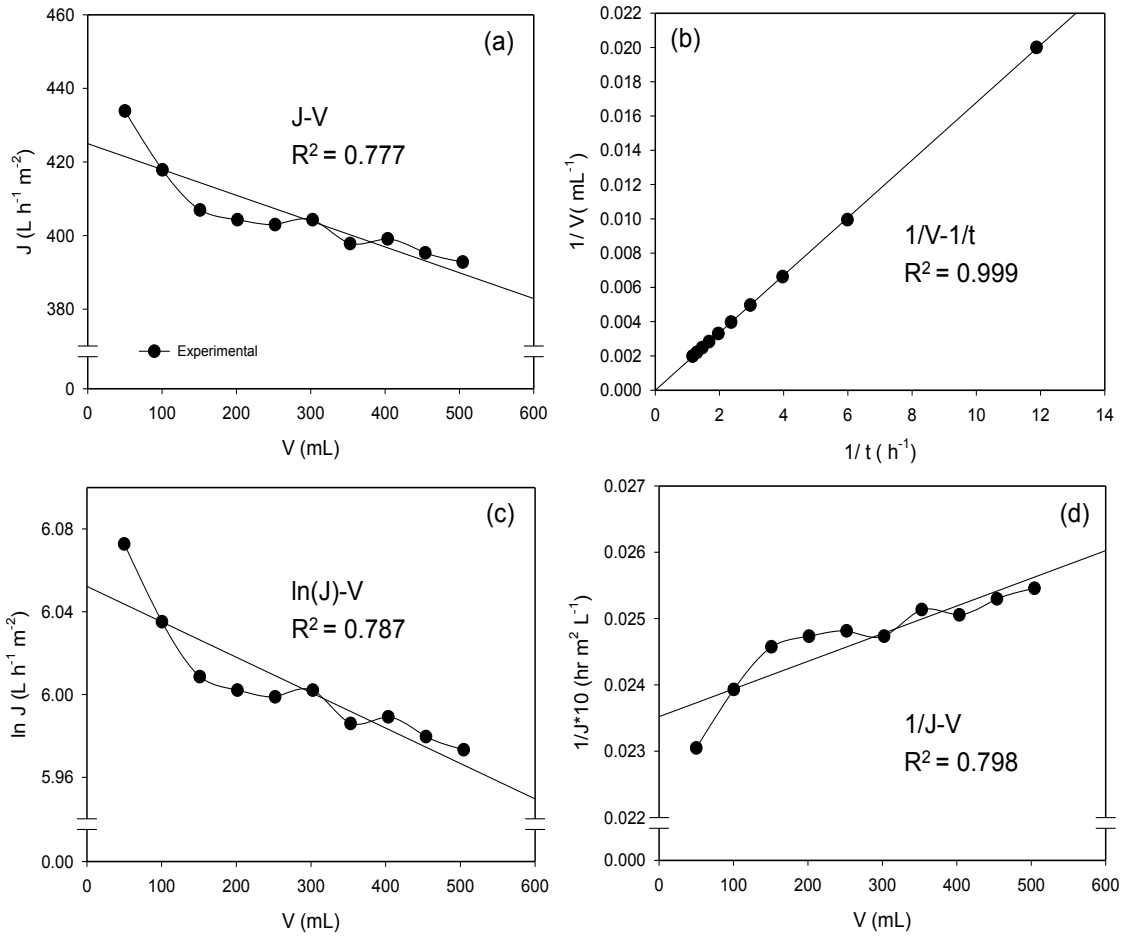


**Figure 4.8** The experimental data fitting of the flux decline using different fouling mechanisms: (a) complete blocking; (b) standard blocking; (c) intermediated blocking; and (d) cake filtration. Operating conditions:  $\Delta P = 827$  kPa (120 psi); stirring speed = 300 rpm; recovery = 50%; DOC =  $8 \text{ mg L}^{-1}$ ; SWNTs =  $10 \text{ mg L}^{-1}$ ; conductivity =  $500 \mu\text{S cm}^{-1}$ ; pre-contact time with SWNTs = 2 h.

#### 4.3.5. Effect of Pressure on BPA and E2 Removal

The BPA and E2 retention experiments were performed with pure water at a constant flux to minimize artifacts from mass transfer at the membrane interface (Figure 4.6). However, the retention of BPA and E2 varied with different applied pressures (138, 414, and 827 kPa) in the presence of SWNTs ( $10 \text{ mg L}^{-1}$ ) and NOM ( $8 \text{ mg L}^{-1}$ ), as shown in Figure 4.9.

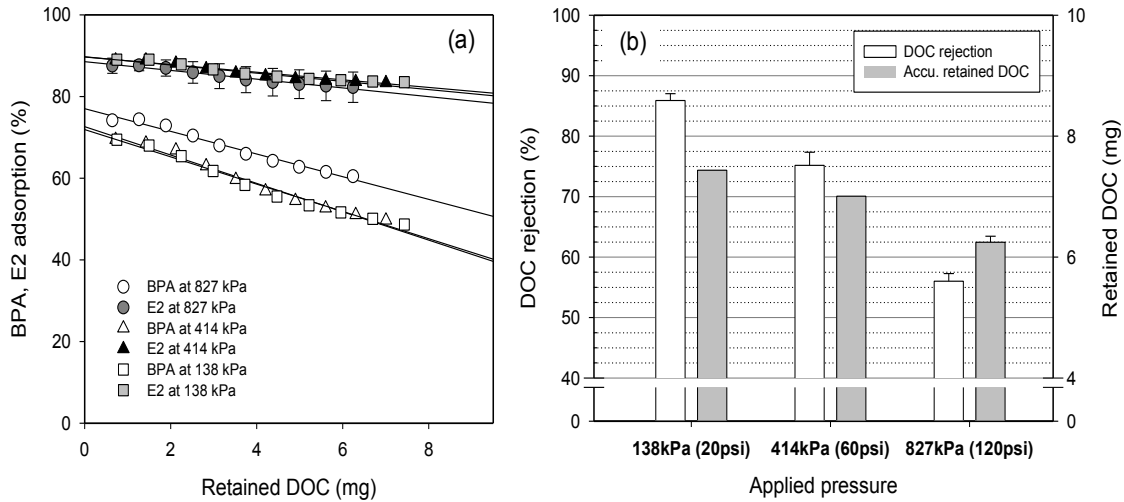


**Figure 4.9** Comparison of (a) retained DOC and adsorption for BPA and E2 and (b) applied pressure, DOC rejection, and retained DOC in the UF5K filtration in the presence of NOM and SWNTs. Operating conditions:  $\Delta P = 827$  kPa (120 psi), 414 kPa (60 psi), 138 kPa (20 psi); stirring speed = 300 rpm; recovery = 50%; DOC =  $8 \text{ mg L}^{-1}$ ; SWNTs =  $10 \text{ mg L}^{-1}$ ; conductivity =  $500 \mu\text{S cm}^{-1}$ ; pH = 7.5; pre-contact time with SWNTs = 2 h.

The adsorbed amounts of BPA and E2 increased linearly with increasing amounts of delivered BPA and E2. The adsorption of E2 is greater than BPA due to more hydrophobic interactions between E2 and the membrane and/or SWNTs. The E2 adsorption was almost constant at all the measured pressures, while the adsorption of BPA was observed to reduce with decreasing pressure (Figure 4.9a). Also, BPA adsorption at an applied pressure of 827 kPa was higher than that at 138 and 414 kPa. The results were explained in terms of retained DOC and DOC rejection (Figure 4.9b). BPA and E2 adsorption decrease linearly with increasing retained DOC, while DOC rejection by the UF5K membrane was approximately 15-30% lower at an applied pressure of 827 kPa than at 414 and 138 kPa. As a result, more DOC was retained at the membrane surface at low applied pressures, resulting in greater competition for adsorption sites and greater pore blockage by DOC. This combination of factors was

responsible for lower adsorption capacity values for BPA, which is less hydrophobic than E2. From these results, it can be concluded that BPA and E2 adsorption and retention associated with NOM transport is significantly influenced by hydrodynamic operating conditions (in this case, the initial pure water flux associated with pressure), which cause varying concentration polarization at the membrane interface. However, the adsorption and retention of E2 are similar at various applied pressures, suggesting that the concentration polarization is insignificant for E2 transport.

#### **4.3.6. Effect of Membrane Pore Size on BPA and E2 Removal**

The water containing BPA and E2 at concentrations of 1  $\mu\text{M}$  was used for contaminant retention experiments through the UF5K, UF10K, and UF30K membranes in the absence and presence of NOM and SWNTs (with a pre-contact time of 2 h). In general, when the source water contains molecules smaller than the membrane pores, solute passes easily through the membrane pores. If only molecular weight and membrane pore size were considered, BPA and E2 retention by these membranes should be minimal. However, all of the membranes show significant retention of E2 (> 80%) and BPA (> 40%) due to adsorption on the membrane, the SWNTs, and/or NOM, while a significant decrease in retention (30-70%) was observed for BPA and E2 in the presence of NOM only (no SWNTs), as shown in Figure 4.10. All three UF membranes showed similar E2 retention, even though their membrane pore sizes were different. The retention of BPA varied predictably depending on membrane pore size, in the order of UF5K > UF10K > UF30K. These results may be explained in terms of: (1) E2 hydrophobic adsorption onto the

hydrophobic membranes and SWNTs and (2) BPA size-exclusion due to NOM-partitioning.

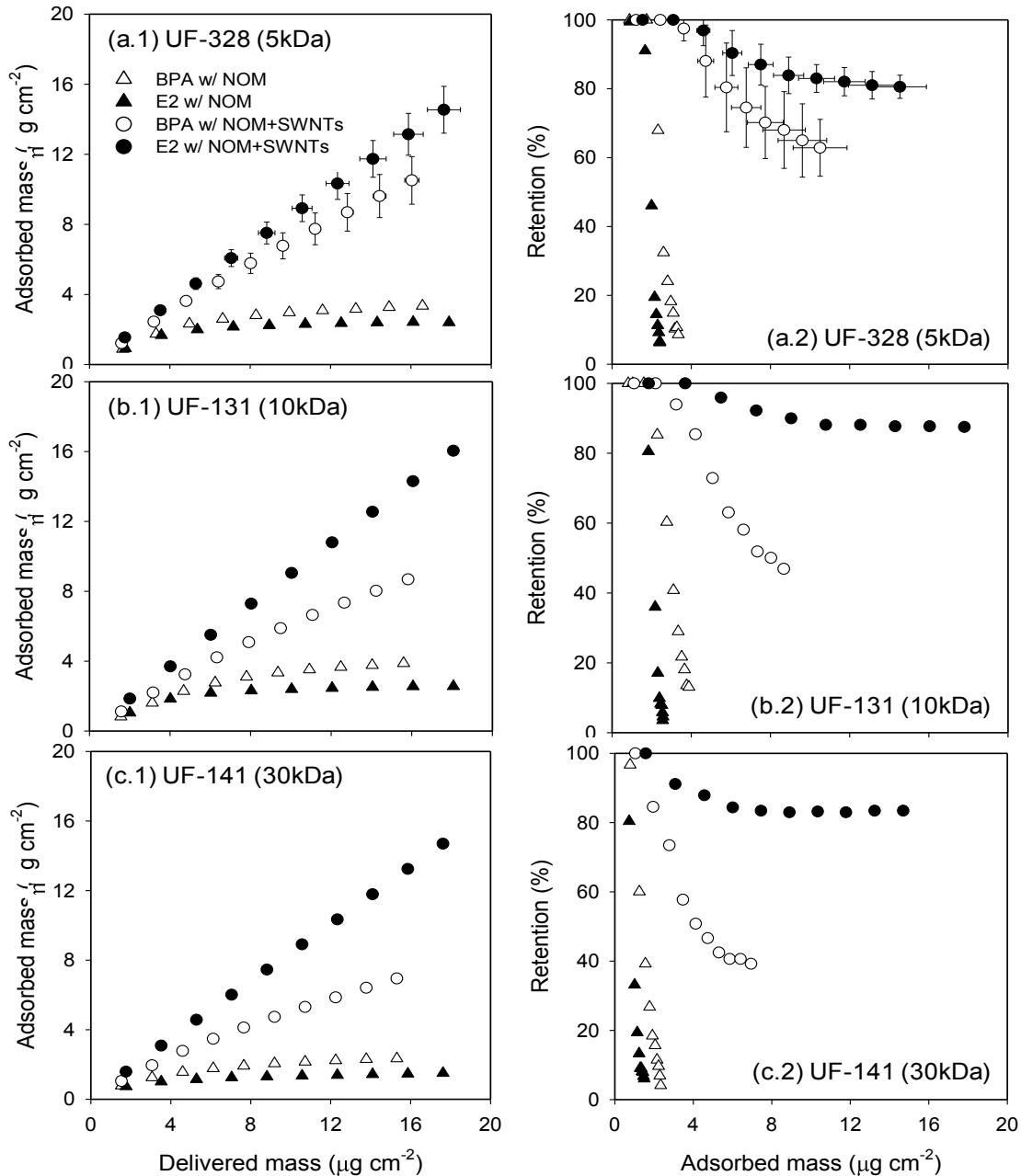


**Figure 4.10** Comparison of delivered and adsorbed mass accumulated, and adsorbed mass and retention for BPA and E2 in three UF (UF5K, UF10K, and UF30K) membrane filtration in the presence of NOM and NOM+SWNTs. Operating conditions:  $\Delta P = 827$  kPa for UF5K, 586 kPa for UF10K, and 228 kPa for UF30K; stirring speed = 300 rpm; recovery = 50%; DOC = 8 mg L<sup>-1</sup>; SWNTs = 10mg L<sup>-1</sup>; conductivity = 500  $\mu$ S cm<sup>-1</sup>; pH = 7.5; pre-contact time with SWNTs = 2 h.

Three-dimensional AFM image analysis was employed to investigate the morphological changes of the fouled UF5K membrane associated with BPA, E2 and NOM in the absence and presence of SWNTs.

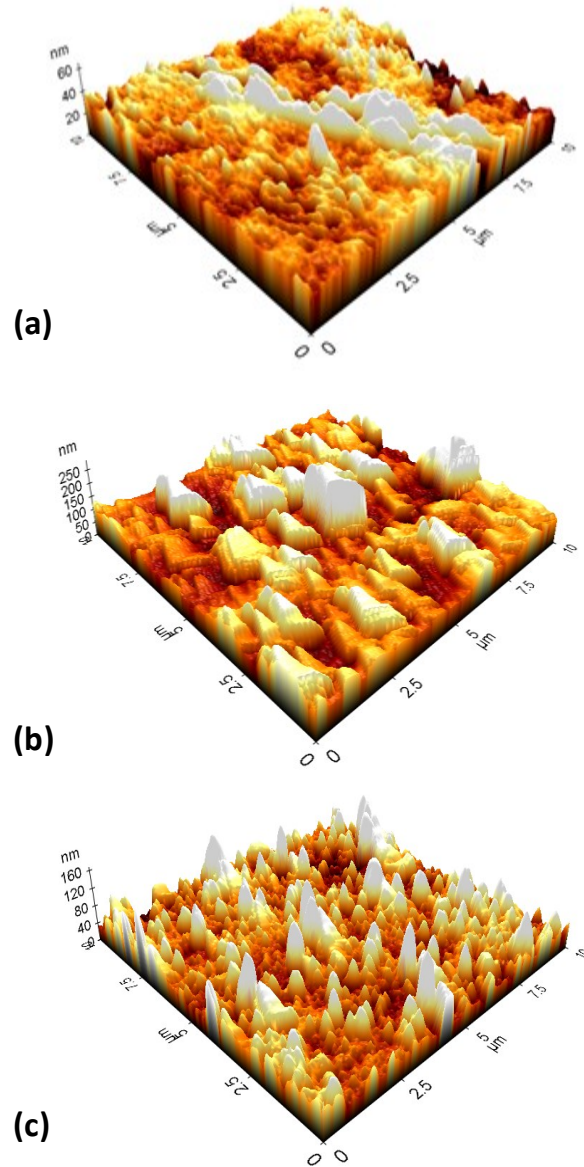


**Figure 4.11** Three-dimensional AFM image (a) cleaned membrane, (b) fouled in the absence of SWNTs, and (c) fouled membrane in the presence of SWNTs. Operating conditions:  $\Delta P = 827$  kPa (120 psi); stirring speed = 300 rpm; recovery = 50%; DOC = 8 mg L<sup>-1</sup>; SWNTs = 10 mg L<sup>-1</sup>; conductivity = 500  $\mu$ S cm<sup>-1</sup>; pre-contact time with SWNTs = 2 h.

Figure 4.11 displays the AFM images of the clean and fouled membranes both in the absence and presence of SWNTs at a scan size of  $10 \mu\text{m}^2$  when imaged in air. The dark and light regions correspond to areas below and above the mean elevation, respectively. The images of the clean and fouled membranes were compared, based on their average roughness values: 30.7 nm (fouled in the absence of SWNTs) > 8.66 nm (fouled in the presence of SWNTs) > 2.43 nm (clean membrane). This suggests that SWNTs reduce membrane fouling, although there are contradictory results concerning the effect of other absorbents (e.g., PAC and aluminum/iron oxide particles) on membrane fouling.

#### 4.4 Conclusions

In this study, flux decline measurements of model water samples containing EDCs (BPA or E2) were conducted using commercially available UF membranes. The sample retention and adsorption values were studied both in the absence and presence of NOM and SWNTs. Results show that the amount of BPA and E2 delivered and adsorbed per unit of membrane area is a better parameter than permeate volume and time, to provide a comparison of their trends in retention and flux decline. The following conclusions were drawn: (i) preferential removal by membrane adsorption occurred for the more hydrophobic E2, compared to BPA, under all of the experimental conditions; (ii) the addition of NOM during UF filtration led to competition for adsorption sites, resulting in lowered adsorption of micropollutants; (iii) membrane fouling by NOM considerably impacted the transport of BPA and E2 in the SWNTs-UF systems due to various NOM-SWNTs-UF-BPA/E2 interactions in the solution; and (iv) SWNTs exhibited a high

adsorptive capacity for the micropollutants BPA and E2. Regarding the micropollutant feed concentration, although the experiments were conducted at high concentrations above typically reported levels in drinking water sources, the results still provide guidelines for SWNTs/UF hybrid membrane filtration since the retention of trace organics at parts per-billion or parts-per-trillion levels are independent of initial concentration [10, 144, 145].

### **Acknowledgements**

This research was supported by GS E&C and the Korea Ministry of Environment, the Korea Ministry of Environment, 'Project, 414-111-004'. The authors also thank Qammer Zaib (University of South Carolina) for the HR-TEM and ZP of SWNTs analysis.

## CHAPTER 5

### NATURAL ORGANIC MATTER REMOVAL IN SINGLE-WALLED CARBON NANOTUBES–ULTRAFILTRATION MEMBRANE SYSTEMS\*

\*Reprinted here with permission of publisher: Heo et al., Natural organic matter removal in single-walled carbon nanotubes–ultrafiltration membrane systems, *Desalination* 298 (2012) 75-84.

#### **Abstract**

Bench-scale ultrafiltration (UF) experiments were performed to address the effects of single-walled nanotubes (SWNTs) on flux and rejection of humic acid (HA) during fouling runs under various hydrodynamic and solution conditions. The performance of SWNTs–UF was also evaluated on the basis of a resistance-in-series model, filtration laws, and dissolved organic matter (DOM) transportation mechanisms. The addition of SWNTs to the UF process did not significantly exacerbate the permeate flux decline and total membrane resistances. Further, it appeared that the SWNTs did not likely increase total resistance because the HA fouling was mainly attributed to the total resistance. In addition, SWNTs–UF produced highly reduced membrane resistance per unit of retained DOM because SWNTs adsorbed some of the HA by offering binding sites. Significantly increased flux trends were observed with unstirred, low pH/high ionic strength, and low solvent flux/mass transfer coefficient ( $J_v/k$ ) conditions. In addition, the rejection of HA increased up to 9–25% in SWNTs–UF. These results suggest that the effect of SWNTs on membrane fouling is a function of hydrodynamic and operational conditions. On the basis



of a filtration laws approach, intermediate blocking was more dominant in the early stages; cake filtration became more dominant as filtration progressed, with development of a fouling layer. The first stages of filtration, unexpectedly, did not clearly show early inner pore blocking even though the main resistance was attributed to adsorptive fouling. DOM transport interactions significantly affected the flux decline and HA rejection trends, which were evaluated through a thermodynamic approach. The HA rejection trends in SWNTs–UF were observed to be higher than that in UF alone. The observed HA rejections of 63, 74, and 87% corresponded to  $J_v/k$  values of 1.7, 0.9, and 0.4, respectively, which indicates an overall reflection coefficient of 0.9 for SWNTs–UF. In addition, a high flux decline observed at high  $J_v/k$  values was due to concentration polarization (CP) and cake/gel layer formation, which hindered the transportation of DOM. It can be concluded that DOM transportation in SWNT–UF systems depends, to a significant extent, on the CP and cake/gel layer formation at the membrane boundary.

*Keywords:* Ultrafiltration; Fouling; Humic Acid; Adsorption; Rejection; Single-Walled Carbon Nanotubes (SWNTs)

## 5.1 Introduction

Natural organic matter (NOM) plays an important role in the most problematic issue concerning water treatment. NOM is a precursor to carcinogenic disinfection byproducts and causes complexation with metals and hydrophobic synthetic compounds. NOM cannot be readily rejected during ultrafiltration (UF) since UF membranes have relatively large membrane pores compared to the molecular size of NOM [11, 12]. Furthermore,

NOM is well known as a major contributor to membrane fouling because it clogs membrane pores or forms a cake layer on the membrane surface. Thus, NOM is a barrier to the extensive application of the UF process in advanced water systems [13-16]. Humic acid (HA), a major hydrophobic fraction of dissolved NOM (DOM), is usually considered to be responsible for severe membrane fouling [17, 18]. HA consists of anionic macromolecules having a wide range of molecular weights. These macromolecules are comprised of both aromatic and aliphatic components with primarily carboxylic (60–90%) and phenolic functional groups in aquatic environments [19]. Compared to other fractions of DOM, HA is found to have the largest impact on membrane fouling because it causes extensive pore adsorption (irreversible fouling).

The past few years have witnessed a significant amount of research interest in the development and use of various carbonaceous nanomaterials (CNMs) for potential environmental applications due to their unique characteristics. These applications include high flux and antifouling membranes, composite filters, sorbents, antimicrobial and antiviral agents, environmental sensing, and renewal energy storage [106, 146, 147]. Among CNMs, carbon nanotubes (CNTs) have been studied as a new sorbent to remove NOM and synthetic micropollutants from water based on the adsorptive capacity of CNTs [74, 148, 149]. CNTs share hexagonal carbon lattices that are a one-dimensional analogues of zero-dimensional spherical fullerene molecules [150]. Unlike many conventional adsorbents, CNTs have an exceptional fibrous shape with high aspect ratios, large surface area-to-volume ratios, and well developed mesopores [151]. These characteristics contribute to higher adsorption capacities [152, 153] and shorter equilibrium times [110, 154]. Previous researchers have studied the adsorption

mechanisms (e.g., hydrophobic interactions and  $\pi$ - $\pi$  bonds) [105] and the adsorptive capacities of NOM onto CNTs [155].

While the source waters are currently given to be in need of more challenging treatment, UF membranes coupled with adsorbents (e.g., powdered activated carbon and aluminum sulfate) are becoming a promising technology to meet stringent regulations [23]. Such integrated systems can be applied even more extensively to water treatment in response to increasing concerns over the removal of NOM. The current understanding of adsorption procedures and fouling of membranes in the presence of DOM clarify that adsorbent addition as a pretreatment may affect membrane performance. However, the effects of the adsorbent have shown somewhat contradictory results, especially in flux decline. These fouling effect scenarios mostly occur through adsorptive fouling from the interaction with HA, the most hydrophobic of the NOM, and the membrane, as noted earlier. On one hand, if the adsorbent successfully removes HA from solution that would otherwise more favorably adsorb onto a membrane surface and pores, membrane fouling is reduced. On the other hand, if the adsorbent itself behaves like the foulants, membrane fouling can be exacerbated. The adsorbent effect on membrane fouling can be a function of adsorbent physicochemical properties (size, charge, and hydrophobicity), membrane characteristics (pore size, charge, and hydrophobicity), and solution water chemistry (pH and conductivity) [12, 121, 156, 157].

The objective of this study is to investigate the feasibility of single-walled carbon nanotubes (SWNTs) contributing to membrane fouling control, and to evaluate potential mechanisms for HA removal in a hybrid system of UF in the presence of SWNTs (SWNTs-UF) under various hydrodynamic and solution conditions. To accomplish this,

the rejection of HA and flux decline in SWNTs-UF systems were investigated as a function of various solution and operating conditions, including extent of conductivity/ionic strength (IS), pH, applied pressure, and SWNT concentrations.

## **5.2 Materials and methods**

### **5.2.1 NOM and UF feed solutions**

HA used in this study was obtained from Sigma-Aldrich Co. (St. Louis, MO, USA), which was used as the model NOM to simulate the hydrophobic constituents of NOM with high molar mass. The dissolved HA is a mixture of complex polyelectrolytes chemically formed by carboxylic and hydroxyl functional groups. Aldrich HA stock solution was prepared by dissolving HA in deionized (DI) ultrapure water. The solution was then sequentially filtered through GF/F (0.7  $\mu\text{m}$ ) glass microfiber filters (Whatman Inc., Piscataway, NJ, USA) and Durapore (0.45  $\mu\text{m}$ ) membrane filters (Millipore Inc., Billerica, MA, USA) to remove any impurities and particulate matter. The feed solution for the UF experiments was prepared by further dilution of HA stock solution with DI water to obtain a desired concentration of 8  $\text{mg L}^{-1}$  as dissolved organic carbon (DOC). The conductivity was adjusted by adding NaCl to maintain a final background conductivity of nearly 300  $\mu\text{S cm}^{-1}$  and up to 11,400  $\mu\text{S cm}^{-1}$  (IS = 0.1 M). The pH was adjusted to 4, 7, and 10 by the addition of 0.1 M NaOH and 0.1 M HCl, as needed, then buffered with 1 mM phosphate buffer solution.

### **5.2.2 Characteristics of SWNTs**

SWNTs (1–2 nm diameter × 5–30 μm length) with over 90% purity were obtained from Cheap Tubes Inc. (Brattleboro, VT, USA). According to the manufacturer, the SWNTs have a specific surface area of 407 m<sup>2</sup> g<sup>-1</sup>. SWNT characteristics have been described in detail in our previous study [158]. In brief, the electrophoretic mobility of SWNTs showed negative surface potential, and values of zeta potential (ZP) ranged from -21 to -67 mV. The negative surface charge of SWNTs increased with increasing solution pH. The diameter of the SWNTs was calculated to be 1.13 nm based on the peak observed at 211.2 cm<sup>-1</sup> through the Raman spectrum. In addition, the aggregation hydrodynamic diameters of SWNTs were measured at approximately 1500 nm by dynamic light scattering [158].

### 5.2.3 UF membrane

One commercially available UF membrane having a nominal molecular weight cut-off (MWCO) of 10 kDa was selected to evaluate its NOM rejection and flux decline properties. The flat sheet membrane, made of polyethersulfone (PES), was obtained from Koch Membrane Systems Inc. (Wilmington, MA, USA). The detailed characteristics of the membrane are listed in Table 5.1. In particular, the PES UF membrane has aromatic rings with two methyl groups and ionizable functional groups (i.e., carboxylic acids), as specified by the manufacturer. Before UF experiments were conducted, each new membrane was soaked in DI water for at least 24 h at a room temperature of 21 ± 1 °C to remove any preservative products prior to use. During this period, the DI water was replaced several times with a new volume of pure water. The DOC of the final rinse water was checked to assure that it was at a negligible level.

**Table 5.1** Ultrafiltration membrane characteristics.

Characteristics of Membrane	PES
Material	Polyethersulfone
MWCO (kDa)	10
ZP (mV) at pH 7	-24.9
Contact angle (°)	48 ± 2
Applied pressure (kPa)	270 – 310
PWP (L/hr-m <sup>2</sup> -kPa)	
<i>Average</i>	0.98
<i>(min-max)</i>	0.93-1.07
<i>c.v.<sup>a</sup> (%)</i>	4.5
Pure water membrane resistance (10 <sup>12</sup> m <sup>-1</sup> )	3.74

PWP is pure water permeability. <sup>a</sup>c.v. is coefficient variance.

#### 5.2.4 SWNTs-UF experiments

All UF filtration experiments were constituted by a feed volume of 300 mL dead-end stirred bench-scale UF cell (HP4750, Sterlitech Corporation, Kent, WA, USA) with an effective membrane area of 14.2 cm<sup>2</sup>. In this study, the filtration cell was coupled with an SWNT reactor and an initial concentration of 8 mg L<sup>-1</sup> DOC as HA was mixed with SWNTs (20–50 mg L<sup>-1</sup>) in the reactor for 1 h prior to the UF experiments. The pre-contact time and dosage were selected to simulate conditions at many full-scale water treatment plants that have employed powdered activated carbon (PAC) contact times of 1–2 h and PAC dosages of 5–50 mg L<sup>-1</sup> [35]. Basically, UF experiments were conducted with and without a stirring rate of 300 rpm to determine the effect of hydrodynamic conditions; transmembrane pressure (TMP) was kept constant at different levels: 1 bar (100 kPa), 3 bar (300 kPa), and 6 bar (600 kPa). Permeate was periodically collected in a

graduated cylinder placed on a digital balance (AV8101, Ohaus, NJ, USA) and weighed. The experimental UF filtration protocol for fouling and rejection runs was performed with three steps: compaction, fouling/rejection, and reversibility. First, the membrane was compacted using high pressure (6 bar) with DI water, and the water flux was checked as a function of time until a stable flux state was obtained (usually within 30 min). Then, the TMP was adjusted to exhibit the desired same initial permeate flux ( $J_o$ ) to ensure the least variation from the various hydrodynamic conditions. Only those membranes for which permeability variances were less than 5% were selected for further SWNTs-UF experiments. The designated UF experiments were conducted by collecting approximately 215 and 85 mL of permeate and retentate, respectively; at that point in time, a volume concentration factor (VCF) of 3.5 was reached.

The observed percentage of HA rejection that was collected  $i$  times,  $R_i$  (%), was calculated using Eq. (5.1):

$$R_i(\text{feed}), \% = \frac{C_F - C_{P,i}}{C_F} \quad (\text{Eq. 5.1})$$

where  $C_F$  and  $C_{P,i}$  are defined as the concentration of feed and  $i$  times permeate, respectively. The permeate flux ( $J_v$ ) was evaluated in terms of the VCF using Eq. (5.2):

$$VCF = \frac{V_F}{V_R} = 1 + \frac{V_P}{V_R} \quad (\text{Eq. 5.2})$$

where  $V_F$ ,  $V_R$ , and  $V_P$  are defined as the volume of feed, retentate, and permeate, respectively. The concentration in the permeate was measured several times until VCF = 1.0–3.5, corresponding to a recovery of 0–71.7%. The adsorbed mass of HA on SWNTs-UF was calculated on the basis of the mass balance of HA in DOC. The adsorbed mass fraction of HA is equal to the HA mass in the feed minus the HA mass out in both the retentate and cumulative permeate, as defined by Eq. (3):

$$M_{Ads} = \frac{C_F V_F - [\sum(C_{P,i} V_{P,i}) + (C_R V_R)]}{C_F V_F} \quad (\text{Eq. 5.3})$$

where  $M_{ads}$ ,  $V_F$ ,  $V_{P,i}$ ,  $V_R$ , and  $C_R$  are the adsorbed mass fraction, feed volume,  $i$  times permeate volume, retentate volume, and retentate concentration, respectively. Analyses of organic HA in the feed, permeate, and retentate of the solutions were performed using a DOC analyzer (Shimadzu Model TOC-5050A) and an ultraviolet absorption spectroscopy at a wavelength of 254 nm (UV<sub>254</sub>).

## 5.3 Results and discussion

### 5.3.1 The influence of SWNTs and hydrodynamic conditions on flux decline and HA rejection

Bench-scale UF experiments were performed to evaluate the performance of both SWNTs–UF (with SWNTs) and the UF process alone (without SWNTs) in terms of flux decline profile and HA rejection. The rejection trends based on DOC and the normalized fluxes of both SWNTs–UF and UF alone are presented in Figure 5.1 as a function of VCF at pH 7 and conductivity of 300  $\mu\text{S cm}^{-1}$ . The VCF provides a more reasonable



comparison of HA rejection and flux decline than permeate volume or time because the retained HA concentration on the membrane surface in dead-end stirred cells is highly variable with respect to condensing volume. This variability significantly influences the physical and chemical properties of the membrane and solute at the interface of the membrane [58, 159].

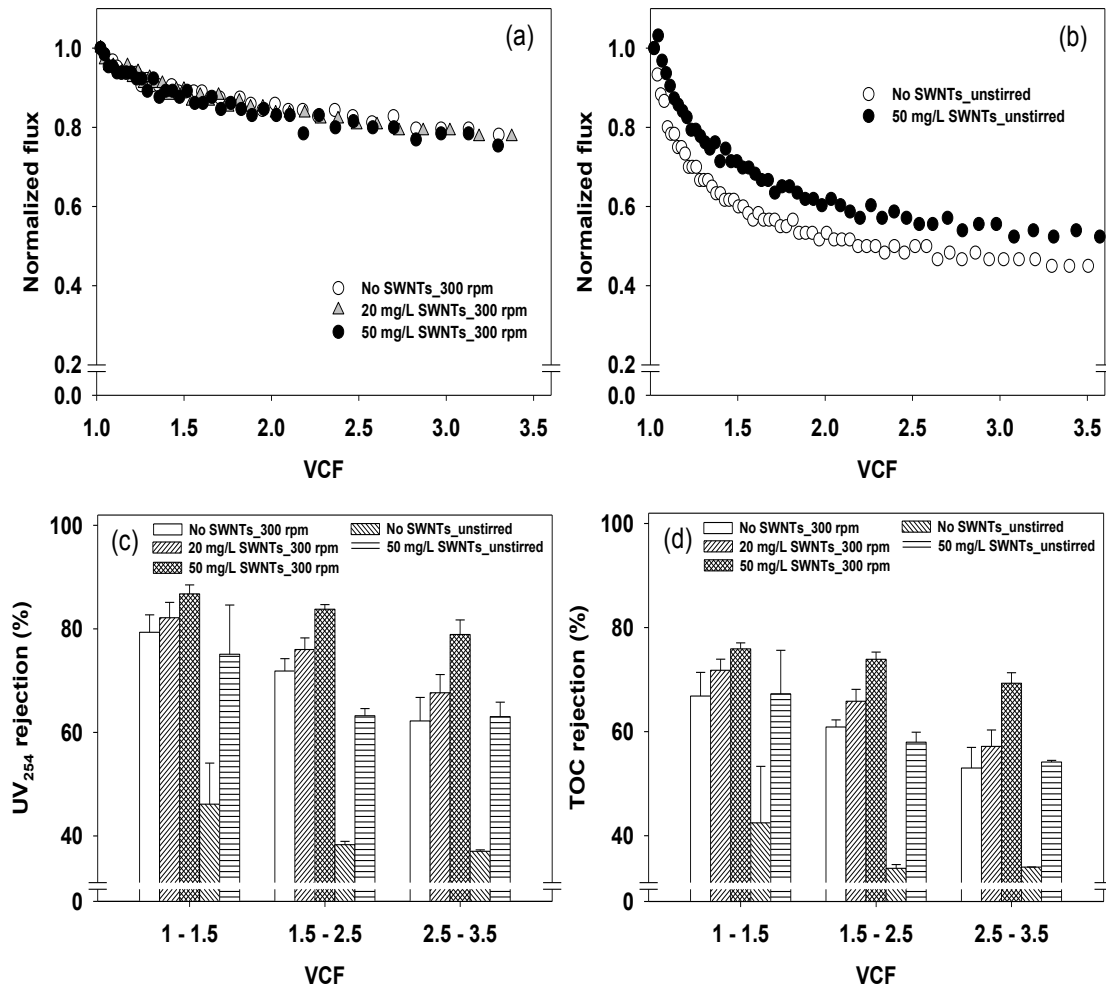


**Figure 5.1** Influence of SWNTs concentrations on flux decline and HA rejection. Flux decline and HA rejection as a function of SWNTs concentration for the 10 kDa PES membrane: (a) Flux decline at 300 rpm, (b) flux decline without stirring, (c) HA rejection based on UV<sub>254</sub>, and (d) HA rejection based on DOC. Operating conditions:  $\Delta P = 1$  bar (300 kPa); DOC = 8 mg L<sup>-1</sup>; SWNTs = 20-50 mg L<sup>-1</sup>; conductivity = 300  $\mu$ S cm<sup>-1</sup>; pH = 7; pre-contact time with SWNTs = 1 h (error bars represent standard deviations).

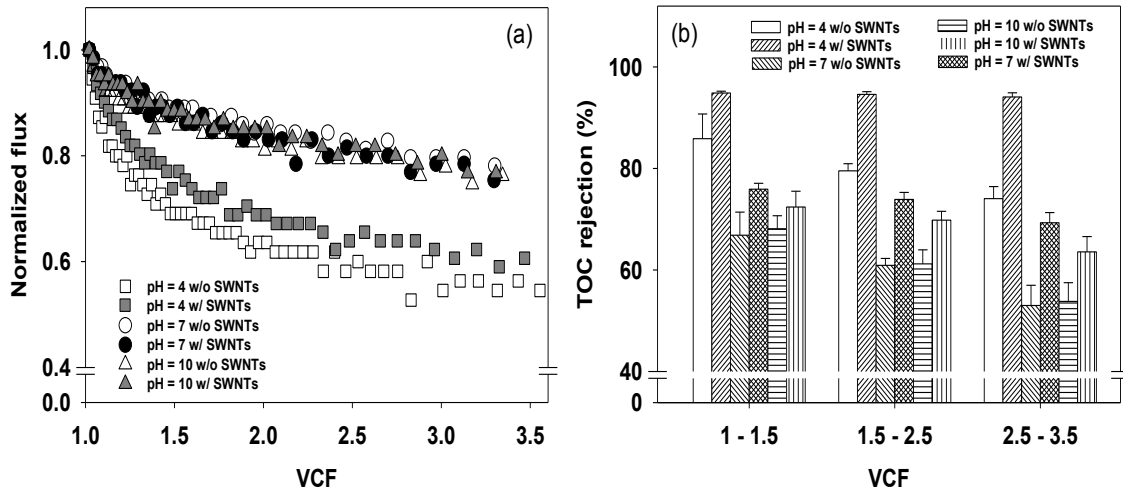
The normalized fluxes of 0, 20, and 50 mg L<sup>-1</sup> SWNT concentrations demonstrate that SWNTs alone do not significantly affect the permeate flux decline in the presence of HA at a stirring speed of 300 rpm (Figure 5.1a) even though SWNTs are presumed to have a high possibility of fouling. Conversely, in the case of unstirred conditions, a slight increase in flux (7–9%) was observed in SWNTs–UF (Figure 5.1b) because SWNTs adsorb some amounts of HA. The levels of SWNT fouling observed under these hydrodynamic conditions are essentially caused by two factors. SWNT particles with lengths of 5–30 μm, outer diameter of 1–2 nm, and an average aggregation hydrodynamic diameter of approximately 1,500 nm are sufficiently large to block membrane pores with a nominal MWCO of 10 kDa. Therefore, the SWNTs stack on the membrane surface to form a porous layer that allows the passage of water with no additional fouling resistance. In particular, the deposition of SWNTs on the membrane surface in an unstirred condition forms a porous grid cell layer, which results in an increase in membrane flux without the addition of fouling resistance in the SWNT–UF system. In addition, the adsorption of HA onto SWNTs increases membrane flux in the unstirred condition, which also reduces membrane cake, gel, and concentration polarization (CP) layers. In general, other studies using adsorbent particles in conjunction with UF have shown considerable advantages in terms of fouling rate reduction and NOM removal efficiency [12, 13, 160].

Figure 5.1c and 5.1d shows the effects of SWNT concentrations and hydrodynamic conditions on HA rejection with the permeate fraction of VCF determined on the basis of UV<sub>254</sub> and DOC. A 9–16% increase in HA rejection was obtained with increasing SWNT concentrations under stirred conditions. SWNT contributions to HA rejection were maximized at the highest permeate VCFs (2.5–3.5). A significant increase (29%) in HA

rejection was shown in terms of  $UV_{254}$  under unstirred conditions with SWNTs–UF over those with the UF process alone. In the comparison of stirred and unstirred conditions, approximately 13–24% less of the HA were rejected in the unstirred case in SWNTs–UF and UF alone, presumably because CP and cake/gel layers increased the concentration of HA on the membrane surface. In addition, the higher rejection in SWNTs–UF should be attributed to the adsorption of HA onto SWNTs under both unstirred and stirred conditions. As a result, the maximized SWNT adsorption effect for HA rejection was obtained for unstirred conditions. The adsorbed amount of HA was calculated using mass balance with the difference in HA concentration among feed, permeate, and retentate (data available on request). The SWNT–UF system showed approximately 30% more HA adsorption than the UF process alone because of HA adsorption onto  $50 \text{ mg L}^{-1}$  SWNTs. Mechanisms of HA adsorption onto SWNTs remain unclear because SWNTs exhibit characteristics of heterogeneity and multiple adsorption mechanisms over time. The adsorption of HA on SWNTs is caused by the energetics of surface reactions through Van der Waals forces and electrostatic repulsion. For example, although the SWNTs surface is electrically balanced, ion exchange can occur because of the energetics of surface reactions associated with electronic charge affinity with functional groups in HA. This phenomenon is part of the Coulombic energy charge, which varies with pH change and surface loading. Therefore, the driving force of SWNT adsorption with HA is a mixed mechanism of hydrophobicity (short range) and Coulombic interaction (longer range) [105, 161, 162].

### 5.3.2 Effects of solution pH and ionic strength

Figure 5.2 shows the effect of pH on HA rejection and flux decline in SWNTs–UF and in UF alone, as a function of VCF. As a general observation, pHs of 7 and 10 showed similar trends of flux decline and rejection of HA in both SWNTs–UF and UF alone. However, Figure 5.2a shows the worst flux decline with UF alone, with an approximate 18–23% increase at pH 4 than that observed for pHs 7 and 10. In the SWNTs–UF process, the normalized flux at pH 4 increased approximately 6–7% over UF alone. In addition, both SWNTs–UF and UF alone showed a significantly high rejection range of 80–95% at pH 4, as compared with pHs 7 and 10 (Figure 5.2b). These rejections decreased with increasing VCF. Several factors can explain these results. The higher rejection at low pH is attributed to membrane pore size reduction through HA adsorption for the hydrophobic PES membrane. As shown in a previous study [163], a consequence of the smaller pore size is a high NOM rejection of 90–95% by UF membranes. These results suggest that HA adsorption occurs more strongly at low pH and that inner pore sites have the top priority for HA adsorption with hydrophobic membranes owing to the strong hydrophobic adsorption. In addition, the charges of the membrane surface and HA become less negative with a decrease in pH, which causes a decrease in the electrostatic repulsion between the membrane and HA. Moreover, the flux difference between SWNTs–UF and UF alone is largely due the adsorption ability of SWNTs, which increases approximately 40% at a low pH over values of 7 and 10.



**Figure 5.2** Influence of pH on flux decline and HA rejection based on DOC in the absence and presence of SWNTs: (a) Normalized flux decline and (b) HA rejection based on DOC at different pH conditions. Operating conditions:  $\Delta P = 1$  bar (300 kPa); DOC =  $8 \text{ mg L}^{-1}$ ; SWNTs =  $50 \text{ mg L}^{-1}$ ; conductivity =  $300 \text{ }\mu\text{S cm}^{-1}$ ; pH = 7; pre-contact time with SWNTs = 1 h.

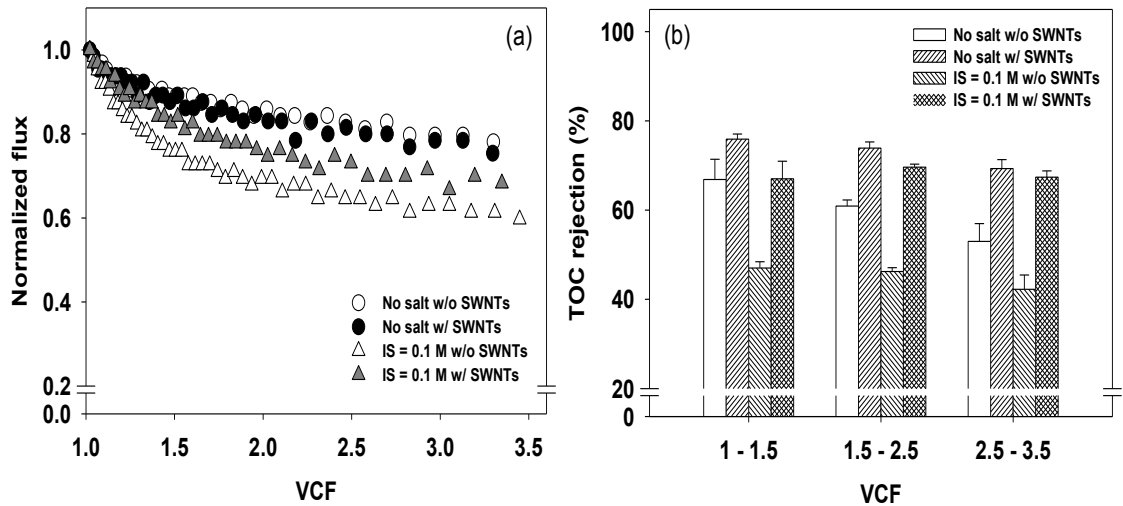


**Figure 5.3** Influence of ionic strengths on flux decline and HA rejection based on DOC in the absence and presence of SWNTs: (a) Normalized flux decline and (b) HA rejection based on DOC at different ionic strength conditions. Operating conditions:  $\Delta P = 3$  bar (300 kPa); DOC =  $8 \text{ mg L}^{-1}$ ; SWNTs =  $50 \text{ mg L}^{-1}$ ; conductivity = 300 and  $11,400 \text{ }\mu\text{S cm}^{-1}$ ; pH = 7; pre-contact time with SWNTs = 1 h.

In general, 0.1 M IS causes an 11–19% greater decrease in flux decline and rejection trends, compared with the no-salt conditions, as shown in Figure 5.3. The UF

process alone showed a larger flux decline of approximately 8% with 0.1 M IS, compared with the SWNTs-UF; the fluxes decreased approximately 32% for SWNTs-UF and 40% for the UF process alone. The HA rejection with 0.1 M IS was lower than that in the no-salt condition, particularly for UF alone. The UF process alone showed the worst rejection, 45%, while the SWNTs-UF rejection was 68%. This phenomenon could be attributed to several factors. High IS can exacerbate fouling by compacting the cake/gel layer, thereby increasing the HA concentration on the membrane surface. In addition, condensing of the HA structure easily allows it to pass through membrane pores, which then leads to lower HA rejection trends [164]. Moreover, in the particular case of SWNTs-UF with a VCF of 2.5–3.5, no difference in rejection of HA was observed between the no-salt and 0.1 M IS conditions, indicating that the adsorption capacity of SWNTs increases as the ionic strength increases because of the screening effect. This, in turn, reduces electrostatic repulsions of surface charge by compressing the double layer with HA solutions [165]. Further, for the UF process alone, reduced electrostatic repulsion between the membrane surface and HA contributes to lower HA rejection trends. These results confirm that the adsorption of NOM on SWNTs varies with solution pH and ionic strength, which could affect the flux decline and rejection trends. In particular, previous reports [105, 166, 167] have determined that pH is the most important factor in the adsorption of NOM on SWNTs, which is related to the point of zero charge on SWNTs (overall net charge) in HA solutions because the adsorption of NOM on SWNTs is driven by electrostatic interactions. The adsorption of NOM on SWNTs in the lower pH range is more electrically balanced than that observed in the case

of high pH. In addition, as pH increases, the adsorbed amount of DOC decreases as a result of the competition between NOM and OH<sup>-</sup> for the same CNT sites [152].

### 5.3.3 Resistances

The effects of SWNT additions and various operating conditions applied by the resistance-in-series model, described in Background (Chapter III), was investigated to evaluate the fouling layer characteristics in terms of flux decline; the results of this analysis are summarized in Table 5.2.

**Table 5.2** Characteristics of the fouling layer and resistances as a function of unit retained DOC mass in the absence and presence of SWNTs and various operating conditions according to resistance in series model.

Process	Solution & operating conditions			Characteristics of the fouling layer and resistances				
	TMP (bar)	pH	IS	$R_m$ ( $10^{12} m^{-1}$ )	$R_t$ ( $10^{12} m^{-1}$ )	$R_c$ ( $10^{12} m^{-1}$ )	$R_c/R_t$	$\delta$ ( $10^{12} m g^{-1}$ )
UF	3.0	7.0	No salts	3.76	5.26	0.50	0.09	4.53
		7.0*		3.86	10.02	4.38	0.44	11.33
		4.0		3.37	8.12	1.92	0.24	6.46
		10.0		3.74	5.45	0.22	0.04	4.90
	3.0	7.0	0.1 M	3.85	8.18	0.25	0.03	8.82
	1.0	7.0	No salts	3.74	4.61	-	-	3.34
6.0	7.0	3.74		6.09	-	-	5.66	
SWNT s-UF (20 mg L <sup>-1</sup> )	3.0	7.0	No salts	3.64	5.03	0.09	0.02	3.95
SWNT s-UF (50 mg L <sup>-1</sup> )	3.0	7.0	No salts	3.85	5.34	0.11	0.02	3.87
		7.0*		3.37	7.14	1.78	0.25	6.47
		4.0		3.74	7.27	1.45	0.20	5.09
		10.0		3.61	5.50	0.12	0.02	4.02
	3.5	7.0	0.1 M	4.49	7.27	0.17	0.02	5.75
	1.0	7.0	No salts	3.63	3.86	-	-	2.67
6.0	7.0	3.74		6.02	-	-	4.53	

\* without stirring.

With the exception of the results for unstirred conditions, the total fouling resistance in SWNTs–UF and UF alone remained roughly similar, with relatively low pH, and high IS. The HA solution applied to the UF membrane in unstirred conditions increased the fouling resistance due to the formation of an additional CP layer or cake/gel layer, since a CP layer could act as one of the resistances for flux decline in the CP–cake/gel layer model [56]. In addition, the cake resistance ratio ( $R_c/R_t$  values) of the cake layer was well developed by increasing the concentration of HA on the UF membrane surface. The unstirred condition clearly showed the contribution of the added SWNTs for mitigating the total fouling resistances. These results, which indicate that the effect of HA adsorption onto the SWNTs is favorable for fouling resistance reduction, can be summarized by several factors. A highly penetrable layer with SWNTs with a less dense cake layer provided better water permeation and was maximized in unstirred conditions, which mitigated the CP effect. In addition, a high concentration of HA in the UF process alone could easily block the membrane by inner pore adsorption and formation of a cake layer. Moreover, during the UF process alone, CP and cake/gel layers provided higher fouling resistance than with SWNTs–UF because the former resulted in a relatively high HA concentration on the membrane surface layer. Regarding the effect of pH and IS, fouling resistances were increased with a low pH of 4 and a high IS of 0.1 M. However, the fouling resistances were significantly decreased in SWNTs–UF at the same values. Under these conditions, adsorption by SWNTs could reduce the larger amount of adsorptive fouling onto the PES membrane. This, in turn, led to lower compaction of HA on the membrane, which ultimately led to smaller increments of fouling resistance in SWNTs–UF.



In particular, the relatively small size of the cake resistance ratio ( $R_c/R_t$ ) in stirred conditions indicated that the adsorptive fouling resistance was the main contributor to the total fouling resistance, rather than cake resistance. This result agrees well with findings of previous research on HA adsorption fouling with UF membranes [15, 18, 168]. In addition, the pure water flux was measured again after filtration to determine the effect of the irreversible fouling, which is consistent with the previous research. No significant difference in irreversible fouling resistance was observed between SWNTs–UF and UF alone.

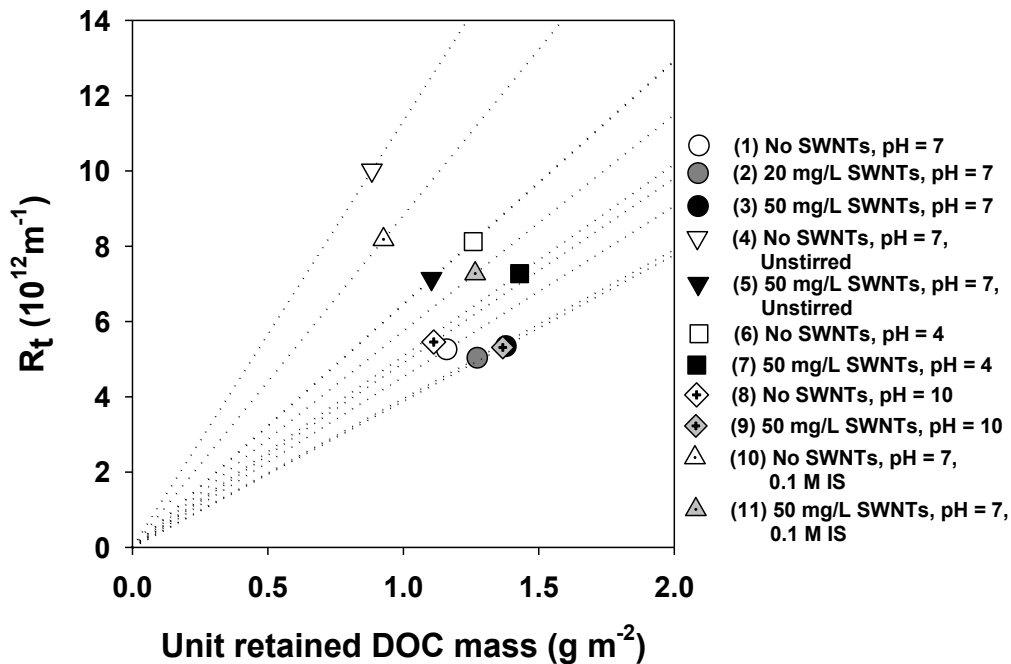


**Figure 5.4.** Comparison of UF fouling resistances as a function of unit retained DOC mass in the absence and presence of SWNTs. Operating conditions:  $\Delta P = 3$  bar (300 kPa); DOC = 8 mg L<sup>-1</sup>; SWNTs = 20 and 50 mg L<sup>-1</sup>; conductivity = 300 and 11,400  $\mu\text{S cm}^{-1}$ ; pH = 7; pre-contact time with SWNTs = 1 h.

The HA deposited on the membrane surface appeared to correlate with the resistance of the cake layer. To observe this effect, the fouling resistance trends in both

SWNTs–UF and UF alone were quantified with membrane resistances per unit retained DOC mass ( $\delta$ ), which is conceptually similar to specific cake resistance [16, 169]. The UF alone and SWNTs–UF at a VCF of 3.5 yielded specific cake resistances per unit retained DOC of  $4.53 \times 10^{12} \text{ m g}^{-1}$ ,  $3.95 \times 10^{12} \text{ m g}^{-1}$ , and  $3.87 \times 10^{12} \text{ m g}^{-1}$  for 0, 20, and 50  $\text{mg L}^{-1}$  SWNTs, respectively. These values clearly showed specific fouling resistances, as plotted in Figure 5.4 and quantified in Table 5.2. After adsorption of HA, most SWNTs–UF cases showed a slightly lower  $R_c/R_f$  ratio than that observed for the UF process alone. Considering the specific fouling resistances, SWNTs–UF resulted in greatly reduced membrane resistances per unit retained DOC mass. It appears that the characteristics of the fouling layer were more dependent on the HA deposition and HA adsorptive fouling since single SWNTs with a length of 5–30  $\mu\text{m}$  are somewhat too large to block the membrane pores. These results showed that membrane fouling resistances per unit retained DOC could be improved with the addition of SWNTs.

### 5.3.4 Fouling mechanism and cake filtration

To analyze the flux decline data of HA solutions during UF filtration,  $J^2$  versus time was plotted for both SWNTs–UF and UF alone in unstirred conditions, as shown in Figure 5a. As discussed in Background (Chapter III), model constants  $\alpha$  and  $\beta$  were evaluated for experimental flux data by flux modeling, as applied in Eq. 3.14. It was previously mentioned that the linear slope after an initial filtration in  $t/V$  versus  $V$  was caused by the formation of a cake layer, and a membrane filtration index (MFI) was obtained to compare SWNTs–UF and UF alone throughout the filtration process, as listed in Table

5.3. The fitting results applied to the flux modeling were well matched, with  $R^2 = 0.94$  and 0.99 for the UF process alone and for SWNTs–UF, respectively.

**Table 5.3** Membrane fouling analyses for HA filtration in UF and UF-SWNTs without stirring.

Process	Flux model				Fouling model					
	$\alpha$ ( $\text{min}^2$ $\text{m}^{-2}$ )	$\beta$ ( $\text{min}$ $\text{m}^{-2}$ )	$r^2$	MFI ( $\text{min}$ $\text{m}^{-2}$ )	Intermediate blocking			Cake filtration		
					a	b	$r^2$	a	b	$r^2$
UF	53,893	4,899	0.94 4	1,225	0.004 4	0.004 8	0.96 5	11.4 7	2.1 7	0.92 1
UF-SWN Ts	47,284	3,170	0.98 5	793	0.004 2	0.004 0	0.97 7	8.78	1.9 2	0.91 9

TMP = 3.0 bar

It was evident that at higher HA concentrations with the UF process alone, the combined HA concentration increased on the membrane surface, and the resultant cake formation led to increasingly more dominant resistance for the solvent flux. This result was attributed to the higher MFI for the UF process alone because the MFI was in proportion to the cake layer formation. As previously stated, many researchers have reported that HA could be a dominant foulant and may cause irreversible fouling. In particular, adsorptive hydrophobic interactions between HA and hydrophobic membranes should cause significant membrane fouling.

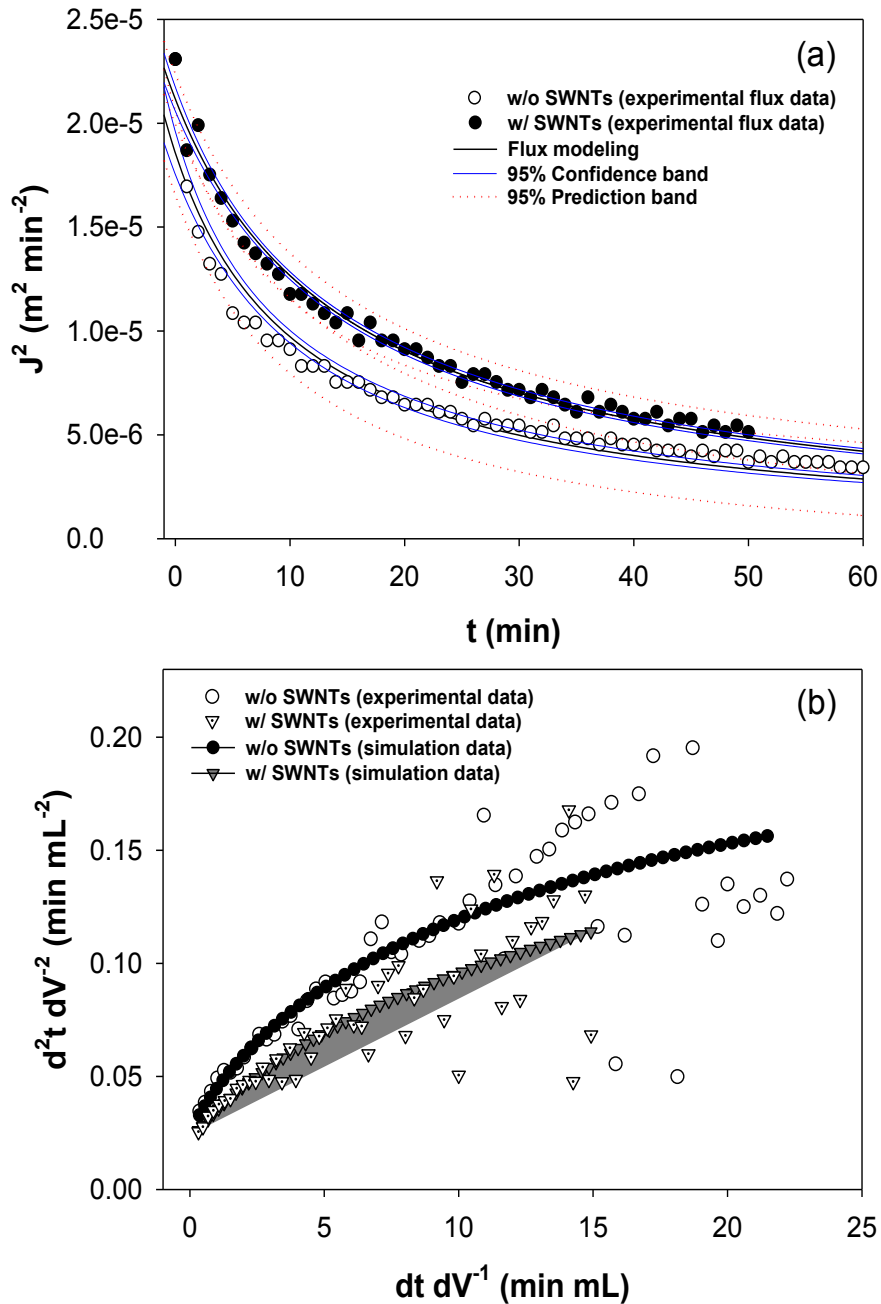


**Figure 5.5** Flux decline analyses for HA filtration in the absence and presence of SWNTs: (a) Flux modeling and (b) membrane fouling analyses. Operating conditions: unstirred with constant  $\Delta P = 3$  bar (300 kPa); DOC =  $8 \text{ mg L}^{-1}$ ; SWNTs =  $50 \text{ mg L}^{-1}$ ; conductivity =  $300 \mu\text{S cm}^{-1}$ ; pH = 7; pre-contact time with SWNTs = 1 h.

Hermia's approach was applied to characterize the fouling mechanisms under constant pressure with dead-end filtration with plots of  $d^2t/dV^2$  versus  $dt/dV$  as shown in

Figure 5.5b. The formed curve was considered to exhibit the blocking behavior index  $\phi$  (discussed in Background, Chapter III). When the experimental data were evaluated directly, the value of the blocking index  $\phi$  was highly sensitive owing to the fluctuation of the flux data, which yielded negative  $\phi$  values in some stages. This result was caused by the failure of fouling mechanisms to explain the experimental data, as shown by two symbols, in Figure 5.5b. Therefore, the simulated fitting polynomials with  $R^2$  values of more than 0.99 were applied to analyze the experimental data for the entire filtration process. The slope of the simulated data curve indicates the blocking index  $\phi$  at that filtration stage. In the early stages of filtration under unstirred conditions,  $\phi$  was 0.5 for both the SWNT–UF and UF-alone processes, which was close to that observed in the intermediate blocking model. Subsequent UF-alone filtrations showed a decreasing slope trend with  $\phi$  values up to 0.4 and 0.3, and finally to 0 (simulated data) for SWNT–UF and UF-alone process. However,  $\phi$  values of SWNTs–UF decreased more slowly than that observed in the UF-alone process. These facts roughly indicate that the early stages of UF filtrations were more dependent on intermediate blocking or a combination of intermediate blocking and cake filtration. However, cake filtration became the more dominant mechanism as filtration progressed and a fouling layer developed. In these subsequent filtrations, the first stages of both SWNTs–UF and UF alone did not clearly show early pore blocking even though the main resistance was attributed to adsorptive fouling. However, on the basis of blocking laws, when the HA concentration was comparatively high in the early stages, all of the membrane pores appeared to have been blocked quickly, and successive delivery of HA began to transition to cake/gel filtration. Cake/gel formation then dominated the entire filtration process, with subsequent HA

arriving at the cake/gel layer that previously formed on the membrane surface. These results complied well with the previous resistance-in-series model results, as tabulated in Table 5.2, in which the cake resistance in the unstirred conditions sharply increased with the buildup of the cake/gel layer.

**Table 5.4** Empirical dead-end filtration blocking laws in their linearized form with blocking indexes.

Blocking Laws	$\phi$	Linearized Equations
Complete blocking	2	$-\ln (J/J_0) = at + b$
Standard blocking	1.5	$t/V = at + b$
Intermediate blocking	1	$1/J = at + b$
Cake filtration	0	$t/V = aV + b$

Note:  $J$ , flux;  $J_0$ , initial flux;  $V$ , filtrated volume;  $t$ , filtration time;  $a$  and  $b$  are constants, respectively.

The linear forms of filtration laws described in section S4 were applied to identify the fouling mechanism functioning with HA and the hydrophobic membrane under unstirred conditions, as summarized in Table 5.4. Further, to observe the stirring effect during filtration, constant pressure filtration laws were applied, as shown in Figure 5.6, that were similar to work previously performed using Aoustin's approach [17]. As demonstrated in Figure 5.6, the effect of stirring was extremely high because both extensive CP during filtration and a high concentration were achieved prior to cake/gel formation.

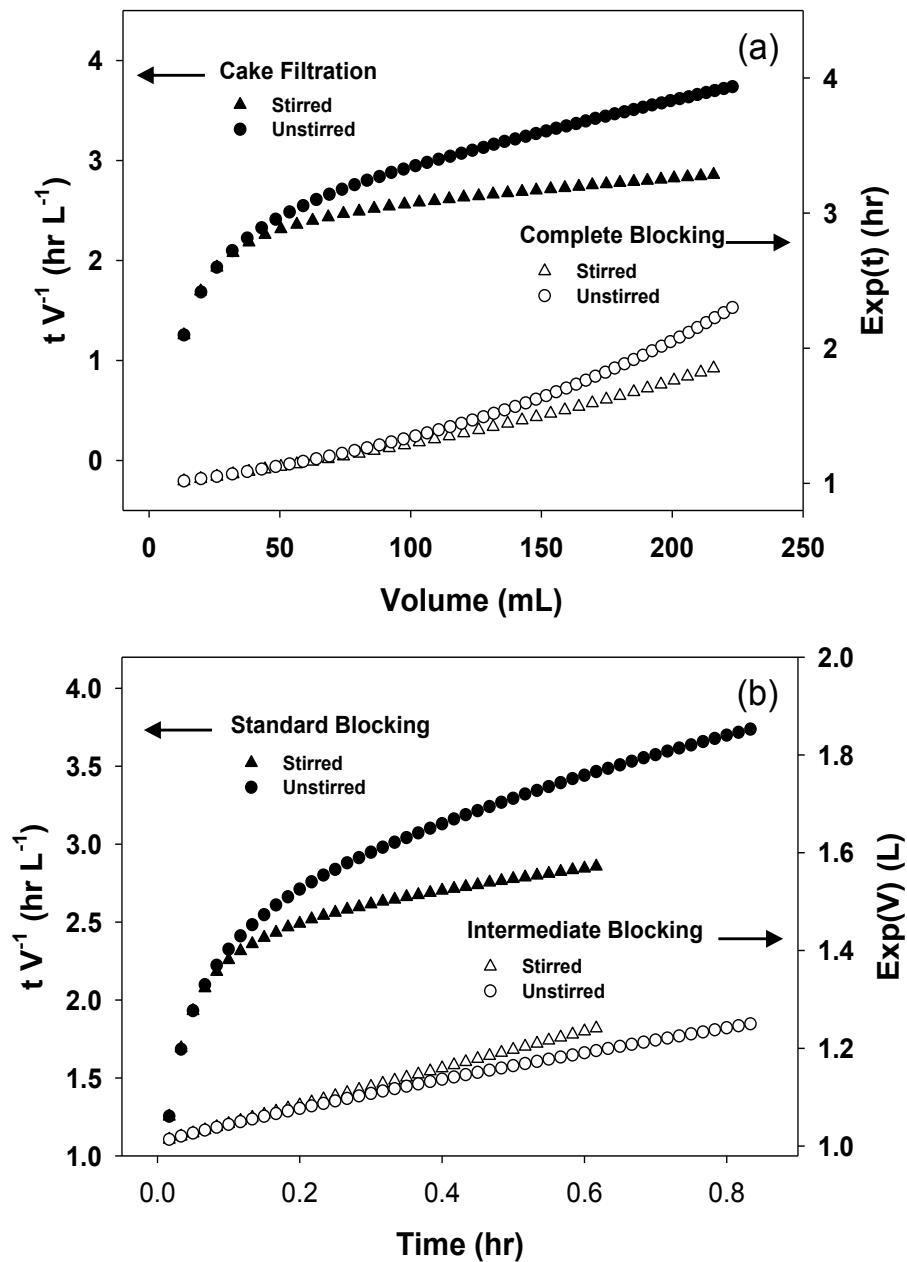


**Figure 5.6** Influence of stirring on filtration law analyses for HA filtration in UF-SWNTs: (a) Cake filtration and complete blocking analysis and (b) standard blocking and intermediate blocking analysis. Operating conditions:  $\Delta P = 3$  bar (300 kPa); DOC = 8 mg L<sup>-1</sup>; SWNTs = 50 mg L<sup>-1</sup>; conductivity = 300  $\mu$ S cm<sup>-1</sup>; pH = 7; pre-contact time with SWNTs = 1 h.

The results after application of the filtration laws demonstrate that intermediate blocking shows an excellent fit ( $R^2 = 0.98$  and  $0.97$  for SWNTs–UF and UF alone) with

the experimental data at ambient conditions (Table 5.3). This finding could be in disagreement with that of previous authors such as Jucker and Clark [163], who reported that membrane inner pore sites have the top priority for the adsorption of humic substances on a hydrophobic membrane, indicating standard blocking. However, under unstirred conditions, it was noted that the fouling mechanisms of HA in SWNTs–UF were mainly linked to cake filtration in later stages, allowing for the possibility that complete blocking was to some extent responsible for membrane fouling due to the wide range of molecular weights in HA.

### 5.3.5 DOM transport in UF-SWNTs system

Figs. 5.7a and 5.7b show the results of normalized permeate flux and HA rejection trends under the influence of various applied pressures for SWNTs–UF (10 kDa and SWNTs of 50 mg L<sup>-1</sup>) and UF alone, respectively. Operational conditions 1, 2, and 3 correspond to the respective applied pressure values of 1 bar (100 kPa), 3 bars (300 kPa), and 6 bars (600 kPa). Figure 5.7a shows an important 11–13% increased flux result at 1 bar with SWNTs and an increased fouling potential of these adsorbents with higher applied pressure (higher permeability), which indicates that the adsorbent on membrane fouling could be a function of hydrodynamic and operational conditions. The average observed rejections of HA as DOC through overall VCF were 87, 74, and 63% in SWNTs–UF and 82, 63, and 56% in UF alone at applied pressures of 1, 3, and 6 bars, respectively. The 3D plot of HA rejection trends in terms of both VCF and applied pressure clearly shows the effect of added SWNTs (Figure 5.8).



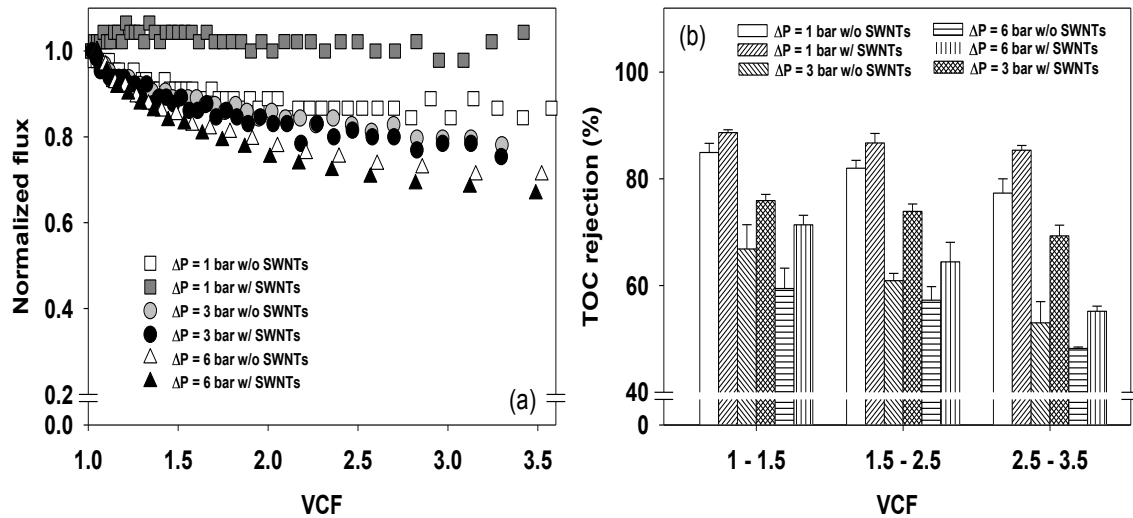


**Figure 5.7** Influence of applied pressure on flux decline and HA rejection based on DOC in the absence and presence of SWNTs: (a) Normalized flux decline and (b) HA rejection at different applied pressures. Operating conditions:  $\Delta P = 1$  bar (100 kPa), 3 bar (300 kPa), and 6 bar (600 kPa); DOC = 8 mg L<sup>-1</sup>; SWNTs = 50 mg L<sup>-1</sup>; conductivity = 300  $\mu$ S cm<sup>-1</sup>; pH = 7; pre-contact time with SWNTs = 1 h.

SWNTs–UF clearly presented improved rejection trends compared to UF alone (Figure 5.8b). The observed HA rejections versus operating pressure were analyzed to match the linear parameter estimation of  $R^2 = 0.86$ – $0.96$ , as described in Chapter III and shown in Figure 5.8. As the applied pressure was increased from 100 to 600 kPa, the rejections were dramatically reduced from 87 to 63% for SWNTs–UF and 82 to 56% for UF alone. It can be concluded that observed DOC rejections decrease when relatively high pressure is applied because such pressure can increase the  $J_v$  magnitude even though other operating conditions such as HA concentration, stirring speed, and VCF remain constant. Similar behavior was previously reported [14, 170] in which NOM rejection in UF membranes varied up to 50% with various applied pressures.

These results could be more specifically explained by several factors. A large solvent flux magnitude with high applied pressure (6 bars) could cause more dominant

convective systems in NOM transport both in SWNTs–UF and UF alone. Therefore, back diffusion could not effectively contribute to observed DOC rejection because it was additionally affected by a stirring speed of 300 rpm. This result was in accordance with earlier studies by Lahoussine-Turcaud [171], which suggest that back transport of HA away from the membrane—essentially, back diffusion—was insufficient to overcome convective transport toward the membrane, leading to the buildup of a cake/gel layer of HA near the membrane surface.

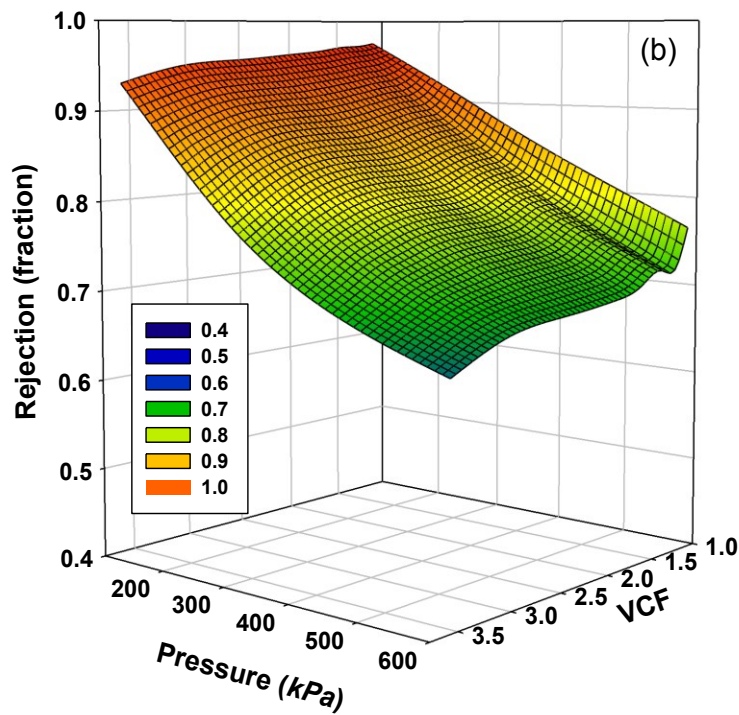
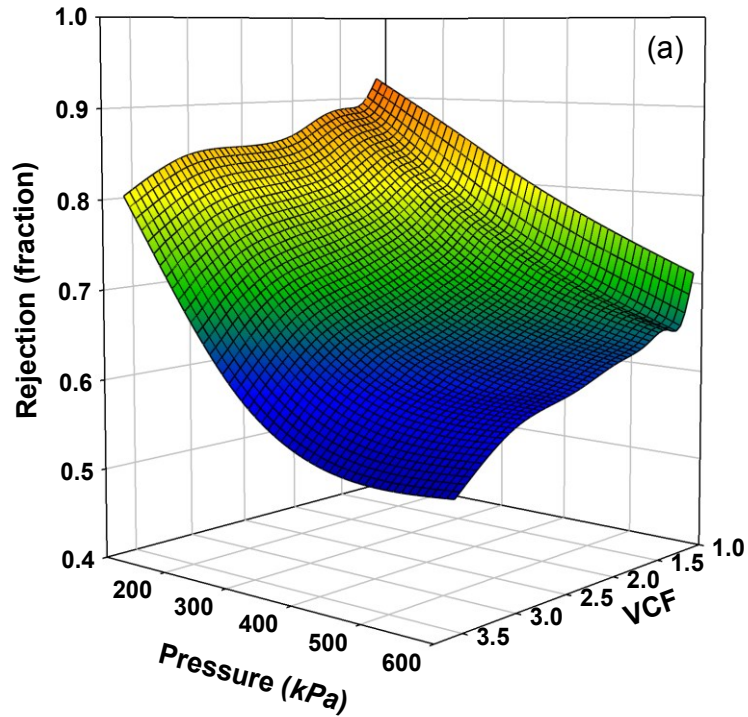


**Figure 5.8** Comparison of HA rejection trends with respect to both VCF and pressure in the absence and presence of SWNTs: (a) In the absence of SWNTs and (b) in the presence of SWNTs. Operating conditions:  $\Delta P = 1$  bar (100 kPa), 3 bar (300 pKa), and 6 bar (600 kPa); DOC = 8 mg L<sup>-1</sup>; SWNTs = 50 mg L<sup>-1</sup>; conductivity = 300  $\mu$ S cm<sup>-1</sup>; pH = 7; pre-contact time with SWNTs = 1 h.

The extent of convective transport depends on flux; thus, its flux decline ( $J/J_o = 71\%$ ) occurred more sharply at high applied pressure than that observed at low applied pressure ( $J/J_o = 87\%$ ). In addition, the high flux for SWNTs–UF and UF alone could cause severe CP and membrane–solute interaction or a cake/gel layer, even with stirring. When the membrane rejects the DOM, the concentration of DOM increases adjacent to the membrane surface rather than in the bulk solution, which in turn leads to the formation of a CP layer. If this CP layer gradually increases the hydraulic resistance across the membrane and limits the permeate flux, the rejection of NOM undergoes a new phase of reduced rejection trends due to the high concentration of NOM on the membrane surface.

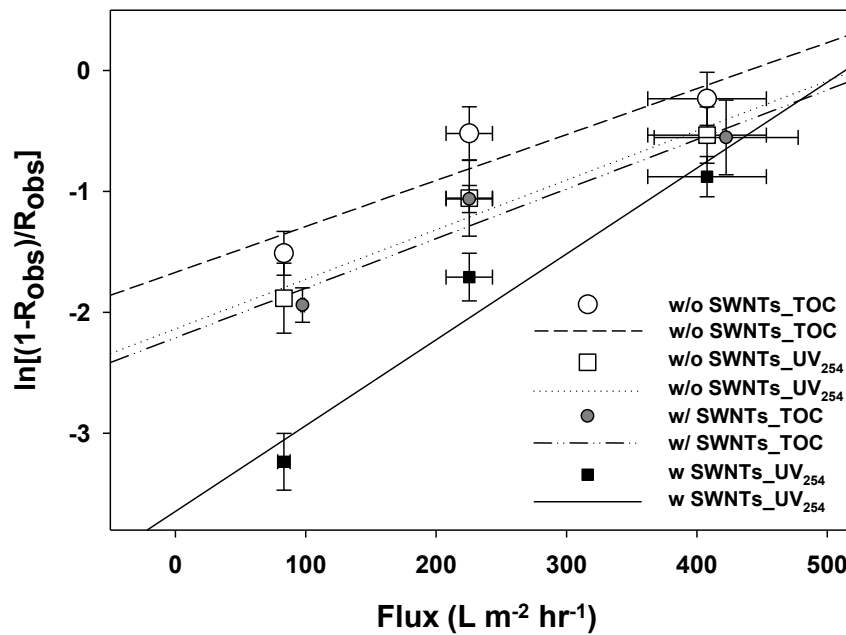


**Figure 5.9** Application of transport mechanisms for real rejection trends and transport parameters ( $l/k$  and  $\sigma$  membrane selectivity) of humic acid with UF-SWNTs. Operating conditions:  $\Delta P = 1$  bar (100 kPa), 3 bar (300 pKa), and 6 bar (600 kPa); DOC = 8 mg L<sup>-1</sup>; SWNTs = 50 mg L<sup>-1</sup>; conductivity = 300  $\mu$ S cm<sup>-1</sup>; pH = 7; pre-contact time with SWNTs = 1 h.

**Table 5.5** Observed and real rejection results of HA in UF and UF-SWNTs according to concentration polarization model.

Process	TMP (bar)	VCF	$J_v$ (LMH)	$J_v/k$	$C_m$ (mg L <sup>-1</sup> )	$R_{obs}$	$R_{real}$	$\sigma$
UF	1.0	1 – 1.5	88.5 (2.1)	0.34 (0.01)	10.7 (0.1)	0.85	0.89	0.84
		1.5 – 2.5	81.5 (1.3)	0.31 (-)	10.3 (0.1)	0.82	0.86	
		2.5 – 3.5	78.0 (-)	0.30 (-)	10.1 (0.1)	0.77	0.82	
	3.0	1 – 1.5	242.7 (7.2)	0.92 (0.03)	17.1 (0.9)	0.67	0.83	
		1.5 – 2.5	223.3 (8.3)	0.85 (0.03)	15.4 (0.5)	0.61	0.78	
		2.5 – 3.5	202.5 (3.5)	0.77 (0.01)	13.7 (0.5)	0.53	0.71	
	6.0	1 – 1.5	455.3 (26.5)	1.73 (0.10)	31.4 (4.1)	0.59	0.89	
		1.5 – 2.5	393.3 (18.6)	1.49 (0.07)	24.8 (2.1)	0.57	0.86	
		2.5 – 3.5	358.0 (5.7)	1.36 (0.02)	19.9 (0.4)	0.48	0.78	
SWNTs-UF	1.0	1 – 1.5	98.3 (1.2)	0.40 (-)	8.9 (-)	0.89	0.92	0.90
		1.5 – 2.5	97.0 (2.0)	0.40 (0.01)	8.8 (0.1)	0.87	0.91	
		2.5 – 3.5	97.0 (-)	0.40 (-)	8.7 (-)	0.85	0.90	
	3.0	1 – 1.5	242.7 (7.2)	0.99 (0.03)	17.8 (4.1)	0.76	0.89	
		1.5 – 2.5	223.3 (8.3)	0.92 (0.03)	15.7 (4.1)	0.74	0.88	
		2.5 – 3.5	202.5 (3.5)	0.83 (0.01)	14.1 (4.1)	0.69	0.84	
	6.0	1 – 1.5	480.4 (24.9)	1.97 (0.10)	36.0 (4.2)	0.71	0.95	
		1.5 – 2.5	407.3 (22.7)	1.67 (0.09)	25.2 (3.1)	0.64	0.90	
		2.5 – 3.5	358.0 (5.7)	1.47 (0.02)	18.9 (0.6)	0.55	0.84	

Standard deviations are indicated in parentheses.

DOM transport characteristics for real rejection trends and transport could be quantified with transport parameters  $J_v/k$  and membrane reflection coefficient  $\sigma$  in both SWNTs–UF and UF alone, as described in Chapter III. Additionally, diffusive and convective transportation of DOM through membrane filtration could be quantitatively

achieved with the pore Péclet number ( $P_e$ ). To investigate the NOM transport characteristics of both SWNTs–UF and UF alone in terms of DOC and  $UV_{254}$ ,  $\ln (1 - R_{obs}/R_{obs})$  against  $J_v$  was plotted to determine  $k$  (mass transfer coefficient) and  $\sigma$  (reflection coefficient), as shown in Figure 5.9. Similar analyses to determine  $k$  were also performed in stirred dead-end ultrafiltration or cross-flow ultrafiltration experiments by previous researchers [170, 172]. By applying Eq. 3.8, which neglects the diffusion portion from Tandon’s approach [Eq. 3.9] because DOM transport phenomenon showed only one trend (decreasing  $R_{obs}$  with increasing  $J_v$ , as shown in Figure 5.7), the results show that DOM transport through UF was dominated by convection rather than diffusion in these UF filtration systems. This result could be confirmed by the determined pore  $P_e$  ( $P_e \gg 1.0$ ). Table 5 shows  $k$  and  $\sigma$  for SWNTs–UF and UF alone under initial conditions of DOC  $8\text{mg L}^{-1}$ , conductivity  $300\ \mu\text{S cm}^{-2}$ , and pH 7.5. The results show  $0.24$  and  $0.26\ \text{m h}^{-1}$  for  $k$  and  $0.90$  and  $0.84$  for  $\sigma$ , respectively. Thus, the membrane selectivity value of SWNTs–UF was higher than that for UF alone, as expected. This result implies that the selectivity of the SWNT–UF system for the DOM was quite high and that the convective transport of DOM largely progressed through SWNT–UF systems. (If  $\sigma$  is 1, DOM transport through the membrane is entirely convection-dependent.) A similar approach was also chosen by previous researchers [61], although their study was performed using an NF membrane. Lee et al. (2004) suggested that the reflection coefficient was not significantly influenced by the system’s hydrodynamic conditions in NF transport systems, which could be attributed to the supposition that the reflection coefficient is an intrinsic membrane characteristic parameter in NF, as is pure water permeability. Hence,

the value remains constant for a given solute–membrane system unless the feed water chemistry and temperature are changed.

#### **5.4 Conclusions**

On the basis of an investigation of SWNTs–UF with controlled membrane fouling and rejections, the following conclusions were derived: (i) The SWNTs–UF exhibited increased rejection trends as a result of SWNT binding site adsorption of HA during VCF-dependent fouling runs under various feed water hydrodynamic and solution conditions. Moreover, the addition of SWNTs to the UF process did not significantly exacerbate the permeate flux decline, which may be due to the stacking of SWNTs on the membrane surface, thereby maintaining a porous layer that permits the passage of water with no additional fouling resistance. (ii) The application of a resistance-in-series model, whereby HA fouling resistances are mainly attributed to adsorptive fouling, indicated that SWNTs–UF likely provides a greatly reduced membrane resistance per unit retained DOC mass, as compared to UF alone. Moreover, the characteristics of the fouling layer and resistances were more dependent on HA deposition and HA adsorptive fouling rather than fouling contribution from SWNTs because the SWNTs were too large to block the membrane pores. (iii) On the basis of blocking laws, the early stages of both SWNTs–UF and UF alone in unstirred conditions were more dependent on intermediate blocking or a combination of intermediate blocking and cake filtration, while cake filtration became the more dominant mechanism as filtration progressed. This result this was caused by the development of the fouling layer. (iv) The SWNTs–UF presented significantly improved rejection trends with various VCFs and applied pressures; this can be seen from the DOM

transport parameters. Overall, SWNTs–UF has been shown to be effective in the improvement of membrane performance through neither attenuate flux nor total membrane resistances. The use of SWNTs to control membrane fouling appears to be a function of hydrodynamic and operational conditions. Therefore, a hybrid membrane process using SWNTs should be useful for future applications to more challenging water treatment issues.

### **Acknowledgements**

This research was supported by the GS E&C Research Institute and the University of South Carolina.



## CHAPTER 6

### REMOVAL OF MICROPOLLUTANTS AND NOM IN SINGLE WALLED CARBON NANOTUBE-UF MEMBRANE SYSTEM FROM SEAWATER\*

\*Reprinted here with permission of publisher: Heo et al., Removal of Micropollutants and NOM in Carbon Nanotube-UF Membrane System from Seawater, Water Science & Technology 63 (2011) 2737-2744.

#### **Abstract**

One of the main problems for seawater reverse osmosis desalination (SWRO) is membrane fouling associated with natural organic matter (NOM). Bisphenol-A (BPA) and 17 $\alpha$ -ethinylestradiol (EE2) are well-known endocrine-disrupting compounds (EDCs) that have been detected in wastewater and seawater. In this study, the contribution of single walled carbon nanotubes (SWNTs, single-walled carbon nanotubes in this study) to membrane fouling control and the potential adsorption mechanisms of BPA and EE2 were investigated using artificial seawater (ASW) in a bench scale ultrafiltration (UF) membrane coupled with SWNTs. For high ionic strength ASW, UVA<sub>254</sub> nm is a good alternative for highly aromatic dissolved organic carbon (DOC) determination, with a very strong linear relationship ( $R^2 \geq 0.99$ ) with increasing DOC concentrations. Approximately 80% of DOC in ASW was rejected by the SWNTs-UF system where DOC of 31% was removed due to adsorption by SWNTs. The presence of SWNTs shows a 20% increase in membrane flux in ASW. A strong linear correlation between retention and adsorption of BPA and EE2 was obtained. The percentage of adsorption/retention of

BPA and EE2 in UF-SWNTs follows the order: 94.0/96.6 (DI+SWNTs, EE2) > 86.2/90.0 (ASW+SWNTs, EE2) > 73.6/78.9 (DI+SWNTs, BPA)  $\geq$  74.1/77.3 (ASW+SWNTs, BPA) > 29.8/29.8 (ASW, EE2)  $\cong$  27.3/27.3 (ASW, BPA)  $\geq$  25.3/25.3 (DI, EE2)  $\cong$  24.8/24.8 (DI, BPA). This indicates that retention by the UF-SWNTs system is mainly due to adsorption. Overall, EE2 adsorption was greater than BPA during the UF-SWNTs experiments, presumably due to the higher hydrophobicity of EE2 than BPA.

**Keywords:** Bisphenol A; 17 $\alpha$ -ethinylestradiol, Artificial seawater, Ultrafiltration, Single walled carbon nanotubes, Adsorption, Retention

## 6.1 Introduction

While water scarcity is common in arid regions, pollution and the use of groundwater aquifers and surface water have led to a reduction in the quantity and/or quality of available natural water resources in many countries. Both desalination and water reuse have been successfully implemented to provide fresh water to communities; these processes use conventional water treatment systems and require fresh water resources, respectively [173, 174]. The use of reverse osmosis (RO) membranes in seawater desalination has increased over the last decade, with materials improving and costs decreasing. One of the major problems for seawater RO (SWRO) is membrane fouling associated with natural organic matter (NOM) and inorganics. Therefore, there is a higher tendency for membrane fouling to occur when seawater and brackish water resources are treated than when surface water and groundwater resources are treated, and thus, sea and brackish water require extensive pretreatment [32].

Organic micropollutants, such as endocrine disrupting compounds (EDCs) and pharmaceuticals and personal care products (PPCPs), can mimic natural hormones in the endocrine system and have been linked to a variety of adverse effects in both humans and animals [3, 175]. More recently, EDCs and PPCPs– groups of emerging contaminants – have been discovered in various surface, wastewater effluent, and seawater near big cities around the world. Some of these contaminants have been linked to ecological impacts at trace concentrations [81, 176-183]. In seawater, levels of several EDCs, including nonylphenolmixture, bisphenol A (BPA), and 17 $\alpha$ -ethinylestradiol (EE2) ranged from 31 to 1,777 ng/L, 11 to 777 ng/L, and 10 to 269 ng/L, respectively [183]. BPA, which is widely used as an important intermediate in the production of epoxy resins, polycarbonate plastics, polysulfone, and certain polyester resins, belongs to the well-known phenolic EDCs [82]. Previous studies have shown that BPA leached out of polycarbonate plastic materials and epoxy resin during autoclaving. This has recently been a matter of interest due to the effects of low doses of BPA on human health, especially in early postnatal exposures [184, 185]. Moreover, 213.1 ng/g of BPA was also detected in locally purchased crab samples [176]. The synthetic estrogen EE2 represents the most active estrogen used in birth control and its toxicity is 10–50 times higher than 17 $\beta$ -estradiol (a natural sex hormone) [186]. In an aquatic environment, EDCs are expected to accumulate in living organisms and negatively affect the reproductive system, such as male fish feminization, sexual disruption, and smoltification [187, 188].

The discussion about the direct effect of EDC in seawater on human health is still controversial because the concentrations of EDCs are expected to be very low (pg to ng/L) due to the higher dilution and/or the short half-life of EDCs in the marine environment

[176, 177, 189, 190]. The release, fate, and potential effect of EDCs in the marine environment, however, have been investigated for the following reasons: (i) There is a potential of net uptake and accumulation of EDCs in living organisms [191], (ii) there is also a possibility for differences in concentration with respect to limited water exchange, different charges of wastewater treatment plant effluent water, and the high variability of water bodies [189], and (iii) due to EDCs' hydrophobic nature, they have the potential for adsorption onto suspended and bed sediments in the marine environment and some of them are characterized as slowly biodegradable in natural and seawater [93, 192].

Thus far, coagulation is the most popular treatment process used for the removal of potential foulants such as aqueous particulate and colloidal matter. However, conventional water treatment such as coagulation, chlorination, flocculation and sedimentation could not completely remove many EDCs and PPCPs [10, 79, 193]. As an advanced treatment technology, the membrane process employing ultrafiltration (UF) is widely used as a separation technology in the filtration of aqueous mixtures for drinking water, wastewater treatment, and seawater desalination. These membranes can remove micropollutants, pathogens and other microbes and natural organic matter (NOM). Also, since the conventional process needs to be carefully designed and diligently operated, there has been an increased tendency toward using UF membranes instead of conventional treatments to provide silt density index values well below 2, which thus enables an SWRO plant to perform at its original design capacity with reduced downtime [194]. Adsorbents are favorable to UF membranes due to the membranes' poor removal efficiency of small substances [195]. The most intensively studied adsorbent for UF filtration is powdered activated carbon (PAC). However, there are contradictory results

concerning the effect of PAC on membrane fouling. Some studies reported an improvement of permeate flux, longer filtration runs, or a reduced frequency of chemical cleaning [120, 157], while others reported similar flux performance or exacerbated flux decline compared to that of a UF membrane alone [122, 196].

Recently, carbon nanotubes (CNTs) have drawn special attention in the research community due to their unique properties and potential environmental applications: sorbents, high-flux membranes, depth filters, antimicrobial agents, environmental sensors, renewable energy technologies, and pollution prevention strategies [105, 106]. In addition, CNT technology has the potential to support point of use water treatment, since unlike many microporous adsorbents, CNTs possess a fibrous shape with a high aspect ratio, large accessible external surface area, and well developed mesopores, all contributing to the superior removal capacities of these macromolecular biomolecules and microorganisms [45]. Due to these unique characteristics of CNTs, the potential applications of CNT-UF can be enormous in water/wastewater treatment/reclamation and seawater desalination, although they have not yet been studied.

The objective of this study is to determine the SWNTs contribution to the transport of micropollutants (BPA and EE2 in this study) and NOM across single-walled carbon nanotubes (SWNTs)-UF membrane treatment systems. Bench-scale experiments were conducted with synthetic seawater spiked with BPA and EE2 in the absence and presence of SWNTs. Seawater spiked with an EDC compound mixture was subjected to several parallel bench-scale experiments to determine the SWNT contribution to the BPA and EE2 removal and the fouling control of the UF membrane. To the best of our knowledge,

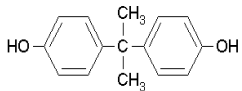
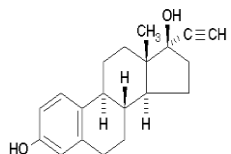
no work has been conducted to date to determine the removal of EDCs and NOM using CNT-UF hybrid systems for seawater.

## **6.2 Materials and methods**

### **6.2.1 Model compounds**

High purity BPA and EE2 (>99%) were purchased from Sigma-Aldrich (Sigma, St. Louis, MO, USA). The physicochemical characteristics of these compounds are described in Table 6.1. For this study, BPA and EE2 were selected because they have been commonly detected in water, wastewater, and wastewater effluent influenced seawater. Because the BPA (plasticizer) and EE2 (synthetic estrogen) have different structure and functional groups, they show different characteristics of hydrophobicity ( $\log K_{OW}$ ), solubility, and  $pK_a$  values. The water solubility of BPA (300 mg/L) is significantly higher than that of EE2 (9.2 mg/L) at 25°C. Both compounds are neutral species at pH below approximately 9.5 based on their  $pK_a$  values. Stock solutions of BPA and EE2 were initially prepared in methanol at 1 mM each to obtain total soluble conditions. The stock solutions were then diluted with ultrapure deionized (DI) water to five different concentrations of 10, 50, 100, 500, and 1,000 nM for the calibration run. The BPA and EE2 solutions, each with a concentration of 1  $\mu$ M, were both placed in together in one beaker and the methanol was evaporated in order to minimize the dissolved organic carbon (DOC) from the solvent introduced into the experiments.

**Table 6.1.** Characteristics of BPA and EE2

Common name (Abbreviation)	Use	MW (g/mole)	Log K <sub>OW</sub>	pK <sub>a</sub>	Water solubility (mg/L) <sup>a</sup>	Structure
Bisphenol A (BPA)	Plasticizer	228.1	3.3	9.6 to 10.2	300	
17 $\alpha$ -ethinylestradiol (EE2)	Ovulation inhibitor	296.2	3.7	~10.5	9.2	

<sup>a</sup>[197].

### 6.2.2 UF membranes

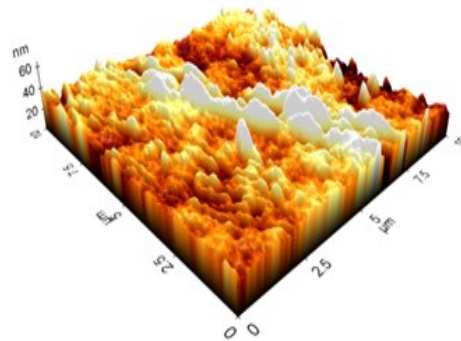
A commercially available flat sheet UF membrane having a nominal molecular weight cut-off (MWCO) of 5,000 Daltons was obtained from Koch Membrane Systems Inc. (Wilmington, MA, USA). The UF membrane, made of polyethersulfone (PES), was selected to examine the effect of adsorption on BPA and EE2 retention. In addition, the UF membrane was desirable for the application of desalination pretreatment due to its durability in high salt environments, as specified by the manufacturer. The detailed characteristics of the membrane are shown in Table 6.2. The membrane zeta potential, associated with the streaming potential, was determined at pH 7.5 and a conductivity of 300 S/cm NaCl using an electro kinetic analyzer (ELS8000, Otsuka Electronics, Osaka, Japan) following an established procedure [124]. The UF membrane is negatively charged based on its zeta potential value. A goniometer (Rame-Hart Inc., Model 100, Netcong, NJ, USA) was used to measure the contact angle of the membrane. Contact angles were measured by a sessile drop method – the water droplet method – based on measuring the contact angles between the water droplet and the membrane surface [124].

According to the contact angle determination, the UF has relatively low hydrophobicity. Atomic force microscopy (AFM, XE-100, PSIA, Seoul, South Korea) was used to analyze the surface morphology and roughness of the membrane. Small squares of the prepared membranes were cut and glued on a glass substrate. The membrane surfaces were imaged in a scan size of  $3\ \mu\text{m} \times 3\ \mu\text{m}$ . The pure water permeability (PWP) measured at 552 kPa using a stirred cell ranged from 0.38 to 0.44 L/hr-m-kPa. Each new membrane was soaked in DI water for at least 24 hr at a temperature of  $21 \pm 1^\circ\text{C}$  prior to use. During this period, the DI water was replaced several times with a new volume of pure water. The DOC of the final rinse water was checked to assure that it was at a negligible level.

**Table 6.2.** Ultrafiltration membrane characteristics

Characteristics of membrane	HFk-328 (UF)
MWCO (Daltons)	5,000
Zeta potential (mV)	-24.9
Contact angle ( $^\circ$ )	42
Applied pressure (kPa)	538– 601
PWP (L/hr-m <sup>2</sup> -kPa)	
<i>Average</i>	<i>0.42</i>
<i>(min-max)</i>	<i>0.38-0.44</i>
<i>c.v.<sup>a</sup> (%)</i>	<i>6.5</i>

AFM image of clean membrane



PWP is pure water permeability.

<sup>a</sup>c.v. is coefficient variance.

### 6.2.3 Preparation of artificial seawater



In order to investigate the removal of BPA, EE2, and NOM, a synthetic solution simulating artificial seawater (ASW) was used. The following salts of ASW were purchased from Sigma-Aldrich (Sigma, MO, USA) and Fisher Scientific (Fisher, MA, USA): NaCl, Na<sub>2</sub>SO<sub>4</sub>, KCl, NaHCO<sub>3</sub>, MgCl<sub>2</sub>, and CaCl<sub>2</sub>. ASW solutions were prepared using DI water according to the Kester and Duedall formula [198]. Trace components-free ASW with a slightly different composition was used in 1 L DI water (23,926 mg NaCl, 4,008 mg Na<sub>2</sub>SO<sub>4</sub>, 677 mg KCl, 196 mg NaHCO<sub>3</sub>, 53.27 mM MgCl<sub>2</sub>·6H<sub>2</sub>O, 10.33 mM CaCl<sub>2</sub>·2H<sub>2</sub>O). DOC (2 mg/L) was added in experiments as Suwannee River humic acid (SHA). SHA stock solutions were dissolved and filtered using a 0.45 µm polyvinylidene fluoride filter (Whatman, Buckinghamshire, UK) prior to use. Table 6.3 describes the characteristics of the ASW. NaOH or HCl were added to adjust the solution pH. The salinity of ASW was measured using a conductivity meter.

**Table 6.3.** Characteristics of standard seawater salt and ionic composition of ASW

Chemical Ion	Standard seawater % of total salt content	Concentration (mg/L)	
		Standard seawater <sup>a</sup>	Artificial seawater
Cl <sup>-</sup>	55.0	19,345	19,346
Na <sup>+</sup>	30.6	10,752	10,763
SO <sub>4</sub> <sup>2-</sup>	7.6	2,701	2,711
Mg <sup>2+</sup>	3.7	1,295	1,295
Ca <sup>2+</sup>	1.2	416	414
K <sup>+</sup>	1.1	390	355
HCO <sub>3</sub> <sup>3-</sup>	0.4	145	142
Br <sup>-</sup>	0.2	66	-
BO <sub>3</sub> <sup>3-</sup>	0.08	27	-
Sr <sup>2+</sup>	0.04	13	-
F <sup>-</sup>	0.003	1	-
DOC	-	-	2
TDS	-	35,000	35,026

<sup>a</sup>[198].

#### 6.2.4 CNT-UF membrane testing unit

BPA and E2 were put in contact with the UF membrane in the absence and presence of SWNTs of 10 mg/L at room temperature. The SWNTs (purity >90%) were purchased from Cheap Tubes, Inc. (Brattleboro, VT, USA) and used without further purification. The SWNTs had a length of 5–30  $\mu\text{m}$  and an outer diameter of 1–2 nm, as provided by the manufacturer. In order to investigate SWNTs-UF, a commercially available bench-scale stainless steel dead-end stirred-cell membrane unit (HP4750, SterliTech Corp., Kent WA, USA) coupled to a SWNTs reactor was used to evaluate flat-sheet membrane specimens for membrane retention and flux-decline. The cell accommodates 14.6  $\text{cm}^2$  flat sheet specimens. All of the experiments were performed at a stirring speed of 300 rpm, a constant initial pure water flux (232  $\text{L}/\text{m}^2\text{-hr}$ ), and pressures of 538–607 kPa. A fresh membrane was used for each experiment. The membrane was pre-compacted with DI water at a pressure of 827 kPa for 1 hr prior to use. The stability of the membrane permeability during the experiment was checked by comparing the pure water flux before and after each experiment. Only those membranes for which the permeability changes were less than 5% were included in the data presented here. A given sample with an initial volume of 100 mL was passed through the membrane until 40 mL of permeate were obtained, and the corresponding retentate was also obtained. This was repeated 10 times until a total of 400 mL of permeate was obtained. A mass balance based on each compound concentration was calculated by measuring the concentration of permeate and retentate, providing an estimate, by difference, of the compound adsorbed both onto the membrane surface and into the membrane pores. The removal of each compound was calculated and the flux-decline monitored as a function of volume, time, and cumulative

delivered or adsorbed mass. Delivered mass is defined as the amount of solute delivered per unit area to the membrane. Adsorbed mass is defined as the amount of solute adsorbed per unit area onto/into the membrane within the stirred-cell. These calculations were described previously [53]. The BPA and EE2 observed retention, collected  $i$  times,  $R_i$ , based on feed concentration, was calculated using Eq. 6.1:

$$R_i(\text{feed}), \% = \frac{C_f - C_p}{C_f} \times 100 \% \quad (6.1)$$

where  $C_f$  is the feed concentration ( $\mu\text{g/L}$ ) and  $C_p$  is the permeate concentration ( $\mu\text{g/L}$ ).

### 6.2.5 Analyses

A total organic carbon analyzer (TOC-V<sub>CSN</sub>, Shimadzu, Columbia, MD, USA) with a detection limit of 0.1 mg/L was used to measure DOC by a non-purgeable organic carbon method with high temperature combustion. This method has been widely used with low salt samples, but for high ionic samples, it gives variable values and uncertainties. Therefore, for the high salinity samples, we used the ultraviolet absorbance (UVA) measurement to indirectly determine DOC since UVA gives a more reliable accuracy for highly aromatic organics particularly humic substances. A UV-Vis spectrometer (Agilent 8453, Santa Clara, CA, USA) was used to determine DOC in ASW. Several membrane permeate and retentate samples were scanned with wavelengths ranging from 180 to 800 nm. Three wavelengths of 200, 254, and 400 nm were selected to determine the DOC. High-performance liquid chromatography (HPLC) was employed to determine BPA and EE2 concentrations using an Agilent 1200 Series (Santa Clara, CA, USA) at an excitation

wavelength of 280 nm and an emission wavelength of 310 nm for BPA and EE2. A Waters 5- $\mu$ m LiChrosorb® RP18 analytical column (4.6 mm $\times$  100 mm) was used for reverse-phase separations with a 100- $\mu$ L sample loop. The mobile-phase solvent profile was 45% DI water, acidified with 10 mM H<sub>3</sub>PO<sub>4</sub> and 55% MeOH for 30 min at a constant flow rate of 1 mL/min. The BPA and EE2 were eluted from the columns at 9.4 and 20.3 minutes, respectively. The detection limits were 0.88 nM (201 ng/L) for BPA and 0.96 nM (283 ng/L) for EE2.

## **6.3 Results and discussion**

### **6.3.1 Comparison of UVA with DOC**

Direct DOC analysis using the high temperature TOC analyzer in seawater has limitations due to the precision and the potential damage to the detector/catalyst of the measuring device. In addition, the limited precision makes it less suitable for analyzing low level DOC in ASW. This uncertainty and limitation of DOC analysis has been reported previously [199]. For DOC analysis with ASW samples, UVA is a good alternative providing high precision at low DOC levels. A similar method was also used in a previous study [200]. In the DI water aqueous conditions, the DOC concentrations of SHA were quantified by both the TOC analyzer and the UVA spectrophotometer.

The correlations between DOC (SHA, 2 mg/L) and UVA at 210, 254, and 400 nm with DI water and ASW are shown in Figure 6.1. Those wavelengths were selected because (i) the NOM has different functional groups and aromatic rings, (ii) the wide absorption wavelengths are observed for aromatics, and (iii) there is recognizable absorption in these wavelengths [201]. For both DI water and ASW samples, UVA

increases with increasing DOC concentration and pH. The effect of pH on 254 nm absorbance in DI is minimal, while the UVA at 400 nm is slightly higher with increasing pH at relatively high DOC concentrations ( $\geq 6$  mg/L). However, the UVA at 210 nm and pH 10.5 in DI water is approximately 15% greater than that at pH 4 and pH 8 due to the presence of OH<sup>-</sup> ions. For ASW, even though it has very high conductivity (52,600  $\mu$ S/cm), UVA exhibits a strong linear relationship with increasing DOC concentrations at all conditions excluding pH 10.5 and 210 nm. The correlation between DOC and UVA is shown to have the strongest linear relationship at 254 nm and pH 8 in both DI water and ASW ( $R^2 \geq 0.99$ ) due to the high aromaticity of SHA (42%) [202]. As a result, UVA at 254 nm ( $UVA_{254}$ ) was selected to determine DOC in ASW with the highest accuracy for high salinity waters.

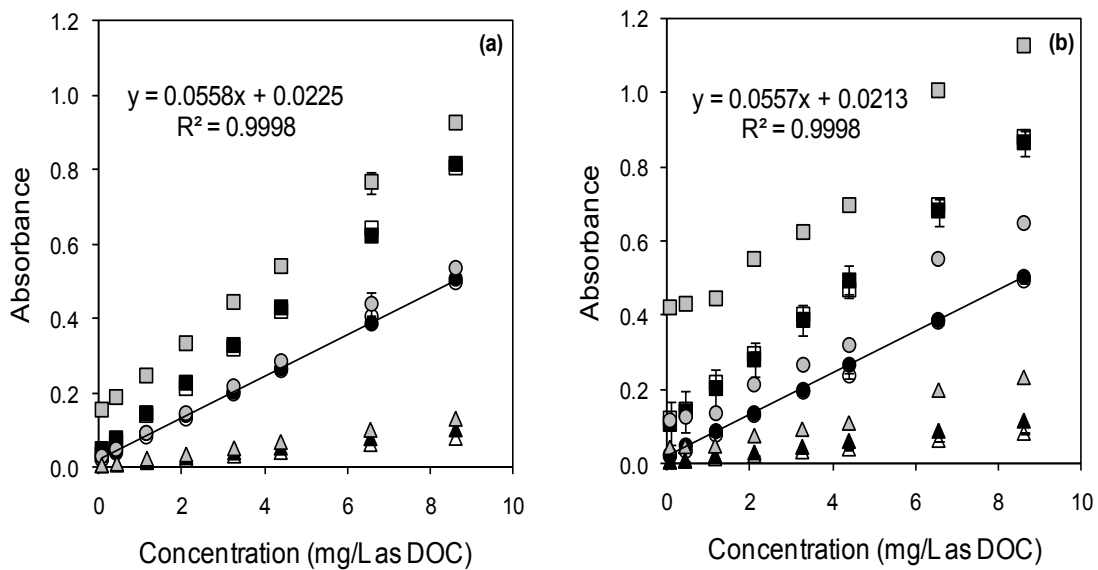


**Figure 6.1.** The relationship between dissolved organic carbon (SHA) and UVA absorbance at various pH values in (a) DI water and (b) ASW. ( $\square$ , 200 nm and pH 4.0;  $\blacksquare$ , 210 nm and pH 8.0;  $\blacksquare$ , 210 nm and pH 10.5;  $\circ$ , 254 nm and pH = 4.0;  $\bullet$ , 254 nm and pH 8.0;  $\odot$ , 254 nm and pH 10.5;  $\triangle$ , 400 nm and pH 4.0;  $\blacktriangle$ , 400 nm and pH 8.0;  $\blacktriangle$ , 400 nm and pH 10.5).

### 6.3.2 Adsorption and retention of BPA and EE2 by SWNTs-UF in DI water and ASW

For the dead-end stirred-cell experiments, each amount of BPA and EE2 removal by the membrane and/or SWNTs was quantified during SWNTs-UF filtration runs with DI, DI+SWNTs, ASW, and ASW+SWNTs. Previous research has demonstrated that for organic compounds, the delivered and adsorbed mass of the solute affects the retention and permeate flux of the membrane. This is because the change of concentration associated with the adsorbed mass during membrane filtration should be influenced by the physicochemical conditions of the membrane (e.g., concentration polarization) and the solute transportation at the membrane interface [58]. The adsorbed/delivered mass accumulated and the retention with adsorbed mass were employed in this study to avoid significant variance depending on the delivered/adsorbed mass of solute and to distinguish between the adsorption on the membranes and other interaction parameters (e.g., dielectric constant, water flux, and octanol-water partition coefficient ( $\log K_{OW}$ )) [203]. In addition, in order to elucidate the SWNTs' contribution to adsorption of BPA and EE2, the amounts of delivered/adsorbed mass in the permeate and retentate were quantified by mass balance over time with the UF membrane in a feed solution of DI water and ASW.

The delivered and adsorbed mass for BPA and EE2, which is influenced by the feed solution and SWNTs presence, is compared in Figure 6.2a. The adsorbed mass of BPA (delivered mass,  $16.1 \mu\text{g}/\text{cm}^2$ ) and EE2 (delivered mass,  $20.9 \mu\text{g}/\text{cm}^2$ ) throughout the UF membrane filtration with an accumulated permeate volume of 400 mL and at a recovery of 40% was  $4.27 \mu\text{g}/\text{cm}^2$  (DI, BPA),  $5.39 \mu\text{g}/\text{cm}^2$  (DI, EE2),  $11.62 \mu\text{g}/\text{cm}^2$  (DI+SWNTs,

BPA), 19.7  $\mu\text{g}/\text{cm}^2$  (DI+SWNTs, EE2), 4.58  $\mu\text{g}/\text{cm}^2$  (ASW, BPA), 6.37  $\mu\text{g}/\text{cm}^2$  (ASW, EE2), 11.6  $\mu\text{g}/\text{cm}^2$  (ASW+SWNTs, BPA), and 17.9  $\mu\text{g}/\text{cm}^2$  (ASW+SWNTs, EE2).

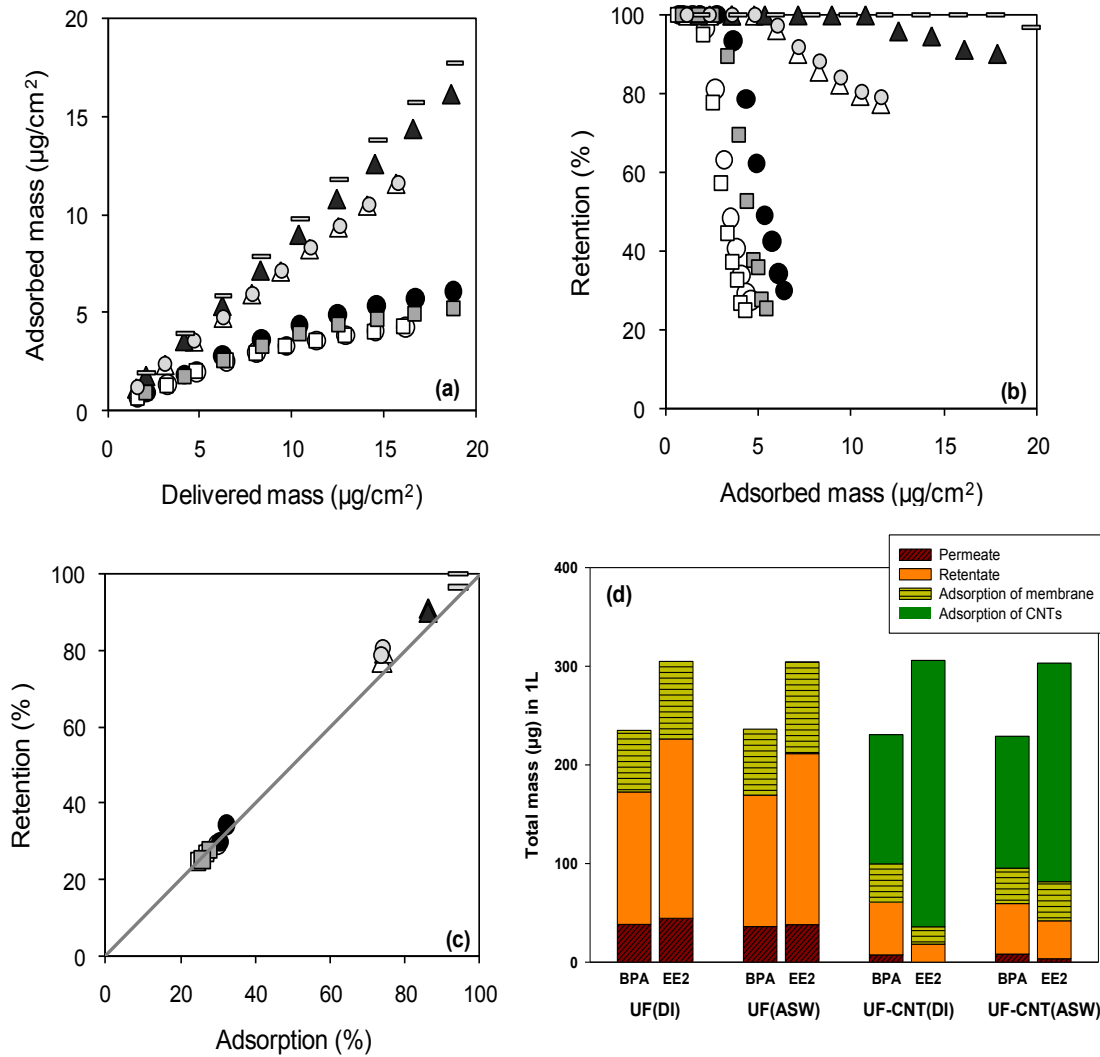


**Figure 6.2.** Comparison of (a) delivered and adsorbed mass accumulated, (b) adsorbed mass and retention, (c) adsorption and accumulated retention, and (d) mass of permeate, retentate, membrane adsorption, and SWNTs adsorption for BPA and EE2 in the SWNTs-UF system with DI water and ASW. Operating conditions:  $\Delta P = 552$  kPa (80 psi); stirring speed = 300 rpm; recovery = 40%; DOC = 2 mg/L; pH = 8; SWNTs = 10 mg/L; conductivity = 200  $\mu\text{S}/\text{cm}$  (DI), 53.2 mS/cm (ASW); pre-contact time with SWNTs = 2 h. ( $\square$ , BPA (DI);  $\blacksquare$ , EE2 (DI);  $\circ$ , BPA w/ SWNTs (DI);  $\blacksquare$ , EE2 w/ CNTs (DI);  $\circ$ , BPA (ASW);  $\bullet$ , EE2 (ASW);  $\Delta$ , BPA w/ SWNTs (ASW);  $\blacktriangle$ , EE2 w/ SWNTs (ASW)).

The percentage of adsorption/retention of BPA and EE2 in UF-CNTs at the same conditions follows the order: 94.0/96.6 (DI+SWNTs, EE2) > 86.2/90.0 (ASW+SWNTs, EE2) > 73.6/78.9 (DI+SWNTs, BPA)  $\geq$  74.1/77.3 (ASW+SWNTs, BPA) > 29.8/29.8 (ASW, EE2)  $\cong$  27.3/27.3 (ASW, BPA)  $\geq$  25.3/25.3 (DI, EE2)  $\cong$  24.8/24.8 (DI, BPA), as shown in Figs. 2b and 2c. While in general, the adsorbed mass increases with increasing delivered mass of BPA and EE2, EE2 retentions greater than BPA in both DI water and ASW in both the absence and presence of CNTs. The DI+SWNTs for EE2 shows the highest slope based on adsorbed/delivered mass. These results can be explained by a combination of the general observations of previous studies and the following phenomena: (i) the higher EE2 adsorption over BPA onto SWNTs is due to EE2's higher hydrophobicity; EE2 (3.7) > BPA (3.3) [35, 74]. (ii) The adsorption coefficient normalized by the hexadecane-water partition coefficient ( $K_{HW}$ ) that causes the screening out of the hydrophobic effect, is 1.5 times higher onto SWNTs in EE2 than in BPA. This is despite BPA's adsorption capacity being double that of EE2 due to the "butterfly" structure of BPA, with two benzene rings adsorbing on the surface, groove area, and interstitial pores of the SWNTs [74]. (iii) Organic compounds containing benzene rings may be strongly driven onto CNTs due to aromatic ( $\pi$ - $\pi$  electron donor-acceptor) interactions [204]. For ASW, the adsorption capacity of carbonaceous materials increases as the ionic strength increases due to the "screening effect", which reduces electrostatic repulsions of surface charge [165]. In addition, the enhancement of hydrophobic-organic adsorption onto carbonaceous materials could be explained by the "salting-out effect", which increases adsorption capacity with decreasing solubility of organic compounds in aqueous salt solutions [205, 206]. However, increasing adsorption trends resulting from



high ionic strength was relatively insignificant for all those experiments. The percentage pre-adsorption of BPA/EE2 onto SWNTs for 2hrs prior to membrane filtration was 56.8/88.3 (DI+SWNTs), and 58.4/73.1 (ASW+SWNTs). We presume that this phenomenon is due to NOM competition for available sites on the CNTs which could be a major governing mechanism of adsorption in ASW (2 mg/L SHA). This result is also somewhat in agreement with the previous study [111].

Unlike the case of UF-SWNTs, the adsorbed/delivered mass trends in the absence of CNTs (Figure 2a) show a flattening out from the steep part of the graph (at the initial stages of the filtration) to a horizontal line (at the end of the filtration) of the delivered mass increment throughout the membrane filtration. This indicates that the primary membrane filtration phase is not completely saturated with BPA and EE2 onto the membrane and that the end of the filtration should be almost saturated with the increment of BPA/EE2 delivered mass (longer filtration may be required for complete saturation of BPA/EE2 to membrane). As described previously, the ratio of adsorbed/delivered mass for BPA/EE2 follows the order: EE2 (ASW) > BPA (ASW) > EE2 (DI) ≥ BPA (DI) throughout the membrane filtration process. These results are due to the fact that the preferential retention associated with the adsorption by the UF membrane adsorption sites, for hydrophobic compounds in the presence of NOM, is positively correlated with log  $K_{ow}$ , while the electrostatic interaction at higher ionic strength is reduced due to the screening out between the organic compound and membrane surface, thus, lower retention was observed [207]. The results of this study show that the retention of BPA is similar in DI water and ASW, while the retention of EE2 was slightly higher in DI water. This result is inconsistent with previous studies, which reported that the organic

compound retention increases with high background salt concentrations that have a significant effect on humic acid fouling [208, 209]. In addition, calcium ions have a significant role in the binding between organic foulants and the membrane surface [210], which also contributed to the organic compound retention. This is presumably because the membrane type, NOM type, and background ions differ. Consequently, different retention of BPA and EE2 could be attributed to the canceling effects of these multiple mechanisms functioning at the same time.

Overall, the results have shown that the BPA and EE2 retention by the UF membrane is more likely attributed to the adsorption of the CNTs and/or the membrane. This is because a different retention mechanism such as size exclusion is unlikely, due to the large pore size of the membrane (nominal MWCO = 5,000 Daltons) compared to the MWs (228.3 g/mol for BPA and 296.4 g/mol for EE2). The transport of BPA and EE2 through the UF-SWNTs system consists of 4 parts with a total mass of 230  $\mu\text{g}$  for BPA and 300  $\mu\text{g}$  for EE2 with a 1 L feed solution, as shown in Figure 2d: permeate, retentate, adsorption onto membrane, and adsorption onto SWNTs. The BPA and EE2 had similar mass composition in both DI water and ASW. However, the adsorption of BPA and EE2 on SWNTs is dominant for both waters in the UF-SWNTs system. The adsorption mass associated with membrane/SWNTs of BPA and EE2 in the presence of SWNTs in DI water and ASW during the filtration run was 38.7/131  $\mu\text{g}$  (DI, BPA), 17.5/270  $\mu\text{g}$  (DI, EE2), 35.9/134  $\mu\text{g}$  (ASW, BPA), and 39.7/222  $\mu\text{g}$  (ASW, EE2). The results clearly show that BPA and EE2 removal is dominant due to the adsorption by SWNTs.

### 6.3.3 Effect of NOM and CNTs on fouling in UF-CNTs

Normalized flux decline and DOC rejection trends based on  $UVA_{254}$  with ASW in UF in the absence and presence of CNTs were monitored over permeate volume, as shown in Figure 6.3. Control experiments with DI water (pH 8 with 1 mM  $Na_2HPO_4$  buffer) were performed to evaluate the implementations of the addition of CNT on UF fouling. As a general observation, the normalized fluxes of DI+SWNTs runs show insignificant flux decline, indicating that SWNTs are not potential foulants, even though it was originally assumed that SWNTs could have high affinity with the UF membrane due to the hydrophobic interaction between CNTs and the membrane surface.

Figure 6.3 shows that ASW had significantly greater flux decline (74%) in the UF-only system than in the UF-SWNTs (54%). In ASW conditions, it is still somewhat controversial which mechanism influences flux decline. Nevertheless, this behavior could be explained by significant seawater characteristics. The seawater has relatively high osmotic pressure due to high ionic strength, which results in a significant decrease in membrane flux. The effect of high ionic strength has been observed in previous studies where flux decline increases with increasing ionic strength [19, 211, 212]. Secondly, multivalent cations such as  $Ca^{2+}$  and  $Mg^{2+}$  in ASW play a significant role in humic acid fouling, which enhances the formation of a fouling layer, although typically inorganic fouling is insignificant to membranes [19, 163, 213]. Thirdly, standard blocking associated with humic acid adsorption onto the membrane might contribute to inside membrane pores [17, 163], which exacerbates more severe irreversible fouling. In general, it is assumed that the hydrophobic NOM (in this study – SHA), as a major foulant, adsorbs to the membrane surface and pores, and its adsorption increases gradually by collecting other NOM particles. Eventually, cake/gel formation occurs on the membrane

surface. However, only a small amount of NOM (2 mg/L) was introduced in this work. Therefore, only inner pore blocking may have occurred, without the formation of cake.

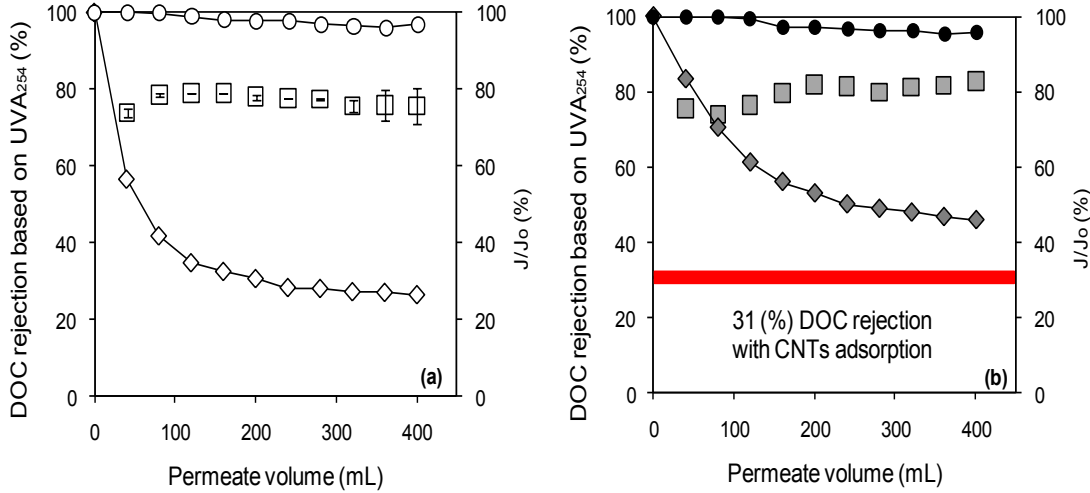


**Figure 6.3.** Comparison of flux-decline, rejection trends based on UVA<sub>254</sub> (a) ASW only and (b) ASW+SWNTs. Operating conditions: pH = 8.0;  $\Delta P = 552\text{kPa}$  (80 psi); stirring speed = 300 rpm; recovery = 40%; DOC = 2 mg/L; SWNTs = 10 mg/L; conductivity = 200  $\mu\text{S/cm}$  (DI), 53.2 mS/cm (ASW); pre-contact time with SWNTs = 2 h. ( $\square$ , DOC rejection without CNTs;  $\blacksquare$ , DOC rejection with SWNTs;  $\circ$ , flux decline w/o SWNTs (DI);  $\bullet$ , flux decline with SWNTs (DI);  $\diamond$ , flux decline without SWNTs (ASW);  $\blacklozenge$ , flux decline with SWNTs (ASW)).

The flux trends of ASW in the presence of SWNTs are 20% higher than in the absence of SWNTs, even though DOC rejection (approximately 80%) exhibited similar trends for both ASW and ASW+CNTs (Figure 6.3b). The lower flux decline in the presence of SWNTs should be attributed to the effect of SWNTs adsorption with humic acid. As the NOM of 30.6% adsorbs onto the SWNTs surface during the 2hrs pre-contact period prior to the membrane filtration run, it contributes to mitigate membrane fouling associated with standard blocking. Even though the same adsorbent was used in the hybrid membrane filtration, the adsorbent fouling effect could be different with respect to

physicochemical conditions such as membrane characteristics, solution water chemistry (pH and conductivity), and hydrodynamic conditions (operating pressure/flux, dosage, and stirring speed) [23]. In this work, the usage of SWNTs 10mg/L with the UF membrane was insignificant for membrane fouling. The SWNTs (with a length of 5–30  $\mu\text{m}$  and an outer diameter of 1–2 nm) are large enough to block membrane pores (nominal MWCO 5,000 Daltons). SWNTs should be stacked on the membrane surface maintaining a porous layer that allows the passage of water without fouling resistance.

Three-dimensional AFM image analysis was employed to investigate the morphological changes of the fouled UF membrane associated with EDCs and NOM in the absence and presence of SWNTs. Figure 6.4 shows the AFM images of the clean and fouled membranes in the absence and presence of SWNTs with ASW at a scan size of 10  $\text{m}^2$  when imaged in air. The dark and light regions correspond to areas below and above the mean elevation, respectively. Comparing the images of the clean and fouled membranes, the fouled membrane in the absence of SWNTs appears to be rougher than the clean membrane and the fouled membrane in the presence of SWNTs based on average roughness values: 17.6 nm (fouled in the absence of CNTs) > 5.03 nm (fouled in the presence of CNTs) > 2.43 nm (clean membrane). This suggests that SWNTs reduce membrane fouling, although there are contradictory results concerning the effect of other absorbents (e.g., PAC and aluminum/iron oxide particles) on membrane fouling.

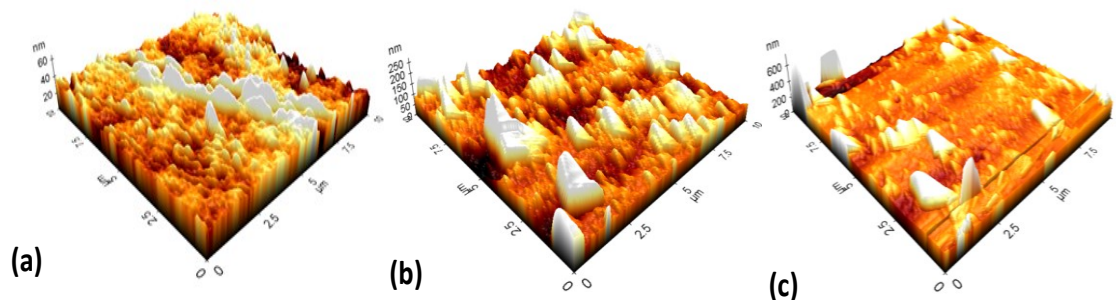


**Figure 6.4.** Three-dimensional AFM image (a) cleaned membrane, (b) fouled in the absence of SWNTs in ASW, and (c) fouled membrane in the presence of SWNTs (ASW).

## 6.4 Conclusions

This study investigated the mechanisms for adsorption and retention of hydrophobic compounds as well as the contribution of SWNTs to mitigating the NOM fouling during UF membrane filtration with ASW. The adsorbed/delivered mass for BPA and EE2 derived from the mass-balance during membrane filtration provided a reasonable comparison of their retention and adsorption trends. In addition, UVA<sub>254</sub> nm absorbance provides reasonable values as an alternative of TOC analysis for highly aromaticity SHA in ASW. The results show that adsorption with an UF membrane and SWNTs has the most significant impact on the retention of hydrophobic compounds in a UF-SWNTs system with ASW, and high adsorption of BPA and EE2 is achieved by the SWNTs. The adsorption of the relatively high hydrophobic EE2 onto SWNTs is more competitive than BPA in the presence of NOM in ASW. The UF-SWNTs system enhances membrane flux due to foulant (i.e., NOM) pre-removal, which also indicates that SWNTs are not potential foulants. Approximately 80% of the DOC in ASW was rejected by the UF-SWNTs systems. These results suggest that this hybrid system can be applied as a pretreatment followed by SWRO. Overall, SWNTs have been shown to be effective in controlling NOM fouling and removing EDCs from seawater. The quantification of

solute adsorption and retention should be useful to develop an existing transport model that will facilitate improved quantitative predictions for other organic compounds which have similar physical and chemical properties to the compounds tested in this study. Future research in hybrid membrane processes using SWNTs should examine the adsorbent effect with respect to physicochemical and hydrodynamic conditions for the application of desalination pretreatment.

### **Acknowledgements**

This research was supported by the GS E&C Research Institute (Korea). Funding was provided by a grant (07SeaHeroB01-01) from the Plant Technology Advancement Program of the Ministry of Land, Transport, and Maritime Affairs of the Korean government and by the University of South Carolina

## CHAPTER 7

### REMOVAL OF SYNTHETIC ORGANIC COMPOUNDS BY FORWARD OSMOSIS AND REVERSE OSMOSIS MEMBRANE\*

\*Reprinted here with permission of publisher: Heo et al., Comparison of flux behavior and synthetic organic compound removal by forward osmosis and reverse osmosis membranes, Journal of Membrane Science 443 (2013) 68-82

#### **Abstract**

Bench-scale forward osmosis (FO) and reverse osmosis (RO) experiments with both FO and RO membranes were used to investigate the retention and adsorption behaviors and the relative hydrophilicities of several synthetic organic compounds (SOCs). In a comparison of membrane characteristics using the solution-diffusion model, the cellulose triacetate (CTA)-based FO membrane exhibited lower selectivity ratios, indicating that the FO membrane has better separation properties than the polyamide-based RO membrane. However, in active layer (AL)-facing-feed solution (FS) configuration in FO mode, the RO membrane exhibited higher removal efficiency at the expense of severe internal concentration polarization (ICP) and flux reduction. Under higher cross-flow velocity (CFV) operations in FO mode, both reduced external concentration polarization (ECP) and retarded SOC diffusion from the reverse flux of sodium chloride contributed to the improved SOC removal performance. The SOC removal percentage by the FO membrane with respect to molecular weight (MW) followed the order (MW, g mol<sup>-1</sup>; removal, %): sulfamethoxazole (296.4; 90%) > carbamazepine (236.3; 83%) >> atrazine



(215.7; 49%) > 4-chlorophenol (128.6; 39%) > phenol (94.1; 22%). For the FO membrane in RO-mode operation with SOCs of relatively small MW, breakthrough release was observed and was attributed to the FO membrane's porous, mesh fabric supporting backing layer. In addition, the batch adsorption and computational modeling in molecular-level studies suggested that adsorption played a dominant role in the removal of SOCs and was generally correlated with the hydrophobicity (log Kow) of the membrane. It was demonstrated that the FO membrane removal behavior was principally related to size exclusion, while the RO membrane removal behavior was related to interactions between hydrophobicity, size, and electrostatic repulsion.

*Keywords:* Forward osmosis; reverse osmosis; synthetic organic chemicals; retention; adsorption; internal concentration polarization

## 7.1 Introduction

Synthetic organic compounds (SOCs) are extensively discharged into conventional wastewater treatment plants because households and industries continue to consume and produce immense quantities of organic compounds [214-216]. SOCs are produced in the laboratory and as by-products of manufacturing for applications in industry, agriculture, burning, and other human activities. The reported human health effects of SOC exposure include damage to the nervous system, liver, and kidney, as well as possible carcinogenic and cancer risks [217-220]. For example, phenolic compounds have been reported to cause liver, cardiovascular system problems with renal papillary damage, and serious alterations of mucosal in sensitive cellular membranes including ocular organs [217]. In

addition, unexpected or uncontrolled exposure to many pharmaceutical SOC's may induce adverse effects in both wildlife and humans; for example, adverse effects have been reported for atrazine (ATZ), carbamazepine (CBM), and sulfamethoxazole (SMT). Extended exposure to ATZ may negatively influence the cardiovascular system as well as damage normal hormone production and reproductive functions [218]. Furthermore, low sperm counts are common in populations where a high concentration of ATZ is present, and damage to the walls of the digestive system are common. CBM and SMT, on the other hand, tend to increase cancer risks, and exposure to these pharmaceutical compounds without medical surveillance is dangerous due to the fragile health of high-risk life forms such as developing fetuses, people with chemical sensitivities, or people with existing diseases taking medications that may adversely react with SOC's in their water source [219, 220].

Previous studies have shown that the use of reverse osmosis (RO) and nanofiltration (NF) membranes are effective approaches for reducing exposure to SOC's; these approaches employ filtration and retention mechanisms, such as size/steric exclusion, electrostatic repulsion, and hydrophobic interactions between solutes and membranes [48, 58, 221, 222]. In these studies, the retention of uncharged organics was mainly controlled by steric hindrance and hydrophobic interactions, whereas the retention of charged organics was usually controlled by electrostatic repulsion [223, 224]. Although RO/NF membrane processes can be effective for retention and removal of SOC's from contaminated waters, these pressure-driven processes are hampered by membrane fouling and considerable energy consumption to maintain normal operation. Thus, forward osmosis (FO) presents a potential alternative to pressure-driven processes; FO provides

an energy-efficient, environmentally friendly membrane technology for sustainable water purification [31, 225].

In recent years, the study of FO has increased due to the need for more sustainable processes in water treatment, as well as in other fields such as desalination of seawater, food processing, electric power production, and pharmaceutical applications [226-228]. FO involves spontaneous water movement by means of a natural chemical gradient in which a solution tends to move from a state of lower osmotic pressure to higher osmotic pressure through a semi-permeable membrane, which can remove target solutes from the sample [31]. The FO process depends on the molar concentrations of the solutions instead of on the actual identity of the solutes. This dependence on concentration imparts versatility to the process and allows for the easy filtration of different kinds of solutions using the same system. Nevertheless, FO is not fully developed technologically; thus, it is not yet used widely in commercial practice [31]. First, specialized membranes (*i.e.*, with low internal concentration polarization (ICP)) must be identified in order to create the most efficient FO system for use with the high osmotic pressures required for creating a high water gradient.

The FO process tends to be much more spontaneous than the RO process; RO requires high hydraulic pressure, making it a much more costly process. In FO, the recovery of a filtered sample from the draw solution (DS) can often be achieved with only a fraction of the power used for the same purpose in RO. Furthermore, FO results in lower fouling propensity and a higher contaminant recovery rate [229]. While fouling still must be controlled in FO, it is typically easier to control than in RO. Currently, both FO-only and hybrid FO/RO processes are being developed to enhance the filtration capability

in water treatment applications [230, 231]. For example, the FO process may be used as a pretreatment method in seawater desalination to reduce both the energy required and extent of fouling in the subsequent RO process.

The adsorption characteristics of SOC<sub>s</sub> on the membrane play an important role in the retention mechanisms of FO and RO processes [127, 232-234]. It has been reported that hydrophobic attraction between SOC<sub>s</sub> and membranes may be the dominant short-term removal mechanism in FO/RO processes. This hydrophobic adsorption may lead to the overestimation of SOC retention efficiency, because equilibrium is not achieved in the initial stages. Furthermore, hydrophobic adsorption of SOC<sub>s</sub> onto the polymeric membranes may adversely affect their ultimate retention efficiency by allowing solution diffusion of SOC<sub>s</sub> through the membrane polymer into the permeate side [127]. Although the effects of adsorption on RO retention behavior have been extensively reported in the literature, only a handful studies have focused on characterization of FO-mode experiments for the retention of SOC<sub>s</sub> [30, 235]. In addition, the solute parameters of SOC retention, such as molecular weight (MW), hydrophobicity (log K<sub>ow</sub>), dipole moment, and solubility, are considered important in FO process applications but are not as well understood. To the best of our knowledge, no work has been conducted to directly compare FO and RO membranes for SOC removal in both FO- and RO-mode experiments under various operating conditions. Therefore, the objective of this study was to conduct a comprehensive experiment to identify factors affecting the SOC retention in RO and FO membranes in both FO- and RO-mode experiments, including computational molecular modeling for membrane adsorption.

## 7.2 Materials and methods

### 7.2.1 Tested SOC compound and solution chemistry

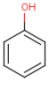
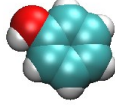
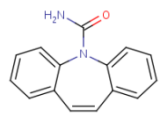
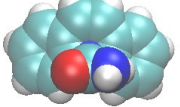
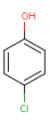
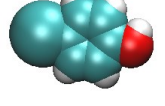
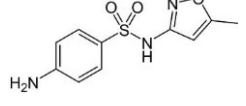
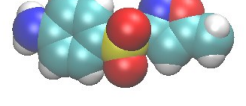
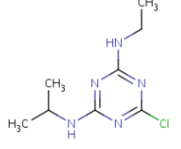
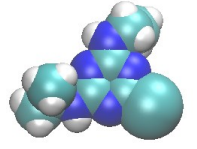
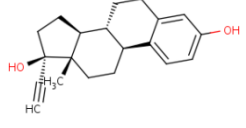
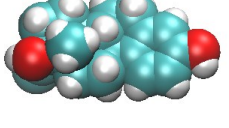
High-purity (> 98%) SOC<sub>s</sub>, namely, phenol (PHN), 4-chlorophenol (4CP), ATZ, CBM, SMT, and 17 $\alpha$ -ethinyl estradiol (EE2), were purchased from Sigma–Aldrich (Saint Louis, MO). MW, hydrophobicity, and water solubility were important factors when selecting these high-purity SOC<sub>s</sub>; environmental relevance was also considered. A summary of the selected key physicochemical properties and molecular structures of the SOC<sub>s</sub> studied are presented in Table 7.1.

These values were obtained from the SRC PhysProp (SRC 2006) and ChemAxon (chemicalize.org 2011). All of the SOC<sub>s</sub>, except PHN and 4CP, were first prepared as a 2-mM stock solution in pure methanol. Then, predetermined volumes of these SOC stock solutions equaling concentrations of 5  $\mu$ M in feed solutions (FS) were placed in separate amber glass jars to minimize co-solvent effects from evaporating methanol solvent. PHN and 4CP were prepared as 5- $\mu$ M stock solutions in Milli-Q<sup>®</sup> water and pure acetonitrile solvent, respectively, and added to the FS directly. Stock solutions were stored below 4°C.

**Table 7.1** Properties of the target compounds spiked to the feed solution.

Compound	ID	MW (g/mol)	Water solubility (mg/L) <sup>a</sup>	Henry's law constant <sup>a</sup> (atm m <sup>3</sup> /mol)	Log K <sub>ow</sub> <sup>b</sup>	pK <sub>a,b</sub> <sup>b</sup>
Phenol	PHN	94.1	8.28×10 <sup>4</sup>	3.33×10 <sup>-7</sup>	1.67	10.02
4-Chlorophenol	4CP	128.6	2.4×10 <sup>4</sup>	6.27×10 <sup>-7</sup>	2.27	8.96
Atrazine	ATZ	215.7	34.7	2.36×10 <sup>-9</sup>	2.20	3.20
Carbamazepine	CBM	236.3	17.7	1.08×10 <sup>-10</sup>	2.77	(-) 3.75
Sulfamethoxazole	SMT	253.3	610	6.42×10 <sup>-13</sup>	0.79	1.97, 7.66
17 $\alpha$ -ethinyl estradiol	EE2	296.4	11.3	7.94×10 <sup>-12</sup>	3.90	10.33

Structure <sup>b</sup>	Space-filling <sup>c</sup>	Structure <sup>b</sup>	Space-filling <sup>c</sup>
			
PHN		CBM	
			
4CP		SMT	
			
ATZ		EE2	

<sup>a</sup> Obtained from the Syracuse Research Corporation (SRC) PhysProp database (<http://www.syrres.com>).

<sup>b</sup> Obtained from the chemicalize.org by ChemAxon (<http://www.chemicalize.org>).

<sup>c</sup> By adjusting the sphere scale so that all target compounds are same scale in size to allow comparison of the overall size of molecules.

## 7.2.2 Membranes and FO mode cross-flow test unit

Two different types of commercially available flat sheet membranes – FO (cellulose triacetate, CTA) and RO (BW30) membranes – were obtained from Hydration Technologies, Inc. (Albany, OR) and Dow Filmtec™, Co. (Kentucky, USA), respectively. The RO membrane was preserved in a refrigerator at 4°C since its purchase in 2009. To reduce the ICP, FO membranes are made of a thin layer of an asymmetric CTA active layer (AL). Each membrane is also embedded with polyester mesh support layers, which vary according to the manufacturer. The RO membrane had a mainly cross-linked aromatic polyamide AL on a polysulfone interlayer with a polyester support layer. A COXEM (CX-200, Daejeon, South Korea) scanning electron microscope (SEM) provided additional details of the supporting layer's patterns and views of the membrane. Membrane samples were prepared with a uniform coating layer of silver conductor and scanned at an accelerating voltage of 20 kV and working distance (WD) of 50.9 to 53.9 mm. In a previous study, the electrophoretic mobility of an FO membrane exhibited relatively less negative surface potential than the RO membrane; the values of zeta potential (ZP) ranged from -4 to -8 mV [235], while the RO membrane had ZPs ranging from -16 to -18 mV [236]. In addition, the RO membrane was more hydrophobic (contact angle of  $76 \pm 7^\circ$ ) [237] than the FO membrane (contact angle of  $62 \pm 7.2^\circ$ ) [238]. In FO-mode experiments, a bench-scale stainless steel plate and frame of an FO cell coupled with an FS tank, a DS tank, a temperature controller (Fisher Scientific Isotemp Chillers, Pittsburgh, PA), variable gear pumps (Micropump, Vancouver, WA), and a pressure transducer (Omega Eng., CT, USA) were employed. Two channels on the sides of the membranes and mesh spacers shaped like diamonds were inserted for the purpose of supporting the FO membrane. Each channel had dimensions of 76 mm length, 27 mm

width, and 2 mm height, providing an effective membrane coupon area of 41.04 cm<sup>2</sup>. The DS tank was placed on a digital balance (AV8101, Ohaus, NJ, USA) and periodically weighed over time, and the co-current cross-flow velocities (CFVs) for both sides of the membrane were maintained at desirable velocities with a cross-flow meter (Dwyer, Michigan City, IN).

### **7.2.3 SOCs retention experiments in FO cross-flow filtration mode**

All FO experiments were performed using the initial volumes of 3 L for the FS and 1 L for the DS; the pH was adjusted to 7 by addition of either 0.1 M NaOH or HCl as needed. The solution was supplemented with phosphate buffered solution (PBS) to maintain the desired pH. Analytical grade NaCl (Fisher Scientific, Pittsburgh, PA) was used to prepare the DS at a concentration of 1 M in Milli-Q® water. The 5- $\mu$ M solutions of SOCs were added to FS. Solutions with concentrations higher than environmental levels were used due to the low effective concentrations of solutes passing through the FO membrane after being diluted in the DS. Therefore, lower concentrations would be difficult to read in the DS in FO-mode operation; in other words, environmental conditions are not ideal to obtain results in FO bench-scale experiments. Each experiment was conducted using a new membrane coupon, and the temperatures of the FS and DS were kept constant at 20  $\pm$  1°C using a recirculating chiller/heater. High-performance liquid chromatography (HPLC) was performed on 1-mL samples from the FS and DS tanks. In addition, pH and temperature were measured throughout testing at regular time intervals. Retention of SOCs in FO processes was measured  $i$  times at a specified interval,  $R_{(i)}$ , based on the feed and draw SOC concentrations; retention was calculated using Eq. 7.1;



$$R_{(i)}(\%) = \frac{C_{F(i)} - C_{P(i)}}{C_{F(i)}} \cdot 100\% \quad (7.1)$$

where  $C_{F(i)}$  and  $C_{P(i)}$  are defined as the concentration of feed and permeate at  $i$  times, respectively. By taking into account dilution effects in the DS, the real permeate concentrations ( $C_{P(i)}$ ) were obtained by differentiated values of the collected DS samples. Mass *versus* time data were evaluated using Eq. 7.2, which was also used in a previous study [239];

$$C_{P(i)} = \frac{C_{DS(i)}V_{DS(i)} - C_{DS(i-1)}V_{DS(i-1)}}{V_{P(i)}} \cdot 100 \quad (7.2)$$

where  $V_{P(i)}$ ,  $V_{DS(i)}$ , and  $V_{DS(i-1)}$  are the permeate and DS volumes at  $i$  times and DS volumes at  $i-1$  times;  $C_{P(i)}$ ,  $C_{DS(i)}$ , and  $C_{DS(i-1)}$  are the permeate and DS concentrations at  $i$  times and DS concentrations at  $i-1$  times, respectively. The mass balance calculation for reverse solute flux of draw solute in FO mode was introduced using an electric compact Thermo Scientific conductivity meter based on the background calibration curves of NaCl ( $R^2 > 0.99$ ).

#### 7.2.4 FO and RO membrane adsorption experiments

Membrane adsorption tests were performed with each type of FO and RO membrane (HTI-CTA, BW-30). The 10 cm × 10 cm membranes were cut into 1 cm × 1 cm sections and then placed in reactors (200-mL amber bottles with Teflon lined screw caps). They

were placed in the same FS conditions and then introduced to the SOCs at a concentration of 2  $\mu\text{M}$ . To control the results, several reactors had only solutes, meaning no membranes were present. This process ensured that the influence of the solutions was taken into account along with any potential compound losses from adsorption on bottle walls and caps. The bottles were placed on a stirrer at a speed of 300 rpm and agitated for 96 h, which is adequate for representing complete pseudo-equilibrium. Aliquots of 1 mL were removed from the reactor bottles for HPLC analyses.

### 7.2.5 Computational methods

The initial structures of the FO and RO membranes used in the simulations consisted of five repeating units of the CTA and BW-30 polyamide monomers, respectively. The coordinates of the membranes and the target SOCs were optimized with dispersion-corrected density functional theory [240, 241] using the BLYP functional and the 6-31++G(d,p) basis set in TeraChem [242, 243]. The initial configurations for the molecular dynamics (MD) simulations were obtained by optimizing fragments of the FO-SOC and RO-SOC complexes by following geometry optimization procedures described in Zaib *et al.* [244]. The complexes were solvated with a box of TIP3P water molecules of dimensions 65 Å  $\times$  72 Å  $\times$  56 Å, and the force fields for the FO, RO, and SOCs were generated using the antechamber module in AMBER 11 [245]. Simulations were performed in the NPT ensemble at 1 atm and 300 K using Langevin dynamics with a collision frequency of 2 ps<sup>-1</sup> for temperature control. The particle mesh Ewald was used to compute the long-range electrostatic interactions, and the cut-off limit for non-bonded interactions was set at 8 Å [246]. The solvated complexes were heated to about 300 K

over a period of 50 ps after an initial optimization. A constant pressure MD simulation was performed for 50 ps to stabilize the system density at  $1.0 \text{ g cm}^{-3}$  and to ensure structural relaxation. In the above simulations, the geometry of the complexes was restrained with a weak harmonic force of  $2.0 \text{ kcal mol}^{-1} \text{ \AA}^{-2}$ , while the hydrogen bonds were constrained using the SHAKE algorithm [247]. The restraint for the complexes was subsequently removed, and the system was equilibrated at 300 K for 500 ps. A 20-ns production run was conducted in the NPT ensemble, and the coordinates were saved every 20 ps. A total of 100 conformational snapshots were extracted from the production simulations at 200-ps intervals for free energy calculations.

The binding free energies between the membranes and the SOCs were computed using the molecular-mechanics/Poisson-Boltzmann surface area (MM/PBSA) approach [248], implemented in the AMBER 11 software package. This approach allows free energy decomposition into contributions originating from different types of interactions or groups of atoms. The free energy is estimated as the summation of the gas-phase molecular mechanic's energy, the solvation free energy, and the conformational entropy upon binding, which is evaluated by means of normal-mode analysis [249].

### 7.2.6 Analytical methods

All of the SOC analyses were conducted with the HPLC-UV method using an Agilent 1200 Series HPLC system (Santa Clara, CA, USA) equipped with diode array detectors (DAD). A Waters 5- $\mu\text{m}$  LiChrosorb® RP18 analytical column was used for reverse-phase separations. The extraction was carried out using non-gradient elution by a mobile phase of 50% Milli-Q® water, acidified with 10 mM  $\text{H}_3\text{PO}_4$ , and 50% acetonitrile at a

constant flow rate of 1.2 mL min<sup>-1</sup> for 7 min. The method detection limits were approximately 50 nM for SOCs, which corresponded to elution times for SMT, PHN, CBM, 4CP, ATZ, and EE2 of 2.2, 2.6, 3.0, 3.7, 5.2, and 6.1 min, respectively. Calibration resulted in typical standard curves, and coefficients of determination (R<sup>2</sup>) greater than 0.99 in the range of the experimental concentrations were used.

### 7.3 Results and discussion

#### 7.3.1 FO and RO membrane characterization

The basic properties of FO and RO membranes were compared to determine the SOC retention performance based on intrinsic membrane properties, as presented in Table 7.2.

**Table 7.2** Properties of the selected FO and RO membranes.

Membrane	Material	Water permeability $W_p$ ( $10^{-7}$ m/s bar)	NaCl permeability $S_p$ ( $10^{-7}$ m/s)	Selectivity $S_p/W_p$ (bar)	Glucose rejection (%)	Contact angle <sup>a</sup> (°)
FO-CTA	Cellulose triacetate	0.858	0.195	0.227	96.6 ± 0.1	60 ± 7.2 <sup>a</sup>
RO-BW30	Polyamide	5.648	4.712	0.834	93.4 ± 0.9	76 ± 7 <sup>b</sup>

<sup>a</sup>[29], <sup>b</sup>[30]

These values were determined independently from a pressurized dead-end configuration of the RO unit (*i.e.*, under RO mode) with a stirring speed of 300 rpm and at 10% recovery to minimize concentration polarization (CP) on the membrane surface. The rejection of NaCl and pure water flux of FO and RO membranes are plotted as a function of applied pressure to calculate the selectivity for the AL of FO and RO membranes based on the solution-diffusion (SD) model, as shown in Figure 7.1.

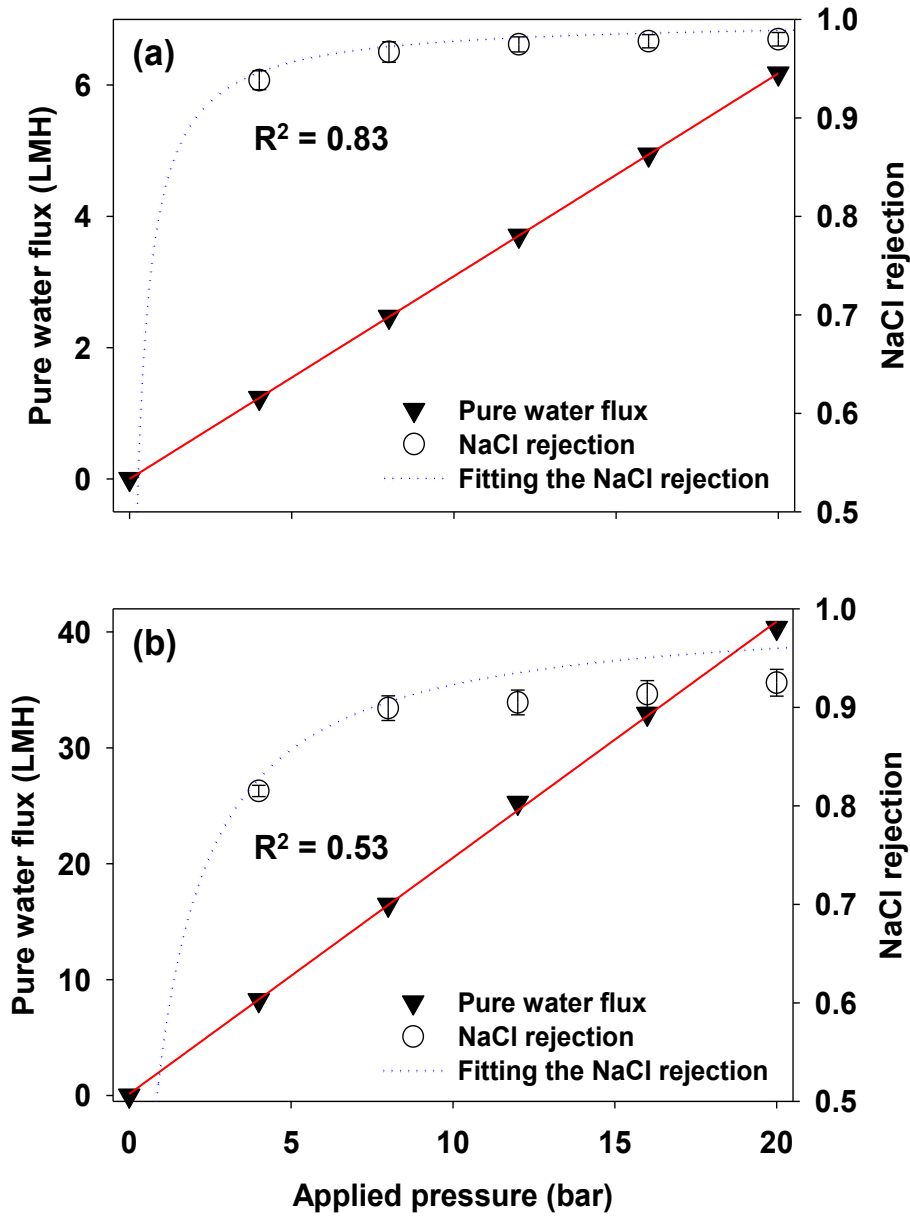


**Figure 7.1** Pure water flux and NaCl rejection trends with respect to applied hydraulic pressure in the RO-mode: (a) FO membrane and (b) RO membrane. Operating conditions:  $\Delta P = 0\text{-}20$  bar; NaCl = 10 mM; stirring speed = 300 rpm.

In Figure 7.1, the slope of the pure water flux corresponds to  $W_p$ , and the fitting of the NaCl rejection curve based on Eq. 3.17 corresponds to  $S_p$  with an assumption that the FO and RO membranes can be correlated to L-S type asymmetric membranes adopted from the SD model [28, 250]. As expected, in both FO and RO membranes, the pure

water flux increased linearly with applied pressure from 0 to 20 bar. The RO polyamide membrane exhibited 6.6 times higher pure water permeability than the FO membrane ( $0.86 \times 10^{-7}$  and  $5.65 \times 10^{-7} \text{ m s}^{-1} \text{ bar}^{-1}$  for FO and RO membranes, respectively). The NaCl rejection rose with increasing applied pressure, as expected from Eq. 3.17, and the typical observed rejection of NaCl was found to be as high as 92 and 98% at 20 bar of applied pressure for RO and FO membranes, respectively. In this study, the RO membrane yielded slightly lower values for NaCl rejection than the commercial, brackish RO membrane rejection values provided by the manufacturer; the difference in NaCl rejection was attributed to the differences in experimental setup, testing protocols, and membrane conditions. When the NaCl rejection data for the RO membrane were evaluated using the SD model, the fitting result value ( $R^2 = 0.53$ ) was highly sensitive, which is consistent with the high values for pure water flux characteristics in RO-mode operation. The degree of CP of salt significantly influenced membrane flux (*i.e.*, greater flux levels) due to the balance of salt convection and back diffusion, which explained why the experimental flux deviated more in the case of the RO membrane compared to the FO membrane. After application of the SD model, the results for the FO membrane exhibited a better sigmoidal curve fit ( $R^2 = 0.83$ ) with the experimental data due to its comparatively low values of water flux characteristics. The RO membrane exhibited 3.7 times higher selectivity ratios ( $S_p/W_p$ ) than the FO membrane, indicating that the FO membrane has better NaCl separation properties than the RO membrane. Previous studies have frequently employed glucose organic solutes as a reference for estimating the mean effective pore size of membranes based on the incorporated steric, hindered convection, and diffusion mass transportation models [239, 251]. In this case, the results for glucose

rejection showed that both FO and RO membranes have a low pore size, with a 180-Da molecular weight cut-off (MWCO), and the FO membrane was estimated to have a relatively smaller membrane pore size than the RO membrane. In addition, the membrane ALs of both FO and RO membranes were similarly hydrophobic, with contact angles of 62° and 72° [237, 238], respectively.

### **7.3.2 Water and reverse salt flux behavior during the FO process**

ICP significantly influences the magnitude of water flux in FO mode, because it greatly reduces the driving force across the membrane from the ideal case in which there is no ICP. This phenomenon is specifically related to the formation of ICP in the membrane support layer, which reduces the flux through the differential concentration built up throughout the membrane support layer [28]. In the ICP model, the degree of ICP exponentially influences the membrane flux upon increasing concentration of DS due to the balance of salt convection and diffusion in the support layer. Furthermore, as shown in Figure 7.2, the fluxes in FO and RO membranes were greatly reduced from the ideal case; previous studies have pointed out that when comparing the AL-facing-DS and the AL-facing-FS configurations, the latter exhibited more severe ICP as a necessary consequence of dilutive ICP [227].

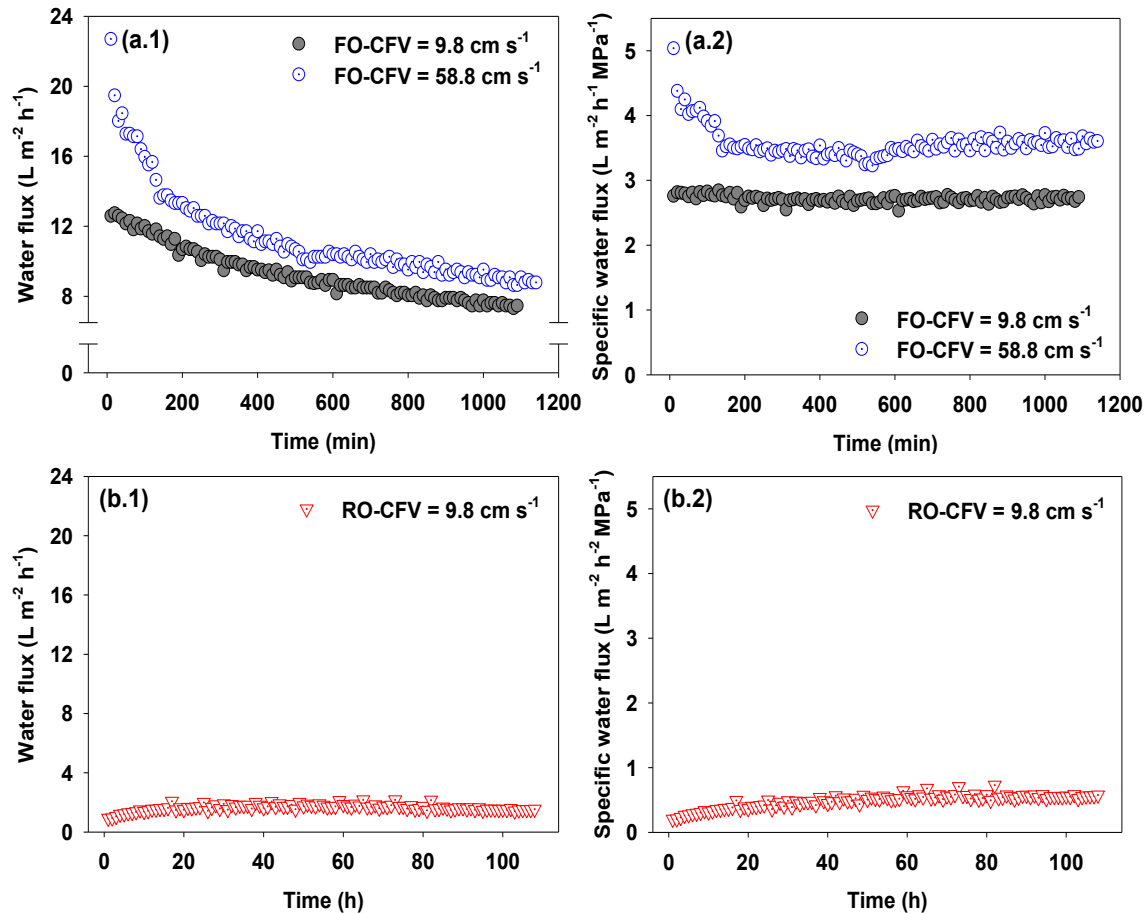


**Figure 7.2** Water flux and specific water flux (flux normalized by osmotic driving force) as a function of time for two FO membrane experiments and one RO experiment: (a) FO membrane (3 and 18 GPH) and (b) RO membrane. Operating conditions: the initial concentration of SOCs = each of 5  $\mu\text{M}$ ; draw solution = 1 M NaCl; cross-flow velocity (CFV) = 3 or 18 GPH; the temperature =  $20 \pm 1$   $^{\circ}\text{C}$ .

With the exception of the initial stage, where the CFV differed between  $9.8 \text{ cm s}^{-1}$  (3 GPH) and  $58.8 \text{ cm s}^{-1}$  (18 GPH), the membranes exhibited similar water flux declining trends, and in the case of a CFV of 18 GPH, the flux increased slightly more than in the case of a CFV of 3 GPH, because the higher CFV can minimize the external concentration polarization (ECP). In addition, the RO membrane in FO-mode operation exhibited approximately five times lower water flux than the FO membrane when the same CFV of  $9.8 \text{ cm}^{-1}$  (3 GPH) was applied. This behavior could be attributed to the



structural differences in the skin and support layers of the membranes [238, 252, 253]. The RO membrane supporting layer parameter was an order of magnitude denser than that of the FO membrane. This difference in density could be attributed to the support layers' tortuosity and porosity, which were clearly visible by SEM, as shown in Figure 7.3. The SEM images of the enlarged cross-section and backside of the FO membrane (Figure 7.3a.2 and 7.3a.3) show the difference compared to that of the thin-film composite (TFC) RO membrane (Figure 7.3b.2 and 7.3b.3). The supporting layer of the FO membrane is comprised of polyester fibers with voids on the order of several tens of micrometers, which are clearly visible on the backside. In contrast, the SEM image of the RO membrane indicates that a dense, non-woven fabric layer existed on the supporting layer, which provided mechanical strength. The porous and spacious supporting layer of the FO membrane contributed to the significantly minimized ICP.

No flux reduction was observed for the RO membrane, but a flux reduction of approximately 30% was observed in the FO membrane with 3 GPH. Surprisingly, the FO membrane with 18 GPH exhibited a dramatically reduced water flux (22.8 to 11.4 L m<sup>-2</sup> h<sup>-1</sup> (LMH)), which corresponds to a reduction of about 50%. The reduction in flux could be attributed to the apparent driving force, which also gradually decreased as water passed through the membrane from the FS to the DS side. Thus, the specific water flux term (flux normalized by the reduced osmotic pressure, refer to the dilution effect of DS) can be used to compare the flux decline in FO mode, as shown in Figure 7.2a.2 and 7.2b.2. Generally, in all cases, the specific water flux increased, indicating that it had no connection with SOC solute fouling and CP during the filtration process. The slight increase in specific water flux was attributed to the stabilization of the FO process.

Interestingly, the specific water flux of FO membranes (both of 3 and 18 GPH) was shown to increase slightly, while the specific water flux of RO membranes increased far more over longer filtration times. This behavior could be explained by the severe ICP, which may have led to compensation of the initial drop in the flux reduction and to less dilutive ICP from less tortuosity and porosity in the supporting layer of the RO membrane [227].

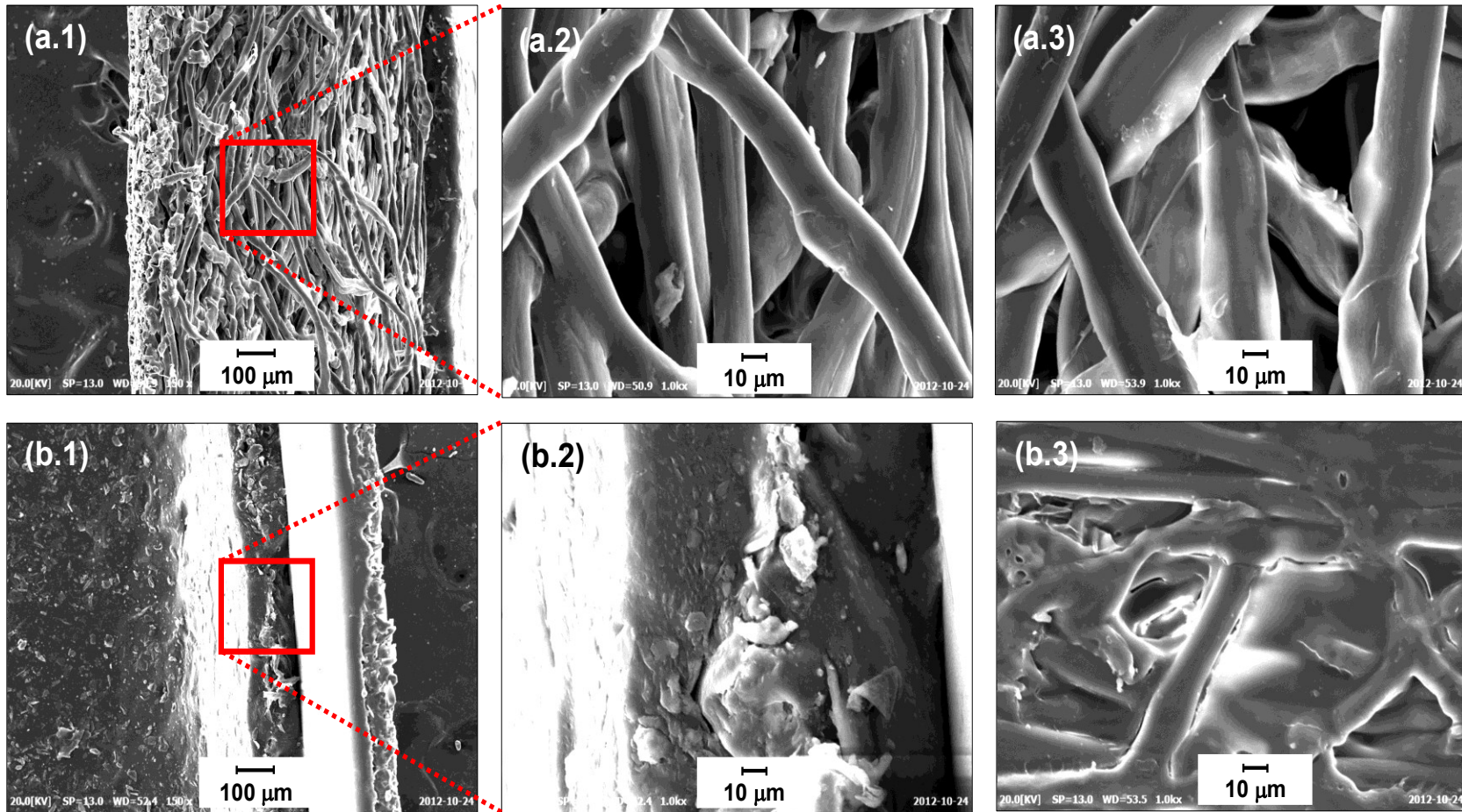


**Figure 7.3** SEM image of FO-CTA and RO-BW30 membrane: (a.1) FO membrane cross-section (×150), (a.2) FO membrane cross-section of supporting layer (×1K), (a.3) FO membrane back side (×1K), (b.1) RO membrane cross-section (×150), (b.2) RO membrane cross-section of supporting layer (×1K), and (b.3) FO membrane back side (×1K).

The reverse solute flux through the FO and RO membranes from the high concentration DS side to the FS side was evaluated by measuring conductivity of the feed water side, as shown in Figure 7.4.

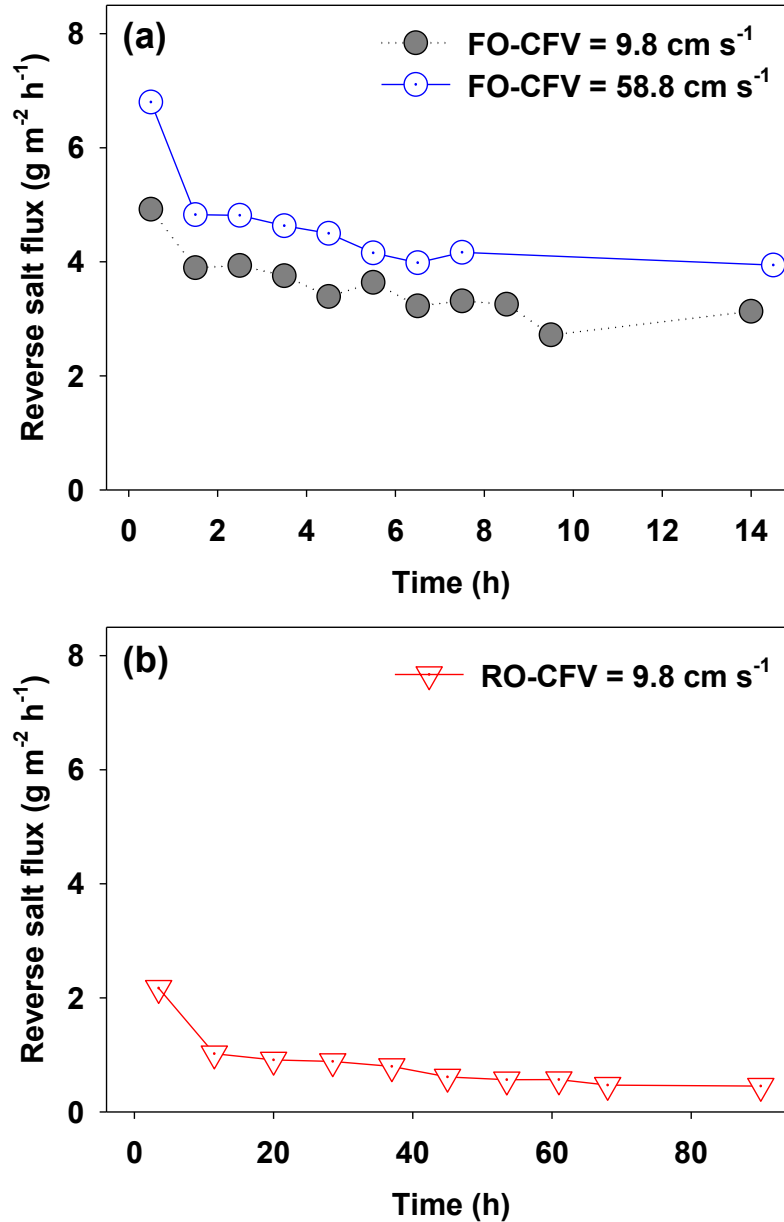


**Figure 7.4** Reverse salt flux as a function of time for two FO membrane experiments and one RO experiment: (a) FO membrane (3 and 18 GPH) and (b) RO membrane. Operating conditions: the initial concentration of SOCs = each of 5  $\mu\text{M}$ ; draw solution = 1 M NaCl; cross-flow velocity (CFV) = 3 or 18 GPH; the temperature =  $20 \pm 1$   $^{\circ}\text{C}$ .

Unlike in ideal semi-permeable membrane conditions, real membranes with AL-facing-FS configurations exhibited reverse solute permeation from the DS entering the porous support as a result of the water flux from the FS to the DS (convection). As shown in Figure 7.4, the reverse salt flux at a CFV of 18 GPH was higher than that at a CFV of 3 GPH. The FO membrane exhibited six times higher reverse salt flux compared to the RO membrane. The reverse salt flux decreased over time for both membranes. These reverse salt flux curves were nearly identical to the water flux trends, thereby indicating that the dilutive ICP, ECP, and osmotic driving force played dominant roles in reverse salt flux and was consistent with previous water flux behavior [254].

### 7.3.3 SOCs retention by FO and RO membranes

Bench-scale FO tests were performed to evaluate the removal of relatively hydrophilic compounds ( $\log K_{ow} < 2.5$ ) in a simple matrix with an AL-facing-FS configuration. Under this condition, permeate water flux behavior in the FO membrane ( $13.25 \pm 0.25$  LMH) was greater than that in the RO membrane ( $1.62 \pm 0.13$  LMH). The CTA-based membranes exhibited higher water flux compared to TFC polyamide membranes during FO-mode processing. This behavior was attributed to the fact that the FO membrane has high water affinity on the membrane AL and lower structural characteristics in FO-mode operations. The rejection values of the SOCs by each FO and RO membrane are presented as a function of permeate volume in DS, as shown in Figs. 7.5–7.

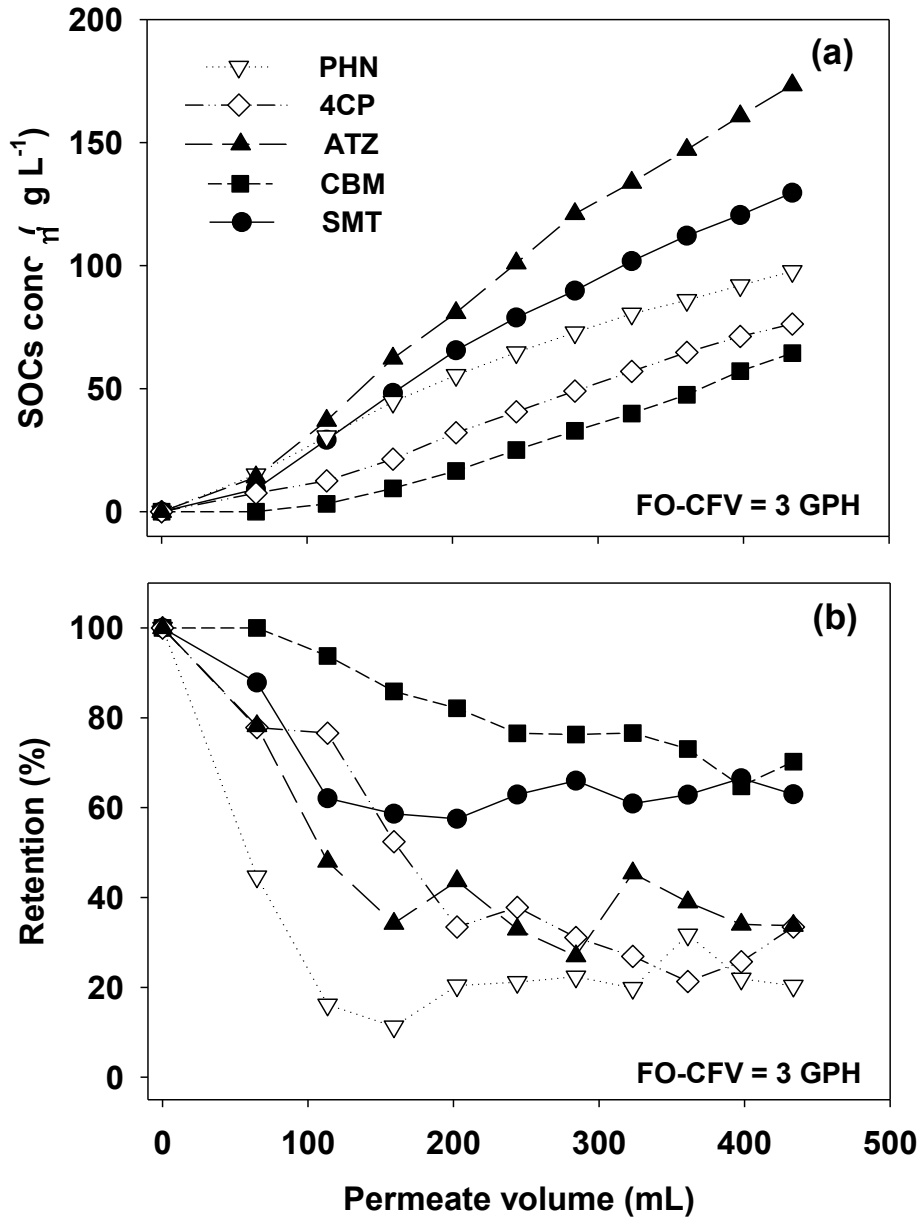


**Figure 7.5** Comparison of (a) SOC concentration in permeate and (b) SOC retention as a function of time with FO membrane in the FO-mode at the cross-flow velocity of 3 GPH. Operating conditions: the initial concentration of SOC = each of 5  $\mu\text{M}$ ; pH = 7; draw solution = 1 M NaCl; the temperature =  $20 \pm 1$  °C.

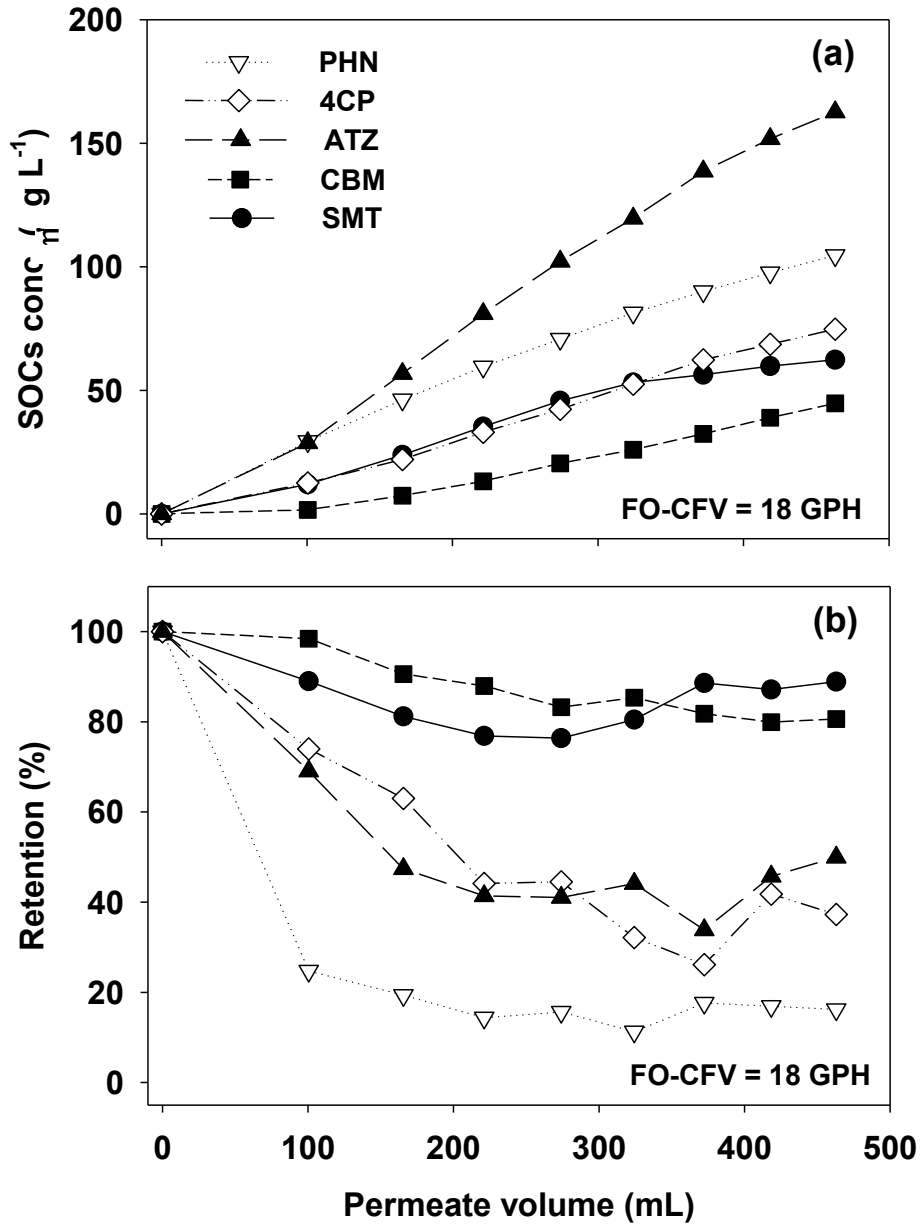


**Figure 7.6** Comparison of (a) SOC concentration in permeate and (b) SOC retention as a function of time with FO membrane in the FO-mode at the cross-flow velocity of 18 GPH. Operating conditions: the initial concentration of SOC = each of 5  $\mu\text{M}$ ; pH = 7; draw solution = 1 M NaCl; the temperature =  $20 \pm 1$  °C.

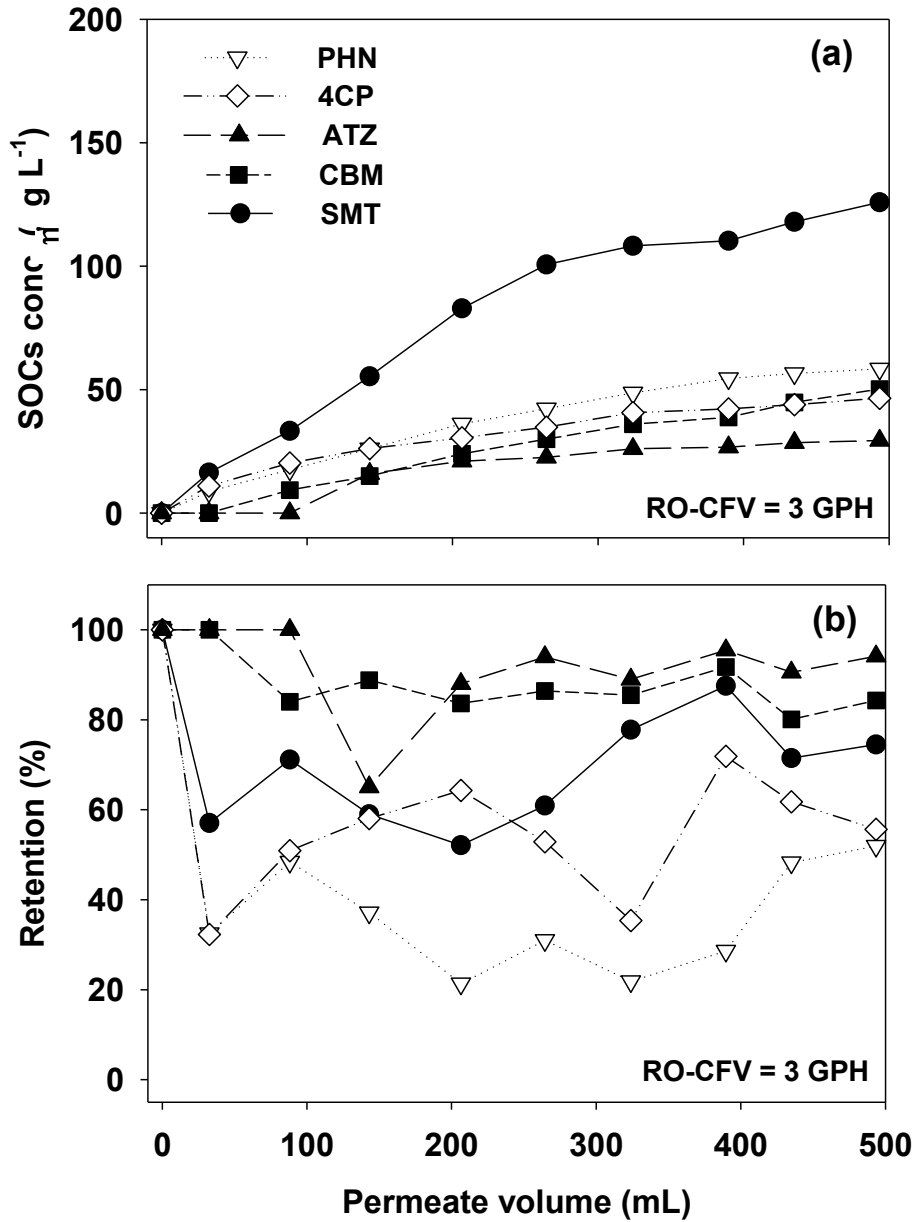


**Figure 7.7** Comparison of (a) SOC concentration in permeate and (b) SOC retention as a function of time with RO membrane in the FO-mode at the cross-flow velocity of 3 GPH. Operating conditions: the initial concentration of SOC = each of 5  $\mu\text{M}$ ; pH = 7; draw solution = 1 M NaCl; the temperature =  $20 \pm 1$  °C.

The SOC retention values at the end of each membrane filtration are also summarized in Figure 7.8a. As shown in Figs. 7.5–7, the SOC retentions had a tendency to fluctuate as a result of experimental error at some permeate volumes, because the SOC



retentions were calculated by mass balance and thus reflected the dilution factor, which was influenced by the mass of the previously collected DS. However, although some experimental error is present, a general trend could be observed: all of the SOC concentrations increased on the DS side as the filtration process progressed. The transport of SOCs through the FO-mode process ranged between 64–173, 45–163, and 29–126  $\mu\text{g L}^{-1}$ , for FO-3 GPH, FO-18 GPH, and the RO membrane at the end of permeate, respectively. The removal of SOCs was between about 20 and > 98% over the whole process, depending primarily on molecular size and charge. For FO membranes with a CFV of 3 and 18 GPH, the average retentions of SOCs at the end of the accumulated 100-mL permeate followed the declining order: SMT ( $66.5 \pm 3.4\%$  and  $89.7 \pm 3.1\%$ )  $\approx$  CBM ( $68.2 \pm 3.0\%$  and  $82.6 \pm 4.1\%$ )  $\gg$  ATZ ( $34.2 \pm 0.6\%$  and  $48.7 \pm 2.6\%$ )  $>$  4CP ( $28.3 \pm 4.4\%$  and  $38.6 \pm 2.8\%$ )  $>$  PHN ( $20.9 \pm 0.9\%$  and  $21.9 \pm 9.3\%$ ), respectively. In FO membranes, retentions of the negatively charged dominant species in some SOCs (CBM and SMT, by their pKa values) were greater than 67%, excluding the chlorinated pesticide compound ATZ, which has a triazine ring and amines, while the rejection of the nonionic and relatively small MW size of other SOCs (PHN and 4CP) was more variable, between approximately 21 and 34%. These results agreed well with previously reported studies that indicated that high CFVs could increase solute rejection in AL-facing-FS configurations. The increase of co-current CFV had a significant influence on the diffusive movement (hindered diffusion of SOCs) and interfered with reverse salt flux by decreasing the ECP [239].

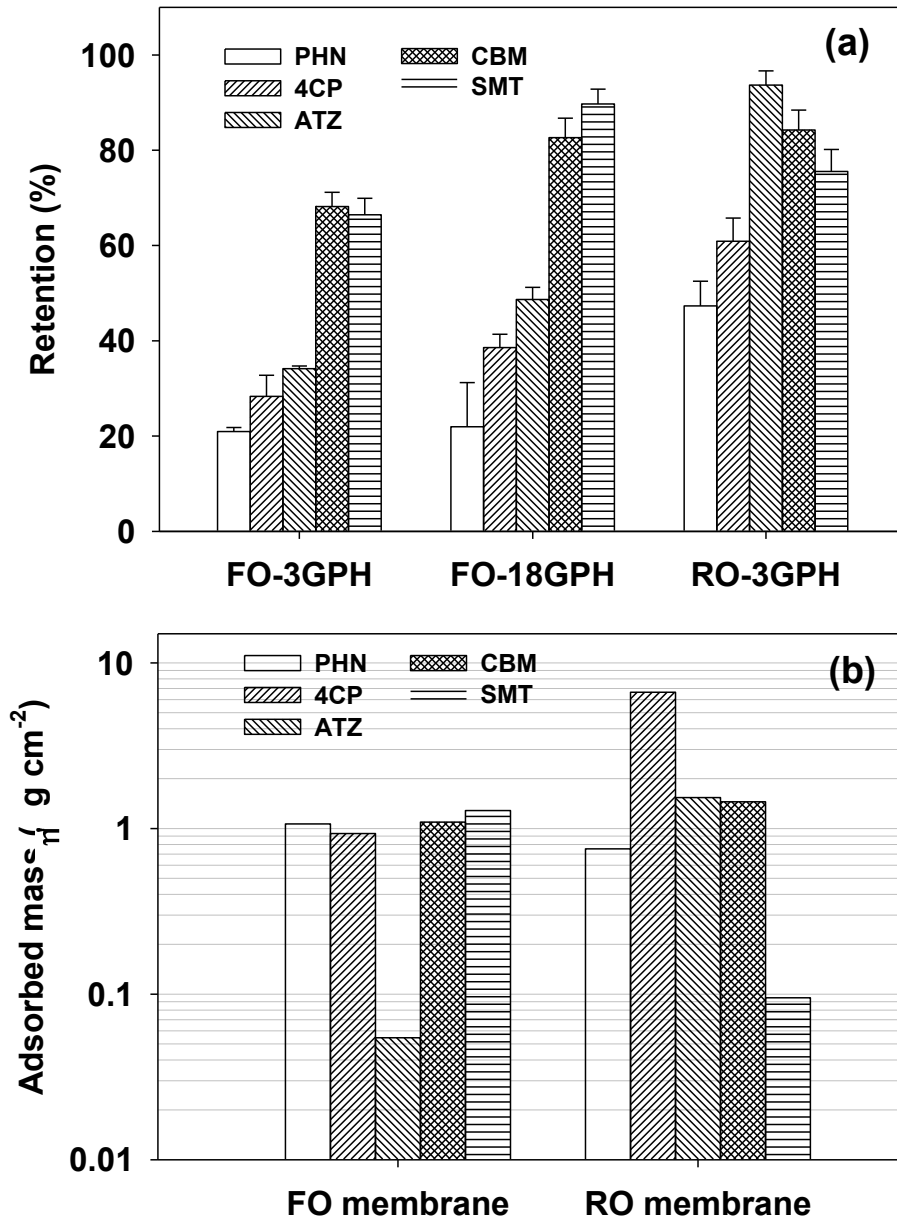


**Figure 7.8** Comparison of (a) SOCs retention between FO and RO membrane and (b) the normalized SOCs adsorbed mass onto FO and RO membrane. Operating conditions: the initial concentration of SOCs = each of 5  $\mu\text{M}$ ; pH = 7; draw solution = 1 M NaCl; cross-flow velocity (CFV) = 3 or 18 GPH; the temperature =  $20 \pm 1$   $^{\circ}\text{C}$ . Adsorption experimental conditions: the initial concentration of SOCs = each of 5  $\mu\text{M}$ ; total membrane area = 20  $\text{cm}^2$ ; contact time = 96 h.

As shown in Figure 7.8, the SOC retention tended to rise with increasing MW, regardless of CFV. This tendency was expected based on hindered diffusion; thus, the

SOC sizes significantly influenced the SOC retention behavior during the FO process. The poor retention of ATZ by FO membranes (compared to CBM and SMT) could be attributed to its lower affinity for the membrane polymer and size-exclusion contributions, because the MW of ATZ is slightly less than that of CBM, although they have similar hydrophobicity. There is no apparent explanation for this behavior except adsorption affinity onto the FO membrane. This behavior was clearly indicated by the adsorption experiment (the specific adsorption mechanism will be discussed in more detail later) with an equivalent concentration and membrane area corresponding to FO-mode, as summarized in Figure 7.8b. The adsorption data were obtained by normalizing the adsorbed SOC capacity by membrane area. The adsorbed mass by the FO and RO membranes were 1.07 and 0.75  $\mu\text{g cm}^{-2}$  (PHN), 0.93 and 6.65  $\mu\text{g cm}^{-2}$  (4CP), 0.05 and 1.54  $\mu\text{g cm}^{-2}$  (ATZ), 1.09 and 1.45  $\mu\text{g cm}^{-2}$  (CBM), and 1.28 and 0.1  $\mu\text{g cm}^{-2}$  (SMT), respectively. These results indicated that the amount of adsorbed ATZ was significantly lower than for the other SOCs. In the RO membrane, the average SOC retentions followed the declining order: ATZ ( $93.7 \pm 3.0\%$ ) > CBM ( $84.3 \pm 4.2\%$ ) > SMT ( $75.2 \pm 4.6\%$ ) > 4CP ( $60.9 \pm 4.9\%$ ) > PHN ( $47.3 \pm 5.2\%$ ). In general, the RO membrane exhibited higher removal efficiency than the FO membrane. The higher removal efficiency of the RO membrane could be attributed to the positively coupled effects from size exclusion, electrostatic repulsion (Donnan exclusion), and adsorption to the membrane surface, while the relatively small water flux in the RO membrane negatively influenced the SOC retentions. In addition, the higher ICP generated by the dense supporting layer may have allowed increased partitioning of SOCs and, thus, increased the SOC retention compared to that observed in the FO membrane.

Along with the previous results, these results indicated that high electrostatic repulsion and severe ICP mechanisms affected the SOC retentions simultaneously, even though the selectivity of salts was lower in the RO membrane than in the FO membrane. The retention of negatively charged SOCs (CBM, SMT, and ATZ) was greater than 75%, while the rejection of the nonionic SOCs (PHN and 4CP) was approximately between 47 and 61%. However, SMT exhibited slightly lower retention than expected based on its size, although SMT compounds were previously found to be highly retained by FO membranes. This unexpected result is likely due to hydrophobic interactions and/or weak hydrogen bonding between SMT and the RO membrane. Among similarly sized compounds, the lower log Kow of SMT exhibited a weak influence on its rejection; an increase in rejection with increasing log Kow was observed in the case of CBM and ATZ. This phenomenon is in agreement with Kiso *et al.* [255], who observed that the rejection of most hydrophobic molecules by CTA membrane material increased with increasing affinity of the solute for the membrane. It should be noted that SOC retentions in the FO-mode experiments were comparatively low in this study. While ionic SOC retentions were greater than about 80% at the initial stage, the general retention of these SOCs was significantly lower than expected based on membrane characteristic experiments, which demonstrated that sodium chloride and glucose were efficiently removed with rejection ranging from approximately 85 to 97%. (The FO-mode is not a pressure-driven process, but its retention mechanisms are expected to follow those of conventional RO processes.) These less optimal SOC retentions might be explained by the following: (i) the relatively low water flux through the membrane can permit solute transportation substantially well across the membrane by hindered diffusion mechanisms [256]; (ii) the relatively low

surface charge of the FO membrane compared to the RO membrane might reduce SOC retentions, while the RO membrane still has higher SOC retention compared to that of the FO membrane [235]; (iii) the high initial concentrations of spiked SOCs were in the range of 485–1,280  $\mu\text{g L}^{-1}$ , which might have affected the higher ECP and SOC diffusion on the membrane surfaces [257], leading to poor removal performance.

#### **7.3.4 Influence of compound characteristics and membrane properties on adsorption**

The initial membrane adsorption of SOCs could be a trivial factor, because the membranes were quickly saturated, and adsorption decreased over long-term operation. However, it is worthwhile to isolate the effect of initial adsorption and predict the exact SOC retention trends for the most appropriate correlations between membrane and SOC properties [127]. Therefore, batch adsorption experiments were employed to determine the FO and RO membrane adsorption capacities under equilibrium conditions (Figure 7.9) as an example of the significant variation in adsorption trends between FO and RO membranes. For comparison, the membrane adsorption tendencies of various hydrophilic SOCs over time were compared with those of EE2. In this experiment, a sufficiently-large membrane area was employed so that SOC adsorption on the membranes could be maximized and free of competitions among the SOCs (membrane area = 100  $\text{cm}^2$ ,  $C_0$  = each of 2  $\mu\text{M}$  SOCs).

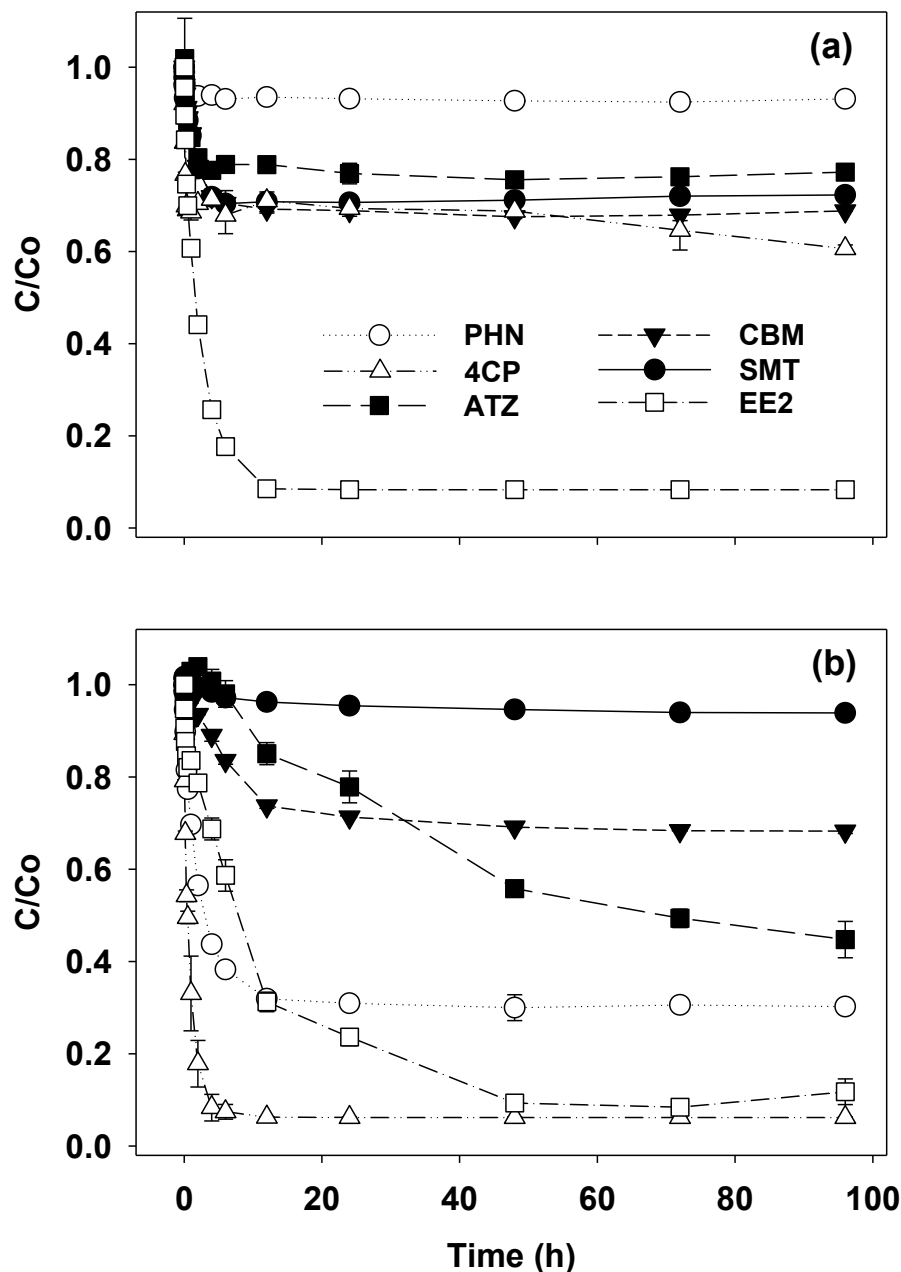


**Figure 7.9** Comparison of SOCs adsorption onto (a) FO membrane and (b) RO membrane as a function of time. Adsorption experimental conditions: the initial concentration of SOCs = each of 2  $\mu\text{M}$ ; pH = 7; total membrane area = 100  $\text{cm}^2$ ; contact time = 0-96 h.

For the FO membrane, in general, the adsorption of most compounds was less than 40%, except for EE2 (92%), which has a higher log  $K_{ow}$  (3.9) than the hydrophilic SOCs.

The compounds exhibited the following adsorption order of normalized  $C/C_0$  values at

equilibrium (removal, 96 h): EE2 ( $91.7 \pm 0.4\%$ )  $\gg$  4CP ( $39.4 \pm 0.8\%$ ) > CBM ( $31.2 \pm 0.1\%$ ) > SMT ( $27.7 \pm 0.6\%$ ) > ATZ ( $22.8 \pm 0.3\%$ )  $\gg$  PHN ( $6.9 \pm 0.1\%$ ). The comparatively hydrophilic SOCs, including SMT, CBM, and ATZ, were observed to have lower adsorption affinity onto the FO membrane compared to EE2 based on their hydrophobicity. However, SMT, CBM, and ATZ did not exhibit any correlation based on log Kow values. In particular, phenolic compounds (PHE and 4CP), which have relatively low MWs compared to the other SOCs used in this study, exhibited different adsorption trends (6.9% for PHE, 39.4% for 4CP) because of their different characteristics (*i.e.*, phenol is highly soluble in water compared to 4CP). The adsorption of 4CP (log Kow = 2.39, pKa = 9.1) was higher than that of PHN, as expected, based on the hydrophobicity of these two SOCs. The charge repulsion caused by de-protonation, which occurred because the solution pH was higher than the compound dissociation constant (pKa) value, did not significantly influence the adsorption process in either membrane compared to log Kow.

For the RO membrane, the adsorption affinity of SOCs roughly correlated with their hydrophobicity, except for phenolic compounds, which have different characteristics (the adsorption affinity of 4CP onto the RO membrane was remarkably higher, and 4CP reached a pseudo-equilibrium state faster than other SOCs). The SOC adsorption affinities on the RO membrane exhibited the following order of normalized C/C<sub>0</sub> values (removal, 96 h): 4CP ( $93.8 \pm 0.1\%$ ) > EE2 ( $89.9 \pm 1.5\%$ )  $\gg$  PHN ( $69.8 \pm 1.5\%$ ) > ATZ ( $55.2 \pm 3.9\%$ ) > CBM ( $31.8 \pm 0.5\%$ )  $\gg$  SMT ( $6.2 \pm 0.2\%$ ). In phenolic compounds, the higher retention by the polyamide RO membrane was caused by the following attributes [224, 258-260]: (i) the physicochemical properties, including the functional groups (-OH

and -Cl), solubility, and hydrophobicity, which impart high affinity to the polyamide materials, (ii) the chlorine functional group of 4CP is an electron-withdrawing group, so the reaction affinity with the membrane polymer might dominate, (iii) water solubility is generally correlated with log  $K_{ow}$ , thus suggesting that the adsorption capacity of 4CP onto the RO membrane increased with lower solubility, and (iv) many studies of membrane adsorption have reported that SOC adsorption onto membranes is influenced by the membrane surface as well as by the supporting layer and the membrane pores. Furthermore, Yoon *et al.* [261] reported that adsorption is related to the membrane pore radius, thereby allowing relatively low MW SOCs (*e.g.*, PHN and 4CP) to access and diffuse to the membrane's internal adsorption sites. Therefore, it could be concluded that, overall, a weak correlation existed between all SOCs; separately between phenolic and other SOCs, a strong correlation was observed between hydrophobicity and adsorption capacity.

### **7.3.5 Molecular modeling of SOCs adsorption behavior onto FO and RO membranes**

The SOCs can bind onto the surfaces of FO and RO membranes at different orientations depending on the medium and the nature of the interactions. Representative MD snapshots in Figure 7.10 show the FO-EE2 and RO-EE2 complexes in aqueous solution (the others are shown in Appendix A).



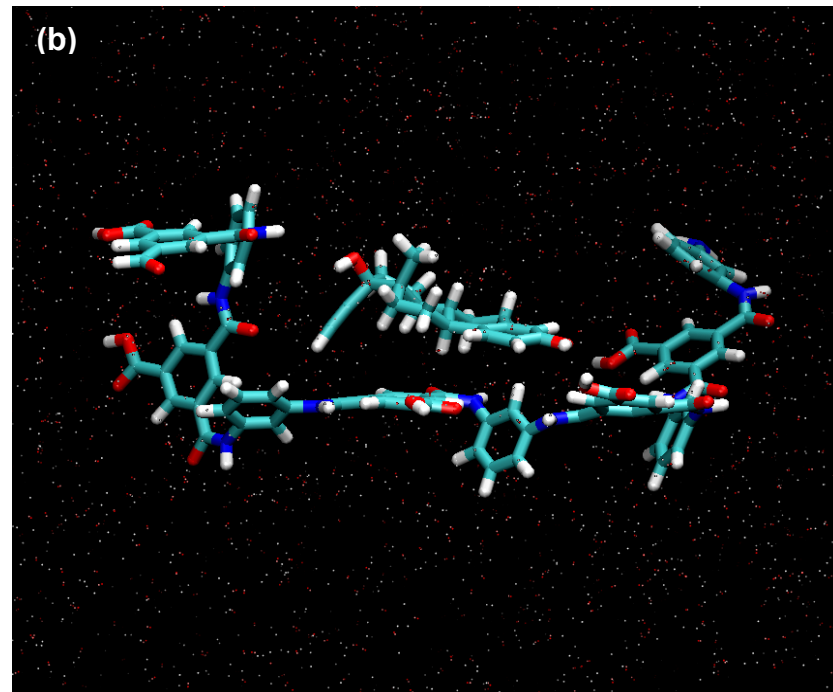
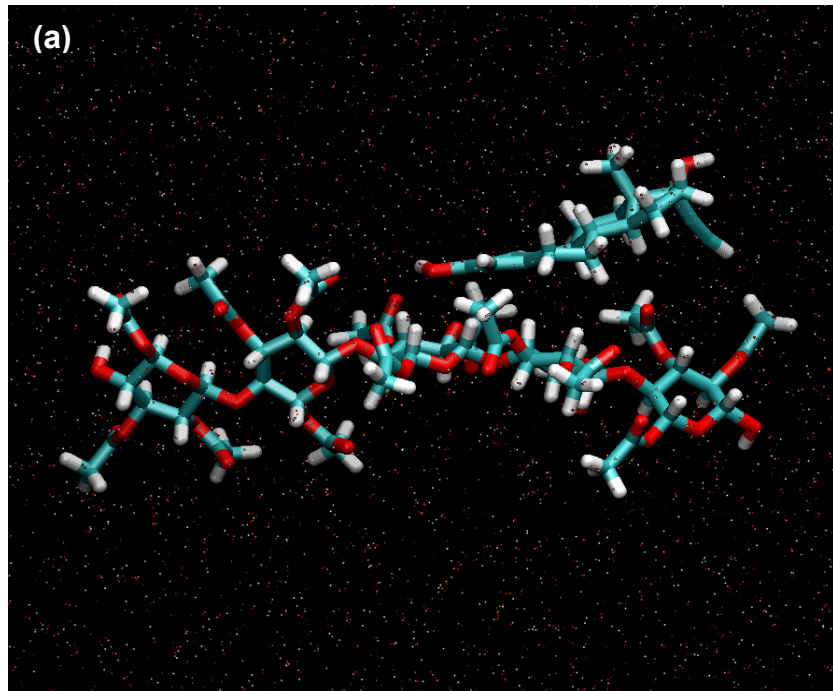


**Figure 7.10** Representative MD snapshot of optimum (a) FO membrane with EE2 and (b) RO membrane with EE2 complexes in aqueous solution.

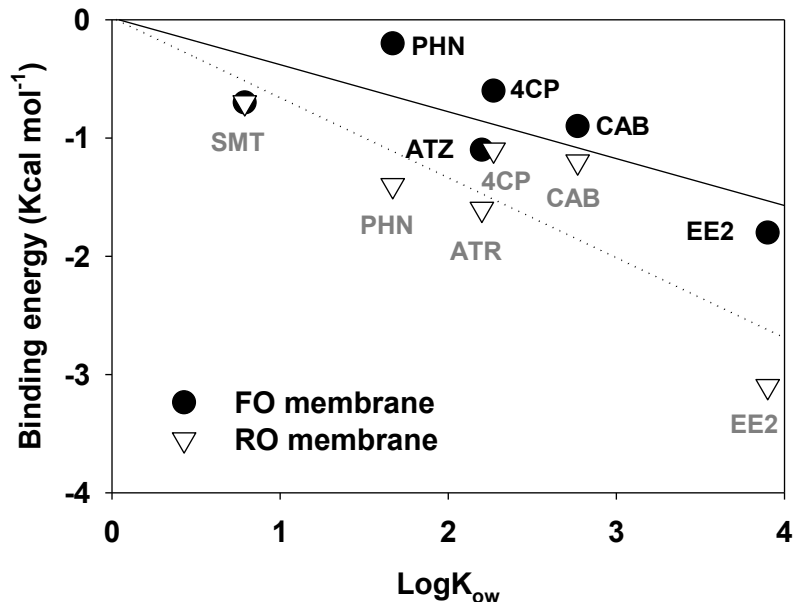


**Figure 7.11** Binding energy of SOCs onto FO and RO membrane with respect to log Kow values (binding energy was computed using AMBER 11 software).

In the case of the RO membrane, cross-linkage of the repeating units of the FT-30 polyamide resulted in the formation of a curled configuration around the SOCs to increase interactions, while the geometry of the CTA-FO membrane remained relatively linear over the course of the simulation. Figure 7.11 shows the dependence of the binding free energies on log Kow. The free energies associated with the binding of the various SOCs onto the membranes show an increasing trend with increasing log Kow. As expected, EE2 had the greatest interaction with both the FO and RO membranes due to its hydrophobic nature and corresponding high log Kow value in comparison to the hydrophilic SOCs. In one of its lower energy configurations, shown in Figure 10, the methyl group is oriented away from the surface of the FT-30 RO membrane, thus allowing for maximum overlap of orbitals between EE2 and the adsorbent. In the case of the FO-EE2 pair however, periodic flips in the orientation of the methyl group towards the surface of the membrane and away from the surface of the membrane resulted in a

smaller  $\pi$ - $\pi$  area of influence and a less favorable binding energy compared to that of the RO-EE2 pair (-1.8 vs. -3.1 kcal mol<sup>-1</sup>). Moreover, binding between the SOCs and the RO membrane was more favorable compared to binding with the FO membrane due to the hydrophobic nature of the FT-30 polyamide RO membrane. Snapshots of the MD simulations show periods of separation between the FO membrane and the hydrophilic SOCs. Based on the 8 Å nonbonded interaction cut off limit, long range interactions between the membranes and SOCs at very far intermolecular separations were not significant and were not included in the free energy calculations. Despite the relatively low log Kow value of PHN, a more favorable interaction was observed between PHN and the RO membrane relative to 4CP and CBM. Thus, it is possible that the aromatic ring in PHN prefers the less polar polyamide membrane to the bulk solution [258], thereby increasing the propensity of PHN to bind onto the surface of the hydrophobic FT-30 RO membrane. This is also consistent with the result of adsorption experiments where the favorable binding translated to increased adsorption of PHN onto the RO membrane. In addition to the binding of phenol onto the surface of the RO membrane and the rapid disappearance of PHN can further be attributed to possible diffusion of the PHN molecules into the membrane pores as observed in the study by Hughes and Gale, 2012 [258].

### **7.3.6 Comparison of SOCs retention and flux behavior during RO process**

RO-mode experiments were performed to verify the performance in terms of flux decline profile and SOC retentions as a function of the volume concentration factor (VCF), as shown in Figure 7.12.

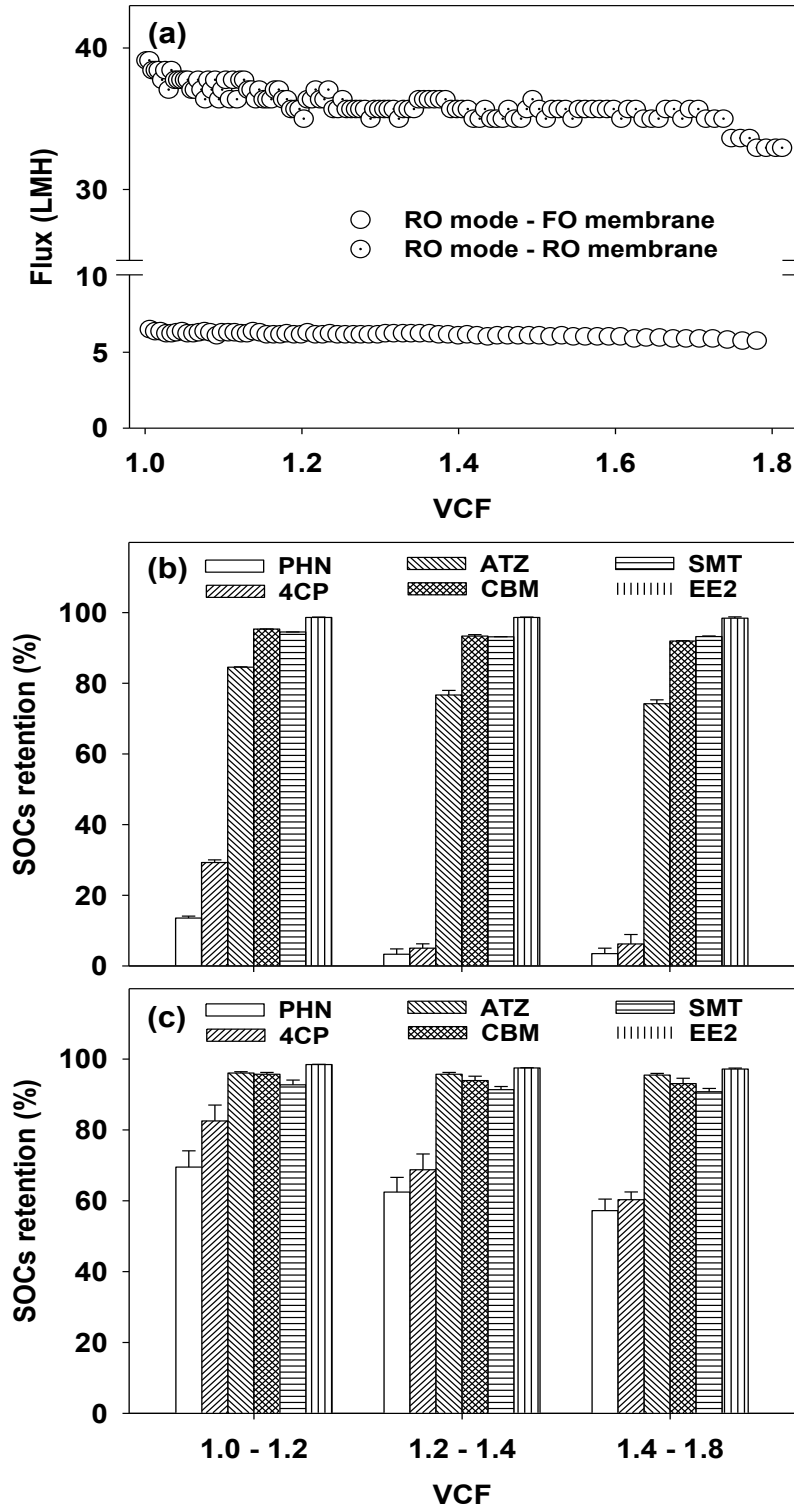


**Figure 7.12** Flux decline and SOC retention as a function of VCF in RO-mode: (a) flux decline between FO and RO membrane, (b) SOC retention with FO membrane, and (c) SOC retention with RO membrane. Operating conditions:  $\Delta P = 20$  bar; stirring speed = 300 rpm; the initial concentration of SOC = each of 5  $\mu\text{M}$ ; pH = 7.

The VCF could be a more meaningful parameter for adsorption characterization, because the retained solute concentration on the membrane surface can mechanistically influence the solute retentions and flux by ECP and diffusion at the interface of the membrane [262]. Conversely, in the comparison of flux curves for both FO and RO membranes, the higher water flux was observed for the RO membrane, which confirms that the FO membrane is mechanistically different than the RO membrane, as previously mentioned. The RO membrane experiences a sharper flux decline than the FO membrane; the flux is 15% less for the RO membrane and only 2–3% reduced for the FO membrane, as shown in Figure 7.12a. For the FO membrane, it is likely that the water flux was not influenced by the SOC concentration in the FS. Finally, the ECP layer formed in the FO membrane had less influence on the flux reduction due to the lack of the solute flux at the same applied pressure of 20 bar. For the RO membrane, higher flux led to the highest osmotic pressure at the membrane surface, which lowered the flux by reducing the effective trans-membrane pressure, because the ECP increased with increasing osmotic pressure. The release and breakthrough of SOCs could be affected by the variation in solution recovery and subsequent VCF. When the stirring speed (300 rpm) was applied to agitate the FS completely, it was expected that the back diffusion phenomenon would diminish. In this condition, to verify the effect of solution recovery between FO and RO membranes, SOC retentions were compared at the same VCF, as shown in Figure 7.12b and 12c. For all selected SOCs, the RO membranes exhibited higher retentions than the FO membranes, which intrinsically caused differences in zeta potential, hydrophobicity, density of active/supporting layers, and pore size. In addition, these results indicated that the membrane selectivity derived from the SD model does not adequately coincide with

SOC retentions in both membranes; however, the SOC retention trended with increasing SOC size (listed by MW) based on greater steric interactions rather than on other mechanisms (electrostatic repulsion and/or hydrophobicity). For phenolic compounds and ATZ, retentions were remarkably lower in the FO membrane than in the RO membrane. The results reported here, indicate that RO-mode operation with FO-type membranes may cause a substantial increase in permeate concentrations of SOCs based on this distinct breakthrough phenomenon, which is often seen in both dead-end and cross-flow filtration operations [131].

#### **7.4. Conclusions**

This study evaluated the removal behavior of several SOCs (PHN, 4CP, ATZ, CBM, SMT, and EE2) by investigating available FO and RO membranes systematically in both FO and RO processes. The study also included computational modeling for membrane adsorption. For the RO membrane in FO mode, ICP was severe and attributed to the lower porosity of the supporting layer of the RO membrane. The lower porosity played a dominant role in the reduction of water and/or reverse salt flux. Compared to the polyamide-based RO membrane, the CTA-based FO membrane exhibited superior water flux performance due to the optimized properties of its active and supporting layers in FO mode. However, higher removal for most of SOCs studied was achieved with the RO membrane at the expense of severe ICP and flux reduction. The results once again confirmed the dominant role of ICP, and the trade-off between flux and removal efficiency depends on the porous supporting layer in AL-facing-FS configurations in the FO process. Therefore, further investigation of this phenomenon is needed, particularly

with respect to membrane properties specialized for the FO process. In the removal of SOCs, the FO membrane, which is mostly uncharged, mainly relied on size exclusion; in contrast, the RO membrane was controlled by both size and electrostatic exclusion. For all SOC compounds studied, except for phenolic compounds, the adsorption capacity generally depended on the log  $K_{ow}$  in both membranes. Although the mechanism is unclear, significant adsorption capacity was observed between phenolic compound 4CP and RO membranes. Compared to the FO membrane, the RO membrane exhibited superior performance in RO mode in terms of higher water permeability and SOC removal. In particular, for the FO membrane in RO-mode operation, possible subsequent breakthrough release of phenolic compounds and ATZ was observed due to their relatively low MWs. It is also worth noting that the comparatively small size and hydrophilic nature of the neutral SOCs significantly increased the transportation to the DS side in the FO-mode configuration, which is expected to be important for the application of FO in environmental water filtration for directly potable usage. Finally, this breakthrough release needs to be further investigated and tested in pilot-scale experiments.

### **Acknowledgements**

This research was supported by the GS E&C Research and Institute Korea Ministry of Environment, ‘GAIA Project, 2012000550022’.

## CHAPTER 8

### OVERALL CONCLUSION AND FUTURE RECOMMENDATIONS

Overall, the results from UF incorporated with SWNTs as adsorbents have demonstrated high removal efficiencies of BPA and E2/EE2 by mainly adsorption mechanisms with SWNTs, as well as the addition of SWNTs to the UF process did not significantly exacerbate the permeate flux decline and total membrane resistances. Significant removal of these compounds and the potential feasibility of FO membrane system to the environmental filtration were observed to meet more stringent treatment goals. In relation to the removal of EDCs from various water sources (Chapters IV and VI), the following conclusions can be derived:

- 1) The adsorbed/delivered mass for BPA and E2/EE2 derived from the mass-balance during membrane filtration provided a reasonable comparison of their retention and adsorption trends.
- 2) A strong linear correlation between the retention and adsorption of BPA and E2 was observed, indicating that adsorption was an important mechanism for the retention of hydrophobic compounds and was dependent on the log  $K_{ow}$ , in which preferential removal by membrane adsorption occurred for the more hydrophobic E2, compared to BPA, leading to increased adsorptive hydrophobic interactions



- 3) The addition of NOM during UF filtration led to competition for adsorption sites, resulting in lowered adsorption of micropollutants. The adsorption of the relatively high hydrophobic EE2 onto CNTs is more competitive than BPA in the presence of NOM in ASW. For ASW, the adsorption capacity of SWNTs resulting from both screening effect and salting-out effect in high ionic strength, was relatively insignificant for all those experiments.
- 4) Membrane fouling by NOM through pore blockage and cake/gel formation considerably impacted the transport of BPA and E2 in the SWNTs-UF systems due to various NOM-SWNTs-UF-BPA/E2 interactions in the solution.

Based on the NOM removal in SWNTs-UF systems (Chapter V), the following conclusions can be derived:

- 1) Applying the SWNTs in conjunction with UF has shown considerable advantages in terms of fouling rate reduction and NOM removal efficiency.
- 2) The adsorption of NOM on SWNTs varies with solution pH and ionic strength, which could affect the flux decline and rejection trends. It is related to the point of zero charge on SWNTs in HA solutions because the adsorption of NOM on SWNTs is driven by electrostatic interactions. For IS effect, IS causes a greater decrease in flux decline and rejection trends, because high IS can exacerbate fouling by compacting the cake/gel layer, thereby increasing the HA concentration on the membrane surface, in addition, condensing of the HA structure easily allows it to pass through membrane pores, which then leads to lower HA rejection trends.

- 3) Considering the specific fouling resistances, SWNTs–UF resulted in greatly reduced membrane resistances per unit retained DOC mass. The characteristics of the fouling layer were more dependent on the HA deposition and HA adsorptive fouling since single SWNTs with a length of 5–30  $\mu\text{m}$  are somewhat too large to block the membrane pores.
- 4) The early stages of both SWNTs–UF and UF alone in unstirred conditions were more dependent on intermediate blocking or a combination of intermediate blocking and cake filtration, while cake filtration became the more dominant mechanism as filtration progressed.
- 5) A high flux decline observed at high  $J_v/k$  values was due to concentration polarization (CP) and cake/gel layer formation, which hindered the transportation of NOM, and NOM transportation in SWNT–UF systems depends, to a significant extent, on the CP and cake/gel layer formation at the membrane boundary.

Based on the removal of synthetic organic compounds by forward osmosis and reverse osmosis membrane (Chapter VII), the following conclusions can be derived:

- 1) In comparison of membrane characteristics identified with the solution-diffusion model, the cellulose triacetate based FO membrane exhibited the lower selectivity ratios, indicating that the FO membrane has the better separation properties than that of polyamide based RO membrane.
- 2) At the RO membrane application in FO-mode, ICP was severe due to less porosity of the supporting layer of RO membrane, and it played a dominant role in the reduction of water and/or reverse salt flux.

- 3) The FO membranes mainly relied on size exclusion since it was almost uncharged while RO membrane was controlled by interactions between size and electrostatic exclusion.
- 4) The free energies associated with the binding of the various SOC<sub>s</sub> onto the membranes show an increasing trend with increasing log K<sub>ow</sub> because EE<sub>2</sub> had the greatest interaction with both the FO and RO membranes due to its hydrophobic nature and corresponding high log K<sub>ow</sub> value in comparison to the hydrophilic SOC<sub>s</sub>
- 5) It has possibility that the comparatively small size and hydrophilic neutral SOC<sub>s</sub> can seriously increase the transportation to the draw side in FO-mode configuration.

Low pressure membranes (LPMs) employing ultrafiltration (UF) and microfiltration (MF) incorporated with SWNTs as adsorbents are an integral part of pretreatment processes for seawater desalination as well as wastewater reclamation and drinking water treatment. However, it should be noted that despite the high adsorption capacities of CNTs in water treatment and purification, they still have several challenges including economic feasibility, health risks, and environmental impacts for practical implementations. Several researchers have reported that the release of CNTs into the environment may cause harmful impacts on ecosystem. In particular, CNTs' health effects on human life with water are still a controversial issue. Also, for the CNT use in drinking water treatment plants, one of the possible problems is the escape of CNTs during the membrane filtration process. In addition, CNTs are still relatively expensive for large scale applications in water treatment. However, continuous mass production of

CNTs will possibly provide large quantities of CNTs with economically viable prices for large scale applications in the near future. Although the experiments were conducted at high concentrations above typically reported levels in drinking water sources, the results still provide guidelines for SWNTs/UF hybrid membrane filtration since the retention of trace organics at parts per-billion or parts-per-trillion levels are independent of initial concentration. In addition, these FO results have shown that the membrane selectivity derived from the SD model does not adequately coincide with SOCs retentions in both membrane cases. Also, in RO-mode, for phenolic compounds and ATR, retentions were remarkably lower with FO membrane than those with RO membranes. The results observed here, consequently, reflect that RO-mode operation with FO type membranes may cause a substantial increase in permeate concentration of SOCs based on this distinct breakthrough phenomenon, therefore when the application of FO to the environmental filtration for directly potable usage, these breakthrough release and SOCs retention model for FO membrane in FO-mode needs to be further investigated and tested in pilot scale experiments.

## REFERENCES

- [1] D.W. Kolpin, E.T. Furlong, M.T. Meyer, E.M. Thurman, S.D. Zaugg, L.B. Barber, H.T. Buxton, Pharmaceuticals, hormones, and other organic wastewater contaminants in US streams, 1999-2000: A national reconnaissance, *Environmental Science & Technology*, 36 (2002) 1202-1211.
- [2] S.A. Snyder, D.L. Villeneuve, E.M. Snyder, J.P. Giesy, Identification and quantification of estrogen receptor agonists in wastewater effluents, *Environ. Sci. Technol.*, 35 (2001) 3620-3625.
- [3] S.A. Snyder, P. Westerhoff, Y. Yoon, D.L. Sedlak, Pharmaceuticals, personal care products, and endocrine disruptors in water: Implications for the water industry, *Environmental Engineering Science*, 20 (2003) 449-469.
- [4] Y. Yoon, J. Ryu, J. Oh, B.G. Choi, S.A. Snyder, Occurrence of endocrine disrupting compounds, pharmaceuticals, and personal care products in the Han River (Seoul, South Korea), *Science of the Total Environment*, 408 (2010) 636-643.
- [5] P.M.D. Foster, B.S. McIntyre, Endocrine active agents: Implications of adverse and non-adverse changes, *Toxicologic Pathology*, 30 (2002) 59-65.
- [6] A. Mantovani, A. Macri, Endocrine effects in the hazard assessment of drugs used in animal production, 21 (2002) 445-456.
- [7] R. Warren, W. B, V.R. Nathan, Environmental factors influencing public health and medicine: Policy implications, *Journal Of The National Medical Association*, 94 (2002) 185-193.
- [8] C. Adams, Y. Wang, K. Loftin, M. Meyer, Removal of antibiotics from surface and distilled water in conventional water treatment processes, *J. Environ. Eng.-ASCE*, 128 (2002) 253-260.
- [9] M. Petrovic, E. Eljarrat, M.J.L. de Alda, D. Barcelo, Analysis and environmental levels of endocrine-disrupting compounds in freshwater sediments, *Trac-Trends Anal. Chem.*, 20 (2001) 637-648.
- [10] P. Westerhoff, Y. Yoon, S. Snyder, E. Wert, Fate of endocrine-disruptor, pharmaceutical, and personal care product chemicals during simulated drinking water treatment processes, *Environmental Science & Technology*, 39 (2005) 6649-6663.

[11] J.W. Cho, G. Amy, J. Pellegrino, Membrane filtration of natural organic matter: comparison of flux decline, NOM rejection, and foulants during filtration with three UF membranes, *Desalination*, 127 (2000) 283-298.

[12] M. Campinas, M.J. Rosa, Assessing PAC contribution to the NOM fouling control in PAC/UF systems, *Water Research*, 44 (2010) 1636-1644.

[13] M.M. Zhang, C. Li, M.M. Benjamin, Y.J. Chang, Fouling and natural organic matter removal in adsorben/membrane systems for drinking water treatment, *Environmental Science & Technology*, 37 (2003) 1663-1669.

[14] Y.M. Yoon, G. Amy, J.W. Cho, N. Her, Effects of retained natural organic matter (NOM) on NOM rejection and membrane flux decline with nanofiltration and ultrafiltration, *Desalination*, 173 (2005) 209-221.

[15] A.W. Zularisam, A.F. Ismail, R. Salim, Behaviours of natural organic matter in membrane filtration for surface water treatment - a review, *Desalination*, 194 (2006) 211-231.

[16] C.-F. Lin, A.Y.-C. Lin, P.S. Chandana, C.-Y. Tsai, Effects of mass retention of dissolved organic matter and membrane pore size on membrane fouling and flux decline, *Water Research*, 43 (2009) 389-394.

[17] E. Aoustin, A.I. Schafer, A.G. Fane, T.D. Waite, Ultrafiltration of natural organic matter, *Separation and Purification Technology*, 22-3 (2001) 63-78.

[18] C.-H. Yu, C.-H. Wu, C.-H. Lin, C.-H. Hsiao, C.-F. Lin, Hydrophobicity and molecular weight of humic substances on ultrafiltration fouling and resistance, *Separation and Purification Technology*, 64 (2008) 206-212.

[19] S.K. Hong, M. Elimelech, Chemical and physical aspects of natural organic matter (NOM) fouling of nanofiltration membranes, *Journal of Membrane Science*, 132 (1997) 159-181.

[20] M.M. Clark, S. Allgeier, G. Amy, S. Chellam, F. DiGiano, M. Elimelech, S. Freeman, J. Jacangelo, K. Jones, J.M. Laine, J. Lozier, B. Marinas, R. Riley, J. Taylor, M. Thompson, J. Vickers, M. Wiesner, A. Zander, A.M.T.R. Comm, Committee report: Membrane processes, *Journal American Water Works Association*, 90 (1998) 91-105.

[21] M.R. Wiesner, S. Chellam, The promise of membrane technologies, *Environmental Science & Technology*, 33 (1999) 360A.

[22] S. Freeman, B. Long, S. Veerapaneni, J. Pressdee, Integrating low-pressure membranes into water treatment plants, *Journal American Water Works Association*, 98 (2006) 26.

- [23] H. Huang, K. Schwab, J.G. Jacangelo, Pretreatment for Low Pressure Membranes in Water Treatment: A Review, *Environmental Science & Technology*, 43 (2009) 3011-3019.
- [24] GWI, *Desalination Markets 2005 - 2015: A Global Assessment and Forecast*, Media Analytics Ltd., Oxford, United Kingdom, in, 2004.
- [25] Q. Yang, K.Y. Wang, T.-S. Chung, A novel dual-layer forward osmosis membrane for protein enrichment and concentration, *Separation and Purification Technology*, 69 (2009) 269-274.
- [26] B. Mi, M. Elimelech, Gypsum Scaling and Cleaning in Forward Osmosis: Measurements and Mechanisms, *Environmental Science & Technology*, 44 (2010) 2022-2028.
- [27] E.R. Cornelissen, D. Harmsen, K.F. de Korte, C.J. Ruiken, J.-J. Qin, H. Oo, L.P. Wessels, Membrane fouling and process performance of forward osmosis membranes on activated sludge, *Journal of Membrane Science*, 319 (2008) 158-168.
- [28] C.Y. Tang, Q. She, W.C.L. Lay, R. Wang, A.G. Fane, Coupled effects of internal concentration polarization and fouling on flux behavior of forward osmosis membranes during humic acid filtration, *Journal of Membrane Science*, 354 (2010) 123-133.
- [29] T.Y. Cath, Osmotically and thermally driven membrane processes for enhancement of water recovery in desalination processes, *Desalination and Water Treatment*, 15 (2010) 279-286.
- [30] N.T. Hancock, P. Xu, D.M. Heil, C. Bellona, T.Y. Cath, Comprehensive Bench- and Pilot-Scale Investigation of Trace Organic Compounds Rejection by Forward Osmosis, *Environmental Science & Technology*, 45 (2011) 8483-8490.
- [31] T.Y. Cath, A.E. Childress, M. Elimelech, Forward osmosis: Principles, applications, and recent developments, *Journal of Membrane Science*, 281 (2006) 70-87.
- [32] L.F. Greenlee, D.F. Lawler, B.D. Freeman, B. Marrot, P. Moulin, Reverse osmosis desalination: Water sources, technology, and today's challenges, *Water Research*, 43 (2009) 2317-2348.
- [33] A. Brehant, V. Bonnelye, M. Perez, Assessment of ultrafiltration as a pretreatment of reverse osmosis membranes for surface seawater desalination, *Water Science and Technology: Water Supply* 3(2003) 437-445.
- [34] J. Lee, H.W. Walker, Effect of process variables and natural organic matter on removal of microcystin-LR by PAC-UF, *Environmental Science & Technology*, 40 (2006) 7336-7342.

- [35] Y.M. Yoon, P. Westerhoff, S.A. Snyder, M. Esparza, HPLC-fluorescence detection and adsorption of bisphenol A, 17 beta-estradiol, and 17 alpha-ethynyl estradiol on powdered activated carbon, *Water Research*, 37 (2003) 3530-3537.
- [36] I.N. Najm, V.L. Snoeyink, B.W. Lykins, J.Q. Adams, Using powdered activated carbon - A critical review, *Journal American Water Works Association*, 83 (1991) 65-76.
- [37] Y. Yoon, P. Westerhoff, S.A. Snyder, Adsorption of H-3-labeled 17-beta estradiol on powdered activated carbon, *Water Air and Soil Pollution*, 166 (2005) 343-351.
- [38] R.H. Baughman, A.A. Zakhidov, W.A. de Heer, Carbon nanotubes - the route toward applications, *Science*, 297 (2002) 787-792.
- [39] M. Valcarcel, B.M. Simonet, S. Cardenas, B. Suarez, Present and future applications of carbon nanotubes to analytical science, *Analytical and Bioanalytical Chemistry*, 382 (2005) 1783-1790.
- [40] M.C. Roco, Environmentally responsible development of nanotechnology, *Environmental Science & Technology*, 39 (2005) 106A-112A.
- [41] P. Ball, Roll up for the revolution, *Nature*, 414 (2001) 142-144.
- [42] Y.H. Li, Z.C. Di, J. Ding, D.H. Wu, Z.K. Luan, Y.Q. Zhu, Adsorption thermodynamic, kinetic and desorption studies of Pb<sup>2+</sup> on carbon nanotubes, *Water Research*, 39 (2005) 605-609.
- [43] J.Y. Chen, W. Chen, D. Zhu, Adsorption of nonionic aromatic compounds to single-walled carbon nanotubes: Effects of aqueous solution chemistry, *Environmental Science & Technology*, 42 (2008) 7225-7230.
- [44] K. Yang, L. Zhu, B. Xing, Adsorption of polycyclic aromatic hydrocarbons by carbon nanomaterials, *Environmental Science & Technology*, 40 (2006) 1855-1861.
- [45] V.K.K. Upadhyayula, S. Deng, M.C. Mitchell, G.B. Smith, Application of carbon nanotube technology for removal of contaminants in drinking water: A review, *Science of the Total Environment*, 408 (2009) 1-13.
- [46] S.A. Snyder, W. E., H. Lei, P. Westerhoff, Y. Yoon, Removal of EDCs and Pharmaceuticals in Drinking and Reuse Treatment Processes, in, *Awwa Research Foundation* 2007.
- [47] Y. Yoon, G. Amy, J. Cho, J. Pellegrino, Systematic bench-scale assessment of perchlorate (ClO<sub>4</sub><sup>-</sup>) rejection mechanisms by nanofiltration and ultrafiltration membranes, *Sep. Sci. Technol.*, In press (2002).



- [48] Y. Yoon, P. Westerhoff, S.A. Snyder, E.C. Wert, Nanofiltration and ultrafiltration of endocrine disrupting compounds, pharmaceuticals and personal care products, *Journal of Membrane Science*, 270 (2006) 88-100.
- [49] C. Combe, E. Molis, P. Lucas, R. Riley, M.M. Clark, The effect of CA membrane properties on adsorptive fouling by humic acid, *Journal of Membrane Science*, 154 (1999) 73-87.
- [50] K. Kimura, G. Amy, J. Drewes, Y. Watanabe, Adsorption of hydrophobic compounds onto NF/RO membranes: an artifact leading to overestimation of rejection, *J. Membrane Sci.*, 221 (2003) 89-101.
- [51] Y. Kiso, A. Mizuno, R. Othman, Y.J. Jung, A. Kumano, A. Arijji, Rejection properties of pesticides with a hollow fiber NF membrane (HNF-1), *Desalination*, 143 (2002) 147-157.
- [52] Y. Yoon, P. Westerhoff, S.A. Snyder, M. Esparza, HPLC-fluorescence detection and adsorption of bisphenol A, 17b-estradiol, and 17a-ethynyl estradiol on powdered activated carbon, *Water Research*, 37 (2003) 3530-3537.
- [53] Y. Yoon, P. Westerhoff, J. Yoon, S.A. Snyder, Removal of 17b-estradiol and fluoranthene by nanofiltration and ultrafiltration, *J. Environ. Eng.-ASCE*, 130 (2004) 1460-1467.
- [54] T.D. Waite, A.I. Schafer, A.G. Fane, A. Heuer, Colloidal fouling of ultrafiltration membranes: Impact of aggregate structure and size, *Journal of Colloid and Interface Science*, 212 (1999) 264-274.
- [55] J.C. Crittenden, G. Tchobanoglous, D.W. Hand, R.R. Trussell, K.J. Howe, *Water Treatment: Principles and Design*, in, John Wiley & Sons Inc, Hoboken, New Jersey, 2005.
- [56] M. Mulder, *Basic Principles of Membrane Technology*, 2nd edition, in, Kluwer Academic Publishers, Dordrecht, The Netherlands, 1996.
- [57] W.R. Bowen, A.W. Mohammad, Characterization and prediction of nanofiltration membrane performance - A general assessment, *Chemical Engineering Research & Design*, 76 (1998) 885-893.
- [58] Y. Yoon, R.M. Lueptow, Removal of organic contaminants by RO and NF membranes, *Journal of Membrane Science*, 261 (2005) 76-86.
- [59] A. Tandon, S.K. Gupta, G.P. Agarwal, MODELING OF PROTEIN TRANSMISSION THROUGH ULTRAFILTRATION MEMBRANES, *Journal of Membrane Science*, 97 (1994) 83-90.

[60] O. Kedem, A. Katchalsky, THERMODYNAMIC ANALYSIS OF THE PERMEABILITY OF BIOLOGICAL MEMBRANES TO NON-ELECTROLYTES, *Biochimica Et Biophysica Acta*, 27 (1958) 229-246.

[61] S. Lee, G. Amy, J. Cho, Applicability of Sherwood correlations for natural organic matter (NOM) transport in nanofiltration (NF) membranes, *Journal of Membrane Science*, 240 (2004) 49-65.

[62] J. Hermia, CONSTANT PRESSURE BLOCKING FILTRATION LAWS - APPLICATION TO POWER-LAW NON-NEWTONIAN FLUIDS, *Transactions of the Institution of Chemical Engineers*, 60 (1982) 183-187.

[63] W.R. Bowen, J.I. Calvo, A. Hernandez, STEPS OF MEMBRANE BLOCKING IN FLUX DECLINE DURING PROTEIN MICROFILTRATION, *Journal of Membrane Science*, 101 (1995) 153-165.

[64] Y. Ye, P. Le Clech, V. Chen, A.G. Fane, B. Jefferson, Fouling mechanisms of alginate solutions as model extracellular polymeric substances, *Desalination*, 175 (2005) 7-20.

[65] E. Turano, S. Curcio, M.G. De Paola, V. Calabro, G. Iorio, An integrated centrifugation-ultrafiltration system in the treatment of olive mill wastewater, *Journal of Membrane Science*, 209 (2002) 519-531.

[66] U. Danis, C. Aydiner, Investigation of process performance and fouling mechanisms in micellar-enhanced ultrafiltration of nickel-contaminated waters, *Journal of Hazardous Materials*, 162 (2009) 577-587.

[67] N.B. Saleh, L.D. Pfefferle, M. Elimelech, Influence of Biomacromolecules and Humic Acid on the Aggregation Kinetics of Single-Walled Carbon Nanotubes, *Environmental Science & Technology*, 44 (2010) 2412-2418.

[68] M.S. Dresselhaus, G. Dresselhaus, A. Jorio, A.G. Souza Filho, R. Saito, Raman spectroscopy on isolated single wall carbon nanotubes, *Carbon*, 40 (2002) 2043-2061.

[69] Gr, uuml, A. neis, R. Saito, T. Kimura, Can, ccedil, L.G. ado, M.A. Pimenta, A. Jorio, A.G. Souza Filho, G. Dresselhaus, M.S. Dresselhaus, Determination of two-dimensional phonon dispersion relation of graphite by Raman spectroscopy, *Physical Review B*, 65 (2002) 155405.

[70] J. Heo, J.R.V. Flora, N. Her, Y.-G. Park, J. Cho, A. Son, Y. Yoon, Removal of bisphenol A and 17 $\beta$ -estradiol in single walled carbon nanotubesâ€“ultrafiltration (SWNTsâ€“UF) membrane systems, *Separation and Purification Technology*, 90 (2012) 39-52.

- [71] C.Y. Lu, H.S. Chiu, Adsorption of zinc(II) from water with purified carbon nanotubes, *Chemical Engineering Science*, 61 (2006) 1138-1145.
- [72] X. Peng, J. Jia, Z. Luan, Oxidized carbon nanotubes for simultaneous removal of endrin and Cd(II) from water and their separation from water, *Journal of Chemical Technology and Biotechnology*, 84 (2009) 275-278.
- [73] H. Yan, A.J. Gong, H.S. He, J. Zhou, Y.X. Wei, L. Lv, Adsorption of microcystins by carbon nanotubes, *Chemosphere*, 62 (2006) 142-148.
- [74] B. Pan, D.H. Lin, H. Mashayekhi, B.S. Xing, Adsorption and hysteresis of bisphenol A and 17 alpha-ethinyl estradiol on carbon nanomaterials, *Environmental Science & Technology*, 42 (2008) 5480-5485.
- [75] B. Halling-Sorensen, S.N. Nielsen, P.F. Lanzky, F. Ingerslev, H.C.H. Lutzhoft, S.E. Jorgensen, Occurrence, fate and effects of pharmaceutical substances in the environment - A review, *Chemosphere*, 36 (1998) 357-394.
- [76] C.H. Huang, D.L. Sedlak, Analysis of estrogenic hormones in municipal wastewater effluent and surface water using enzyme-linked immunosorbent assay and gas chromatography/tandem mass spectrometry, *Environmental Toxicology and Chemistry*, 20 (2001) 133-139.
- [77] S.K. Khanal, B. Xie, M.L. Thompson, S.W. Sung, S.K. Ong, J. Van Leeuwen, Fate, transport, and biodegradation of natural estrogens in the environment and engineered systems, *Environmental Science & Technology*, 40 (2006) 6537-6546.
- [78] S.A. Snyder, T.L. Keith, D.A. Verbrugge, E.M. Snyder, T.S. Gross, K. Kannan, J.P. Giesy, Analytical methods for detection of selected estrogenic compounds in aqueous mixtures, *Environ. Sci. Technol.*, 33 (1999) 2814-2820.
- [79] S.A. Snyder, P. Westerhoff, Y. Yoon, D.L. Sedlak, Pharmaceuticals, personal care products, and endocrine disruptors in water: implications for water treatment, *Environl. Eng. Sci.*, 20 (2003) 449-469.
- [80] B.J. Vanderford, R.A. Pearson, D.J. Rexing, S.A. Snyder, Analysis of endocrine disruptors, pharmaceuticals, and personal care products in water using liquid chromatography/tandem mass spectrometry, *Anal. Chem.*, 75 (2003) 6265-6274.
- [81] Y. Yoon, B. Choi, J. Oh, J. Ryu, S.A. Snyder, Occurrence of endocrine disrupting compounds, pharmaceuticals, and personal care products in the Han River (Seoul, South Korea), *Sci. Total Environ.*, 408 (2010) 636-643.
- [82] Y. Zhang, C. Causserand, P. Aimar, J.P. Cravedi, Removal of bisphenol A by a nanofiltration membrane in view of drinking water production, *Water Research*, 40 (2006) 3793-3799.

- [83] A.V. Krishnan, P. Stathis, S.F. Permuth, L. Tokes, D. Feldman, Bisphenol A: An estrogenic substance is released from polycarbonate flasks during autoclaving *Endocrinology*, 132 (1993) 2279-2286.
- [84] T. Suzuki, Y. Nakagawa, I. Takano, K. Yaguchi, K. Yasuda, Environmental fate of bisphenol A and its biological metabolites in river water and their xeno-estrogenic activity, *Environmental Science & Technology*, 38 (2004) 2389-2396.
- [85] S. Jobling, M. Nolan, C.R. Tyler, G. Brighty, J.P. Sumpter, Widespread sexual disruption in wild fish, *Environmental Science & Technology*, 32 (1998) 2498-2506.
- [86] R. Loos, G. Locoro, S. Contini, Occurrence of polar organic contaminants in the dissolved water phase of the Danube River and its major tributaries using SPE-LC-MS2 analysis, *Water Research*, 44 (2010) 2325-2335.
- [87] S. Rodriguez-Mozaz, M.L. de Alda, D. Barcelo, Analysis of bisphenol A in natural waters by means of an optical immunosensor, *Water Research*, 39 (2005) 5071-5079.
- [88] B.L.L. Tan, D.W. Hawker, J.F. Muller, L.A. Tremblay, H.F. Chapman, Stir bar sorptive extraction and trace analysis of selected endocrine disruptors in water, biosolids and sludge samples by thermal desorption with gas chromatography-mass spectrometry, *Water Research*, 42 (2008) 404-412.
- [89] T. Hashimoto, K. Onda, Y. Nakamura, K. Tada, A. Miya, T. Murakami, Comparison of natural estrogen removal efficiency in the conventional activated sludge process and the oxidation ditch process, *Water Research*, 41 (2007) 2117-2126.
- [90] P.T. Thuy, K. Moons, J.C. van Dijk, N.V. Anh, B. Van der Bruggen, To what extent are pesticides removed from surface water during coagulation-flocculation?, *Water and Environment Journal*, 22 (2008) 217-223.
- [91] C.X. Zhang, Y.X. Wang, Removal of dissolved organic matter and phthalic acid esters from landfill leachate through a complexation-flocculation process, *Waste Management*, 29 (2009) 110-116.
- [92] B. De Gussemme, B. Pycke, T. Hennebel, A. Marcoen, S.E. Vlaeminck, H. Noppe, N. Boon, W. Verstraete, Biological removal of 17 alpha-ethinylestradiol by a nitrifier enrichment culture in a membrane bioreactor, *Water Research*, 43 (2009) 2493-2503.
- [93] S.A. Snyder, J. Leising, P. Westerhoff, Y. Yoon, H. Mash, B. Vanderford, Biological and physical attenuation of endocrine disruptors and pharmaceuticals: Implications for water reuse, *Ground Water Monitoring and Remediation*, 24 (2004) 108-118.

- [94] Z.R. Yu, S. Peldszus, P.M. Huck, Adsorption characteristics of selected pharmaceuticals and an endocrine disrupting compound - Naproxen, carbamazepine and nonylphenol - on activated carbon, *Water Research*, 42 (2008) 2873-2882.
- [95] F. Yuan, C. Hu, X.X. Hu, J.H. Qu, M. Yang, Degradation of selected pharmaceuticals in aqueous solution with UV and UV/H<sub>2</sub>O<sub>2</sub>, *Water Research*, 43 (2009) 1766-1774.
- [96] F. Mendez-Arriaga, R.A. Torres-Palma, C. Petrier, S. Esplugas, J. Gimenez, C. Pulgarin, Ultrasonic treatment of water contaminated with ibuprofen, *Water Research*, 42 (2008) 4243-4248.
- [97] R.P.S. Suri, T.S. Singh, S. Abburi, Influence of Alkalinity and Salinity on the Sonochemical Degradation of Estrogen Hormones in Aqueous Solution, *Environmental Science & Technology*, 44 (2010) 1373-1379.
- [98] K. Kimura, S. Toshima, G. Amy, Y. Watanabe, Rejection of neutral endocrine disrupting compounds (EDCs) and pharmaceutical active compounds (PhACs) by RO membranes, *J. Membrane Sci.*, 245 (2004) 71-78.
- [99] X. Jin, J.Y. Hu, S.L. Ong, Influence of dissolved organic matter on estrone removal by NF membranes and the role of their structures, *Water Research*, 41 (2007) 3077-3088.
- [100] K. Kimura, G. Amy, J. Drewes, T. Heberer, T. Kim, Y. Watanabe, Rejection of organic micropollutants (disinfection by-products, endocrine disrupting compounds, and pharmaceutically active compounds) by NF/RO membranes, *J. Membrane Sci.*, 227 (2003) 113-121.
- [101] L.D. Nghiem, S. Hawkes, Effects of membrane fouling on the nanofiltration of pharmaceutically active compounds (PhACs): Mechanisms and role of membrane pore size, *Separation and Purification Technology*, 57 (2007) 176-184.
- [102] L.D. Nghiem, A. Manis, K. Soldenhoff, A.I. Schafer, Estrogenic hormone removal from wastewater using NF/RO membranes, *J. Membrane Sci.*, 242 (2004) 37-45.
- [103] A.I. Schafer, L.D. Nghiem, T.D. Waite, Removal of the natural hormone estrone from aqueous solutions using nanofiltration and reverse osmosis, *Environ. Sci. Technol.*, 37 (2003) 182-188.
- [104] D. Jermann, W. Pronk, M. Boller, A.I. Schafer, The role of NOM fouling for the retention of estradiol and ibuprofen during ultrafiltration, *Journal of Membrane Science*, 329 (2009) 75-84.
- [105] B. Pan, B.S. Xing, Adsorption Mechanisms of Organic Chemicals on Carbon Nanotubes, *Environmental Science & Technology*, 42 (2008) 9005-9013.

- [106] M.S. Mauter, M. Elimelech, Environmental applications of carbon-based nanomaterials, *Environmental Science & Technology*, 42 (2008) 5843-5859.
- [107] X.K. Wang, C.L. Chen, W.P. Hu, A.P. Ding, D. Xu, X. Zhou, Carbon nanotubes, *Environmental Science & Technology*, 39 (2005) 2856-2860.
- [108] N.V. Perez-Aguilar, E. Munoz-Sandoval, P.E. Diaz-Flores, J.R. Rangel-Mendez, Adsorption of cadmium and lead onto oxidized nitrogen-doped multiwall carbon nanotubes in aqueous solution: equilibrium and kinetics, *Journal of Nanoparticle Research*, 12 (2010) 467-480.
- [109] G.C. Chen, X.Q. Shan, Y.S. Wang, B. Wen, Z.G. Pei, Y.N. Xie, T. Liu, J.J. Pignatello, Adsorption of 2,4,6-trichlorophenol by multi-walled carbon nanotubes as affected by Cu(II), *Water Research*, 43 (2009) 2409-2418.
- [110] C.S. Lu, Y.L. Chung, K.F. Chang, Adsorption of trihalomethanes from water with carbon nanotubes, *Water Research*, 39 (2005) 1183-1189.
- [111] S.J. Zhang, T. Shao, S.S.K. Bekaroglu, T. Karanfil, Adsorption of synthetic organic chemicals by carbon nanotubes: Effects of background solution chemistry, *Water Research*, 44 (2010) 2067-2074.
- [112] P. Oleszczuk, B. Pan, B.S. Xing, Adsorption and Desorption of Oxytetracycline and Carbamazepine by Multiwalled Carbon Nanotubes, *Environmental Science & Technology*, 43 (2009) 9167-9173.
- [113] K. Kostarelos, The long and short of carbon nanotube toxicity, *Nature Biotechnology*, 26 (2008) 774-776.
- [114] C.W. Lam, J.T. James, R. McCluskey, S. Arepalli, R.L. Hunter, A review of carbon nanotube toxicity and assessment of potential occupational and environmental health risks, *Critical Reviews in Toxicology*, 36 (2006) 189-217.
- [115] N. Savage, M.S. Diallo, Nanomaterials and water purification: Opportunities and challenges, *Journal of Nanoparticle Research*, 7 (2005) 331-342.
- [116] H. Dumortier, S. Lacotte, G. Pastorin, R. Marega, W. Wu, D. Bonifazi, J.-P. Briand, M. Prato, S. Muller, A. Bianco, Functionalized carbon nanotubes are non-cytotoxic and preserve the functionality of primary immune cells, *Nano Letters*, 6 (2006) 1522-1528.
- [117] K.J. Howe, A. Marwah, K.P. Chiu, S.S. Adham, Effect of coagulation on the size of MF and UF membrane foulants, *Environmental Science & Technology*, 40 (2006) 7908-7913.

- [118] J. Kim, Q.R. Deng, M.M. Benjamin, Simultaneous removal of phosphorus and foulants in a hybrid coagulation/membrane filtration system, *Water Research*, 42 (2008) 2017-2024.
- [119] J.S. Kim, Z.X. Cai, M.M. Benjamin, Effects of adsorbents on membrane fouling by natural organic matter, *Journal of Membrane Science*, 310 (2008) 356-364.
- [120] C.W. Lee, S.D. Bae, S.W. Han, L.S. Kang, Application of ultrafiltration hybrid membrane processes for reuse of secondary effluent, *Desalination*, 202 (2007) 239-246.
- [121] M. Tomaszewska, S. Mozia, Removal of organic matter from water by PAC/UF system, *Water Research*, 36 (2002) 4137-4143.
- [122] P. Zhao, S. Takizawa, H. Katayama, S. Ohgaki, Factors causing PAC cake fouling in PAC-MF (powdered activated carbon-microfiltration) water treatment systems, *Water Science and Technology*, 51 (2005) 231-240.
- [123] Y. Yoon, R.M. Lueptow, Reverse osmosis membrane rejection for ersatz space mission wastewaters, *Water Research*, 39 (2005) 3298-3308.
- [124] S. Kim, N. Park, S. Lee, J. Cho, Membrane characterizations for mitigation of organic fouling during desalination and wastewater reclamation, *Desalination*, 238 (2009) 70-77.
- [125] J.W. Cho, G. Amy, J. Pellegrino, Membrane filtration of natural organic matter: Initial comparison of rejection and flux decline characteristics with ultrafiltration and nanofiltration membranes, *Water Research*, 33 (1999) 2517-2526.
- [126] A.I. Schafer, I. Akanyeti, A.J.C. Semiao, Micropollutant sorption to membrane polymers: A review of mechanisms for estrogens, *Advances in Colloid and Interface Science*, 164 (2011) 100-117.
- [127] A.M. Comerton, R.C. Andrews, D.M. Bagley, P. Yang, Membrane adsorption of endocrine disrupting compounds and pharmaceutically active compounds, *Journal of Membrane Science*, 303 (2007) 267-277.
- [128] P.A. Neale, B.I. Escher, A.I. Schafer, Quantification of solute-solute interactions using negligible-depletion solid-phase microextraction: Measuring the affinity of estradiol to bulk organic matter, *Environmental Science & Technology*, 42 (2008) 2886-2892.
- [129] B. Van der Bruggen, L. Braeken, C. Vandecasteele, Evaluation of parameters describing flux decline in nanofiltration of aqueous solutions containing organic compounds, *Desalination*, 147 (2002) 281-188.

- [130] J. Chen, W. Chen, D. Zhu, Adsorption of nonionic aromatic compounds to single-walled carbon nanotubes: Effects of aqueous solution chemistry, *Environmental Science & Technology*, 42 (2008) 7225-7230.
- [131] L.D. Nghiem, J. McCutcheon, A.I. Schafer, M. Elimelech, The role of endocrine disrupters in water recycling: risk or mania?, *Water Science and Technology*, 50 (2004) 215-220.
- [132] Y. Kiso, Y. Nishimura, T. Kitao, K. Nishimura, Rejection properties of non-phenylic pesticides with nanofiltration membranes, *Journal of Membrane Science*, 171 (2000) 229-237.
- [133] L.D. Nghiem, A.I. Schafer, Adsorption and transport of trace contaminant estrone in NF/RO membranes, *Environ. Eng. Sci.*, 19 (2002) 441-451.
- [134] H. Ozaki, H.F. Li, Rejection of organic compounds by ultra-low pressure reverse osmosis membrane, *Water Research*, 36 (2002) 123-130.
- [135] J. Heo, L. Joseph, Y. Yoon, Y.-G. Park, N. Her, J. Sohn, S.-H. Yoon, Removal of micropollutants and NOM in carbon nanotube-UF membrane system from seawater, *Water Science and Technology*, 63 (2011) 2737-2744.
- [136] D. Jermann, W. Pronk, S. Meylan, M. Boller, Interplay of different NOM fouling mechanisms during ultrafiltration for drinking water production, *Water Research*, 41 (2007) 1713-1722.
- [137] A.R. Costa, M.N. de Pinho, M. Elimelech, Mechanisms of colloidal natural organic matter fouling in ultrafiltration, *Journal of Membrane Science*, 281 (2006) 716-725.
- [138] W. Yuan, A.L. Zydney, Humic acid fouling during ultrafiltration, *Environmental Science & Technology*, 34 (2000) 5043-5050.
- [139] T. Carroll, N.A. Booker, J. Meier-Haack, Polyelectrolyte-grafted microfiltration membranes to control fouling by natural organic matter in drinking water, *Journal of Membrane Science*, 203 (2002) 3-13.
- [140] J. Cho, G. Amy, J. Pellegrino, Membrane filtration of natural organic matter: factors and mechanisms affecting rejection and flux decline with charged ultrafiltration (UF) membrane, *Journal of Membrane Science*, 164 (2000) 89-110.
- [141] R. Boussahel, S. Bouland, K.M. Moussaoui, A. Montiel, Removal of pesticide residues in water using the nanofiltration process, *Desalination*, 132 (2000) 205-209.
- [142] A. Seidel, M. Elimelech, Coupling between chemical and physical interactions in natural organic matter (NOM) fouling of nanofiltration membranes: implications for fouling control, *J. Membrane Sci.*, 203 (2002) 245-255.



- [143] Y. Shen, W. Zhao, K. Xiao, X. Huang, A systematic insight into fouling propensity of soluble microbial products in membrane bioreactors based on hydrophobic interaction and size exclusion, *Journal of Membrane Science*, 346 (2010) 187-193.
- [144] D.R.U. Knappe, Y. Matsui, V.L. Snoeyink, P. Roche, M.J. Prados, M.M. Bourbigot, Predicting the capacity of powdered activated carbon for trace organic compounds in natural waters, *Environmental Science & Technology*, 32 (1998) 1694-1698.
- [145] D. Bruce, P. Westerhoff, A. Brawley-Chesworth, Removal of 2-methylisoborneol and geosmin in surface water treatment plants in Arizona, *Journal of Water Supply Research and Technology-Aqua*, 51 (2002) 183-197.
- [146] G.L. Che, B.B. Lakshmi, E.R. Fisher, C.R. Martin, Carbon nanotubule membranes for electrochemical energy storage and production, *Nature*, 393 (1998) 346-349.
- [147] K.R. Rogers, Recent advances in biosensor techniques for environmental monitoring, *Analytica Chimica Acta*, 568 (2006) 222-231.
- [148] D. Lin, B. Xing, Tannic acid adsorption and its role for stabilizing carbon nanotube suspensions, *Environmental Science & Technology*, 42 (2008) 5917-5923.
- [149] Z.-P. Zhu, K.-L. Huang, Y. Zhou, Study on Kinetics, Thermodynamics and Mechanism for Carbon Nanotubes Adsorbing Humic Acid, *Journal of Inorganic Materials*, 26 (2011) 170-174.
- [150] S. Iijima, HELICAL MICROTUBULES OF GRAPHITIC CARBON, *Nature*, 354 (1991) 56-58.
- [151] V.K.K. Upadhyayula, S.G. Deng, M.C. Mitchell, G.B. Smith, Application of carbon nanotube technology for removal of contaminants in drinking water: A review, *Science of the Total Environment*, 408 (2009) 1-13.
- [152] C. Lu, F. Su, Adsorption of natural organic matter by carbon nanotubes, *Separation and Purification Technology*, 58 (2007) 113-121.
- [153] X. Zhang, B. Pan, K. Yang, D. Zhang, J.A. Hou, Adsorption of sulfamethoxazole on different types of carbon nanotubes in comparison to other natural adsorbents, *Journal of Environmental Science and Health Part a-Toxic/Hazardous Substances & Environmental Engineering*, 45 (2011) 1625-1634.
- [154] X.J. Peng, Y.H. Li, Z.K. Luan, Z.C. Di, H.Y. Wang, B.H. Tian, Z.P. Jia, Adsorption of 1,2-dichlorobenzene from water to carbon nanotubes, *Chemical Physics Letters*, 376 (2003) 154-158.

- [155] X. Wang, S. Tao, B. Xing, Sorption and Competition of Aromatic Compounds and Humic Acid on Multiwalled Carbon Nanotubes, *Environmental Science & Technology*, 43 (2009) 6214-6219.
- [156] C.F. Lin, Y.J. Huang, I.J. Hao, Ultrafiltration processes for removing humic substances: Effect of molecular weight fractions and PAC treatment, *Water Research*, 33 (1999) 1252-1264.
- [157] K. Konieczny, G. Klomfas, Using activated carbon to improve natural water treatment by porous membranes, *Desalination*, 147 (2002) 109-116.
- [158] L. Joseph, Q. Zaib, I.A. Khan, N.D. Berge, Y.-G. Park, N.B. Saleh, Y. Yoon, Removal of bisphenol A and 17 alpha-ethinyl estradiol from landfill leachate using single-walled carbon nanotubes, *Water Research*, 45 (2011) 4056-4068.
- [159] S. Lee, J.W. Cho, M. Elimelech, Combined influence of natural organic matter (NOM) and colloidal particles on nanofiltration membrane fouling, *Journal of Membrane Science*, 262 (2005) 27-41.
- [160] J. Kim, Z. Cai, M.M. Benjamin, Effects of adsorbents on membrane fouling by natural organic matter, *Journal of Membrane Science*, 310 (2008) 356-364.
- [161] L. Vaisman, H.D. Wagner, G. Marom, The role of surfactants in dispersion of carbon nanotubes, *Advances in Colloid and Interface Science*, 128 (2006) 37-46.
- [162] X. Zhao, J.K. Johnson, Simulation of adsorption of DNA on carbon nanotubes, *Journal of the American Chemical Society*, 129 (2007) 10438-10445.
- [163] C. Jucker, M.M. Clark, ADSORPTION OF AQUATIC HUMIC SUBSTANCES ON HYDROPHOBIC ULTRAFILTRATION MEMBRANES, *Journal of Membrane Science*, 97 (1994) 37-52.
- [164] I. Sutzkover-Gutman, D. Hasson, R. Semiat, Humic substances fouling in ultrafiltration processes, *Desalination*, 261 (2011) 218-231.
- [165] M.A. Fontecha-Camara, M.V. Lopez-Ramon, M.A. Alvarez-Merino, C. Moreno-Castilla, Effect of surface chemistry, solution pH, and ionic strength on the removal of herbicides diuron and amitrole from water by an activated carbon fiber, *Langmuir*, 23 (2007) 1242-1247.
- [166] H. Hyung, J.-H. Kim, Natural organic matter (NOM) adsorption to multi-walled carbon nanotubes: Effect of NOM characteristics and water quality parameters, *Environmental Science & Technology*, 42 (2008) 4416-4421.

[167] H. Wang, A.A. Keller, F. Li, Natural organic matter removal by adsorption onto carbonaceous nanoparticles and coagulation, *Journal of Environmental Engineering-ASCE*, 136 (2010) 1075-1081.

[168] K.L. Jones, C.R. O'Melia, Protein and humic acid adsorption onto hydrophilic membrane surfaces: effects of pH and ionic strength, *Journal of Membrane Science*, 165 (2000) 31-46.

[169] H. Susanto, M. Ulbricht, High-performance thin-layer membranes for ultrafiltration hydrogel composite of natural organic matter, *Water Research*, 42 (2008) 2827-2835.

[170] N. Hilal, M. Al-Abri, H. Al-Hinai, Characterization and retention of UF membranes using PEG, HS and polyelectrolytes, *Desalination*, 206 (2007) 568-578.

[171] V. Lahoussineturcaud, M.R. Wiesner, J.Y. Bottero, FOULING IN TANGENTIAL-FLOW ULTRAFILTRATION - THE EFFECT OF COLLOID SIZE AND COAGULATION PRETREATMENT, *Journal of Membrane Science*, 52 (1990) 173-190.

[172] P. Pradanos, J.I. Arribas, A. Hernandez, MASS-TRANSFER COEFFICIENT AND RETENTION OF PEGS IN LOW-PRESSURE CROSS-FLOW ULTRAFILTRATION THROUGH ASYMMETRIC MEMBRANES, *Journal of Membrane Science*, 99 (1995) 1-20.

[173] M.A. Sanz, V. Bonnelye, G. Cremer, Fujairah reverse osmosis plant: 2 years of operation, *Desalination*, 203 (2007) 91-99.

[174] B. Sauvet-Goichon, Ashkelon desalination plant - A successful challenge, *Desalination*, 203 (2007) 75-81.

[175] C.G. Campbell, S.E. Borglin, F.B. Green, A. Grayson, E. Wozel, W.T. Stringfellow, Biologically directed environmental monitoring, fate, and transport of estrogenic endocrine disrupting compounds in water: A review, *Chemosphere*, 65 (2006) 1265-1280.

[176] C. Basheer, H.K. Lee, K.S. Tan, Endocrine disrupting alkylphenols and bisphenol-A in coastal waters and supermarket seafood from Singapore, *Marine Pollution Bulletin*, 48 (2004) 1161-1167.

[177] D. Li, M. Dong, W.J. Shim, U.H. Yim, S.H. Hong, N. Kannan, Distribution characteristics of nonylphenolic chemicals in Masan Bay environments, Korea, *Chemosphere*, 71 (2008) 1162-1172.

[178] O. Braga, G.A. Smythe, A.I. Schafer, A.J. Feitz, Steroid estrogens in ocean sediments, *Chemosphere*, 61 (2005) 827-833.

- [179] P. Stefanelli, A. Ausili, A. Di Muccio, C. Fossi, S. Di Muccio, S. Rossi, A. Colasanti, Organochlorine compounds in tissues of swordfish (*Xiphias gladius*) from Mediterranean Sea and Azores islands, *Marine Pollution Bulletin*, 49 (2004) 938-950.
- [180] M.C. Fossi, S. Casini, L. Marsili, Endocrine disruptors in Mediterranean top marine predators, *Environmental Science and Pollution Research*, 13 (2006) 204-207.
- [181] M.M. Storelli, G.O. Marcotrigiano, Occurrence and accumulation of organochlorine contaminants in swordfish from Mediterranean Sea: A case study, *Chemosphere*, 62 (2006) 375-380.
- [182] A. Belfroid, M. van Velzen, B. van der Horst, D. Vethaak, Occurrence of bisphenol A in surface water and uptake in fish: evaluation of field measurements, *Chemosphere*, 49 (2002) 97-103.
- [183] Y. Liu, Y.T. Guan, N.F.Y. Tam, T. Mizuno, H. Tsuno, W.P. Zhu, Influence of Rainfall and Basic Water Quality Parameters on the Distribution of Endocrine-Disrupting Chemicals in Coastal Area, *Water Air and Soil Pollution*, 209 (2010) 333-343.
- [184] J. Sekizawa, Low-dose effects of bisphenol A: a serious threat to human health?, *Journal of Toxicological Sciences*, 33 (2008) 389-403.
- [185] F.S. Vom Saal, C. Hughes, An extensive new literature concerning low-dose effects of bisphenol A shows the need for a new risk assessment, *Environmental Health Perspectives*, 113 (2005) 926-933.
- [186] H. Segner, J.M. Navas, C. Schafers, A. Wenzel, Potencies of estrogenic compounds in in vitro screening assays and in life cycle tests with zebrafish in vivo, *Ecotoxicology and Environmental Safety*, 54 (2003) 315-322.
- [187] S.S. Madsen, A.B. Mathiesen, B. Korsgaard, Effects of 17 beta-estradiol and 4-nonylphenol on smoltification and vitellogenesis in Atlantic salmon (*Salmo salar*), *Fish Physiol. Biochem.*, 17 (1997) 303-312.
- [188] K.E. Liney, J.A. Hagger, C.R. Tyler, M.H. Depledge, T.S. Galloway, S. Jobling, Health effects in fish of long-term exposure to effluents from wastewater treatment works, *Environmental Health Perspectives*, 114 (2006) 81-89.
- [189] I.C. Beck, R. Bruhn, J. Gandrass, W. Ruck, Liquid chromatography-tandem mass spectrometry analysis of estrogenic compounds in coastal surface water of the Baltic Sea, *Journal of Chromatography A*, 1090 (2005) 98-106.
- [190] O.P. Heemken, H. Reincke, B. Stachel, N. Theobald, The occurrence of xenoestrogens in the Elbe river and the North Sea, *Chemosphere*, 45 (2001) 245-259.

- [191] S. Atkinson, M.J. Atkinson, A.M. Tarrant, Estrogens from sewage in coastal marine environments, *Environmental Health Perspectives*, 111 (2003) 531-535.
- [192] G.G. Ying, R.S. Kookana, Degradation of five selected endocrine-disrupting chemicals in seawater and marine sediment, *Environmental Science & Technology*, 37 (2003) 1256-1260.
- [193] T.A. Ternes, M. Meisenheimer, D. McDowell, F. Sacher, H.J. Brauch, B.H. Gulde, G. Preuss, U. Wilme, N.Z. Seibert, Removal of pharmaceuticals during drinking water treatment, *Environmental Science & Technology*, 36 (2002) 3855-3863.
- [194] C.V. Vedavyasan, Pretreatment trends - an overview, *Desalination*, 203 (2007) 296-299.
- [195] A.I. Schafer, A.G. Fane, T.D. Waite, Cost factors and chemical pretreatment effects in the membrane filtration of waters containing natural organic matter, *Water Research*, 35 (2001) 1509-1517.
- [196] C.W. Li, Y.S. Chen, Fouling of UF membrane by humic substance: Effects of molecular weight and powder-activated carbon (PAC) pre-treatment, *Desalination*, 170 (2004) 59-67.
- [197] A. Shareef, M.J. Angove, J.D. Wells, B.B. Johnson, Aqueous solubilities of estrone, 17 beta-estradiol, 17 alpha-ethynylestradiol, and bisphenol A, *Journal of Chemical and Engineering Data*, 51 (2006) 879-881.
- [198] D.R. Kester, I.W. Duedall, D.N. Connors, Pytkowic.Rm, PREPARATION OF ARTIFICIAL SEAWATER, *Limnology and Oceanography*, 12 (1967) 176-&.
- [199] S. Kim, K. Chon, S.J. Kim, S. Lee, E. Lee, J. Cho, Uncertainty in organic matter analysis for seawater reverse osmosis (SWRO) desalination, *Desalination*, 238 (2009) 30-36.
- [200] R. Al-Rasheed, D.J. Cardin, Photocatalytic degradation of humic acid in saline waters. Part 1. Artificial seawater: influence of TiO<sub>2</sub>, temperature, pH, and air-flow, *Chemosphere*, 51 (2003) 925-933.
- [201] N. Her, G. Amy, J. Sohn, U. von Gunten, UV absorbance ratio index with size exclusion chromatography (URI-SEC) as an NOM property indicator (vol 57, pg 35, 2008), *J. Water Supply Res Technol.-Aqua*, 57 (2008) 289-289.
- [202] J. Hur, M.A. Schlautman, Effects of mineral surfaces on pyrene partitioning to well-characterized humic substances, *Journal of Environmental Quality*, 33 (2004) 1733-1742.

- [203] B. Van der Bruggen, L. Braeken, C. Vandecasteele, Evaluation of parameters describing flux decline in nanofiltration of aqueous solutions containing organic compounds, *Desalination*, 147 (2002) 281-288.
- [204] W. Chen, L. Duan, D.Q. Zhu, Adsorption of polar and nonpolar organic chemicals to carbon nanotubes, *Environmental Science & Technology*, 41 (2007) 8295-8300.
- [205] W.H. Xie, W.Y. Shiu, D. Mackay, A review of the effect of salts on the solubility of organic compounds in seawater, *Marine Environmental Research*, 44 (1997) 429-444.
- [206] M.A. Schlautman, S.B. Yim, E.R. Carraway, J.H. Lee, B.E. Herbert, Testing a surface tension-based model to predict the salting out of polycyclic aromatic hydrocarbons in model environmental solutions, *Water Research*, 38 (2004) 3331-3339.
- [207] L.D. Nghiem, A.I. Schafer, M. Elimelech, Role of electrostatic interactions in the retention of pharmaceutically active contaminants by a loose nanofiltration membrane, *Journal of Membrane Science*, 286 (2006) 52-59.
- [208] L.D. Nghiem, D. Vogel, S. Khan, Characterising humic acid fouling of nanofiltration membranes using bisphenol A as a molecular indicator, *Water Research*, 42 (2008) 4049-4058.
- [209] S.H. Yoon, C.H. Lee, K.J. Kim, A.G. Fane, Effect of calcium ion on the fouling of nanofilter by humic acid in drinking water production, *Water Research*, 32 (1998) 2180-2186.
- [210] A. Seidel, M. Elimelech, Coupling between chemical and physical interactions in natural organic matter (NOM) fouling of nanofiltration membranes: implications for fouling control, *Journal of Membrane Science*, 203 (2002) 245-255.
- [211] X.H. Zhu, M. Elimelech, Colloidal fouling of reverse osmosis membranes: Measurements and fouling mechanisms, *Environmental Science & Technology*, 31 (1997) 3654-3662.
- [212] H.Q. Chen, A.S. Kim, Prediction of permeate flux decline in crossflow membrane filtration of colloidal suspension: a radial basis function neural network approach, *Desalination*, 192 (2006) 415-428.
- [213] K. Katsoufidou, S.G. Yiantsios, A.J. Karabelas, A study of ultrafiltration membrane fouling by humic acids and flux recovery by backwashing: Experiments and modeling, *Journal of Membrane Science*, 266 (2005) 40-50.
- [214] R.C. Hale, M.J. La Guardia, Have risks associated with the presence of synthetic organic contaminants in land-applied sewage sludges been adequately assessed?, *New solutions : a journal of environmental and occupational health policy* : NS, 12 (2002) 371-386.

- [215] E.Z. Harrison, S.R. Oakes, M. Hysell, A. Hay, Organic chemicals in sewage sludges, *Science of the Total Environment*, 367 (2006) 481-497.
- [216] C. Miega, J.M. Choubert, L. Ribeiro, M. Eusebe, M. Coquery, Fate of pharmaceuticals and personal care products in wastewater treatment plants - Conception of a database and first results, *Environmental Pollution*, 157 (2009) 1721-1726.
- [217] J. Michalowicz, W. Duda, Phenols - Sources and toxicity, *Polish Journal of Environmental Studies*, 16 (2007) 347-362.
- [218] T.B. Hayes, V. Khoury, A. Narayan, M. Nazir, A. Park, T. Brown, L. Adame, E. Chan, D. Buchholz, T. Stueve, S. Gallipeau, Atrazine induces complete feminization and chemical castration in male African clawed frogs (*Xenopus laevis*), *Proceedings of the National Academy of Sciences of the United States of America*, 107 (2010) 4612-4617.
- [219] S.K. Khetan, T.J. Collins, Human pharmaceuticals in the aquatic environment: A challenge to green chemistry, *Chemical Reviews*, 107 (2007) 2319-2364.
- [220] K. Kuemmerer, The presence of pharmaceuticals in the environment due to human use - present knowledge and future challenges, *Journal of Environmental Management*, 90 (2009) 2354-2366.
- [221] C. Bellona, J.E. Drewes, P. Xu, G. Amy, Factors affecting the rejection of organic solutes during NF/RO treatment - a literature review, *Water Research*, 38 (2004) 2795-2809.
- [222] C.F. Schutte, The rejection of specific organic compounds by reverse osmosis membranes, *Desalination*, 158 (2003) 285-294.
- [223] K. Kimura, G. Amy, J.E. Drewes, T. Heberer, T.U. Kim, Y. Watanabe, Rejection of organic micropollutants (disinfection by-products, endocrine disrupting compounds, and pharmaceutically active compounds) by NF/RO membranes, *Journal of Membrane Science*, 227 (2003) 113-121.
- [224] K. Kimura, S. Toshima, G. Amy, Y. Watanabe, Rejection of neutral endocrine disrupting compounds (EDCs) and pharmaceutical active compounds (PhACs) by RO membranes, *Journal of Membrane Science*, 245 (2004) 71-78.
- [225] T.-S. Chung, S. Zhang, K.Y. Wang, J. Su, M.M. Ling, Forward osmosis processes: Yesterday, today and tomorrow, *Desalination*, 287 (2012) 78-81.
- [226] J.R. McCutcheon, M. Elimelech, Influence of concentrative and dilutive internal concentration polarization on flux behavior in forward osmosis, *Journal of Membrane Science*, 284 (2006) 237-247.

- [227] S. Zou, Y. Gu, D. Xiao, C.Y. Tang, The role of physical and chemical parameters on forward osmosis membrane fouling during algae separation, *Journal of Membrane Science*, 366 (2011) 356-362.
- [228] S. Chou, R. Wang, L. Shi, Q. She, C. Tang, A.G. Fane, Thin-film composite hollow fiber membranes for pressure retarded osmosis (PRO) process with high power density, *Journal of Membrane Science*, 389 (2012) 25-33.
- [229] R.W. Holloway, A.E. Childress, K.E. Dennett, T.Y. Cath, Forward osmosis for concentration of anaerobic digester centrate, *Water Research*, 41 (2007) 4005-4014.
- [230] O.A. Bamaga, A. Yokochi, E.G. Beaudry, Application of forward osmosis in pretreatment of seawater for small reverse osmosis desalination units, *Desalination and Water Treatment*, 5 (2009) 183-191.
- [231] O.A. Bamaga, A. Yokochi, B. Zabara, A.S. Babaqi, Hybrid FO/RO desalination system: Preliminary assessment of osmotic energy recovery and designs of new FO membrane module configurations, *Desalination*, 268 (2011) 163-169.
- [232] K. Kimura, G. Amy, J. Drewes, Y. Watanabe, Adsorption of hydrophobic compounds onto NF/RO membranes: an artifact leading to overestimation of rejection, *Journal of Membrane Science*, 221 (2003) 89-101.
- [233] A.I. Schaefer, I. Akanyeti, A.J.C. Semiao, Micropollutant sorption to membrane polymers: A review of mechanisms for estrogens, *Advances in Colloid and Interface Science*, 164 (2011) 100-117.
- [234] J. Heo, J.R.V. Flora, N. Her, Y.-G. Park, J. Cho, A. Son, Y. Yoon, Removal of bisphenol A and 17 beta-estradiol in single walled carbon nanotubes-ultrafiltration (SWNTs-UF) membrane systems, *Separation and Purification Technology*, 90 (2012) 39-52.
- [235] X. Jin, J. Shan, C. Wang, J. Wei, C.Y. Tang, Rejection of pharmaceuticals by forward osmosis membranes, *Journal of Hazardous Materials*, 227 (2012) 55-61.
- [236] H. Buksek, T. Luxbacher, I. Petrinic, Zeta Potential Determination of Polymeric Materials Using Two Differently Designed Measuring Cells of an Electrokinetic Analyzer, *Acta Chimica Slovenica*, 57 (2010) 700-706.
- [237] M. Pontie, H. Dach, J. Leparc, M. Hafsi, A. Lhassani, Novel approach combining physico-chemical characterizations and mass transfer modelling of nanofiltration and low pressure reverse osmosis membranes for brackish water desalination intensification, *Desalination*, 221 (2008) 174-191.



[238] J.R. McCutcheon, M. Elimelech, Influence of membrane support layer hydrophobicity on water flux in osmotically driven membrane processes, *Journal of Membrane Science*, 318 (2008) 458-466.

[239] M. Xie, L.D. Nghiem, W.E. Price, M. Elimelech, Comparison of the removal of hydrophobic trace organic contaminants by forward osmosis and reverse osmosis, *Water Research*, 46 (2012) 2683-2692.

[240] S. Grimme, J. Antony, S. Ehrlich, H. Krieg, A consistent and accurate ab initio parametrization of density functional dispersion correction (DFT-D) for the 94 elements H-Pu, *Journal of Chemical Physics*, 132 (2010).

[241] S. Grimme, S. Ehrlich, L. Goerigk, Effect of the Damping Function in Dispersion Corrected Density Functional Theory, *Journal of Computational Chemistry*, 32 (2011) 1456-1465.

[242] J. Kaestner, J.M. Carr, T.W. Keal, W. Thiel, A. Wander, P. Sherwood, DL-FIND: An Open-Source Geometry Optimizer for Atomistic Simulations, *Journal of Physical Chemistry A*, 113 (2009) 11856-11865.

[243] I.S. Ufimtsev, T.J. Martinez, Quantum Chemistry on Graphical Processing Units. 3. Analytical Energy Gradients, Geometry Optimization, and First Principles Molecular Dynamics, *Journal of Chemical Theory and Computation*, 5 (2009) 2619-2628.

[244] Q. Zaib, I.A. Khan, N.B. Saleh, J.R.V. Flora, Y.-G. Park, Y. Yoon, Removal of Bisphenol A and 17 beta-Estradiol by Single-Walled Carbon Nanotubes in Aqueous Solution: Adsorption and Molecular Modeling, *Water Air and Soil Pollution*, 223 (2012) 3281-3293.

[245] D.A. Case, T.E. Cheatham III, T.A. Darden, C.L. Simmerling, R.E.D. J. Wang, R. Luo, R.C. Walker, W. Zhang, K.M. Merz, B.P. Roberts, S. Hayik, A. Roitberg, G. Seabra, J. Swails, A.W. Götz, I. Kolossváry, K.F. Wong, F. Paesani, J. Vanicek, R.M. Wolf, J. Liu, X. Wu, S.R. Brozell, T. Steinbrecher, H. Gohlke, Q. Cai, X. Ye, J. Wang, M.-J. Hsieh, G. Cui, D.R. Roe, D.H. Mathews, M.G. Seetin, R. Salomon-Ferrer, C. Sagui, V. Babin, T. Luchko, S. Gusarov, A. Kovalenko, P.A. Kollman, AMBER 11, University of California, San Francisco, USA, (2011).

[246] A. Segura-Cabrera, V. Bocanegra-Garcia, C. Lizarazo-Ortega, X. Guo, J. Correa-Basurto, M.A. Rodriguez-Perez, A computational analysis of the binding mode of closantel as inhibitor of the *Onchocerca volvulus* chitinase: insights on macrofilaricidal drug design, *Journal of Computer-Aided Molecular Design*, 25 (2011) 1107-1119.

[247] J.P. Ryckaert, G. Ciccotti, H.J.C. Berendsen, Numerical integration of the Cartesian equations of motion of a system with constraints: Molecular dynamics of n-alkanes, *Journal of Computational Physics*, 23 (1977) 327-320.

[248] J. Srinivasan, T.E. Cheatham, P. Cieplak, P.A. Kollman, D.A. Case, Continuum solvent studies of the stability of DNA, RNA, and phosphoramidate - DNA helices, *Journal of the American Chemical Society*, 120 (1998) 9401-9409.

[249] T. Hou, J. Wang, Y. Li, W. Wang, Assessing the Performance of the MM/PBSA and MM/GBSA Methods. 1. The Accuracy of Binding Free Energy Calculations Based on Molecular Dynamics Simulations, *Journal of Chemical Information and Modeling*, 51 (2011) 69-82.

[250] S. Loeb, L. Titelman, E. Korngold, J. Freiman, Effect of porous support fabric on osmosis through a Loeb-Sourirajan type asymmetric membrane, *Journal of Membrane Science*, 129 (1997) 243-249.

[251] L.D. Nghiem, A.I. Schafer, M. Elimelech, Removal of natural hormones by nanofiltration membranes: Measurement, modeling, and mechanisms, *Environmental Science & Technology*, 38 (2004) 1888-1896.

[252] X. Jin, Q. She, X. Ang, C.Y. Tang, Removal of boron and arsenic by forward osmosis membrane: Influence of membrane orientation and organic fouling, *Journal of Membrane Science*, 389 (2012) 182-187.

[253] K.L. Lee, R.W. Baker, H.K. Lonsdale, MEMBRANES FOR POWER-GENERATION BY PRESSURE-RETARDED OSMOSIS, *Journal of Membrane Science*, 8 (1981) 141-171.

[254] N.T. Hancock, T.Y. Cath, Solute Coupled Diffusion in Osmotically Driven Membrane Processes, *Environmental Science & Technology*, 43 (2009) 6769-6775.

[255] Y. Kiso, Y. Sugiura, T. Kitao, K. Nishimura, Effects of hydrophobicity and molecular size on rejection of aromatic pesticides with nanofiltration membranes, *Journal of Membrane Science*, 192 (2001) 1-10.

[256] T.-U. Kim, J.E. Drewes, R.S. Summers, G.L. Amy, Solute transport model for trace organic neutral and charged compounds through nanofiltration and reverse osmosis membranes, *Water Research*, 41 (2007) 3977-3988.

[257] R.V. Linares, V. Yangali-Quintanilla, Z. Li, G. Amy, Rejection of micropollutants by clean and fouled forward osmosis membrane, *Water Research*, 45 (2011) 6737-6744.

[258] Z.E. Hughes, J.D. Gale, Molecular dynamics simulations of the interactions of potential foulant molecules and a reverse osmosis membrane, *Journal of Materials Chemistry*, 22 (2012) 175-184.

[259] S.H. Yuan, X.H. Lu, Comparison treatment of various chlorophenols by electro-Fenton method: relationship between chlorine content and degradation, *Journal of Hazardous Materials*, 118 (2005) 85-92.

[260] A.L. Ahmad, K.Y. Tan, Reverse osmosis of binary organic solute mixtures in the presence of strong solute-membrane affinity, *Desalination*, 165 (2004) 193-199.

[261] Y. Yoon, P. Westerhoff, J. Yoon, S.A. Snyder, Removal of 17 beta estradiol and fluoranthene by nanofiltration and ultrafiltration, *J. Environ. Eng.-ASCE*, 130 (2004) 1460-1467.

[262] J. Heo, H. Kim, N. Her, S. Lee, Y.-G. Park, Y. Yoon, Natural organic matter removal in single-walled carbon nanotubes-ultrafiltration membrane systems, *Desalination*, 298 (2012) 75-84.

APPENDIX A - MD SNAPSHOT OF OPTIMUM SOCs WITH FO AND RO  
MEMBRANE COMPLEXES IN AQUEOUS SOLUTION

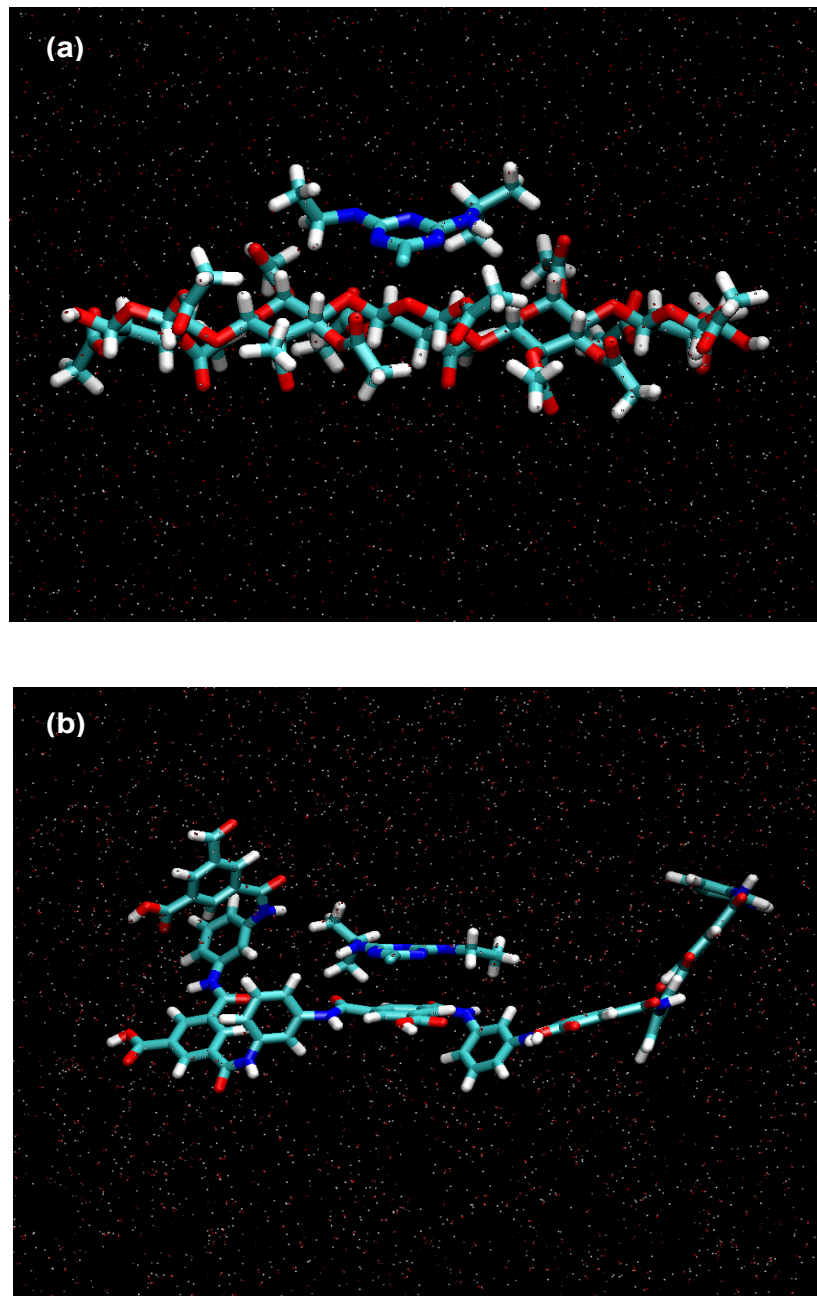


**Figure A.1** Representative MD snapshot of (a) FO-ATZ and (b) RO-ATZ complexes in aqueous solution.

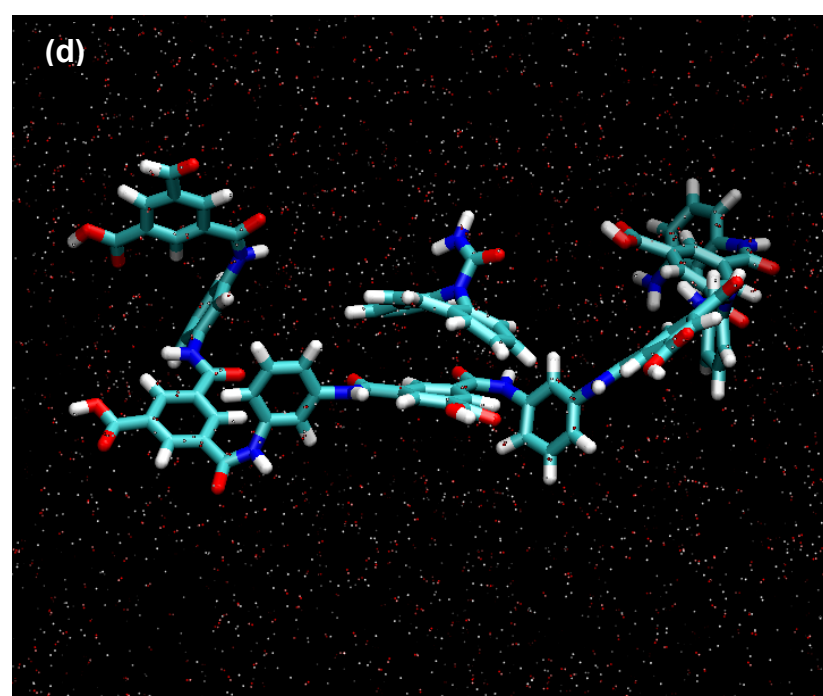
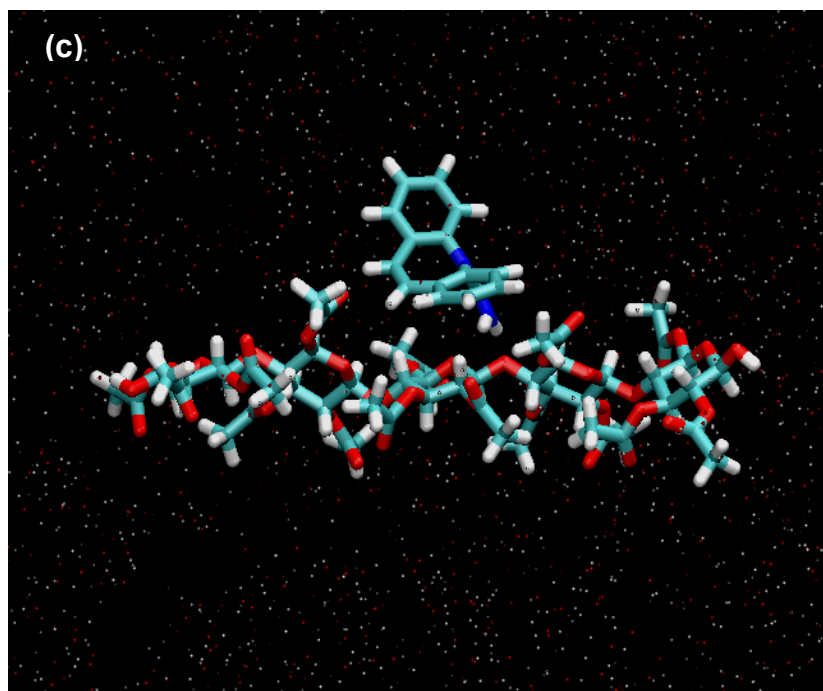


**Figure A.2** Representative MD snapshot of (c) FO-CBM and (d) RO-CBM complexes in aqueous solution.

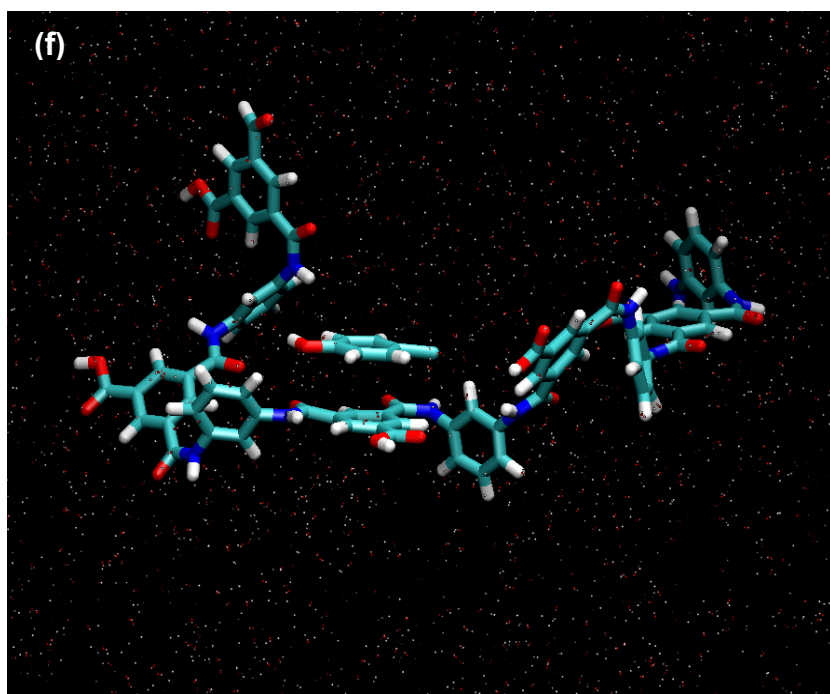
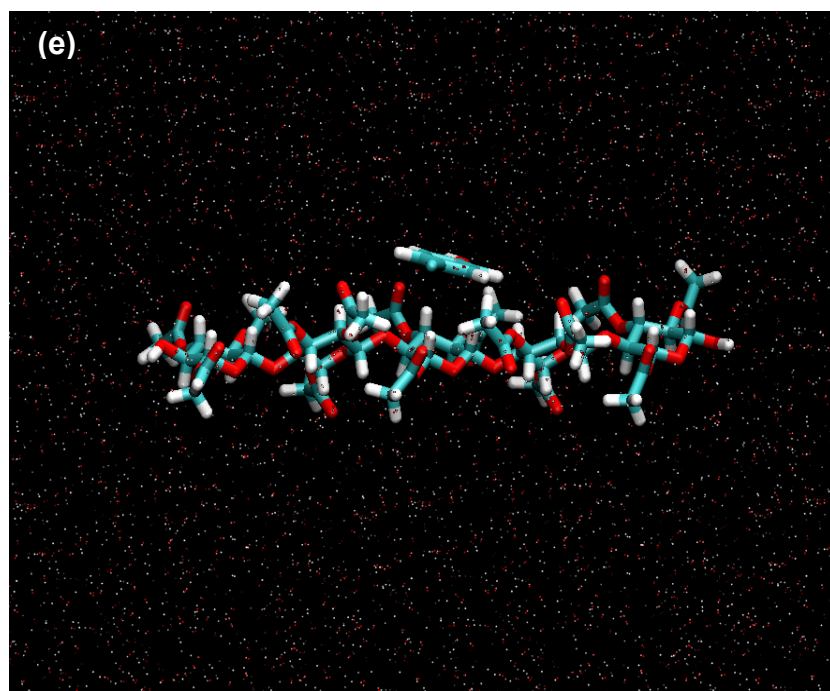


**Figure A.3** Representative MD snapshot of (e) FO-4CP and (f) RO-4CP complexes in aqueous solution.

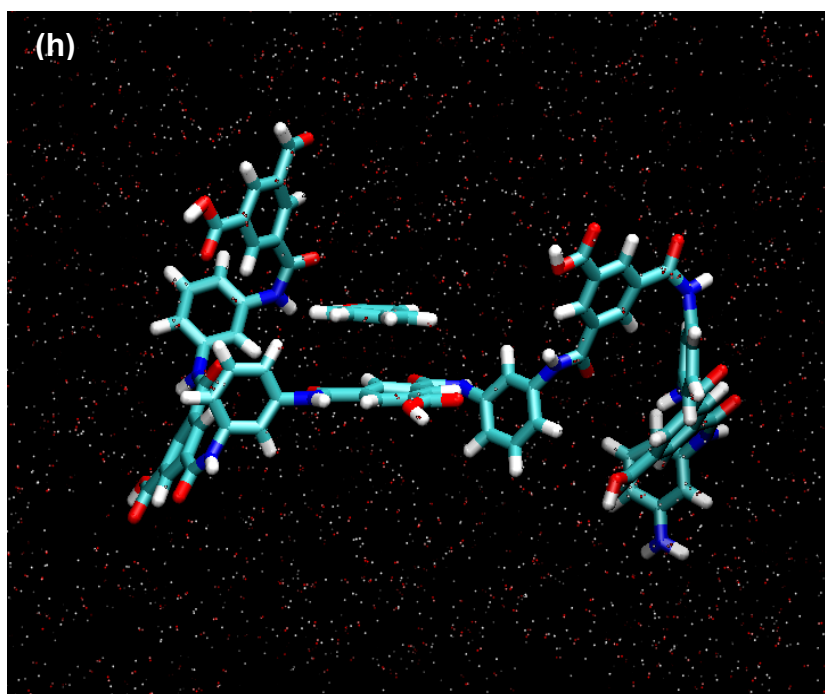
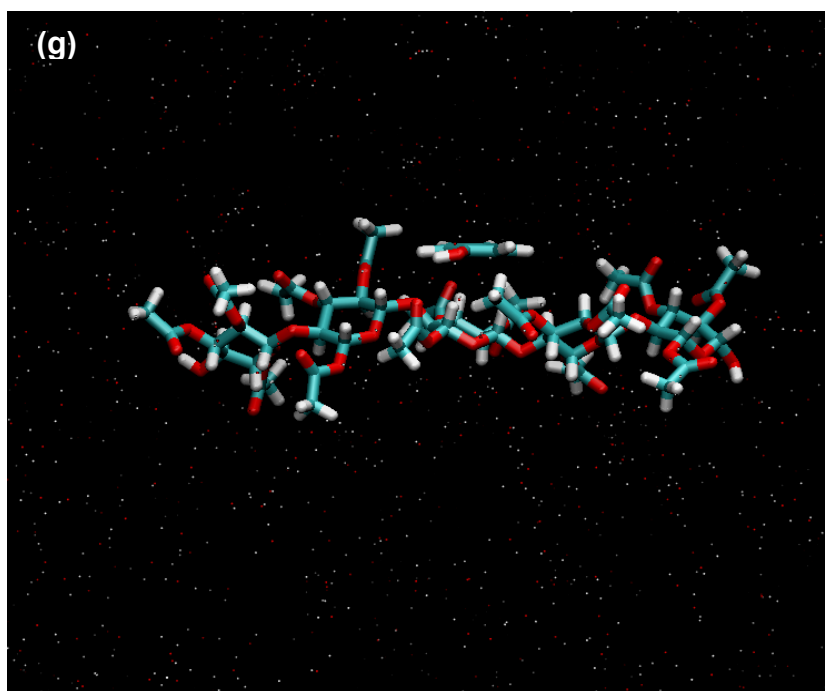


**Figure A.4** Representative MD snapshot of (g) FO-PHN and (h) RO-PHN complexes in aqueous solution.

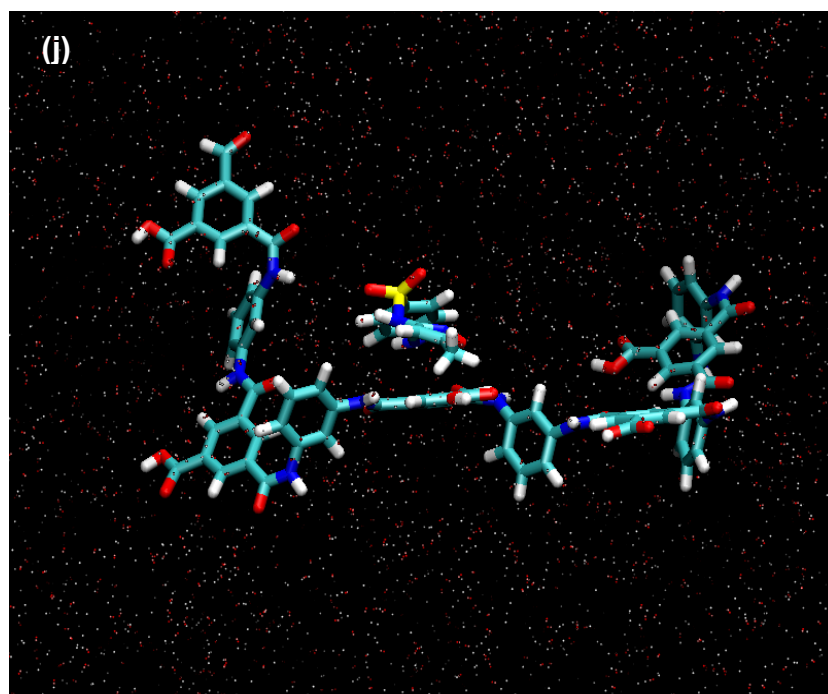
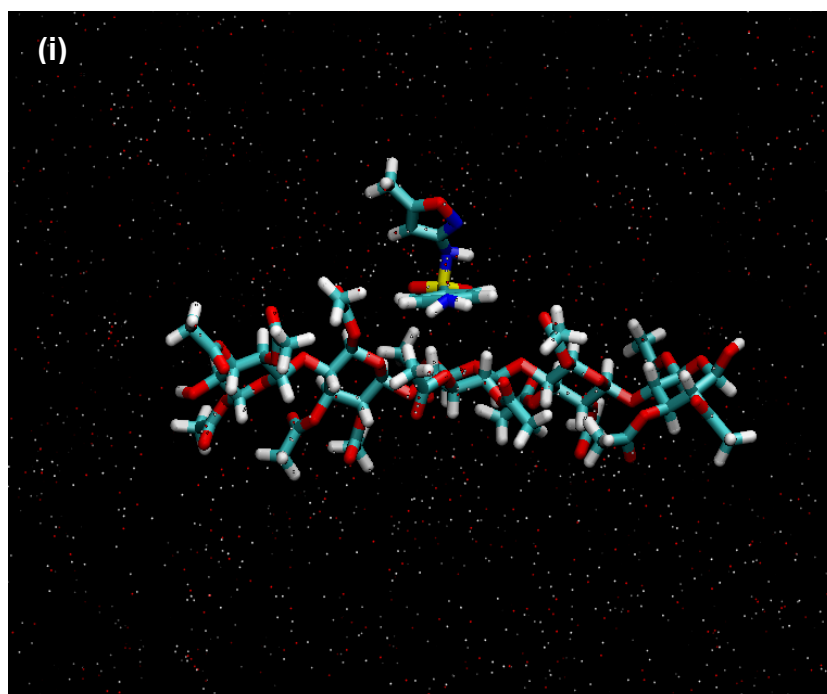


**Figure A.5** Representative MD snapshot of (i) FO-SMT and (j) RO-SMT complexes in aqueous solution.



## APPENDIX B - PRINTABLE AUTHORSHIP LICENSE

Rightslink Printable License	Page 1 of 5
<b>ELSEVIER LICENSE</b> <b>TERMS AND CONDITIONS</b>	
Jul 18, 2013	
<p>This is a License Agreement between Jiyong Heo ("You") and Elsevier ("Elsevier") provided by Copyright Clearance Center ("CCC"). The license consists of your order details, the terms and conditions provided by Elsevier, and the payment terms and conditions.</p> <p><b>All payments must be made in full to CCC. For payment instructions, please see information listed at the bottom of this form.</b></p>	
Supplier	Elsevier Limited The Boulevard, Langford Lane Kidlington, Oxford, OX5 1GB, UK
Registered Company Number	1982084
Customer name	Jiyong Heo
Customer address	751 Mallet Hill Rd APT #1105 COLUMBIA, SC 29223
License number	3192050614654
License date	Jul 18, 2013
Licensed content publisher	Elsevier
Licensed content publication	Separation and Purification Technology
Licensed content title	Removal of bisphenol A and 17 $\beta$ -estradiol in single walled carbon nanotubes-ultrafiltration (SWNTs-UF) membrane systems
Licensed content author	Jiyong Heo, Joseph R.V. Flora, Namguk Her, Yong-Gyun Park, Jaeweon Cho, Ahjeong Son, Yeomin Yoon
Licensed content date	27 April 2012
Licensed content volume number	90
Licensed content issue number	
Number of pages	14
Start Page	39
End Page	52
Type of Use	reuse in a thesis/dissertation
Portion	full article
Format	both print and electronic
Are you the author of this Elsevier article?	Yes
Will you be translating?	No
Order reference number	
<p><a href="https://s100.copyright.com/App/PrintableLicenseFrame.jsp?publisherID=70&amp;publisherNa...">https://s100.copyright.com/App/PrintableLicenseFrame.jsp?publisherID=70&amp;publisherNa...</a> 7/18/2013</p>	

**ELSEVIER LICENSE  
TERMS AND CONDITIONS**

Order reference number: 1982084  
 Title of your thesis/dissertation: Natural organic matter removal in single-walled carbon nanotubes-ultrafiltration membrane systems  
 Date of purchase: Jul 18, 2013

This is a License Agreement between Jiyong Heo ("You") and Elsevier ("Elsevier") provided by Copyright Clearance Center ("CCC"). The license consists of your order details, the terms and conditions provided by Elsevier, and the payment terms and conditions.

**All payments must be made in full to CCC. For payment instructions, please see information listed at the bottom of this form.**

Supplier	Elsevier Limited The Boulevard, Langford Lane Kidlington, Oxford, OX5 1GB, UK
Registered Company Number	1982084
Customer name	Jiyong Heo
Customer address	751 Mallet Hill Rd APT #1105 COLUMBIA, SC 29223
License number	3192050900919
License date	Jul 18, 2013
Licensed content publisher	Elsevier
Licensed content publication	Desalination
Licensed content title	Natural organic matter removal in single-walled carbon nanotubes-ultrafiltration membrane systems
Licensed content author	Jiyong Heo, Hwan Kim, Namguk Her, Sangho Lee, Yong-Gyun Park, Yeomin Yoon
Licensed content date	16 July 2012
Licensed content volume number	298
Licensed content issue number	
Number of pages	10
Start Page	75
End Page	84
Type of Use	reuse in a thesis/dissertation
Intended publisher of new work	other
Portion	full article
Format	both print and electronic
Are you the author of this Elsevier article?	Yes
Will you be translating?	No

<https://s100.copyright.com/App/PrintableLicenseFrame.jsp?publisherID=70&publisherNa...> 7/18/2013



**Publishing**

Alliance House  
12 Caxton Street  
London SW1H 0QS  
Tel: +44 (0)20 7654 5500  
Fax: +44 (0)20 7654 5555

Jiyong Heo  
University of South Carolina,  
Customer address: 751 Mallet Hill Road Apt #1105  
Columbia, SC 29223, USA

Friday, 19 July 2013

Dear Jiyong Heo

Permissions request relating to material published in *Water Science and Technology*

In response to your request for copyright clearance to use the article below from *Water Science and Technology* in your dissertation:

Heo, J., Joseph, L., Yoon, Y., Park, Y-G. Her, N., Sohn, J. And Yoon, S-H. 2011  
Removal of micropollutants and NOM in carbon nanotube-UF membrane system from  
seawater. *Water Science and Technology* 63(11) 2737-2744

We are very happy to grant you permission to reproduce the material specified above at no charge, provided that:

- the material to be used has appeared in our publication without credit or acknowledgement to another source;
- suitable acknowledgement to the source is given in accordance with standard editorial practice, e.g.,

"Reprinted from *Water Science and Technology*, volume x, issue number y, pages zz-zzz, with permission from the copyright holders, IWA Publishing."

- reproduction of this material is confined to the purpose for which this permission is given.

I trust this permission will be satisfactory; if any point needs clarification or you have any further queries, please do not hesitate to contact us again.

Yours sincerely

Michelle Herbert  
Journals Editorial Co-ordinator  
IWA Publishing

Order reference number: **ELSEVIER LICENSE**  
**TERMS AND CONDITIONS**  
 Title of your thesis/dissertation: **Wetted Carbon Nanotubes-Ultrafiltration and Forward Osmosis** Jul 18, 2013  
 Expected completion date: **Aug 2013**

This is a License Agreement between Jiyong Heo ("You") and Elsevier ("Elsevier") provided by Copyright Clearance Center ("CCC"). The license consists of your order details, the terms and conditions provided by Elsevier, and the payment terms and conditions.

**All payments must be made in full to CCC. For payment instructions, please see information listed at the bottom of this form.**

Supplier	Elsevier Limited The Boulevard, Langford Lane Kidlington, Oxford, OX5 1GB, UK
Registered Company Number	1982084
Customer name	Jiyong Heo
Customer address	751 Mallet Hill Rd APT #1105 COLUMBIA, SC 29223
License number	3192051216015
License date	Jul 18, 2013
Licensed content publisher	Elsevier
Licensed content publication	Journal of Membrane Science
Licensed content title	Comparison of flux behavior and synthetic organic compound removal by forward osmosis and reverse osmosis membranes
Licensed content author	Jiyong Heo, Linkel K. Boateng, Joseph R.V. Flora, Heebum Lee, Namguk Her, Yong-Gyun Park, Yeomin Yoon
Licensed content date	15 September 2013
Licensed content volume number	443
Licensed content issue number	
Number of pages	14
Start Page	69
End Page	82
Type of Use	reuse in a thesis/dissertation
Intended publisher of new work	other
Portion	full article
Format	both print and electronic
Are you the author of this Elsevier article?	Yes
Will you be translating?	No

<https://s100.copyright.com/App/PrintableLicenseFrame.jsp?publisherID=70&publisherNa...> 7/18/2013